ELUCIDATION OF THE STRUCTURE AND RECOGNITION PROPERTIES OF ANTIMONY(III)-TARTRATE USING ELECTROSPRAY IONIZATION MASS SPECTROMETRY

by

ARUNA B. WIJERATNE

Presented to the Faculty of the Graduate School of

The University of Texas at Arlington in Partial Fulfillment

of the Requirements

for the Degree of

DOCTOR OF PHILOSOPHY

THE UNIVERSITY OF TEXAS AT ARLINGTON

August 2010

ACKNOWLEDGEMENTS

It is with my greatest pleasure I convey my sincere appreciation to all who made my doctoral degree a success.

First and foremost I express my deepest gratitude to my co-supervisors; Dr. Kevin A. Schug and Dr. Daniel W. Armstrong, professors of the Department of Chemistry and Biochemistry, at the UT-Arlington for the enthusiasm, encouragement, guidance and supervision they have granted me to carry out effective and efficient research. Throughout my graduate-study period they provided sound advice, ideas and corrected various drafts, spending their valuable time on me. They made my research experience memorable and I would have been lost without them.

I am indebted to Dr. Jose Gracia and Dr. Peter Kroll, post-doctoral associate and professor, respectively, of the Department of Chemistry and Biochemistry, at the UT-Arlington, for their invaluable support in carrying out molecular calculations and advise on structural elucidations. I am also indebted to Dr. Richard B. Timmons, from whom I acquired plasma-Chemistry knowledge related to my research and Dr. Carl J. Lovely, from whom I took continuous consultation in NMR-spectroscopy.

I am thankful for my dissertation committee members Dr. Carl J. Lovely and Dr. Richard X. Guan for their support towards my dissertation work. Special thanks are also conveyed to Dr. Brian Edwards and Mr. Charles Savage, technical staff members of the Department of chemistry and Biochemistry, at the University of Texas at Arlington, for their utmost technical support provided throughout my research. I gratefully thank our present and past group members from both groups, Pritesh S. Sharma, Samuel H. Yang, Bilal H. Bazzi, Sandra E. Spencer and others for their support in carrying out research, friendship and anonymous help throughout my stay at UT-Arlington.

Last but not least, I am deeply thankful for my beloved wife, Bhagya K. Wijayawardena, my mother S. Wijeratne, my parents in law, Mr. and Mrs. Wijayawardena, my uncle W. M. J. Kumarasinghe and my very best friend D. N. Wijesundera, Physics-PhD graduate student at the University of Houston, TX, for their warm support, love and company throughout my graduate-study period, which made me accomplish my Ph.D.

July 19, 2010

ABSTRACT

ELUCIDATION OF THE STRUCTURE AND RECOGNITION PROPERTIES OF ANTIMONY(III)-TARTRATE USING ELECTROSPRAY IONIZATION MASS SPECTROMETRY

Aruna B. Wijeratne, PhD

The University of Texas at Arlington, 2010

Supervising Professors: Kevin A. Schug and Daniel W. Armstrong

Chirality of molecules is a major topic in the design, discovery and development of new drugs. Currently, analytical chemistry research divisions are challenged to find new methods to screen enantiospecific molecular recognition properties of potential chiral drug candidates with targeted biological molecules in a time-sensitive environment. Recently, mass spectrometry (MS) has received significant attention for its use in studying molecular recognition systems. Electrospray ionization mass spectrometry (ESI-MS) has received the most attention for the investigation of stereochemical association phenomena, due to its capacity to transfer solution phase chiral interactions into the gas phase for analysis in single-stage mass spectra. ESI-MS based chiral molecular recognition studies on cinchona alkaloid-carbamate model systems had been initiated by our group in order to test the viability of mass spectrometric techniques to trace solution phase enantiomeric interactions in their respective mass spectra. Importantly, these studies have returned results in good correlation with those found previously by in liquid phase separation techniques. It was realized that mass spectrometry is an invaluable tool to pre-screen such recognition systems. In order to further corroborate this argument, our group

had been in search of novel, less well understood chiral molecular recognition systems to be analyzed using ESI-MS, where other frequently used analytical techniques have failed to clarify their underlying mechanistic details.

Antimony(III) tartrate also known as “tartar emetic”, the bis-potassium salt of dianionic antimony(III)-L-tartarate, has a long history which traces back to medieval times and is filled with intrigue and peril. It has also been used as a therapeutic indication for diseases like typhoid, bronchitis, pneumonia and schistosomiasis. To date, mechanistic details of its actions, especially its biomolecular recognition properties, are not very well understood. While trying to indicate ESI-MS as an invaluable tool to study molecular recognition phenomena, we also hypothesized that ESI-MS based noncovalent binding studies of antimony(III)-D/L-tartrate complexes may provide useful information about its molecular recognition capacity. Since tartar emetic has also shown antibacterial properties, ESI-MS studies were carried out to visualize tartar emetic’s selective binding towards biologically relevant amino acid enantiomers. Consequently, a previously unprecedented proton-assisted enantioselective character of “tartar emetic” towards neutral D-amino acid enantiomers was revealed. A serendipitous observation resulted from these studies was its ability to capture unusual solvent reaction products generated during negative ionization mode ESI, which in fact provided a new understanding for the overall electrospray ionization mechanism. Additionally, theoretical studies, accompanied by multinuclear magnetic resonance experiments revealed that tartar emetic can assume a previously unknown structural isomer which is proven to co-exist with its crystallographically-determined structure. These findings and many ongoing research efforts suggest that this phenomenon may be responsible for many of tartar emetic’s inexplicable observations. This dissertation discusses our ongoing efforts to indicate ESI-MS for studying interesting molecular recognition phenomena of antimony(III)-tartrate binding to amino acids as well as providing useful molecular information of an inexpensive organo-metallic complex which could potentially be structurally altered to be used in many applications.

TABLE OF CONTENTS

LIST OF ILLUSTRATIONS

Figure Page

LIST OF TABLES

Table Page

CHAPTER 1

INTRODUCTION

1.1 Chirality

In chemistry, molecules with structures that have non-superimposable mirror images are said to carry the property, “chirality” [1]. The term “chiral” means hand in Greek. Right and left hands can be considered mirror images of each other and they cannot be superimposed. This example of right and left hands which is used to explain this phenomenon eventually has become the term used to describe molecules, which exhibit handedness. In 1815, the French physicist J. B. Biot was the first to discover that solutions containing organic substances such as tartaric acid are capable of rotating the polarization-plane of a linearly polarized light. This phenomenon was later termed as optical rotation. Then about three and half decades later, L. Pasteur related the optical rotation to a molecular property. In 1883, J. H. van’t Hoff and J. A. Le Bel had postulated that this molecular property originates from stereochemical factors; that is, the three dimensional arrangement of atoms or groups of atoms in a single molecule. Lord Kelvin, in his Baltimore lectures on “molecular dynamics and the Wave Theory of Light”, had proposed the term, “chirality” to explicitly describe this molecular property to any geometrical figure or group of points which is chiral [2].

1.1.1 Significance of chirality in drug development or therapeutics

Chirality is a key feature of the living world. Most biologically-active molecules are chiral. Naturally-occurring amino acids (building blocks of proteins), naturally-occurring mono-saccharides (building blocks of carbohydrates), and nucleotides (building blocks of nucleic acids that carry genetic information) are chiral [3]. For each category of such biomolecules found in the human body, identical chirality or handedness is observed. For example, the 21 essential amino acids are found predominantly in the *L*-configuration, while most carbohydrates are found

in the *D*-configuration (Note: "*D*-" or "*L*-" signifies one image-piece of a non-superimposable mirror-images-couple, referred to as enantiomers. The *D*/*L*-nomenclature system uses glyceraldehyde as the reference for indicating the chirality of sugars and their derivatives. More specifically, assigning *D*- or *L*- for a particular enantiomer depends on the original *D*- or *L*-glyceraldehyde that it was derived from). This chiral molecularity observed in the human body makes essential physiological processes highly stereoselective [4]. In fact, when exogenous chiral compounds are introduced into the body, physiological processes can show a high degree of chiral discrimination [5]. This is due to their differential interaction with chiral targets such as receptors, enzymes and ion channels [1].

Before the early 1980's, pharmacopoeia had been dominated by racemates. A racemate is composed of 1:1 mixture of enantiomers. However, with the emergence of new synthetic technologies, which have allowed the preparation of pure enantiomers in desirable amounts, renewed interests were established in understanding the stereochemical aspects of drug action [1]. This further resulted in placing a new awareness on the significance of stereoselective pharmacokinetics and disposition of therapeutics [1, 6-8]. With extensive advances in bio-molecular recognition studies, it is now well established, if one enantiomer is biologically-active for a desired purpose, its mirror-image stereoisomer could be inactive, be a competitor for the active enantiomer, or give rise to adverse biological actions [1, 6-9]. Therefore, chirality of drugs is a major topic in the "design, discovery and development of new drugs" [1]. Since a significant portion of currently-used drugs are in a single enantiomeric form, the focus in developing these drugs has made scientists in synthetic divisions discover "new methods and materials to obtain enantiomerically pure products" [10]. With an ever increasing number of single enantiomer compounds to evaluate, analytical scientists are currently challenged to find new methods to determine enantiomeric composition (i.e. enantiomeric purity) of new chiral materials in a time-sensitive environment. Analytical scientists are

simultaneously challenged to devise new ways to screen enantiospecific molecular recognition properties of potential chiral drug candidates with targeted biological molecules [10-12].

1.1.2 Measurement of Enantioselectivity

In a chemical reaction, the preferential formation or discrimination of one enantiomer over the other is referred to as enantioselectivity [13]. The quantitative measurement used to signify enantioselectivity is referred to as enantiomeric excess (e.e). In a mixture of *D*- and *L*-enantiomers, provided with the composition as the mole or weight fractions as F_D and F_L (where $F_D + F_L = 1$) the e.e. is given by $| F_D - F_L |$ [13]. Traditional methods utilized to determine enantiomeric excess include polarimetry, isotope dilution, gas chromatography (GC), liquid chromatography (LC) and nuclear magnetic resonance (NMR) spectroscopic methods [14]. Additional techniques that are currently in use or tested for enantiomeric discrimination studies include subcritical and supercritical fluid chromatography (SFC), capillary electrophoresis (CE), capillary electrophoretic chromatography (CEC), counter current chromatography (CCC) and centrifugal partition chromatography (CPC) [12]. In terms of accuracy and generality, LC and GC methods (using chiral stationary phases) are the current state-of-art techniques used for the measurement of enantioselectivity [10-12].

Except for analytical techniques that take advantage of measuring optical rotation and/or circular dichroism (CD), to separate enantiomers which carry the same physicochemical properties, all above mentioned techniques essentially utilize a complementary chiral reference compound (a “chiral selector”, a non-racemic chiral molecule either naturally occurring or synthetically produced) [10]. Efficiency of resolving enantiomers relies primarily on preferential association of one enantiomer over the other with this chiral reference. As it is illustrated in the Figure 1.1, if the difference in free energies of association between the chiral selector and the enantiomers is not zero (i.e. $\Delta\Delta G \neq 0$), then the chiral selector is said to be enantioselective for a particular enantiomer-couple [15]. GC and LC use chiral stationary phases (CSPs) to separate enantiomers. In LC, a chiral selector is either immobilized on a stationary phase such as silica

gel to create CSPs or incorporated into the mobile phase to create a pseudo-CSP. In order to obtain an effective enantiomeric separation, in all chromatographic techniques, it is essential that enantiomers interact with the stationary phase and migrate with the mobile phase differentially due to enantiospecific association and/or dissociation (non-covalently) with the chiral selector [10].

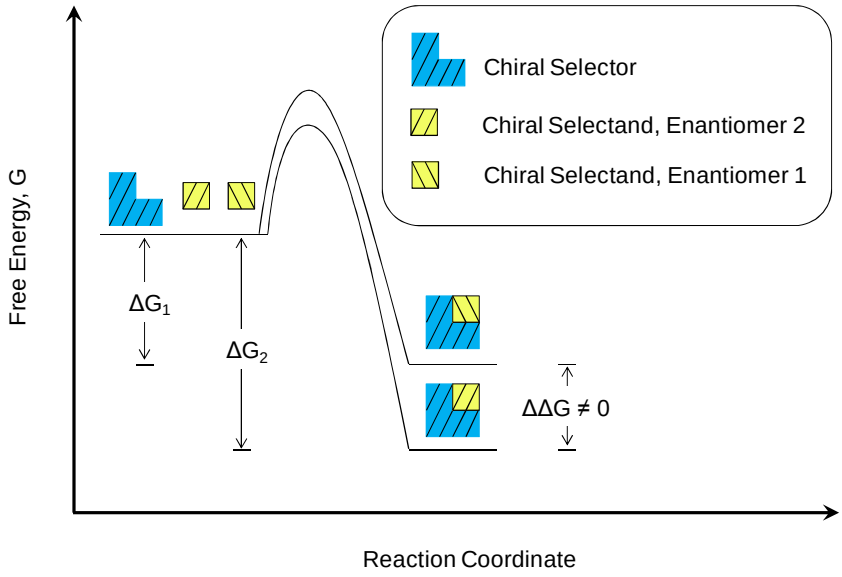

Figure 1.1 Enantioselective association by a chiral selector which shows differential binding ($\Delta\Delta G \neq 0$) to enantiomers. Here, the chiral selector exhibits a preferential binding to selectand enantiomer 2 ($\Delta G_2 > \Delta G_1$).

Currently, separation of enantiomers and determination of enantiomeric excess for racemic and non-racemic mixtures, in most cases, is achievable. Even so, since chiral compounds used in therapeutics are continuingly evolving, development of new chiral selectors having novel chiral association and dissociation mechanisms are required [10]. Also, a universal chiral selector that is capable of resolving all racemic mixtures is yet to be discovered and this challenges scientists to identify such chiral selectors. When fast combinatorial approaches were used to produce new chiral selectors, analytical techniques were challenged to provide faster

analysis and greater sensitivity [10. 12]. Sensitivity becomes an issue when small sample amounts are synthesized.

Recently, mass spectrometry (MS) has received significant attention for its use in studying molecular recognition systems. Small sample consumption and rapid analysis have made MS analyses more attractive compared to other analytical techniques. MS has also shown promise to study chiral molecular recognition phenomena [10-12]. However, compared to the level of general practice of chromatographic (LC and GC) and capillary electrophoretic (CE) separation techniques for enantiomeric excess determinations, MS is yet to reach such levels. While these separation techniques are still considered the "gold standard" for e.e. determinations, steady developments of new MS-techniques and their use in various chiral molecular recognition systems have shown the versatility of MS which can provide useful mechanistic information [10, 12].

1.1.3 Mass Spectrometry (MS) for Screening Enantioselectivity

Since the first observation by Fales and Wright, the stereochemical self-association phenomena of dialkyl-*D* and *L*-tartrate esters in chemical ionization (CI)-MS studies [15, 16], MS techniques have been effectively used to study a wide variety of chiral recognition systems and to provide useful insights into their underlying recognition mechanisms. Fast atom bombardment (FAB) [17, 18], matrix-assisted laser desorption/ionization (MALDI) [19] and electrospray ionization (ESI) [10, 12 and the references provided in 10] techniques, coupled with different mass spectrometric analyzers were used to study enantioselective phenomena generated from solution or condensed phases. Gas-phase stereoselective phenomena were also monitored by ion-molecule or guest-exchange reactions [20-22], the kinetic method [23], the direct dissociation of diastereomeric complexes [24-26], and with some other less common experimental techniques [27-29]. However, ESI-MS has received the most attention for the investigation of stereochemical association phenomena, due to its capacity to transfer solution phase chiral interactions into the gas phase for analysis in single-stage mass spectra [10].

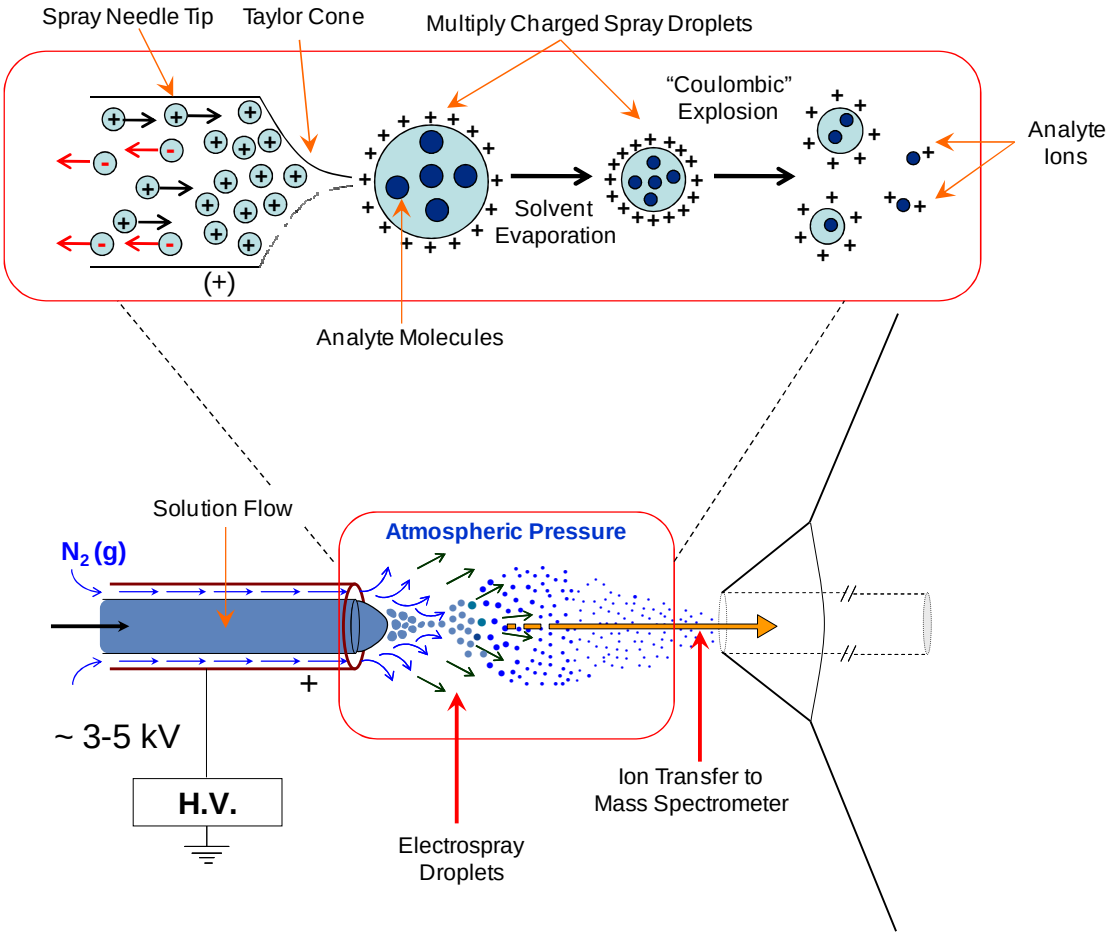

Figure 1.2 Electrospray ionization (ESI) process.

1.2 Electrospray Ionization Mass Spectrometry (ESI-MS)

A significantly high potential (~ 3-5 kV) applied to a stainless steel capillary tip (75-150 micrometers i.d.), which carries a liquid at a flow rate between 1 µL/min and 1 mL/min, is capable of producing an aerosol of highly-charged droplets [30, 31]. In general, if the flowing solution is composed of an analyte (carrying ionizable functional groups such as carboxylic acids and/or amines) dissolved in a polar, volatile solvent (such as methanol or acetonitrile), the aerosol containing highly charged droplets eventually produces analyte ions (frequently through protonation in the positive mode and through deprotonation in the negative mode) with minimal fragmentation. This ionization technique is referred to as electrospray ionization (Figure 1.2).

ESI is one of the most attractive atmospheric pressure ionization (API) techniques (because the ionization takes place at atmospheric pressure) and is well-suited for the mass spectroscopic analysis of polar molecules ranging from less than 100 Da to more than 1,000,000 Da. The most noted use of ESI-MS, for the analysis of large biomolecules such as proteins was pioneered by John Fenn and co-workers, and he won a share of the 2002 Nobel Prize in Chemistry [32]. Even so, ESI-MS is widely used in many research environments such as biotechnological (analysis of proteins, peptides, oligonucleotides), pharmaceutical (drug discovery, combinatorial chemistry, pharmacokinetics, drug metabolism), clinical (neonatal screening, haemoglobin analysis, drug testing), environmental (water quality, food contamination) and geological (oil composition) sciences [33].

1.2.1 Electrospray Ionization Mechanism

During electrospray ionization, ionization of intact molecules from a solution, flowing through a spray capillary, is achieved by applying a high voltage, as schematically depicted in Figure 1.2. At the end of the capillary tip a "Taylor cone" forms [33-34], from the apex of which, highly charged droplets dispense into the atmospheric pressure spray chamber. Due to solvent evaporation, which is pneumatically-assisted by a flow of nitrogen gas, these charged droplets shrink in size. This causes the surface charge density of the droplets to increase and to become very unstable due to Coulombic repulsions. On the other hand, the surface tension of the liquid tries to hold the droplets intact. However, when the excess charge repulsions overcome the surface tension, termed the Rayleigh stability limit [35], a "coulombic explosion" takes place. This process causes the droplets to disintegrate and eventually leads to the release of charged analytes or complex ions into the gas phase. These generated ions are then sampled into a high vacuum region and mass resolved to obtain ESI-mass spectra.

1.2.2 Electrospray Ionization Mass Spectrometry (ESI-MS) for Enantioselective Molecular Recognition

ESI-MS is by far the most popular choice of ionization used to study diastereomeric noncovalent complexes by MS. Henion and coworkers [36] were the first to study noncovalent interactions by ESI-MS. Since then, it has been proven to be capable of generating ion responses of noncovalently bound molecular adducts that were preformed in condensed media (e.g. in solution). Single-stage ESI-mass spectra have effectively traced useful information about solution phase dependent mass spectra as a function of solvent, pH, and ionic strength, among other variables [10]. Techniques such as titrations, competitive binding, and thermal dissociation threshold measurements have been applied to study solution-phase dependent solvated ionic complexes by ESI-MS [10]. Also, once these ionic complexes (noncovalently bound diastereomeric complexes) are transferred into the gas-phase and isolated, gas phase dissociation techniques, for example collisional and radiative dissociation, have been used to study intrinsic binding properties, in the absence of solvent molecules [37]. Such techniques used for gas-phase dissociation studies are referred to as “MS/MS” or tandem MS approaches. However, obtaining quantitative information from solution-phase is tricky and highly dependent on specific binding systems under investigation [38]. Usually, solution phase targeting ESI-MS experiments are further validated by complimentary solution-phase methods such as UV/Vis, fluorescence, nuclear magnetic resonance (NMR), CE, or calorimetric experiments. [10, 39-41]. While a significant number of chiral molecular recognition studies have been carried out using ESI-MS [10], cinchona alkaloid-carbamate chiral molecular recognition system has been extensively studied as a model chiral recognition system by the Schug, K.A. and co-workers [42-47].

1.2.3 Cinchona Alakaloid-Carbamate: Model Chiral Molecular Recognition System Studied using ESI-MS

Cinchona alkaloid-carbamate chiral selectors (tBuCQN (8*S*,9*R*) and tBuCQD(8*R*,9*S*), Figure 1.3) have been effectively employed for separation of enantiomers [48-60], particularly chiral acids (N-blocked amino acid enantiomers, *L*- and *D*-DNB-Leu, Figure 1.3), using liquid phase separation techniques. These chiral selectors have been immobilized on stationary phases and are even commercially available in several HPLC column formats [52]. The underlying mechanism for the resolution of these chiral acid enantiomers was fully detailed using various experimental and theoretical techniques such as NMR, calorimetry, IR and quantum mechanical calculations [51, 53, 55, 57, 60]. An anion exchange-type mechanism was defined to be the most important for the resolution of chiral acid enantiomers [55].

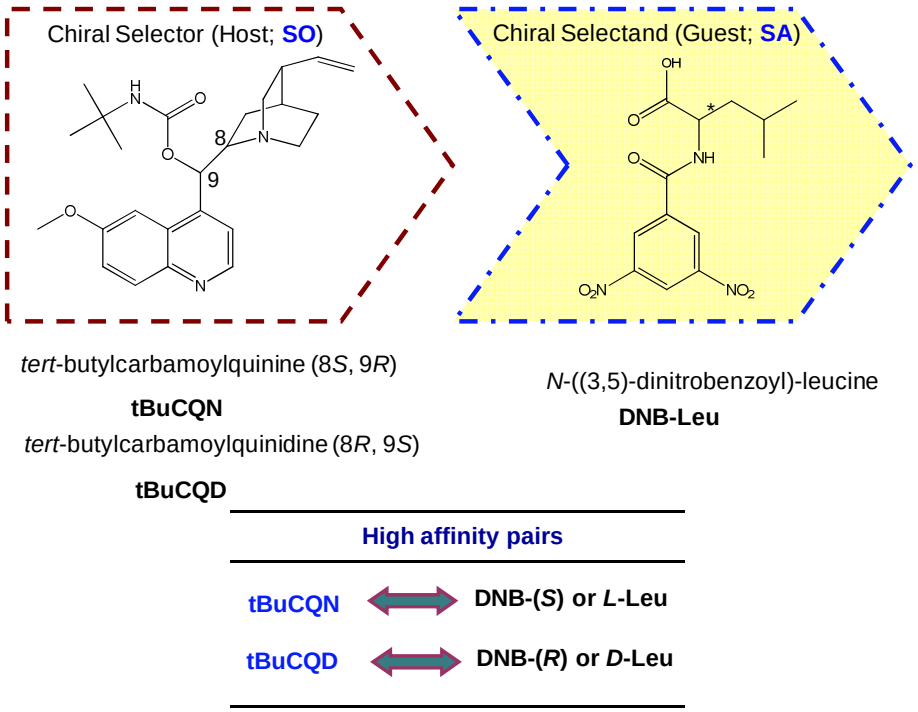

Figure 1.3 Cinchona alakaloid-carbamate-based model chiral molecular recognition systems.

The chiral selector-selectand association was proven to be primarily governed by the electrostatic interaction between the “protonated tertiary amine on the quinuclidene group of the chiral selector (tBuCQN) and deprotonated carboxylic acid group on the chiral selectands (DNB-

Leu)" [15, 55]. Secondary interactions that have also contributed for the chiral molecular recognition for these pairs include hydrogen bonding, π-π, and van der Waals forces. Stereochemically aligned 1:1 selector-selectand association of tBuCQN and *L*-DNB-Leu has been the most favorable association couple. In fact, diastereomeric complexes of chloro-tBuCQN with *L*-DNB-Leu were readily crystallized; whereas crystallization of chloro-tBuCQN with *D*-DNB-Leu was not accomplished. X-ray crystallographic measurements were carried out to study the preferential association of the chiral selector-selectand pair. The optimal alignment of the non-covalent interactions is illustrated in Figure 1.4. On another note, though they are not enantiomers, tBuCQD and tBuCQN have displayed cross-chiral (opposing) configurational preferences for the binding of *D*- and *L*-enantiomers of N-blocked amino acids, and was used in many of these studies as complementary cross-chiral studies to further validate the findings [15].

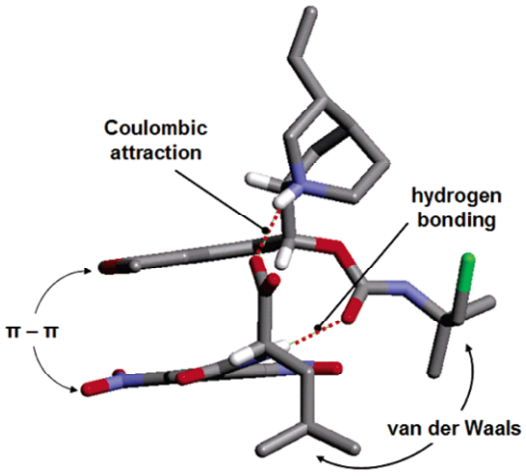

Figure 1.4 X-ray crystal structure illustration of favorable stereospecific interactions observed between *L*-DNB-Leu (bottom) in complex with chloro-tBuCQN (top). Reprinted from reference 43 with permission from American Chemical Society.

Since the fully detailed understanding of chiral molecular recognition properties of this cinchona alkaloid-carbamate model system, a wide variety of mass spectrometric molecular recognition studies have been performed by Schug, K.A. et.al [42-47]. These MS studies had been initiated in order to test the viability of mass spectrometric techniques to trace solution

phase enantiomeric interactions in their respective mass spectra. Most importantly, these studies have returned results in good correlation with those found previously by in liquid phase separation techniques. Overall, it was realized that mass spectrometry is an invaluable tool to pre-screen such recognition systems, especially given its analytical merits such as high sensitivity and rapidity of analysis.

1.3 Metal-tartrates or Binuclear Tartrato(4-) Metal Bridged Complexes

Our group had been in search of novel, less well understood chiral molecular recognition systems to be analyzed using ESI-MS, where other frequently used analytical techniques failed to clarify their underlying mechanistic details. We identified a set of complex molecular ions, namely binuclear tartrato(4-)-metal bridged complexes (for a general depiction, see Figure 2.1 in Chapter 2), potentially capable of containing a wide range of metal or metal-oxo centers such as As(III), Sb(III), Bi(III), Cr(III), Cu(II), Fe(III), In(III), Ti(III), V(IV)O, and W(VI), among others. These metal complexes have been of significant interest in asymmetric catalysis [61], medicinal chemistry [62-65] and enantiomeric separations [66-77]. From these complexes, antimony(III) tartrate was particularly interesting due to its long history (since medieval times) of therapeutic uses and due to the poor understanding of its detailed biomolecular recognition mechanism [65]. Structure of metal-tartrates are flexible, it is not only the metal-ion centers can be altered, but also the tartrate-ligands can be easily functionalized [66]. While trying to indicate ESI-MS as an invaluable tool to study molecular recognition phenomena, we also hypothesized that ESI-MS based non-covalent binding studies of antimony(III)-*D*/*L*-tartrate complexes would provide some useful information about its molecular recognition capacity. It was anticipated, an improved understanding of this metal-tartrate complex could be used to better optimize its previously tested applications. Research work documented in this dissertation, in fact is in support for our hypotheses and has contributed significantly to ESI-MS chiral molecular recognition studies, in understanding of the structural chemistry of metal-tartrates, and also an

unexpected contribution for the underlying mechanism for the electrospray ionization process [15, 78-82].

1.4 Antimony(III)-tartrates

Potassium antimony(III) tartrate, also referred as “tartar emetic”, has been a pharmaceutically important compound for centuries [65]. The long history of tartar emetic traces back to medieval times and is filled with intrigue and peril. The term “emetic” signifies its original use, as a medicine that was used to induce vomiting. It has also been used as a therapeutic indication for diseases like typhoid, bronchitis, pneumonia and schistosomiasis. Improperly administered, tartar emetic has exhibited severe side effects, which meant its use was generally dissuaded. To date, mechanistic details of its actions, especially its biomolecular recognition properties, are not very well understood [64-65, 78]. Since tartar emetic has also shown antibacterial properties [65], electrospray ionization mass spectrometric (ESI-MS) studies were carried out to visualize tartar emetic’s selective binding towards neutral amino acid enantiomers. Consequently, a previously unprecedented proton-assisted enantioselective character of “tartar emetic” towards *D*-amino acid enantiomers was observed. Antibacterial therapeutics, such as vancomycin and ristocetin, has shown similar selective binding towards *D*-amino acids which allows inhibition of peptidoglycan polymer regulation in the cell wall of Gram positive bacteria. The peptidoglycan is a stress bearing polymer containing *D*-amino acids [79]. Extended ESI-MS studies were also carried out to test the solvent composition dependence of these observed phenomena [80]. These studies have further revealed the ability of antimony(III)-tartrate to trap unusual solvent reaction intermediates, presumably formed during negative ionization mode electrospray ionization (ESI), which provided an unprecedented view for ESI processes [81]. Additionally, theoretical studies, accompanied by nuclear magnetic resonance experiments revealed that tartar emetic possesses a previously unknown structural isomer which is proven to co-exist in both the gas phase and in solution media [82]. These findings suggest this newly

identified isomer might be responsible for many of tartar emetic's previously inexplicable properties.

1.5 Dissertation Overview

Solution phase and gas phase chiral molecular recognition properties of tartrates (salts or esters of tartaric acid) and metal tartrates (binuclear tartrato(4-)-metal-bridged complexes), in conjunction with their applications in enantiomeric separation sciences and their mass spectrometric chiral discrimination properties, are comprehensively reviewed in Chapter 2 [78].

Chapter 3 provides our initial work, that is, to use ESI-MS to study antimony(III)-*L*-tartrate ("tartar emetic") association to leucine enantiomeric isotopomers [79]. These studies have revealed remarkable proton-assisted enantioselective molecular recognition phenomena and made us infer that recognition of neutral side-chain amino acid-enantiomers by antimony(III)-*L*-tartrate complex requires the association of a proton to become enantioselective. Interestingly, the dianionic selector itself failed to show enantiomeric discrimination capacity. This observation was proven to be consistent in both solution-phase-targeting full scan and gas-phase targeting collision threshold dissociation (CTD) experiments. Importantly, as it is described in Chapter 2, this disparity in enantioselective binding capacity between the dianionic and the protonated monoanionic representatives of antimony(III)-*D*- and -*L*-tartrates could have only be clearly revealed by ESI-MS and tandem mass spectrometry experiments. These studies have also urged more in-depth studies of mechanisms associated with exhibited enantiomeric resolving capacity of antimony tartrates in HPLC and CE applications, as well as for former antimony(III)-*D*, *L*-tartrate based ESI-MS association studies.

The effect of solvent systems on ESI-MS based proton-assisted enantioselective molecular recognition phenomena of tartar emetic, antimony(III)-*L*-tartrate, was evaluated and the results are discussed in Chapter 4 [80]. A series of competitive binding experiments using chiral selectors, bis(sodium) antimony(III)- *D*- and -*L*-tartrates with chiral selectands, neutral side-chain amino acid enantiomeric isotopomers of alanine (Ala), valine (Val), leucine (Leu) and

phenylalanine (Phe), in three different solvent systems, ACN/H_2O (75/25 v/v), H_2O (100%) and H_2O/MeOH (25/75 v/v) were carried out. Observations from these experiments have suggested that the effect of solvent systems on the proton-assisted chiral recognition capacity of antimony(III)- *D*,*L*-tartrates is small, but not negligible. It was also observed that an ACN/H_2O (75/25 v/v) solvent system facilitates and enhances the chiral discrimination capacity of protonated $\{[Sb_2\text{- }D, L\text{-tar}_2][H]\}^-$ ionic species. Further, amino acid enantiomers have showed a general trend of increasing selectivity order, Val ≤ Ala < Leu ≈ Phe towards the protonated $\{[Sb_2\text{- }D, L\text{-tar}_2][H]\}^-$ ionic species which was independent of the solvent system employed. The lack of enantioselective binding by $\{[Sb_2\text{- }D,L\text{-tar}_2]\}^{2-}$ ionic species with all four amino acids was consistently recorded in respective mass spectra from all performed experiments.

Chapter 5 explains the extended gas-phase targeting collision threshold dissociation (CTD) experiments carried out on diastereomeric ions generated by the association of dianionic as well as protonated monoanionic antimony(III)-*D*,*L*-tartrates with alanine (Ala), valine (Val) and phenylalanine (Phe) amino acid enantiomers [15]. These studies were aimed to compare the enantioselective capacity of antimony(III)-tartrate with a wider range of amino acid enantiomers. A consistent pattern of proton-assisted enantioselectivity was observed for all diastereomeric ions generated with each amino acid. It was realized that either a fundamental difference exists in the structural and functional arrangement of stereoselective recognition motifs between the dianionic and protonated monoanionic forms, or that some other unforeseen factor is contributing to the decreased stereoselective performance provided by the dianionic forms.

Chapter 6 describes a rather serendipitous observation that eventually resulted in providing new insight into the fundamental understanding of the electrospray process [81]. More specifically, negative-ionization mode ESI-MS analysis of antimony(III)-tartrate in frequently used solvent systems, ACN/H_2O and MeOH/H_2O, revealed that antimony(III)-tartrate dianions are capable of associating to solvent reaction products generated by free radical formation and

recombination during negative-ionization mode electrospray process. A systematic increase and decrease in negative spray capillary voltage (SCV) from normal operational voltage ranges of a conventional quadrupole ion trap instrument during these analyses have shown initially unobserved adduct ions to correspondingly increase and diminish in relative ion intensity. The identity of the adducted species, including products such as H_2O_2, $NCCH_2CH_2CN$, and $CH_2(OH)_2$, were confirmed by experiments with deuterated and non-deuterated solvent mixtures. Relative intensity dependence of these adducted-ions was also monitored as the volume composition of each solvent system was changed. Results have clearly indicated that the relative intensity of $\{[Sb_2\text{-}tar_2][H\text{-}O\text{-}O\text{-}H]\}^{2-}$ and $\{[Sb_2\text{-}tar_2][NC\text{-}CH_2\text{-}CH_2\text{-}CN]\}^{2-}$ adduct ions increased with the volume percent of H_2O and CH_3CN, respectively. Similarly, an increase in volume percent of CH_3OH have increased the relative intensity of $\{[Sb_2\text{-}tar_2][H\text{-}O\text{-}CH_2\text{-}O\text{-}H]\}^{2-}$ adducted-ions. Based on these pieces of evidence, findings described in this chapter made us propose that homolytic cleavage of C-H bonds for CH_3CN and CH_3OH molecules, and O-H bonds for H_2O molecules, produces a series of free radicals during negative-ionization mode ESI, and subsequent self-recombination or cross-recombination of these free radicals then occurs to form the neutral solvent products, which are observed in mass spectra as dianionic $[Sb_2\text{-}tar_2]$-adducted ion species.

It was clear that explicating our observations, particularly the proton-assisted enantioselective character of tartar emetic, was not trivial using the crystallographically determined structure of dianionic antimony(III)-*L*-tartrate. Therefore, to end this tale of the binding chemistry of antimony(III)-*D*- and *L*-tartrates, a more thorough understanding of the structure of dianionic antimony(III)-*L*-tartrate was required. Chapter 7 reports the results of theoretical calculations and NMR (nuclear magnetic resonance) experiments carried out on antimony(III)-*L*-tartrate dianionic structure [82]. Experiments have revealed a new structural isomer for the antimony(III)-*L*-tartrate dianion, which is predicted to co-exist in solution and in the gas phase. Overall, these studies have provided a new insight into a dynamic structural

character for antimony(III)-*L*-tartrate. These studies urge researchers to revisit and consider both structures when investigating the molecular recognition properties of antimony(III)-*L*-tartrate.

Overall, while the work documented here has significantly supported our ongoing efforts to show that ESI-MS is an important analytical tool to study molecular recognition phenomena, extended studies are currently being carried out to further elucidate this assertion. On the other hand, interesting structural and molecular recognition properties of antimony(III) tartrate have taken a step forward to provide an improved mechanistic understanding for its less well-understood intricacies. Though more work is required to fully describe its mode of resolving action, the information exposed in this dissertation indicate metal-tartrates may very well still be tuned to provide optimum performance both as an analytical separations reagent, and even as a useful therapeutic entity.

CHAPTER 2

MOLECULAR RECOGNITION PROPERTIES OF TARTRATES AND METAL-TARTRATES IN SOLUTION MEDIA AND GAS PHASE

2.1 Introduction

Tartrates (salts or esters of tartaric acid) and metal-tartrates (binuclear tartrato(4-)-metal-bridged complexes), depicted as shown in Figure 2.1, are an important class of chiral molecules due to their application in separation science as enantioselective recognition elements (chiral probes; chiral selectors; chiral references). The history of tartrates is inextricably linked with the seminal work of Louis Pasteur on elaborating the presence of chirality or "handedness" in molecules [83, 84]. Tartrate-esters were the first compounds to be used to demonstrate the capacity for mass spectrometry to study stereospecific interactions in the gas phase [16]. L-tartaric acid can be found naturally in its enantiopure form. Its enantiomer, *D*-tartaric acid, is also readily available commercially. All other tartrate salts and esters, as well as metal-tartrates, are derived from these tartaric acid enantiomers. Substantial versatility is afforded by this highly functional scaffold, and molecularly modified forms of tartaric acid include alkoxy (-OR) derivatives, ester (-COOR) or amide (-$CONR_1R_2$) transformations, and even C-H alkylation. The capability for obtaining metal-tartrates with different metal ions is also attractive to generate a broader range of arrangements with interesting molecular recognition, as well as magnetic and even, medicinal properties [61, 65,66, 85-90].

Antimony-tartrate in particular has been used since medieval times for its pharmaceutical significance. History tells of its variable indications as an emetic-drug, an anti-parasitic drug, and a therapeutic agent for wide-spread inflammatory conditions, like bronchitis and pneumonia [65]. However, due to a large number of deleterious side effects, its use has been substituted by other less toxic substances. Still, antimony tartrate, and other metal tartrates have remained in the curious eye of many scientists throughout the years. Their

variable capacity for enantioselective recognition towards biomolecular, as well as synthetic organic and inorganic substrates, makes them flexible and broadly applicable. A number of viable system-dependent models have been proffered to explain observed recognition behavior, although a review of the literature tells of a system which requires more examination to be truly well understood.

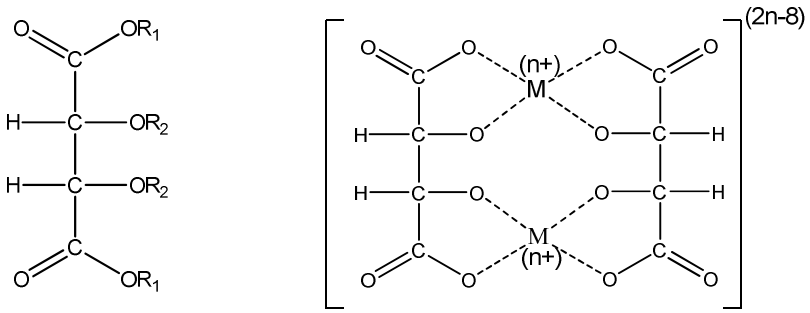

(A) (B)

Figure 2.1 General structural depiction of (A) tartrates [R=alkyl or H] and (B) metal-tartrates (M = V(IV)O, Sb(III), Cr(III), As(III), Bi(III), Cu(II), Fe(III), W(VI)). Reprinted from reference 78 with permission from John Wiley & Sons, Inc.

Tartrates and metal-tartrates have shown their capacity for resolving enantiomers in a wide variety of separation techniques. In synthetic applications, using these compounds, successful enantioselective separations by diastereomeric salt formation have been achieved. For example, tartaric acid is capable of resolving enantiomeric mixtures of chiral amines [91]. Similarly, metal-tartrates, such as sodium salts of antimony(III)- and arsenyl(III)-*D*,*L*-tartrates have been able to separate Δ and Λ enantiomers of Co(III)/Ru(II) complexes by diastreomeric salt formation [92-96, 67] (Δ and Λ correspond to helical chiral designations where Δ and Λ represent right-handed and left-handed helices, respectively). Tartrates have also been investigated for use as chiral selectors in gas-chromatography (GC) [97], liquid-liquid extraction [98-99], counter-current dialysis [100], counter-current chromatography [101], super critical fluid chromatography [102], capillary electrophoresis (CE) [103-104], and high performance liquid chromatography (HPLC) [105-119]. Comparably less number of applications has been reported

for metal-tartrates relative to that for tartrates. However, metal-tartrates have illustrated their potential to resolve enantiomers especially in HPLC [68, 70-74] and CE [69, 75-77] applications.

Preferential association of the chiral selector with one enantiomer of a racemic mixture is the key to separating enantiomers [11, 120-121]. In-depth understanding of favorable or unfavorable diastereomeric interactions originated between analytes and selector molecules not only clarifies experimental observations in separation sciences, but also provides vital information for optimizing recognition systems so that efficient and effective enantiomeric separations can be achieved. X-ray crystal structure determinations of diastereomeric salts is by far the most utilized technique for understanding specific interactions between chiral standards and enantiomeric analytes in the solid state. However, these solid-state determinations may be questionable for use as means to explain solution phase separations. Stereospecific recognition in the solution phase is utilized predominantly in chromatographic and electrophoretic separation techniques, but more direct methods, such as NMR, are needed to unequivocally define interaction mechanisms in the presence of solvent. More recently, with the advent of soft ionization techniques coupled to mass spectrometry (MS), it has become possible to directly study both the solution phase and the gas phase binding interactions in noncovalent diastereomeric complexes [12, 17, 19, 37, 122] . Single-stage mass spectral analysis has been used to carry out solution-phase chiral molecular interaction studies. In this case, it is often assumed that solution-phase-directed intermolecular interactions are preserved and represented by the variation of gas phase ion intensities in the recorded mass spectra. In practice, such correlation can be system-dependent and should be rigorously examined. Gas phase intermolecular interaction studies in MS are also common [10, 27], having been carried out by different methods, including collisional dissociation of diastereomeric complexes [26], the Kinetic Method [23], ion-molecule guest-exchange reactions [20, 22], and a variety of other more complicated set-ups [29, 123]. In these studies, while enantioselective interactions can be investigated directly in the absence of solvent, this also provides a drawback regarding the

formulation of conclusions with respect to solvent-dependent recognition mechanisms. However, comparison of molecular recognition studies in all three (solid, solution, and gas) phases would provide complementary pieces of information which can be united to fully characterize interaction mechanisms and optimize their use.

The first identification of chiral interactions using mass spectrometry involved the self-bound complexes of tartrate-esters studied by Fales and Wright using chemical ionization-MS [16]. Since then, much of the early work in this field was carried out by fast atom bombardment experiments [124-126], while electrospray ionization – mass spectrometry (ESI-MS) has taken a more prominent role in recent years as the technology has matured. ESI-MS is well known for providing high sensitivity, minimal sample consumption, high speed of analysis, and a capacity for preserving and studying noncovalent complexes formed in solution [10, 12, 20, 23, 27, 37, 46, 122, 127].

The aim of this chapter is to provide the reader a brief overview of solution phase and gas phase molecular recognition properties of tartrates and metal-tartrates. Solution phase enantiomeric separations, especially in liquid chromatographic and capillary electrophoretic formats, utilizing tartrates and metal-tartrates as chiral selectors are reviewed. Mass spectrometric solution phase and gas phase molecular recognition properties of tartrates and metal tartrates which are supported by literature are also discussed. Overall, this review serves to collect and present experimental results which have helped shape perceptions of enantioselective recognition relevant to these interesting classes of compounds. However, it is also brought to light that many aspects related to the mechanistic interpretation of these results remain to be further elaborated.

2.2 Solution Phase Molecular Recognition Properties of Tartrates

Using *L*-(+)-diacetyltartaric acid anhydride, chemical modification of silica gel has produced useful chromatographic stationary phases for separating enantiomers based on a *L*-(+)-tartaric acid chiral selector [105-106]. An acetylated derivative of *L*-(+)-tartaric acid can be bonded to the silica support via 3-(trimethoxysilyl)propylamine to create the chiral stationary phase (CSP) shown in Figure 2.2A. After removal of the protecting groups and treatment with Cu^{2+}, the *L*-(+)-tartaric acid-modified CSP shown in Figure 2B was able to resolve enantiomers of catecholamines. CSPs tested with acetylated hydroxyl groups (-OAc) were not successful in resolving the enantiomers, indicating the important role of the hydroxyl groups for enantioselective recognition.

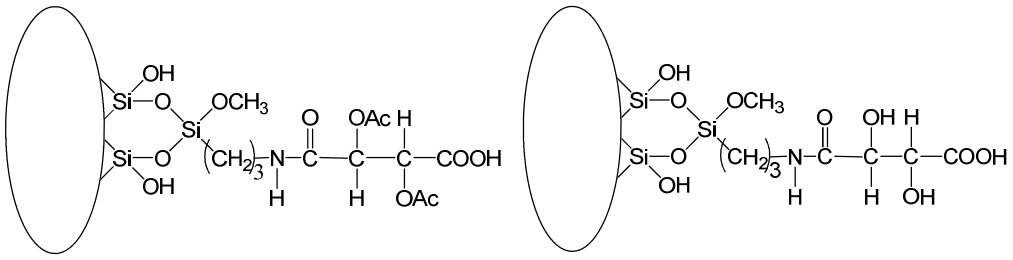

(A) (B)

Figure 2.2 Chemically modified silica-gel-based chiral stationary phases with (A) O-acetylated *L*-tartaric acid and (B) *L*-tartaric acid chiral selector units [105,106]. Reprinted from reference 78 with permission from John Wiley & Sons, Inc.

Even so, (*R*,*R*)-O,O-diacetyltartaric acid diamide bonded phases have been successful in providing enantiomeric separations for 3,5-dinitrobenzoyl derivatives of leucine and phenylglycine methyl esters [107]. Further, the direct separation of amino acid, hydroxy acid, and amino-alcohol enantiomers has been achieved using octadecylsilyl-bonded (ODS) silica gel coated with a monoamide derivative of (*R*,*R*)-tartaric acid (derived from (*S*)-valine-(*S*)-1-(α-naphthyl)ethylamide), using aqueous or hydro-organic eluents containing copper(II) ion in the mobile phase [110]. A subsequent study was carried out by preparing three monoamide derivatives of (*R*,*R*)-tartaric acid derived from (*R*)-1-(α-naphthyl)ethylamine, (*S*)-valine-(*S*)-1-(α-

naphthyl)ethylamide and (*R*)-valine-(*R*)-1-(α-naphthyl)ethylamide, respectively, and examining their chromatographic properties as chiral selectors by HPLC [111]. These chiral selectors containing carboxylic acid groups were ionically bonded to 3-aminopropyl silica-gel stationary phases by carrying out acid base reactions in methanol and were used to separate enantiomers of derivatives of amino acids, amines, carboxylic acids and alcohols. In order to achieve direct separation of underivatized racemic amino acids and hydroxyl acids, copper(II) complexes of these chiral selectors were coated on reversed-phase materials. This study has revealed that (*R*,*R*)-tartaric acid amide derivatives can act as bi-functional chiral selectors, applicable for the enantiomeric separation of a wide range of racemic compounds.

Tartaric acid based CSPs have also been commercialized for use. A tert-butylbenzoylated tartaric acid-based CSP (Kromasil-CHI-TBB) is available which has been shown to be applicable for resolving racemic mixtures of mandelic and tropic acid derivatives on both analytical and preparative scales [113]. Although these analytes have relatively simple structures, their enantiomeric forms have proved to be difficult to resolve by other means.

Immobilization of tartrate-based chiral selectors on solid supports to produce useful chiral solid or liquid stationary phases has been pursued by many research groups. Adsorption of structurally modified (*R*,*R*)-tartaric acid diamides, such as (*R*,*R*)-N-isopropyl-N'-(1-pyrenyl)tartaramide, (*R*,*R*)-N-(2-chrysenyl)-N'-isopropyltartaramide and (*R*,*R*)-N-(2-chrysenyl)-N'-(3-nitrophenyl)tartaramide on to porous graphitic carbon to create carbon-based CSPs has been reported by Monser et al [112]. Excellent enantioselectivity was demonstrated for various types of compounds including aromatic alcohols, binaphthyl derivatives, β-blocking agents and anti-inflammatory agents. Tartaric acid-based selectors ((*R*, *R*)-O, O'-bis(dimethylbenzoyl)-N,N'-diallyl-N, N'-dimethyl tartaramide) and ((*R*,*R*)-N-allyl-O,O'-bis(dimethylbenzoyl) tartarimide) were also synthesized and immobilized on silica-gel for evaluation as chiral stationary phases by Oxelbark and Sellen [115]. These were compared for enantiomeric separations of chiral compounds with the commercially available column Kromasil-CHI-1, which is based on the

selector: (*R*, *R*)- O, O'-bis(dimethylbenzoyl)-N,N'-diallyl tartaramide. It was concluded that amide-NH functions are essential for achieving retention and enantioselective discrimination of most analytes. Further, the flexibility of the benzoyl moieties has also been deemed essential for providing additional steric information to differentiate enantiomers.

In related work, polymeric chiral stationary phases based on O,O'-di(3,5-dimethylbenzoyl)-N,N'-diallyl-*L*-tartaric diamide (Kromasil CHI-DMB) have been used to baseline resolve 1,1'-bi-2-naphthol (BINOL) enantiomers [116]. Even so, 1,1'-bi-2-naphthyl di-p-toluenesulfonate, 1,1'-bi-2-naphthyl diacetate and 1,1'-bi-2-naphthyl dicinnamate enantiomeric mixtures could not been resolved using this method. Chiral liquid stationary phases were prepared on solid supports by immobilizing organic stationary phases prepared by dissolving tartaric acid derivatives in solvents such as hexane or dichloromethane [109]. Both hydrophilic (Nucleosil CN) and hydrophobic (porous graphitic carbon) solid supports were used in a comparative analysis. Among the tartrate derivatives tested, only tartrates with free –OH groups have affected enantioselective retention for ephedrine stereoisomers. Liquid stationary phases with (2*R*,3*R*)-di-n-butyl tartrate (DBT) in hexane were shown to provide greater stereoselectivity than DBT in dichloromethane for amino-alcohol separations. The different solid supports were also shown to alter the retention and resolution of the analyte enantiomers.

In reversed phase LC, tartaric acid has been successful in aiding enantiomeric separations as a mobile phase additive. Tartaric acid derivatives were used as chiral complexing agents to generate diastereomeric complexes with amino-alcohol enantiomers, facilitating their separation on an achiral stationary phase [109]. The enantiomeric resolution of *D*-(-)- and *L*-(+)-ascorbic acid was also demonstrated by this approach and the method was applied to identify vitamin C in medical formulations [108] .

L-(+)-tartaric acid has been tested as a chiral mobile phase additive in supercritical fluid chromatography (SFC) and capillary zone electrophoresis (CZE). In SFC, good enantioselective resolution was observed for tertiary amine homologues of 2-amino alcohols

which are used as β-adrenoreceptor-blocking drugs [102]. Intermediate selectivities have also been observed for aromatic compounds when there was a second substituent at the ortho-position. Overall, the mechanism of retention was concluded to be most influenced by aromaticity, as well as the presence of free electron pairs, in the analytes to be separated. In CZE, enantiomeric separation of MK-0677 {(*R*)-2-amino-N-[2-[1,2-dihydro-1-(methylsulfonyl)spiro [3H-indole-3,4'-piperidin]-1'-yl]-2-oxo-1-[(phenylmethoxy)methyl]ethyl]-2-methylpropanamide-monomethane sulfonate}, an orally-active growth hormone secretagogue, has been achieved using β-cyclodextrin (β-CD) as the chiral selector in a phosphate buffer containing *L*-tartaric acid and ethanol. Addition of *L*-tartaric acid as an ion-pairing reagent was demonstrated to be essential for achieving separation of the enantiomers [103].

2.3 Gas Phase Molecular Recognition Properties of Tartrates

In 1977, Fales and Wright reported the first gas phase chiral recognition using chemical ionization mass spectrometry (CI-MS). In brief, they observed self-recognition of dimethyl-d_6-*D*-tartrate (d_6-*D*-DMT) and dimethyl-*L*-tartrate (d_0-*L*-DMT) by the inspection of protonated dimer ion ($[2M+H]^+$) signals in mass spectra produced when an equimolar mixture of d_0-*L*-DMT and d_6-*D*-DMT was subjected to CI-MS using isobutene as a reagent gas. From a theoretical point of view, the protonated dimer ion signal should consist of three isotopic peaks due to the formation of both homo- and heteroisotopomeric ion forms. The three combinations expected would be: One signal at m/z 357 representing the self-bound d_0-*L*-DMT protonated dimer ion; a second peak at m/z 363 representing the heteroisotopomeric mixed dimer ion; and a third peak at m/z 369 representing the self-bound d_6-*D*-DMT protonated dimer ion. The expected ratio of peak intensities for these ions is 1:2:1 according to the quadratic relation (d_0-*L*-DMT+ d_6-*D*-DMT)^2. Unexpectedly, the mixed dimer ion intensity was only a fraction (78%) of the expected ion intensity. On the other hand, the expected 1:2:1 pattern was only observed when equimolar mixtures of d_0-*D*-DMT and d_6-*D*-DMT were subjected to CI-MS. The latter observation in fact rules out any contributions based on isotope effects in the former experiment. The observed

effect is then attributable to enantioselective self-association in the gas phase. A more pronounced effect was observed when an equimolar mixture of esters, diisopropyl-d_0-*D*-tartrate (d_0-*D*-DIPT) and its enantiomeric isotopomer diisopropyl-d_{14}-*L*-tartrate (d_{14}-*L*-DIPT) was analyzed. In this case, the signal intensity of mixed ion form was less than half (46%) of the expected value [16].

A concrete explanation for this phenomenon was pursued. The reported chiral recognition mechanism states that proton (H^+) solvation by five strain-free linear H-bonds are exerted between pairs of tartrate esters. The minimum energy conformations are illustrated in Figure 3 [128]. Association to form the heterochiral pair results in a weaker H-bonding interaction at an extreme of the zip-type chelate complex proposed. This is further explained by a weak dialkyl-gauche interaction formed when the enantiomers having opposite configurations bind through a proton, resulting in a less favorable association of tartrate-esters [128].

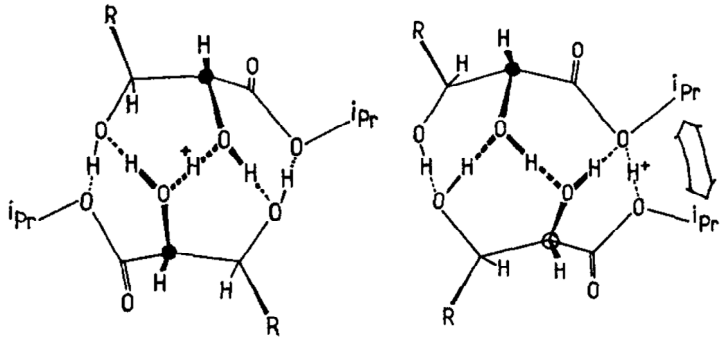

Figure 2.3 Chirospecific conformations of diastereomeric protonated dimers of diisopropyl tartrates. (A) homo-chiral dimer ([diisopropyl-d_{16}-*L*-tartrate]$_2$[H]$^+$) and (B) hetero-chiral dimer ([diisopropyl-d_{16}-*L*-tartrate] [diisopropyl-*D*-tartrate][H]$^+$). Reprinted from reference 78 with permission from John Wiley & Sons, Inc.

The consistency of these self-recognition features by tartrate-esters was further confirmed by fast atom bombardment (FAB) experiments [124]. Using diisopropyl tartrate as a matrix, tandem mass spectrometry was performed following FAB to determine absolute configuration of some diol compounds [125]. Mass analyzed ion kinetic energy (MIKE) spectra

and kinetic energy release (KER) measurements of diastereomeric octahedral cobalt complexes of alkyl tartrate esters have also shown that diastereomeric complexes can be differentially evaluated in the gas phase. Different KER values of product ions were generated from $[Co(acac)_2][D\text{-},L\text{-diisopropyl tartrate}]^+$ (acac = acetylacetonate ion) and it was concluded that the presence of a chemical kinetic resolving agent like *RR*- or *SS*-threohydrobenzoyn (THB) is essential for this chiral recognition system [126]. The enantiomers of analytes, such as isopropyl threo- and erythro-3-cyclohexylglycerates, 2,3-butanediol, trans-1,2-cyclohexanediol and 1,4-dimethoxy-2,3-butanediol were studied in the gas phase by CI-MS using labeled diisopropyl tartrates as a chiral reference [129]. The protonated mixed dimers of iso-propyl threo-3-cyclohexylglycerates and trans-1,2-cyclohexanediol showed small but significant chiral discrimination, whereas the other analytes failed to display any chiral discrimination by this method.

Investigation of noncovalent gas phase association between chiral dialkyltartrates (T) and multiprotic-onium (A) ions such as hydronium, ammonium and primary aminium ions using CI-MS has resulted in the observation of trimer ion adducts of the form T_3AH^+ (5% to 55% of the substrate ions) where the expected 1:3:3:1 pattern has deviated substantially, ranging from 1:1:1:1 to 5:3:3:5 [128]. Homochiral adducts were shown to yield three to four times greater intensities than the heterochiral adducts. A term was introduced to provide a measure of chiral discrimination shown by trimer-adducts of dialkyltartrate-esters. The “chiral discrimination ratio” (CDR) is defined as the observed ratios of sums of the homo-chiral versus hetero-chiral trimer adduct abundances divided by the corresponding statistical ratio of one-third:

$$\text{CDR (Chiral discrimination ratio)} = \frac{3\,([sss.AH^+] + [sss.AH^+])}{([ssr.AH^+] + [srr.AH^+])} \quad \cdots\cdots\cdots (2.1)$$

This definition assumes that the measurements are performed with equimolar mixtures of dialkyltartrate enantiomers which are differentially labeled. This is a very useful parameter to illustrate the stereospecific binding power of trimeric tartrate complexes in the presence of

variable additives in the direct insertion probe in CI-MS along with tartrates. For example, when the bases ammonia and water were used as multiprotic onium ion producers, CDR values of 2.1 and 2.7-3.6 were obtained, respectively. Chiral discrimination properties of tartrate esters were also dependent on the specific CI conditions employed. A detailed comparison of CDR values for trimeric homochiral clusters of diisopropyl tartrates with varying multiprotic onium (A) ions can be found in the work from Winkler et al [130].

CDR is also useful in comparing the effect of different MS-techniques for chiral discrimination properties of diisopropyl tartrate clusters. Experiments similar to those carried out by Winkler et al [130] were performed using self-CI Fourier Transform ion cyclotron resonance (FT-ICR) mass spectrometry by Denisov et. al.[131]. A much greater degree of chiral discrimination was observed using FT-ICR-MS. For example, a CDR value of 25 was obtained for trimeric diisopropyl tartrate clusters with $MeNH_3^+$ in FT-ICR. Comparatively, a lower value of CDR = 4.5 was obtained in similar CI-MS experiments [130]. In FT-ICR experiments, the diastereomeric clusters of diisopropyl tartrates have deviated from the expected statistical abundances of 1:3:3:1 to closer to 10:1:1:10. In order to explain homo-/heterochiral trimer association of dialkyl-tartrates along with multiprotic-onium (A) ions, semi-empirical molecular orbital calculations (PM3) were performed. The homochiral and heterochiral propeller structures of the methylammonium dimethyl-tartrate trimer clusters of $(DMT)_3$ adducted to methylammonium ($CH_3NH_3^+$) are represented in Figure 2.4. The –OH group (labeled with an asterisk) points outward in the ssr.$MeNH_3^+$ structure. Therefore, one of the additional N–H···O interactions (not explicitly delineated in Figure 2.4) with inner –OH groups found in the sss.$MeNH_3^+$ structure is absent in the heterochiral ssr.$MeNH_3^+$ cluster. The origin of chiral discrimination was thus speculated to be based on the enthalpic difference resulting from this difference in H-bonding [130].

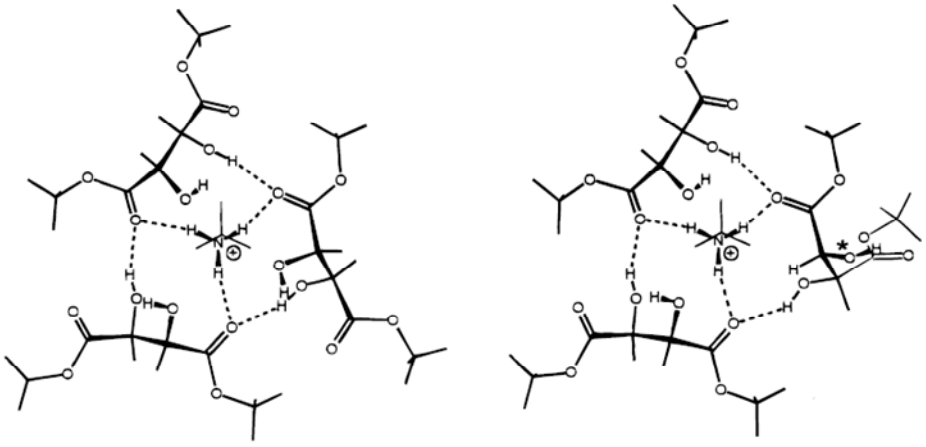

Figure 2.4 Structures of diastereomeric ion clusters $(DMT)_3.CH_3NH_3^+$ calculated by PM3. The hydroxyl group (marked with an asterisk on the right) provides a distinct difference between the two molecular associated depicted. Reprinted from reference 78 with permission from John Wiley & Sons, Inc.

Chiral molecular recognition properties of dialkyl tartrate ion clusters with varying coordination centers, ranging from proton, ammonium and alkyl ammonium to alkali ions Li^+, Na^+, K^+ have also been investigated [132]. The systems were examined using both CI-MS and FT-ICR-MS. Chiral discrimination properties in these studies comparing the MS techniques were found to be identical within experimental error. Particularly strong effects were found for protonated dimer ions, whereas tartrate dimer ions charged through alkali metal ion coordination failed to exhibit any significant discrimination. Theoretical calculations at the Hartree-Fock level were performed to offer a rational basis for this molecular recognition. Multiple H-bonds were found in both heterochiral and homochiral dimers when associated through an H^+ coordination center. Similar to previous work [130, 131], one less H-bond was observed in the heterochiral dimer. The calculations predicted ~ 5 kcal/mol preference, based on heat of formation, for the formation of the homochiral dimer form, consistent with the experimental observations. Replacing the proton by a lithium ion, and adjusting the electron-core, have resulted in a tetrahedral bridged structure that has positioned tartrate moieties too far

apart to establish any H-bonds. This finding further corroborated the absence of chiral discrimination observed for heterochiral and homochiral dimer ions when they are associated via alkali metal ion adduction.

Homochiral vs. heterochiral recognition properties of tartrate complexes have been further analyzed using electrospray ionization mass spectrometry with a quadrupole mass analyzer [133]. The cationization of supramolecular timeric dialkyl-tartrate complexes by alkali metal salts was investigated. A significant stabilization of the complex was observed in the presence of K^+ ion and the selectivities were shown to decrease in the order of $K^+ > Na^+ > Rb^+ > Cs^+ > Li^+$. The calculated trimer ion chiral discrimination ratios in this case were very large (CDR = 18 for K^+ and Rb^+ adducts with dimethyl-tartrate), favoring the homochiral clusters over the heterochiral clusters. This CDR value however falls in between comparable maximum values observed in the CI-MS studies (CDR = 5) and FT-ICR-MS studies (CDR = 45) described previously. The specific factors governing this order of selectivities with respect to cation size of these alkali metal cations were not reported because comparison of CDR values with ionic radii have shown no correlation, in general.

Chiral recognition by di-*O*-benzoyl-tartaric acid di-butyl ester (**T**) was observed in the gas phase when different forms of diastereomeric ion clusters containing Cu(II)/Zn(II) associated with **T** and *L*-tryptophan (**A**) were dissociated using electrospray ionization FT- ICR-MS [134]. The readily observed diastereomeric clusters were singly charged protonated dimeric $[\mathbf{TA}H]^+$, doubly charged copper(II)-bound tetrameric $[\mathbf{TA}CuH]_2^{2+}$, and doubly charged zinc(II)-bound tetrameric $[\mathbf{TA}ZnH]_2^{2+}$ ions, together with other complexes. The relative intensities of ion signals following dissociation of $[\mathbf{TA}H]^+$, $[\mathbf{TA}CuH]_2^{2+}$ and $[\mathbf{TA}ZnH]_2^{2+}$ were studied to assess the presence of enantioselective recognition. Evaluating the ratios of daughter ion to parent ion abundances, a higher degree of stereoselectivity was observed for the $[\mathbf{TA}CuH]_2^{2+}$ and $[\mathbf{TA}ZnH]_2^{2+}$ cluster ions. The authors thus concluded that Cu(II)/Zn(II) ions can direct the chiral

recognition capacity of di-o-benzoyl-tartaric acid di-butyl esters; however no speculation regulating mechanistic an explanation for these observations was postulated.

In a comparative study carried out on chiral-recognition properties of dimers and trimers of dimethyl tartrate esters using corona discharge ionization and thermal ionization techniques in MS, it was shown that both techniques are capable of producing dimers and trimers of the dimethyl tartrate molecules with pronounced stereoselective association effects. In corona discharge ionization, H_3O^+ and H_2O^+ based dimers and trimers have been detected; and in thermal ionization-generated mass spectra, K^+-bound dimers and trimers have dominated. The addition of water molecules has been shown to strongly influence the relative stabilities of hetero-/homo-dimer ions. In fact, addition of one molecule was observed to make the heterodimeric complex more stable than the homodimeric complex. Further additions of two or more water molecules to the complex completely abolished the influence of chirality in dimer ion stability [135].

In general, gas phase self association of tartrates, in particularly dialkyl-tartrate enantiomeric isotopomers studied using different mass spectrometric techniques showing different CDR values, indicate that the amplification of enantiomeric discrimination can vary with the method utilized for the analysis. Originally observed preferential self-association phenomena, in one case of dialkyltartrate enantiomeric isotopomers by CI-MS (CDR ~ 5), were magnified when ESI-MS (CDR ~ 18) was employed, and even more so when FT-ICR-MS (CDR = 45) was utilized. More importantly, the observed effects of additives on CDR values to cause different chiral discrimination effects for the self-association of tartrate provide some vital pieces of information on the change of molecular recognition properties of tartrates. Though solid-state crystallographic structural determinations have often been used to correlate observed solution phase chiral discriminations, to our knowledge no efforts have been attempted to link these gas phase molecular recognition properties of tartrates to solution phase chiral discrimination studies. The bridging of information obtained from different phases is required so that more

useful solution phase separations (which are predominantly associated with different buffer additives) can be achieved.

2.4 Solution Phase Molecular Recognition Properties of Metal-Tartrates

Despite the fact that there is a range of metal-tartrates known [66], only a few, in particularly Sb(III)-, Cu(II)-, and As(III)-tartrates, have been tested or proven to be useful as chiral selectors for enantioselective separations [68-69, 70-77]. The application of metal-tartrates, especially for HPLC and CE chiral separations, is also sparse. In mass spectrometry, only a couple of reports have probed the use of metal-tartrates (specifically, Sb(III)-tartrate) as chiral selectors [136-138]. All of these have been solution phase-targeting single-stage mass spectrometry experiments. Even so, the demonstrated effectiveness of this compound class for the separation of a wide range of analyte types, from amino acids to metal complexes, warrants further investigation. With the relatively few reports, additional experiments would certainly be required to gain better mechanistic insight into their enantioselective recognition properties, and may also shed some light on their reported medicinal indications [65].

The separation of optical isomers of cobalt(III) complexes, $[Co(en)_3]^{3+}$, cis-α-$[Co(trien)(en)]^{3+}$, cis-β-$[Co(trien)(en)]^{3+}$, u-fac-$[Co(dien)_2]^{3+}$, s-fac-$[Co(dien)_2]^{3+}$ and mer-$[Co(dien)_2]^{3+}$ (en = ethylenediamine, trien = ethylenetriamine; u = unsymmetrical, s = symmetrical, fac = facial, mer = meridinal) has been examined using potassium antimony(III)-*D*-tartrate [$K_2(Sb_2$-*D*-$tar_2)$] as the chiral selector in HPLC using SP-Sephadex C-25 as the stationary phase [70]. Based on these results, the authors have speculated a lock and key-type association model to explain the observations. In particular, Λ-enantiomers of Co(III) complexes possess a special topographical feature that is absent in the Δ-enantiomers. An N-H proton at the apex of the Λ-form can be depicted to point vertically out of the paper (Figure 2.5A) and only one ethylenediamine (en) chelate ring is present at the bottom left side. As shown in Figure 2.5B, if the Co(III) complex has a Λ-configuration, the space ("channel") between the ethylenediamine ligands takes an *L*-shape, whereas a J-shape geometry can be shown for the

complex in the Δ-configuration (Figure 2.5C). In general, with $[Sb_2(D\text{-tar})_2]^{2-}$ used as a chiral mobile phase additive, Λ-enantiomers eluted first. This means that the $[Sb_2(D\text{-tar})_2]^{2-}$ ion associates preferentially with Λ-enantiomers, facilitating their elution. Figure 2.6 is presented in order to explain this mechanism more clearly. Figure 2.6A shows the structure of $[Sb_2(D\text{-tar})_2]^{2-}$, where one of the associated tartrate groups is highlighted. This highlighted portion is proposed to form a "key" (Figure 2.6B) which fits the *L*-shaped "lock" of Λ-$[Co(en)_3]^{3+}$ as shown in Figure 2.6C. One carbonyl oxygen of $[Sb_2(D\text{-tar})_2]^{2-}$ is directed towards the N-H proton of ethylenediamine (en). This specific lock-and-key interaction is not formed between the chiral selector $[Sb_2(D\text{-tar})_2]^{2-}$ and Δ-$[Co(en)_3]^{3+}$. This analysis provides a reasonable basis for the mechanism of enantioselective association between $[Sb_2(D\text{-tar})_2]^{2-}$ and optical isomers of cobalt(III) complexes, however further application of this model to other inorganic systems would be necessary to assess its generality.

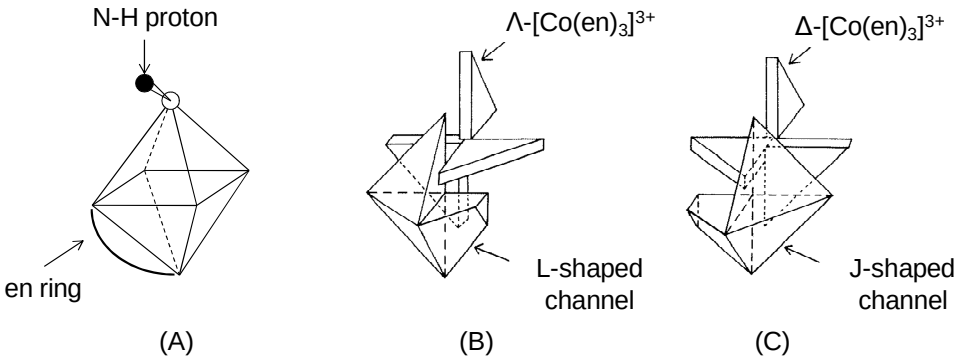

Figure 2.5 A) Topographic geometry of Λ-$[Co(en)_3]^{3+}$ depicting the spatial position of the amine proton and the ethylenediamine chelate. Resolution of Λ- and Δ- enantiomers by association with the chiral selector $[Sb_2(D\text{-tar})_2]^{2-}$ is facilitated by the opposing channel structures of (B) Λ-$[Co(en)_3]^{3+}$ ("*L*-shaped") and (B) Δ-$[Co(en)_3]^{3+}$ ("J-shaped"). Reprinted from reference 78 with permission from John Wiley & Sons, Inc.

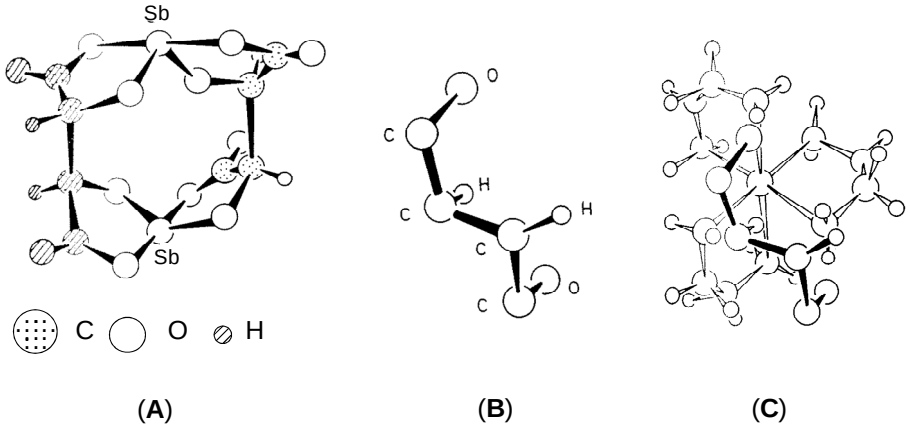

(**A**) (**B**) (**C**)

Figure 2.6 (A) Structure of $[Sb_2(D\text{-tar})_2]^{2-}$. In (B), the hatched atoms from (A) are shown to form a "key" which can (C) stereoselectively recognize the *L*-shaped channel of $\Delta\text{-}[Co(en)_3]^{3+}$. Reprinted from reference 78 with permission from John Wiley & Sons, Inc.

Resolution of the uncharged chiral metal complexes, fac-[Co(*D*/*L*-Ser)$_3$], fac-[Co(β-Ala)$_3$], and mer-[Co(β-Ala)$_3$] (Ser = serinate anion and β-Ala = β-alaninate anion) was also attempted using $[Sb_2(D\text{-tar})_2]^{2-}$ as a chiral selector, both in the mobile phase, using aqueous solutions of $Na_2[Sb_2(D\text{-tar})_2]$ as eluent, and in the stationary phase, by immobilizing the chiral selector on the stationary phase in the form of an anion-exchanger [70]. When used as a mobile phase additive, baseline resolution of fac/mer Co-complexes was achieved. The separation factor (α) increases with increasing concentration of the chiral selector. When the chiral selector was immobilized on an anion-exchange resin, good enantiomeric separations were again observed for the fac/mer Co-complexes using different mixtures of ethanol/water as mobile phases. It was observed that the facial (fac) isomers were retained more than the meridinal (mer) isomers. This was attributed to the larger dipole moment of the facial (fac) isomers, allowing them to be more strongly adsorbed by the selector anion on the stationary phase than the meridional (mer) isomers. It was also observed that an increase of ethanol content of the mobile phase resulted in greater chiral discrimination. A reasonable explanation was provided for this observation. For chiral discrimination to take place, analytes first should come close to the stationary phase and become dehydrated. The addition of ethanol likely aids effective dehydration to facilitate stronger interaction of analytes with the stationary phase.

A subsequent analysis focused on the stereoselective separation of hexa-amine cage complexes, $[Co(sep)]^{3+}$ (sep = 1,3,6,8,10,13,16,19-octaazabicyclo[6.6.6]eicosane) and $[Co(diNOsar)]^{3+}$ (diNOsar = 1,8-dinitro-3,6,10,13,16,19-hexaazabicyclo[6.6.6]eicosane), using ion-exchange chromatography with $(Sb_2\text{-}D\text{-}tar_2)^{2-}$ as chiral eluent [71]. From this work, a mechanism by which $[Sb_2(D\text{-}tar)_2]^{2-}$ exerts its molecular recognition towards these complexes was interpreted. The Λ-enantiomers always eluted first and enantiomers of cage complexes presenting bulky alkyl caps were resolved to a greater degree. These empirical observations were explained by invoking a C2 association model in which 2 NH protons directed along the (pseudo) C2 axis of the Co-complexes are H-bonded to 2 O atoms of the $[Sb_2(D\text{-}tart)_2]^{2-}$ ion as shown in Figure 2.7. It was concluded that stereoselective recognition of the cage complex is originated by the steric repulsion between the alkyl cap of the Δ-enantiomer and the distal carboxylate group of the chiral anion.

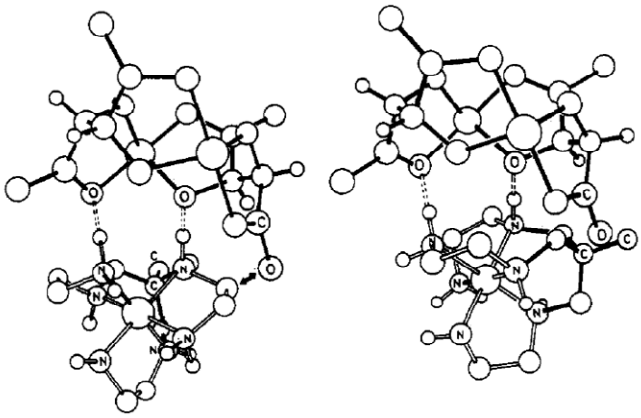

(A) (B)

Figure 2.7 C2 stereoselective association model for (A) Λ-$[Co(sen)]^{3+}$ and (B) Δ-$[Co(sen)]^{3+}$ with $[Sb_2(D\text{-}tar)_2]^{2-}$. Reprinted from reference 78 with permission from John Wiley & Sons, Inc.

In another study, reversed-phase ion-pair chromatography (RPIPC) was performed to resolve $[CoL_6]^{3+}$ (L = amine) using $[M_2(D\text{-}tart)_2]^{2-}$ (M = Sb, As) as ion-pairing chiral reagents [72]. For both metal-tartrate types, satisfactory resolution was achieved for racemic mixtures of $[Co(en)_3]^{3+}$, $[Co(tn)_3]^{3+}$, $[Co(sen)]^{3+}$, $[Co(sep)]^{3+}$, and $[Co(diNOsar)]^{3+}$ (tn = trimethylenediamine;

sen = 1,1,1-tris[[(2-aminoethyl)amino]methyl]ethane; sep = 1,3,6,8,10,13,16,19-octaazabicyclo[6.696]eicosane; and diNOsar = 1,8-dinitro-3,6,10,13,16,19-hexaazabicyclo[6.6.6]eicosane) compounds. However, in comparison, $[As_2(D\text{-tart})_2]^{2-}$ was shown to provide more effective separations compared to $[Sb_2(D\text{-tart})_2]^{2-}$. This study in fact illustrates the variable molecular recognition capacity of different metal-tartrates, an aspect that may be fruitful to expand upon in future work.

Similarly, resolution of a diastereomeric mixture of tris(trans-1,2-diaminocyclohexane)cobalt(III) complexes, including Λ-ob_3-, Δ-ob_3-, Λ-lel_3-, and Δ-lel_3-$[Co(chxn)_3]^{3+}$ (chxn = trans-1,2-diaminocyclohexane) using $[Sb_2(D\text{-tart})_2]^{2-}$ anion as a mobile phase additive was demonstrated using ion-exchange chromatography by Mizuta et al [74]. Here, it is important to note that ethylenediamine type ligands (en) are non-planar. When they coordinate to central metal atoms and form pentagonal rings, the en backbone can be either parallel ("lel") or obverse ("ob") to the C_3-axis of the metal-complex. An elution order of Λ-ob_3 > Λ-lel_3 > Δ-lel_3 > Δ-ob_3 was observed. The authors have explained a general association phenomenon between $[Co(chxn)_3]^{3+}$ and $[Sb_2(D\text{-tart})_2]^{2-}$ by noting that lone electron pairs on three O atoms in $[Sb_2(D\text{-tart})_2]^{2-}$ which can form triple H-bonds with three N-H groups of $[Co(chxn)_3]^{3+}$ directed along the C3-axis. This is depicted in Figure 2.8. The origin of chiral discrimination was explained by considering the helical arrangement of functional groups. Due to the right handed helicity of the three N-H groups of the Λ-ob_3 isomer, stronger H-bonds are speculated to be formed with the three spirally oriented O-lone-pairs of $[Sb_2(D\text{-tart})_2]^{2-}$. In contrast, the -$lel_3$ isomers, with no such helicity, form weaker H-bonds. The Δ-ob_3 isomer, having the opposite helicity to that of Λ-ob_3, was characterized by the weakest interaction of all in this analysis. The association models proposed by the authors were also verified by crystal structure determinations of the diastereomeric salts.

Copper(II) complexes of N,S-dioctyl-*D*-penicillamine and (*R,R*)-tartaric acid mono-(*R*)-1-(α-naphthyl)ethylamide coated on silica gel were also tested for direct resolution of some

carboxylic acid and amine enantiomers [73]. Diastereomeric copper(II) complex formation was assumed for the separation of these racemic carboxylic acids and amines when these promising copper(II)-tartrate based CSPs were employed. The results have shown that the carboxyl or amino groups attached to the asymmetric carbon atom are mainly responsible for the formation of Cu-directed diastereomeric complexes with the CSP. Though it was emphasized that complexation of analytes through Cu is crucial for these separations, a detailed explanation of molecularity effects for the chiral discrimination of these tested analytes was not stated.

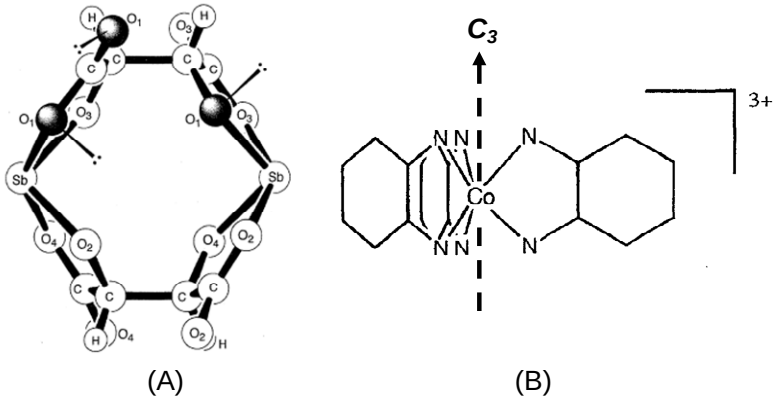

Figure 2.8 (A) Molecular structure of $[Sb_2(D\text{-tar})_2]^{2-}$ ion emphasizing three (shaded) O-atoms which form a network of hydrogen bonds. The wedges indicate the directions by which lone pairs on each O-atom (O_1) are directed. (B) Shows the molecular structure of $[Co(chxn)_3]^{3+}$, emphasizing its inherent C_3 axis. Reprinted from reference 78 with permission from John Wiley & Sons, Inc.

The enantiomeric purity of a range of transition metal complexes of the type M(α-diimine)$_3^{2+}$ (M(II) = Ru(II), Ni(II), Fe(II); α-diimine = 1,10-phenanthroline or 2,2'-bipyridine) have been determined by CE using $K_2[Sb_2(D\text{-tart})_2]$ as the chiral selector [75]. The enantiomers of $[Ru(diimine)_3]^{2+}$ complexes have been resolved using either $K_2[Sb_2(D\text{-tart})_2]$ or dibenzoyl-*L*-tartrate as chiral resolving agents in CE [69]. CE enantiomeric separations carried out on transition metal complexes with metal ions Ru^{2+}, Ni^{2+}, Cr^{3+}, and Co^{3+} using $[Sb_2(D\text{-tart})_2]$ and dibenzoyl-*L*-tartrate as chiral standards have interestingly exhibited reversals of enantiomeric

elution orders when metal complexes have carried a total 3+ charge [76]. However, no molecular recognition mechanism has been offered to explain these results. Using copper(II)-*L*-tartrate, enantiomeric separation of native *D*/*L*-malic acid [77] and a series of sympathomimetics and β-blockers has been also achieved by capillary electrophoresis [104].

2.5 Gas Phase Molecular Recognition Properties of Metal-Tartrates

To our knowledge Arakawa et al. reported the first use of metal-tartrates as a chiral reference to study enantioselective discrimination by this compound class using mass spectrometry [135]. Chiral recognition of metal bis(*L*-alaninate)ethylenediamine cobalt(III) complexes using $[Sb_2(D,L\text{-tart})_2]$ as chiral standards have been studied by differential association of the optical isomers using electrospray ionization mass spectrometry (ESI-MS). ESI-MS results have indicated that $[Sb_2(L\text{-tart})_2]^{2-}$ recognizes the chirality of some Δ- and Λ-Co(III) complexes in single-stage mass spectra by showing large differences in the intensities of the associated diastereomeric ions. In support of their observations, ion-exchange chromatography has been performed and the association preferences matched that observed in ESI-MS results. Though enantioselective discrimination in ESI mass spectra and enantiomeric separations in ion-exchange chromatography were observed when $[Sb_2(L\text{-tart})_2]^{2-}$ was employed as a chiral standard to discriminate Δ- and Λ-Co(III) complexes, reciprocal relationships revealed through changes in ion abundances or reversal of elution orders in ion-exchange chromatography have not been necessarily observed when $[Sb_2(L\text{-tart})_2]^{2-}$ was replaced with $[Sb_2(D\text{-tart})_2]^{2-}$. The lack of a reciprocal binding relationship was explained by the prevalence of complicated steric interactions in the association of $[Sb_2(L\text{-tart})_2]^{2-}$ and $[Sb_2(D\text{-tart})_2]^{2-}$ with the Co(III)-complexes. However more rigorous theoretical explanation either by molecular modeling techniques or by some other means is required to fully understand this chiral recognition system.

A subsequent report, employing metal-tartrates in MS-based chiral recognition experiments also used the same chiral standards $[Sb_2(L\text{-tart})_2]^{2-}$ and $[Sb_2(D\text{-tart})_2]^{2-}$ in order to

illustrate solution-phase isomerization of optically active 2-thiazolidinecarboxylic acid (2-THC), a substrate for *D*-amino acid oxidase in animal kidney known to undergo racemization in solution [137]. The intensities of diastereomeric ions formed by association of (+)-2-THC and (-)-2-THC with $[Sb_2(L\text{-tart})_2]^{2-}$ were shown to increase and decrease, respectively, with time as (+)-2-THC underwent racemization to the (-)-isomer (and vice versa) in solution. For this chiral recognition system, unlike that reported for the metal complexes [136], reciprocal effects on the intensities of the associated ions were observed when $[Sb_2(D\text{-tart})_2]^{2-}$ was employed instead of $[Sb_2(L\text{-tart})_2]^{2-}$ as the chiral standard. Stereochemical associative models of the optical isomers with $[Sb_2(L\text{-},D\text{-tart})_2]^{2-}$ have been constructed to explain these observations, considering H-bonding between the NH-group of THC and the O-atom on $[Sb_2(L\text{-},D\text{-tart})_2]^{2-}$, and invoking HSAB (hard and soft acid and base) theory to describe the interaction of S from THC with Sb atoms of $[Sb_2(L\text{-},D\text{-tart})_2]^{2-}$, as shown in Figure 2.9.

In order to show that the Sb-S interaction of the proposed associative model plays an important role in this chiral recognition, similar experiments were performed using proline instead of THC. Though structurally similar, functionally, the sulfur atom in THC is replaced by a carbon in proline. No differential association between either of the $[Sb_2(L\text{-},D\text{-tart})_2]^{2-}$ chiral selector ions with proline enantiomers was observed, supporting the importance of the proposed S-Sb differential interaction “trigger” for this chiral recognition system [137].

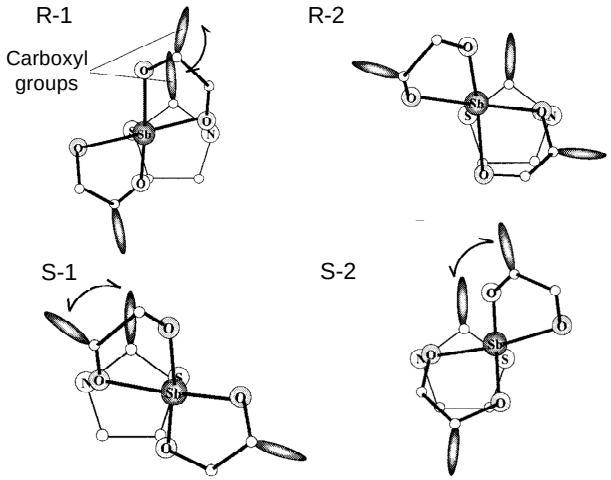

Figure 2.9 Proposed association models based on two types of intermolecular interactions; NH-O hydrogen bonding and S-Sb weak affinity. R-1 and R-2 show the interaction of $[Sb_2(L\text{-tar})_2]^{2-}$ with R-2-THC and S-1 and S-2 show those of $[Sb_2(L\text{-tar})_2]^{2-}$ with S-2-THC [83]. Reprinted from reference 78 with permission from John Wiley & Sons, Inc.

In summary, although a limited number of studies have been performed using metal-tartrates as chiral selectors, significant applications for segregating a variety of enantiomeric mixtures has been demonstrated in both solution phase and gas phase experiments. Various mechanistic models have been proposed, however some discrepancies have remained difficult to explain. It is possible that such uncertainties have lead to the utility of this chiral selector class being overlooked. However, given their demonstrated application for discriminating both small molecule analytes and a wide range of metal complexes, further studies to elucidate whether a general molecular recognition model for metal-tartrates exists should be pursued.

2.6 Summary and Concluding Remarks

Tartrates and metal-tartrates can be jointly categorized as an important class of enantioselective recognition elements that have been utilized for the separation of various types of enantiomers ranging from metal-complexes to pharmaceutically/biologically significant organic molecules. Tartrates and metal-tartrates have mainly been used in HPLC and CE for a range of enantiomeric separations, owing to their versatile molecular structures which can be functionalized in many ways. In HPLC, tartaric acid-derived compounds and metal-tartrates

have been used as chiral selectors either as bonded/immobilized stationary phases or as mobile phase additives to affect enantiomeric separations. In many instances, mechanistic explanations have been provided depending on the various separations observed. In order to account for their solution phase chiral discrimination properties, mechanisms have been proposed which are built from solid-state crystallographically-determined structures of chiral standards, particularly for metal-tartrates. However, in solution it is reasonable to anticipate that these solid-state structures might change their molecular orientation in the presence of solvent and associated buffers that are composed of ions. Therefore, more rigorous experiments to explicate solution based separations by jointly using solid, solution, and gas phase molecular recognition studies of these molecules/ions are required.

Mass spectrometry (MS) has become a viable approach to study both solution phase and gas phase binding interactions of noncovalently-bound diastereomeric complexes. Following the first identification of self-bound chiral interactions of tartrate-esters using CI-MS by Fales and Wright [16], the chiral discrimination properties of various tartrate derivatives have been studied using a variety of MS techniques. Self association phenomena in particular have been extensively studied in this regard. The variation of chiral recognition properties for tartrates in the presence of various forms of cations (e.g. alkali metal ions, “onium” ions from various types of organic bases, ions of heavy metals, etc.) have also been studied. These forms of self bound tartrate clusters associated to various types of cations can be anticipated to also form in solution, making these studies particularly relevant to HPLC and CE separations in the presence of various buffers. Still, comprehensive experimental verification of this link is yet to be reported.

Metal-tartrates have been studied by MS to a lesser degree. In some cases, solution phase chiral recognition properties have successfully matched their ESI-MS chiral discrimination responses illustrating the feasibility of ESI-MS to be used as a method to identify solution phase chiral molecular recognition properties of this compound class. Still, more

experiments demonstrating the utility of metal-tartrates in solution phase using MS techniques are required to assess the generality of this approach. In summary, the solution phase and gas phase chiral recognition properties of tartrates and metal-tartrates can be probed in a complementary manner using both traditional separation science and emerging MS methods.

CHAPTER 3

ANTIMONY(III)-*D*,*L*-TARTRATES EXHIBIT PROTON-ASSISTED ENANTIOSELECTIVE BINDING IN SOLUTION AND IN THE GAS PHASE

3.1 Introduction

Inextricably tied to the notion of chirality through their incorporation of tartaric acid [83], metal-tartrates have been the subject of research in asymmetric catalysis [61], chiral separations [66-69], and medicinal chemistry [62, 63]. Antimony(III)-*L*-tartrate, known as "tartar emetic" when administered as a dipotassium salt [65], is believed to exist primarily as a doubly-charged binuclear tartrato(4-)-metal-bridged complex as shown in Figure 3.1. Antimony(III)-*L*-tartrate has enjoyed an especially turbulent history as a therapeutic indication, but it has shown significant utility as an analytical separations reagent, as an antifilarial drug for treatment of schistosomal blood flukes (schistosomiasis), and as an antibiotic [64,65]. Despite these uses, the mechanistic basis for understanding the modes of enantioselective molecular recognition by antimony tartrates has remained somewhat a mystery. Electrospray ionization – mass spectrometry (ESI-MS), in particular, is attractive for investigating molecular recognition phenomena [12,122,139]. Focusing on a relevant model for biomolecular recognition, specifically amino acids, it was hypothesized that ESI-MS-based binding experiments would be able to provide further insight into the enantioselective recognition capacity of antimony(III)-*D*- and -*L*-tartrates and, potentially, guide further research on elucidating the reported biological activity of these compounds.

Arakawa et al. were the first to investigate the enantioselective binding by potassium antimony(III)-*D*- and -*L*-tartrate to Co(III) complex and 2-thiazolidinecarboxylic acid enantiomers using ESI-MS [78, 136, 137]. Importantly, the results of these MS-based experiments were shown to be consistent with those from independent solution phase measurements. For instance, enantioselective association of antimony(III)-*D*- and -*L*-tartrate with Co(III) complexes

observed in ion-exchange chromatographic experiments correlated well with data from ESI-MS based solution-phase-targeting experiments [136]. Also, the observation of time-dependent racemization of 2-thiazolidinecarboxylic acid (2-THC) enantiomers in solution were effectively tracked in single-stage mass spectra when antimony(III)-*D*- and -*L*-tartrate selectors were utilized [137]. These solution-phase correlations to the recorded ESI mass spectra may be due in part for the utility of acetonitrile/water (ACN/H_2O) solvent systems. Recent reports by Kass et.al. show solution phase species are produced and recorded in respective mass spectra when ACN/H_2O (compared to MeOH/H_2O) mixtures are employed as the electrospray solvent [140-142]. Nevertheless, while metal-tartrates have been demonstrated to be useful for enantioselective resolution of a variety of compound classes in the solution phase [78], a general model for describing their relevant binding chemistry is still missing.

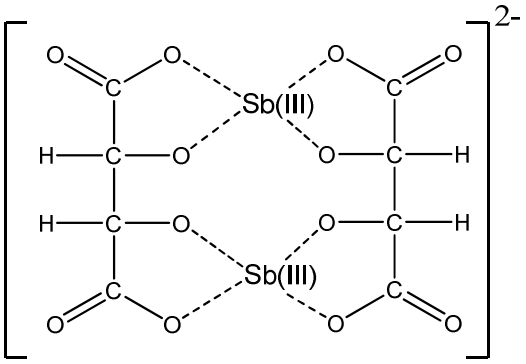

Figure 3.1 Doubly charged binuclear tartrato(4-)-antimony(III) bridged complex. Reprinted from reference 79 with permission from Elsevier B.V.

Competitive binding (solution phase-targeting) and collision threshold dissociation (gas phase-targeting) experiments between isotopomeric enantiomers of the amino acid leucine (Leu) and disodium antimony-*D*- and -*L*-tartrates were performed to study enantioselective association and dissociation in this system. Interestingly, a remarkable charge-state-dependent (proton-assisted) enantioselectivity was observed in both solution phase and gas phase measurements where the protonated monoanion of antimony(III)-*D*- and -*L*-tartrate exhibited

significant enantioselective association/dissociation to leucine enantiomers in a cross-chiral (reciprocal) fashion. Conversely, the dianionic form failed to show enantioselective recognition. Overall, the results for both ion forms were observed to be consistent in solution-phase-targeting and in gas-phase experiments.

3.2 Proton-assisted enantioselectivity of antimony(III)-*D*,*L*-tartrate in solution phase targeted single-stage ESI-MS

Disodium antimony(III)-*L*-tartrate ($[Na]_2[Sb_2$-*L*-$tar_2]$) was first analyzed in the negative ionization mode (100 µM solution in 75:25 acetonitrile (ACN)/H_2O (v/v) with 100 mM formaldehyde). All measurements were performed using a Thermo LCQ Deca XP ion trap instrument equipped with a conventional electrospray ion source. The solvent system (75:25 ACN/H_2O (v/v)) was chosen to be consistent with prior antimony(III)-*D*, *L*-tartrate ESI-MS association studies [78, 136, 137] and to enhance the probability of observing ions characteristic of solution phase equilibria in single-stage mass spectra [140-142]. Formaldehyde was incorporated in the solution in order to reduce noise and enhance signal quality of negative ion spectra according to prior reports in the literature [143]. The disodium salt was employed instead of the potassium salt (tartar emetic) due to the reported reduced toxicity of the former [144]. In the spectra, a doubly-charged $[Sb_2$-*L*-$tar_2]^{2-}$ (268.1 Th) ion was observed, accompanied also by protonated $\{[Sb_2$-*L*- $tart)_2][H]\}^-$ (536.8 Th) and sodiated $\{[Sb_2$-*L*-$tar_2][Na]\}^-$ (558.9 Th) singly-charged anion forms (Figure 3.2). Confirmatory observations are, briefly, in each of the three main peaks, three isotopic peaks were observed as a result of the two isotopes of Sb (^{121}Sb, 57.36% natural abundance and ^{123}Sb, 42.64% natural abundance). Also, isotopic peaks of the two singly charged $\{[Sb_2$-*L*-$tar_2][H]\}^-$ and $\{[Sb_2$-*L*-$tar_2][Na]\}^-$ ions were separated by 2 Th, whereas isotopic peaks of the doubly charged $[Sb_2$-*L*-$tar_2]^{2-}$ were separated by 1 Th.

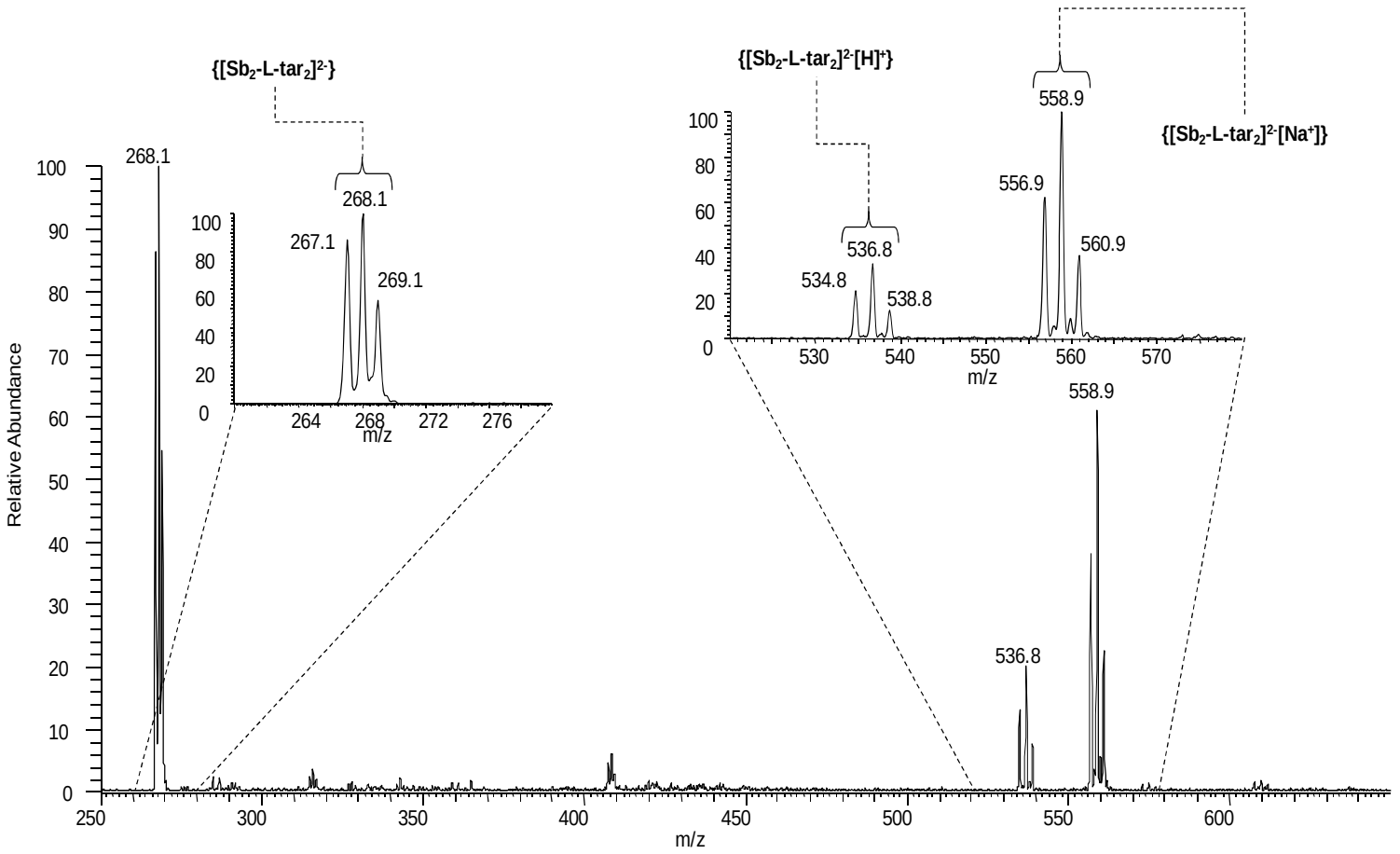

Figure 3.2 ESI-mass spectrum obtained by direct infusion (10 µL min^{-1}) of the solution containing 100 µM $Na_2[Sb_2$-*L*- $tar_2]$ (solvent system: CH_3CN/H_2O, 75/25 v/v + HCHO, 100 mM). Reprinted from reference [79] with permission from Elsevier B.V.

Competitive binding experiments were then performed to measure the differential association exhibited by both antimony(III)-*D*- and -*L*-tartrate (in separate experiments) to enantiomeric isotopomers of leucine (*D*-Leu vs. *L*-d10-Leu). Leucine was chosen as a representative biologically-relevant amino acid and the d10-deuteration of *L*-Leu allowed observation of well-separated diastereomeric complex ion signals in representative mass spectra, as shown in Figure 3.3. Diastereomeric ionic complexes were observed only at 333.3 Th and 667.5 Th values (Figure 3.3A, Figure 3.3B insets), despite the use of the disodium salt for preparation of solutions. The composition of each diastereomeric complex was confirmed by collision induced dissociation (Figure 3.4). Additionally, β-deuterium isotope binding effects were also evaluated (e.g. $[Na]_2[Sb_2$-*L*-$tar_2]$ + L-Leu + *L*-d10-Leu) (Figure 3.5).

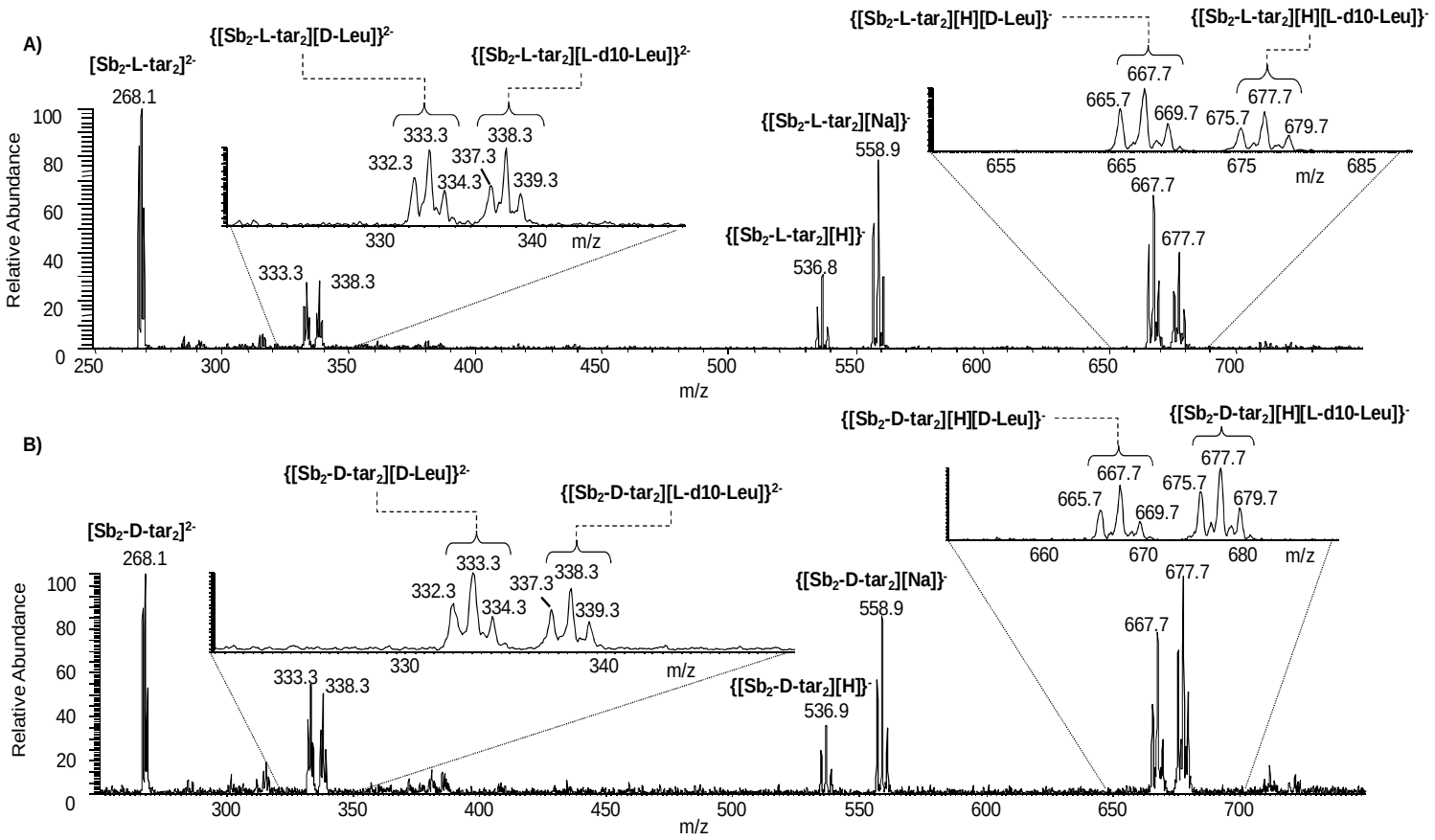

Figure 3.3 Competitive binding ESI mass spectra obtained by direct infusion of a solution containing equimolar (100 μM) A) *D*-Leu, *L*-d10-Leu and $Na_2[Sb_2$-*L*-$tar_2]$ and B) *D*-Leu, *L*-d10- Leu and $Na_2[Sb_2$-*D*-$tar_2]$ in CH_3CN/H_2O (75/25 v/v) with 100 mM HCHO. Reprinted from reference 79 with permission from Elsevier B.V.

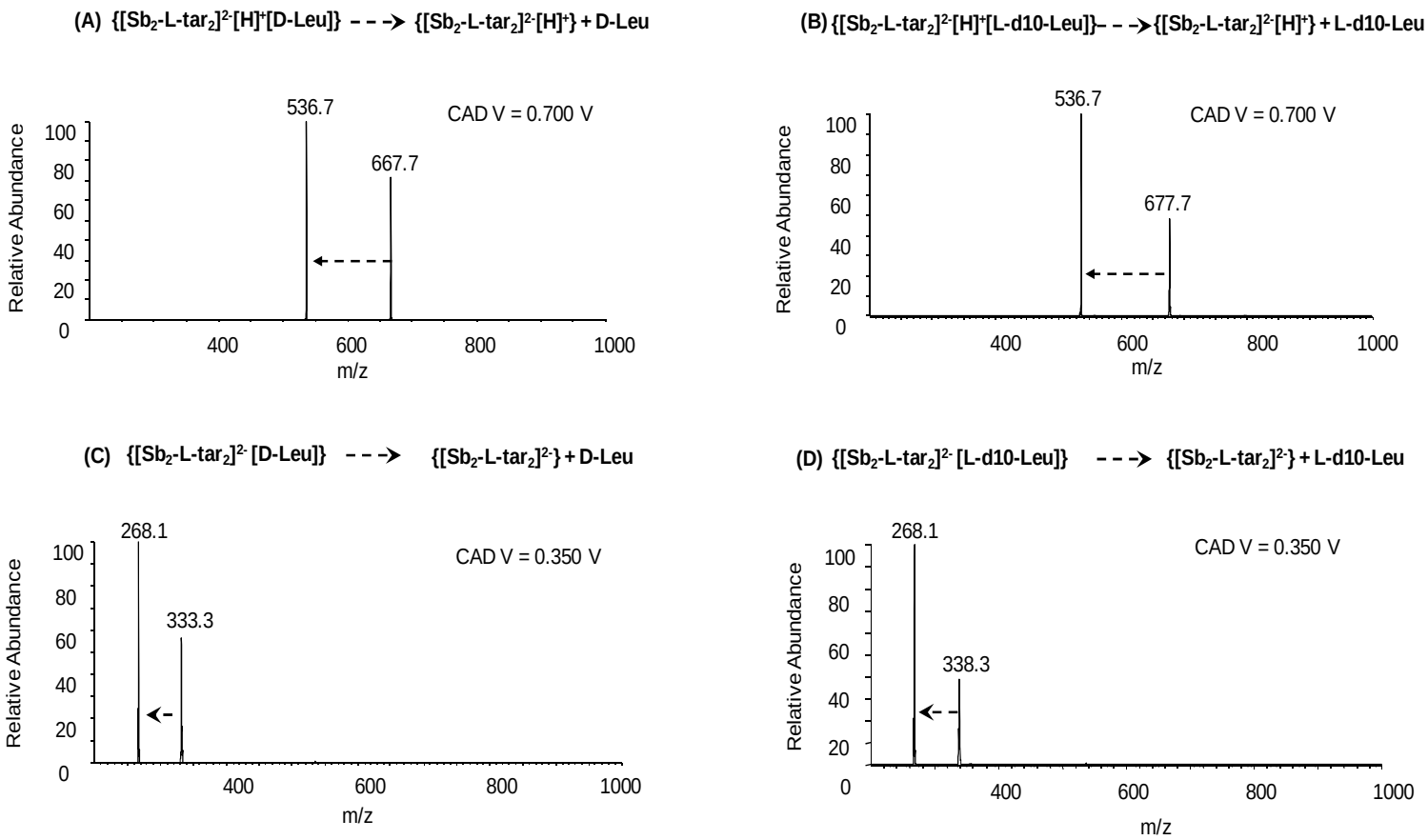

Figure 3.4 Competitive binding ESI mass spectra (control experiment) obtained by direct infusion of a solution containing equimolar (100 µM) **A**) *L*-Leu, *L*-d_{10}-Leu and $Na_2[Sb_2$-*L*-$tar_2]$ and **B**) *L*-Leu, *L*-d_{10}-Leu and $Na_2[Sb_2$-*D*-$tar_2]$ in CH_3CN/H_2O (75/25 v/v) with 100 mM HCHO. Reprinted from reference 79 with permission from Elsevier B.V.

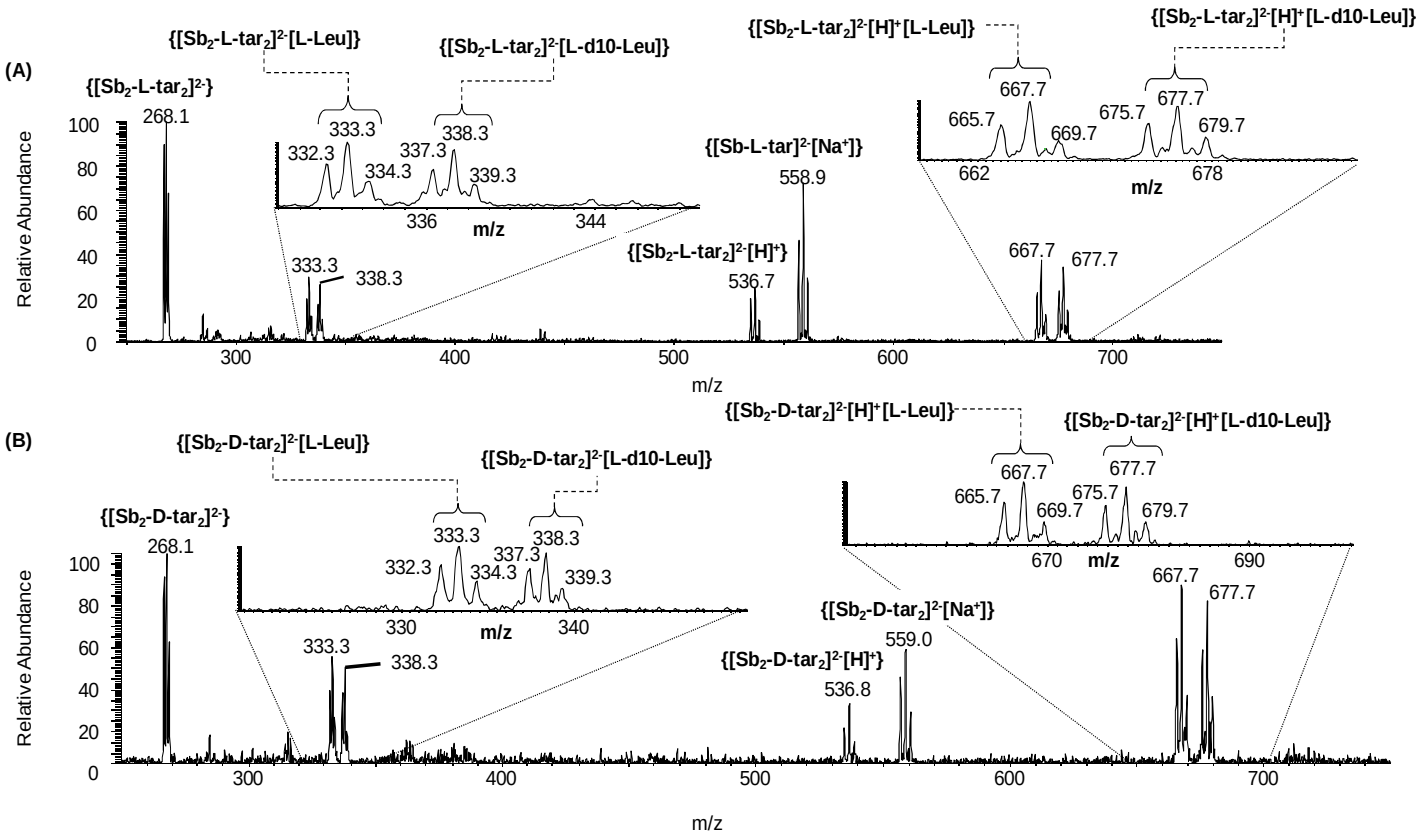

Figure 3.5 Competitive binding ESI mass spectra (control experiment) obtained by direct infusion of a solution containing equimolar (100 μM) **A**) *L*-Leu, *L*-d_{10}-Leu and $Na_2[Sb_2$-*L*-$tar_2]$ and **B**) *L*-Leu, *L*-d_{10}-Leu and $Na_2[Sb_2$-*D*-$tar_2]$ in CH_3CN/H_2O (75/25 v/v) with 100 mM HCHO. Reprinted from reference 79 with permission from Elsevier B.V.

Additionally, the ionizable nature of both the selector and the amino acid selectand further warranted an evaluation of their individual charge states in the observed complexes. More specifically, observed diastereomeric complexes can be assumed to form between the selector (2-, 1-, and neutral) and a) neutral or zwitterionic Leu (667.5 Th corresponding to$\{[Sb_2\text{-}L\text{-}tar_2][H][Leu]\}^-$ and 333.3 Th corresponding to$\{[Sb_2\text{-}L\text{-}tar_2][Leu]\}^{2-}$) or b) anionic Leu (667.5 Th corresponding to $\{[Sb_2\text{-}L\text{-}tar_2][H]_2[Leu\text{-}H]\}^-$ and 333.3 Th corresponding to$\{[Sb_2\text{-}L\text{-}tar_2][H][Leu\text{-}H]\}^{2-}$). The involvement of cationic Leu, however, can be ruled out because 333.3 Th is observed in our mass spectra and 333.3 Th (a 2- complex) cannot be assigned using [Leu+H]. In order to identify which form of Leu exists in these observed mass spectra, similar competitive binding experiments (against *L*-d10-Leu) were performed using N-acetylated Leu (Ac-Leu). N-acetylation ensures the formation of the anionic form of the amino acid under the solution conditions employed. Figure 3.6 clearly illustrates that a very different profile of sodiated diastereomeric complexes, relative to unblocked Leu, was observed when Ac-*L*-Leu binding was evaluated. MS/MS experiments Figure 3.7 verify that the observed diastereomeric complexes formed between the selector and Ac-*L*-Leu were $\{[Sb_2\text{-}L\text{-}tar_2][Na]_2[Ac\text{-}L\text{-}Leu - H]\}^-$ (753.7 Th) and $\{[Sb_2\text{-}L\text{-}tar_2][Na]_3\ [N\text{-}Ac\text{-}L\text{-}Leu{-}H]_2\}^-$ (948.7 Th). These experiments with N-acetyl amino acid reveal more insight into the ionic-states of the amino acids. More specifically, non-formation of similar diastereomeric complexes with N-acetyl Leucine to that formed with leucine suggests that a charged amino group is necessary for the formation of diastereomeric complexes with $\{[Sb_2\text{-}D,L\text{-}tar_2]\}^{2-}$ and $\{[Sb_2\text{-}D,L\text{-}tar_2][H]\}^{1-}$ ions. Then it further tells that leucine exists in its zwitterionic form rather than its neutral form. This not only clarifies the ionic states of the complexes but also supports the fact that solution-phase data are recorded in single-stage mass spectral analysis. Because it is well established that amino acids exists in their zwitterionic states in neutral aqueous media. However, it should be clarified in the monoanionic diastereomeric complexes where the proton resides. More specifically, does the proton associate more preferentially to the dianionic $[Sb_2\text{-}D,L\text{-}tar_2]^{2-}$ core or to the zwitterionic [Leu]

core ? CAD experiments performed on mono-anionic diastereomeric complexes {[Sb_2-*D*,*L*-tar_2][H][Leu]}$^{1-}$ show fragment ions of {[Sb_2-*D*,*L*-tar_2][H]}$^{1-}$ at 536.7 Th rather than [Sb_2-*D*,*L*-tar_2]$^{2-}$ ions at 268.1 Th. This observation supports that proton affinity of dianionic [Sb_2-*D*,*L*-tar_2]$^{2-}$ core is greater than that of zwitterionic [Leu] core. If zwitterionic [Leu] had had a greater proton affinity than the dianionic [Sb_2-*D*,*L*-tar_2]$^{2-}$, then the CAD mass spectra would have produced {[Sb_2-*D*,*L*-tar_2]}$^{2-}$ (268.1 Th) ions. These rationale and experiments favor the assignment of zwitterionic Leu in the complex with antimony(III)-tartate. It also supports the notion that ionization state of antimony(III)-tartrate in the complex varies from doubly deprotonated (dianionic) to singly deprotonated (monoanionic).

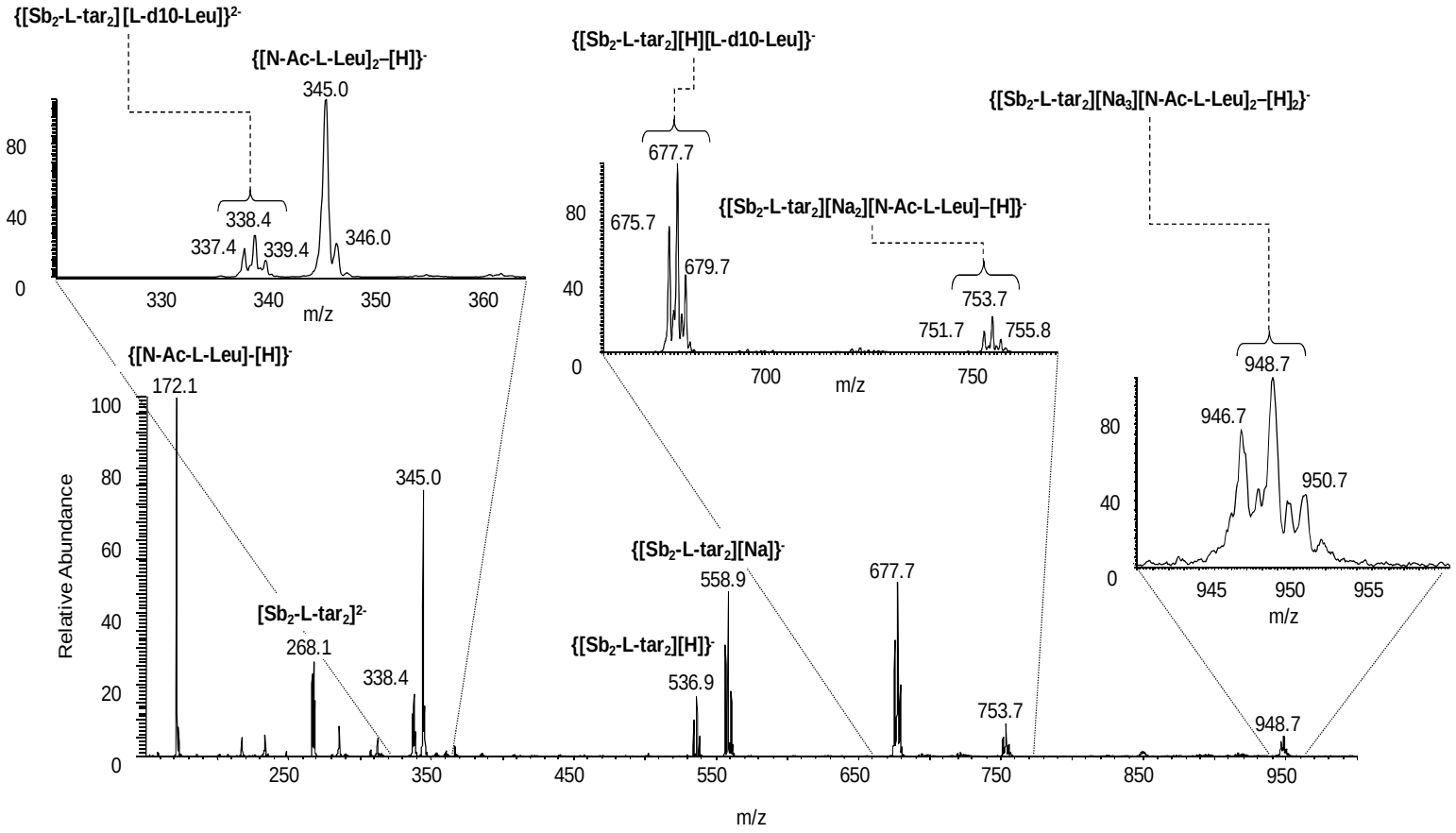

Figure 3.6 Competitive binding ESI mass spectrum (control experiment) obtained by direct infusion of a solution containing equimolar (100 µM) N-Ac-*L*-Leu, *L*-d_{10}-Leu and $Na_2[Sb_2(L\text{-tart})_2]$ in CH_3CN/H_2O (75/25 v/v) with 100 mM HCHO. Reprinted from reference 79 with permission from Elsevier B.V.

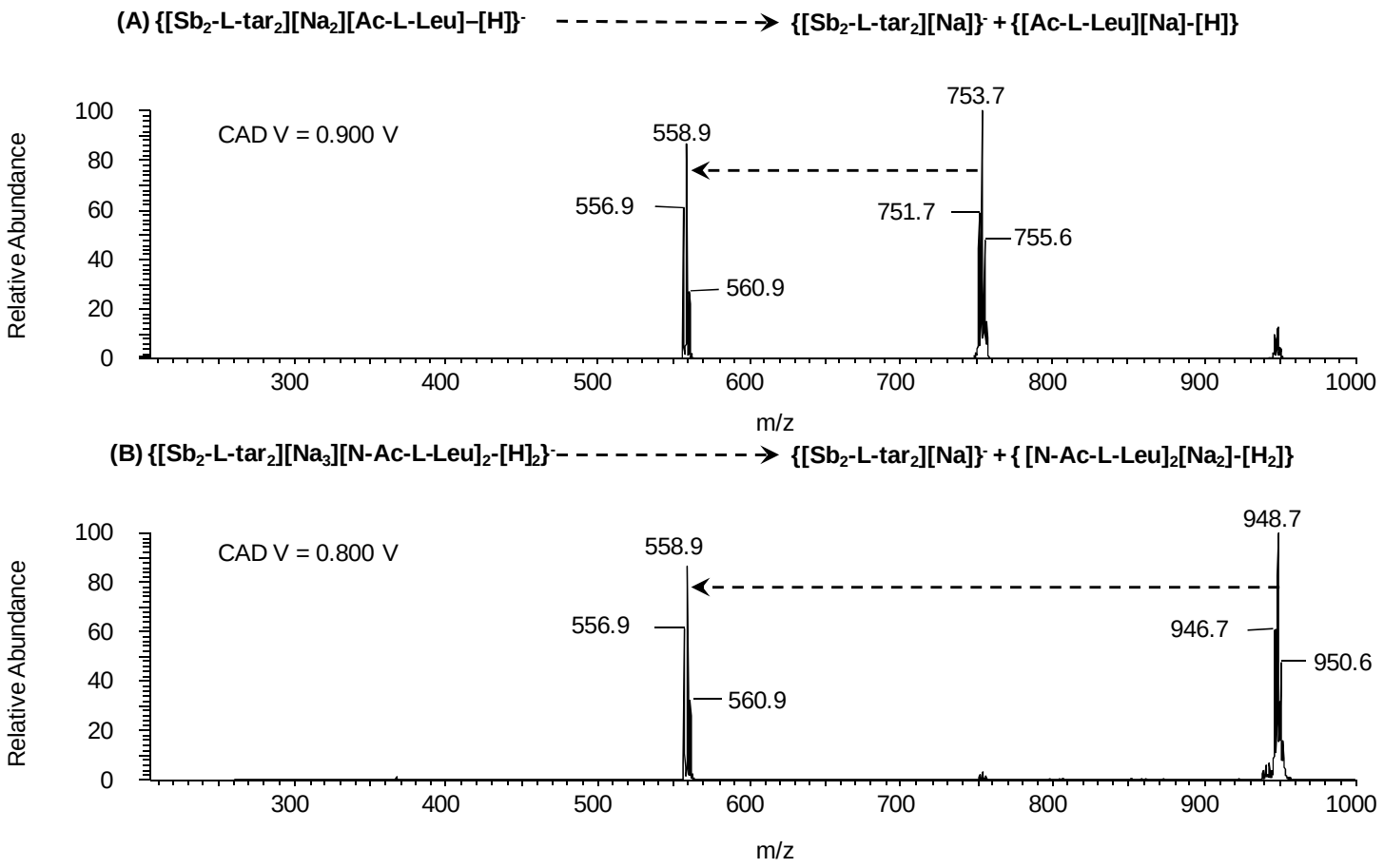

Figure 3.7 Collision activated dissociation of diastereomeric ion complexes formed between antimony(III)-*L*-tartrate and N-Ac-*L*-Leu in quadrupole ion trap. Reprinted from reference [79] with permission from Elsevier B.V.

Interestingly, the $[Sb_2\text{-}L,D\text{-}tar_2]^{2-}$ dianion and the $\{[Sb_2\text{-}L,D\text{-}tar_2][H]\}^{-}$ monoanion showed significantly different enantioselectivities. Table 3.1 shows the selectivity (α) values, calculated as a ratio of ion abundances for each of the isotopomeric diastereomeric ion complex pairs of a given charge state (equation 3.1).

$$\text{Selectivity } (\boldsymbol{\alpha}) = \frac{\text{int } \{[Sb_2\text{-}\mathbf{X}\text{-}tar_2][H]_{\mathbf{a}}[\mathbf{Y}\text{-Leu}]\}^{\mathbf{p}-}}{\text{int } \{[Sb_2\text{-}\mathbf{X}\text{-}tar_2][H]_{\mathbf{a}}[\mathbf{Z}\text{-Leu}]\}^{\mathbf{p}-}} \quad \text{----------} \quad (3.1)$$

Also shown are values for competitive binding control experiments to discern any contributions from the deuterium labeling [44]. For the dianionic form, no discernable enantioselectivity was observed (Cases **I** and **V**). For the monoanionic form, a significant preference for binding *D*-Leu by $\{[Sb_2\text{-}L\text{-}tar_2][H]\}^{-}$ (Case **III**), and a cross-chiral preference of similar magnitude for binding *L*-Leu by $\{[Sb_2\text{-}D\text{-}tar_2][H]\}^{-}$ (Case **VII**), was recorded. While deuterium isotope effects were observed, the magnitudes of these effects were less pronounced than that for the measured enantioselectivities.

Table 3.1 Calculated average selectivity values (n = 5) and standard deviations from competitive binding experiments according to the given standard equation. **X** denotes the stereochemistry of the tartrates, **Y** and **Z,** respectively, denote the configuration of *L*eu in the numerator and denominator, **a** denotes the number of protons associated with the complex, and **p-** denotes the charge state of the complex. Cases for evaluation of enantioselectivity (**I**, **III**, **V**, **VII**) are shaded in grey. Control experiments for determination of deuterium isotope effect contributions are shown in cases **II**, **IV**, **VI**, and **VIII**.

Case	X	Y	Z	a	p-	α
I	*L*	*D*	*L*-d_{10}	0	2-	1.09 ± 0.15
II	*L*	*L*	*L*-d_{10}	0	2-	0.96 ± 0.14
III	*L*	*D*	*L*-d_{10}	1	1-	1.62 ± 0.20
IV	*L*	*L*	*L*-d_{10}	1	1-	1.13 ± 0.07
V	*D*	*L*-d_{10}	*D*	0	2-	0.82 ± 0.15
VI	*D*	*L*-d_{10}	*L*	0	2-	0.77 ± 0.07
VII	*D*	*L*-d_{10}	*D*	1	1-	1.65 ± 0.42
VIII	*D*	*L*-d_{10}	*L*	1	1-	0.81 ± 0.03

3.3 Proton-assisted enantioselectivity of antimony(III)-*D*,*L*-tartrate in gas phase-targeted collision activated dissociation (CAD) ESI-MS

To further elucidate the proton assisted enantioselectivity observed in competitive binding experiments, the diastereomeric ionic complexes were isolated in the quadrupole ion trap and subjected to collision threshold dissociation (CAD). In these gas phase experiments, the stabilities of isolated ionic complexes were monitored as a function of activation voltage [145, 146] (q = 0.250; 30 msec activation time). In Figure 3.8, it can be seen that the overall trend for selective dissociation in the gas phase is consistent with that observed in the solution phase. For the monoanionic diastereomeric complexes, a distinct enantioselective binding preference was observed, where a higher activation voltage was required to dissociate *D*-Leu from $\{[Sb_2\text{-}L\text{-}tar_2][H][D\text{-}Leu]\}^-$ (Figure 3.8A). Similarly, the complex between $\{[Sb_2\text{-}D\text{-}tar_2][H]\}^-$ and *L*-Leu was more stable than that for *D*-Leu (Figure 3.8B). Although absolute binding energies are difficult, if not impossible, to determine due to the multi-collision environment in the ion trap, the differences between voltages required to dissociate 50% of the precursor ion complexes (V_{50}) can be used as a measure of relative stability.

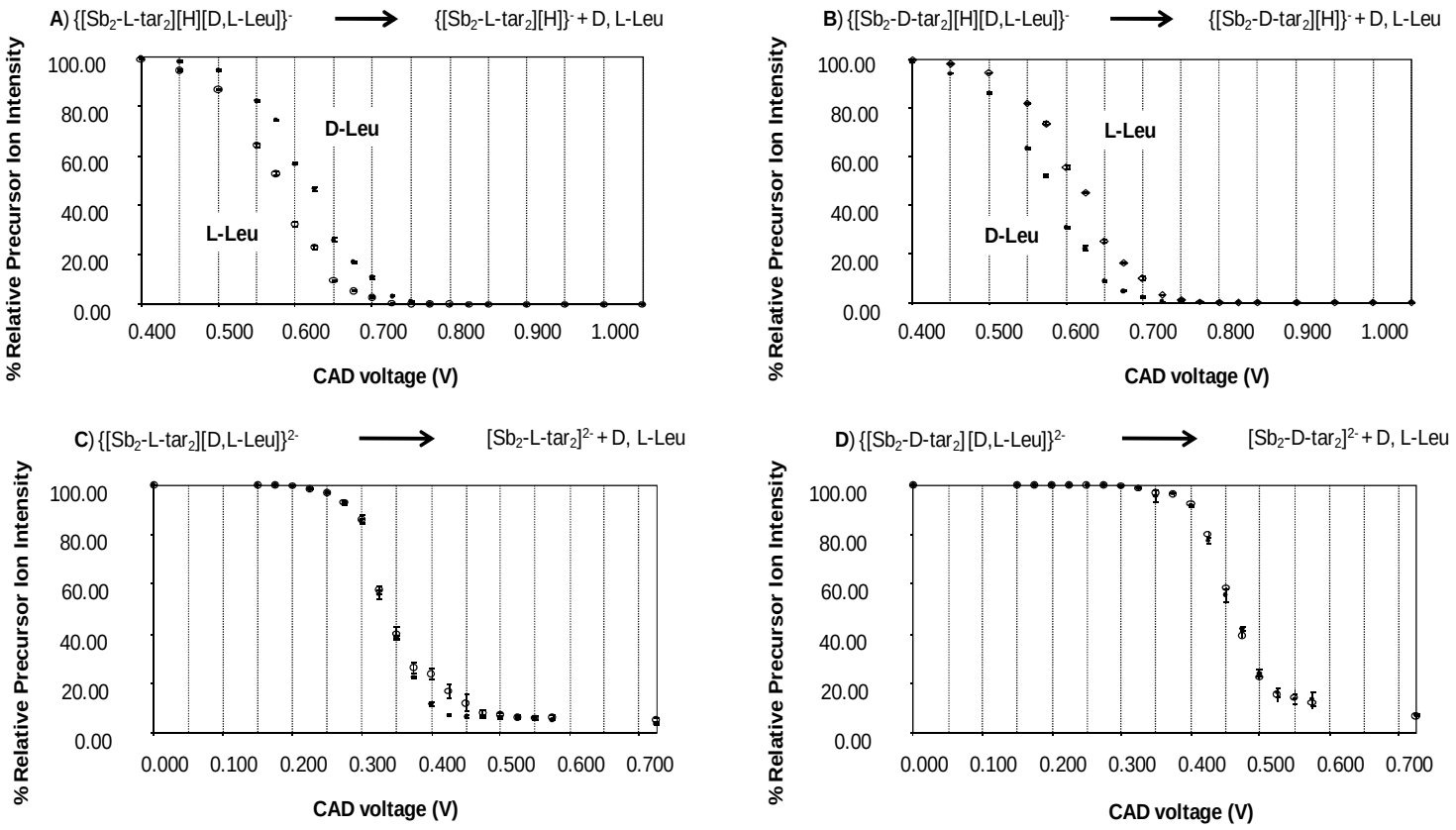

Figure 3.8 Collision threshold dissociation of diastereomeric ion complexes: A) $\{[Sb_2\text{-}L\text{-}tar_2][H][D\text{-}Leu]\}^-$ (•) and $\{[Sb_2\text{-}L\text{-}tar_2][H][L\text{-}Leu]\}^-$ (○); B) $\{[Sb_2\text{-}D\text{-}tar_2][H][D\text{-}Leu]\}^-$ (•) and $\{[Sb_2\text{-}D\text{-}tar_2][H][L\text{-}Leu]\}^-$ (○); C) $\{[Sb_2\text{-}L\text{-}tar_2][D\text{-}Leu]\}^{2-}$ (•) and $\{[Sb_2\text{-}L\text{-}tar_2]\ [L\text{-}Leu]\}^{2-}$ (○); *D*) $\{[Sb_2\text{-}D\text{-}tar_2]\ [D\text{-}Leu]\}^{2-}$ (•) and $\{[Sb_2\text{-}D\text{-}tar_2]\ [L\text{-}Leu]\}^{2-}$ (○) in a quadrupole ion trap. Data points are reported as average values (n = 3) with error bars representing one standard deviation from the mean. Reprinted from reference 79 with permission from Elsevier B.V.

The average V_{50} values (n = 3) for dissociation of {[Sb_2-*L*-tar_2][H][*D*-Leu]}$^-$, {[Sb_2-*L*-tar_2][H][*L*-Leu]}$^-$, {[Sb_2-*D*-tar_2][H] [*L*-Leu]}$^-$, and {[Sb_2-*D*-tar_2][H][*D*-Leu]}$^-$ diastereomeric ions obtained from the threshold dissociation plots were 0.615 ± 0.005 V , 0.575 ± 0.005 V, 0.610 ± 0.005 V and 0.570 ± 0.005 V, respectively. The differences in V_{50} values (with error propagation) which are indicative of Δ(ΔG) for the dissociation of the diastreomeric complexes were 0.040 ± 0.007 V (*D*-Leu > *L*-Leu with {[Sb_2-*L*-tar_2][H]}$^-$) and 0.040 ± 0.007 V (*L*-Leu > *D*-Leu with {[Sb_2-*D*-tar_2][H]}$^-$), demonstrating enantioselective binding in the gas phase with a perfect quantitative cross-chiral relationship (assuming the constant of proportionality between V_{50} and ΔΔG values are constant during all CAD experiments). A similar analysis was carried out for evaluating the results from dissociation of the dianionic diastereomeric complexes (Figure 3.8C, 3.8D). The experiments indicated no enantioselective dissociation in the gas phase for the dianionic forms, which is consistent with solution-phase-based competitive binding results.

While non-correlation between solution phase and gas phase binding preference is common, this marked correlation of proton-assisted enantioselective discrimination capacity of antimony(III)-*D*- and -*L*-tartrate between solution-phase and gas-phase association and dissociation phenomena can provide some insight into the binding chemistry between antimony(III)-*D*,*L*-tartrates and leucine enantiomers. Specifically, for the protonated monoanionic system, the solvent can be assumed to play a minor role relative to the stereochemical orientation of the associates in providing enantioselective binding. In other words, solvation is not necessarily needed to maintain a delicate balance of noncovalent forces, contrary to that shown for other enantioselective systems [26]. Further studies incorporating different solution conditions (% organic, pH, and ionic strength) are needed to confirm this assertion.

Of greater interest is the nature of proton-assistance which gives rise to enantioselective binding. This finding suggests that the display of functional motifs responsible

for enantioselective binding to leucine is significantly different between the dianionic and the protonated monoanionic forms. The necessity of ammonium portion for the formation of diastereomeric complexes between $\{[Sb_2\text{-}D,L\text{-}tar_2]\}^{2-}$ and $\{[Sb_2\text{-}D,L\text{-}tar_2][H]\}^{1-}$ ions and zwitterionic *L*eu however provide some insight to provide a reasonable rationale for the variation of stereo-recognition for the two types of ions. The dianionic $\{[Sb_2\text{-}D,L\text{-}tar_2]\}^{2-}$ core would coordinate with the ammonium portion to minimize electrostatic repulsion and carboxylate anionic portion would avoid the dianionic core which then result in a poor orientation for stereo-recognition. In the monoanion, though Leu is zwitterionic, its carboxylate anionic portion is capable of hydrogen bonding to the proton where it resides on the $\{[Sb_2\text{-}D,L\text{-}tar_2]\}^{2-}$ core and the ammonium portion coordinates to the more electro-negative portion of $\{[Sb_2\text{-}D,L\text{-}tar_2][H]\}^{1-}$ core which would conduct more to stereo-recognition. To investigate this more fully, both theoretical computational and solution phase NMR experiments have been initiated [147]. Preliminary computational results indicate that the lack of enantioselectivity observed for the dianionic form is due to the presence of an additional low energy conformation in equilibrium with the X-ray-predicted crystallographic form. These forms appear to exhibit opposing enantioselectivities, manifesting experimentally in an overall lack of enantioselectivity observed for the dianion form during ESI-MS measurements. For the protonated case, which has never been previously investigated in this manner, a single dominant conformation has been preliminarily isolated, explaining the observation of its enantioselective binding capacity in the mass spectra. The detailed computations necessary to fully explain this behavior require significant time to complete. These results, along with data from NMR experiments and ESI-MS data for additional analyte enantiomers, are needed to fully elaborate the mechanistic basis for the observations reported here, will be reported in due course.

3.4 Conclusions

In conclusion, fundamental mass spectrometric investigations have provided key pieces of evidence towards rationalizing the enantioselective binding capacity of antimony(III)-*L*-tartrate. It is reasonable to assume that the dianion $[Sb_2\text{-}L\text{-}tar_2]^{2-}$ is in equilibrium with the protonated monoanion $\{[Sb_2\text{-}L\text{-}tar_2]^{2-}[H]^{+}\}$ in aqueous solutions. The fact that these different ion forms yield different enantioselective discrimination capacity holds promise for reconciling the use of antimony(III)-*D*- and -*L*-tartrate as analytical separations reagents. In the work by Martin et.al. [69], resolution of Ru(II) tris-diimine complexes by capillary electrophoresis was achieved at pH 2.5, a condition where the protonated monoionic complex would be highly favored. At higher pH values, enantioselectivity would be expected to diminish as the dianionic form is populated. Other reports in the literature also assert the importance of pH on enantioselective solution phase separations [148-145]. With regard to mass spectrometry, these findings may prompt further evaluation of previous work using antimony(III)-tartrate in ESI-based enantioselective association experiments [136, 137] to discern if similar behavior, especially for the protonated monoanion $\{[Sb_2\text{-}L\text{-}tar_2][H]\}^{-}$, may have been overlooked. Overall, the notion of charge-state-dependent enantioselective reactions has been previously reported in protein-ligand systems [151], but to our knowledge, this is the first report of such behavior for small molecule enantioselective binding systems, recorded in both solution-phase-targeting ESI-MS and gas-phase MS/MS dissociation experiments. This study sheds new light on the dynamic nature of antimony(III)-tartrate chiral selectors and prompts further investigation into a system that could indeed still be found quite useful for analytical separations (and therapeutic indications) if it can be controlled to a greater extent.

CHAPTER 4

ESI-MS INVESTIGATION OF SOLVENT EFFECTS ON THE CHIRAL RECOGNITION CAPACITY OF TARTAR EMETIC TOWARDS NEUTRAL SIDE-CHAIN AMINO ACIDS

4.1 Introduction

Metal-tartrate complexes, particularly antimony tartrates, are an attractive class of compounds for use in separation science as chiral reference compounds, e.g. in chromatographic and electrophoretic enantioselective separations [68-72, 74-76]. Their capacity for use as a resolving agent has also helped synthetic chemists resolve enantiomers by diastereomeric salt formation [95]. Additionally, the history of medicinal indications for *L*-antimony(III)-tartrate ("tartar emetic") traces back to medieval times as an emetic drug, and also as a therapeutic indication for diseases like typhoid, bronchitis, pneumonia and schistosomiasis [65, 152-155].

Tartar emetic's long history had been filled with intrigue and peril [65]. Improperly administered, tartar emetic has been associated with side effects including severe nausea, vomiting, diarrhea, renal failure, cardiovascular collapse, and even, death. Therefore, during the sixteenth century, medicinal practice employing antimony was banned by the Paris faculty of medicine. It was then brought back into use by popular demand, partly because in 1657, it was believed to have cured King *L*ouis XIV from typhoid fever [65, 152]. Through the beginning of the nineteenth century it was considered the "strong arm of fever therapy," [152] but then, again, its use went into decline, presumably due to its unwanted side effects. In the middle of the twentieth century, it was recalled and used for a totally different disease, parasitic disorders caused by schistosomal blood flukes [154-156]. However, it was later replaced with less toxic alternatives. Overall, the therapeutic potential of tartar emetic as an anti-infective has been overshadowed by its associated toxicity. This could, however, be a slight historical

misconception compounded due to the lack of understanding of its mechanism of action and the limited investigation of its pharmacodynamics [157, 158].

Due to the debates about metal-tartrate structures in the 1970s [85] and questions about *L*-antimony(III)-tartrate's mode of action in biological systems, e.g. its reported anti-bacterial activity at relatively high concentrations compared to penicillin by Duffin et al. [64, 65], an attempt to understand its enantioselective discrimination character towards biologically relevant amino acid enantiomers at the molecular level was carried out in our group using electrospray ionization mass spectrometry (ESI-MS). ESI-MS has been used to study gas-phase dissociation as well as solution-phase association phenomena of enantiomers with a variety of chiral selectors [10, 12, 23]. Since tartar emetic has shown antibacterial properties, it was hypothesized that selective solution-phase binding towards *D*-amino acids by *L*-antimony(III)-tartrate or tartar emetic might be visualized in some form in single-stage ESI-mass spectra. A great deal of work has been previously performed to study the association between depsipeptide models of bacterial peptidoglycan cell wall synthesis intermediates (e.g. *D*-Ala-*D*-Ala motifs) and antibiotics, such as vancomycin and ristocetin, using ESI-MS [159]. It was also recently reported that a dedicated enzyme in bacteria produces *D*-amino acids (e.g. *D*-Leu, *D*-Met, *D*-Phe etc.) in order to modulate synthesis of the peptidoglycan polymer of the bacterial cell wall [160]. The peptidoglycan is an essential component of the bacterial cell wall in Gram positive bacteria, which is a sturdy and elastic polymer that serves as a stress-bearing component used by bacteria to adapt in varying environmental settings. Thus, experiments designed to probe the properties of therapeutic compounds that show a selective binding preference for amino acids in the *D*-configuration could also have implications for understanding their ability to inhibit bacterial cell wall synthesis, perhaps in a manner similar to vancomycin.

Arakawa et al. were the first to study chiral molecular recognition properties of *D*,*L*-antimony(III)-tartrates using ESI-MS. Their single-stage ESI-MS-based results have effectively shown the trends that were observed in independent solution phase experiments [136, 137].

Our recent studies in single-stage ESI-MS experiments of *D*,*L*-antimony(III)-tartrates and enantiomers of leucine showed previously unprecedented proton-assisted enantioselectivity [79]. More specifically, it was observed that proton-associated *L*-antimony(III)-tartrate showed selective binding towards *D*-Leu over *L*-Leu. However, when there was no proton association, *D*,*L*-antimony(III)-tartrate dianionic hosts failed to show enantioselective molecular recognition phenomena toward the amino acid guests. Nevertheless, several questions still remain to be answered in order to construct a general model for these observed phenomena. Is this proton-assisted enantioselectivity of *D*,*L*-antimony(III)-tartrates maintained with other similar neutral side-chain amino acids? Also, if it is maintained, what is the solvent dependence of these phenomena? Will similar results be observed when 100% aqueous solutions and aqueous systems mixed with other common organic modifiers like methanol are used? The latter questions arise in part due to recent work by Kass and coworkers [140-142]. They have reported that experimental electrospray conditions, such as solvent composition, can alter the isomeric form of an anion. For example, singly deprotonated tyrosine, where deprotonation can take place either at the carboxylic or at the phenolic sites, can assume a carboxylate form if the spray solvent is composed of methanol/water or a phenolate form if the spray solvent is composed of acetonitrile/water. More importantly, based on theoretical calculations, they have pointed out that acetonitrile and water (ACN/H_2O) solvent systems better preserved the solution-phase molecular form of tyrosine (i.e. the carboxylate form), which were appropriately represented in the respective mass spectra. They further assert that electrospraying methanol and water ($MeOH/H_2O$) solvent systems predominantly produces gas phase ion structures of tyrosine (i.e. the phenolate ion form). In order to probe whether similar solvent effects in our own chiral molecular recognition system are present, several single-stage ESI-MS competitive binding experiments were performed and the results are described herein.

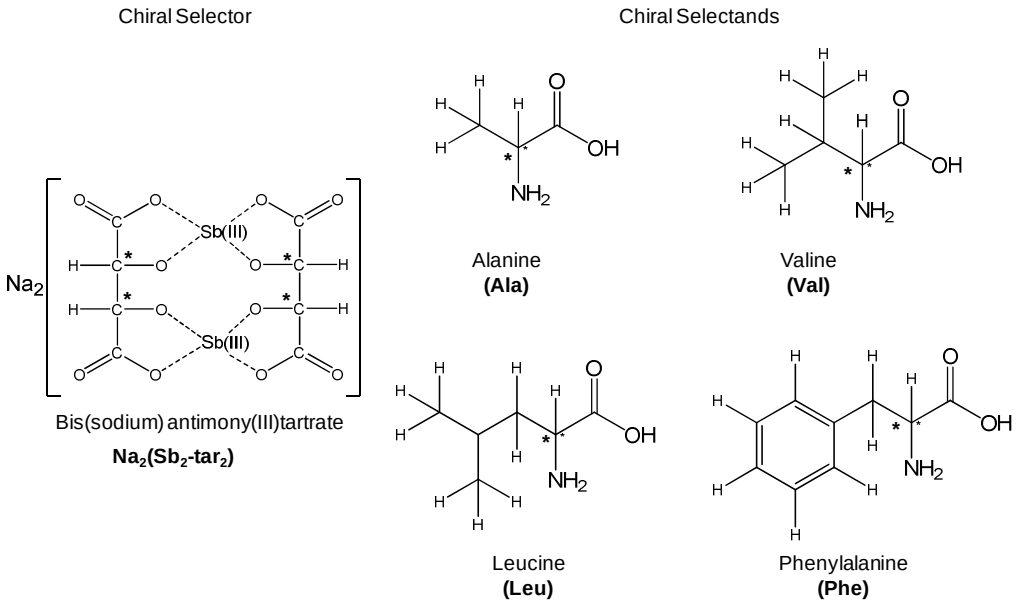

Figure 4.1 Structures of the chiral selectors, Na_2[*D*-, *L*-Sb_2-tar_2] and selectands, neutral side chain amino acids alanine, valine, leucine and phenylalanine. Note: Chiral centers are marked with an asterisk. Reprinted from reference 80 with permission from John Wiley & Sons, Inc.

This chapter shows that *D*, *L*-antimony(III)-tartrates maintain their proton-assisted enantioselective molecular recognition capacity for several neutral side-chain amino acids. This was achieved by carrying out single-stage ESI-MS competitive binding experiments between isotopomeric enantiomers of the amino acids alanine (Ala), valine (Val), leucine (Leu) and phenylalanine (Phe) (see Figure 4.1 for chiral selectors and selectands employed for this study). These amino acids were selected so that the effect of the hydrophobic substituent group on the enantioselective molecular recognition capacity of *D*,*L*-antimony(III)-tartrates could be evaluated. Also, general trends governed by different electrospray solvent systems on chiral molecular recognition properties by *D*,*L*-antimony(III)-tartrates were monitored. This manuscript reports that the effect on the chiral recognition capacity of *D*,*L*-antimony(III)-tartrates by the electrospray-friendly organic modifiers, like acetonitrile and methanol, is small but not negligible, with respect to that observed in pure water. The proton-assisted enantioselectivity between *D*,*L*-antimony(III)-tartrates and neutral side-chain amino acid binding systems, with respect to aqueous solutions, was maintained.

4.2 Experimental

4.2.1 Materials

Enantiomerically-pure (> 98%) *D*- and *L*-forms of amino acids alanine (Ala) and phenylalanine (Phe) were obtained from Sigma-Aldrich Inc. (St. Louis, MO USA), whereas those of valine (Val) and leucine (Leu) were obtained from Fluka Chemie (Buchs, Switzerland)). Enantiomerically-pure deuterated amino acid standards *L*-2,3,3,3-d4-alanine (*L*-d4-Ala), *L*-2,3,4,4,4,5,5,5-d8-valine (*L*-d8-Val), *L*-2,3,3,4,5,5,5,6,6,6-d10-leucine (*L*-d10-Leu) and *L*-d5-phenyl-2,3,3-d3-alanine (*L*-d8-Phe) were obtained from C/D/N Isotopes Inc.(Pointe-Claire, Quebec, Canada). All solvents utilized for ESI-MS analyses (water, methanol (MeOH), acetonitrile (ACN)) were LC-MS grade and purchased from Mallincrodt-Baker (Phillipsburg, NJ USA). Antimony(III) oxide (Sb_2O_3) was purchased from Alfa Aesar (Ward Hill, MA USA) and 5.0 M sodium hydroxide aqueous solution was from Sigma-Aldrich. Enantiomerically-pure *D*- and *L*-tartaric acids were obtained from Sigma-Aldrich. Ethyl alcohol used for synthesis purposes was obtained from Pharmco-AAPER (USA).

4.2.2 Methods

4.2.2.1 Synthesis of Chiral Selector Bis(sodium) *D*- and -*L*-antimony(III)-tartrate Complex Salts

Bis(sodium) *D*- and -*L*-antimony(III)-tartrates, were prepared according to a previously published procedure [85]. Briefly (Scheme 4.1), *L*-tartaric acid (1.0000 ± 0.0001 g, 6.66 x 10^{-3} mol) was dissolved in LC-MS grade water (~ 30 mL) in a round-bottomed flask (100 ml). While stirring the content in the round-bottomed flask, aqueous sodium hydroxide solution (1.330 ± 0.005 mL from 5.0 M, 6.66 x 10^{-3} mol, 1.0 equiv.) was added in order to make the mono-sodium salt of *L*-tartaric acid. Antimony(III) oxide (0.8714 ± 0.0001 g, 3.33 x 10^{-3} mol, 0.5 equiv.) was then added into the round-bottomed flask and refluxed for 12 hours. Hot-filtration was carried out for the removal of any residual antimony oxide. White crystalline bis(sodium) *L*-antimony(III)-tartrate salt was precipitated by careful addition of 99.98% ethanol (~ 500 mL) into the warm, hot-filtered solution. The compound, collected by suction filter, was then washed with aqueous

ethanol and acetone, and air dried (yield > 90%). The same technique was employed to synthesize bis(sodium) *D*-antimony(III)-tartrate salt by employing *D*-tartaric acid instead of *L*-tartaric acid. In order to characterize the compounds using methods described in our previous report [79], ESI-mass spectra of the selectors were obtained. Both negative ionization mode ESI-mass spectra of synthesized bis(sodium) *D*- and *L*-antimony(III)-tartrate salts showed consistent doubly charged [*D*, *L*-Sb_2-tar_2]$^{2-}$ (268.1 Th) ions accompanied by protonated {[*D*, *L*-Sb_2-tar_2][H]}$^{1-}$ (536.8 Th) and sodiated {[*D*, *L*-Sb_2-tar_2][Na]}$^{1-}$ (558.9 Th) singly-charged anion forms. All peaks showed consistent isotopic distributions that resulted due to the presence of two isotopes of Sb (^{121}Sb, 57.36% NA and ^{123}Sb, 42.64% NA). It was also observed that isotopic peaks of the two singly charged {[*D*, *L*-Sb_2-tar_2][H]}$^{1-}$ (536.8 Th) and {[*D*, *L*-Sb_2-tar_2][Na]}$^{1-}$ (558.9 Th) ions were separated by m/z = 2, whereas signals of isotopic peaks for the doubly charged [*D*, *L*-Sb_2-tar_2]$^{2-}$ (268.1 Th) ions were separated by m/z = 1.

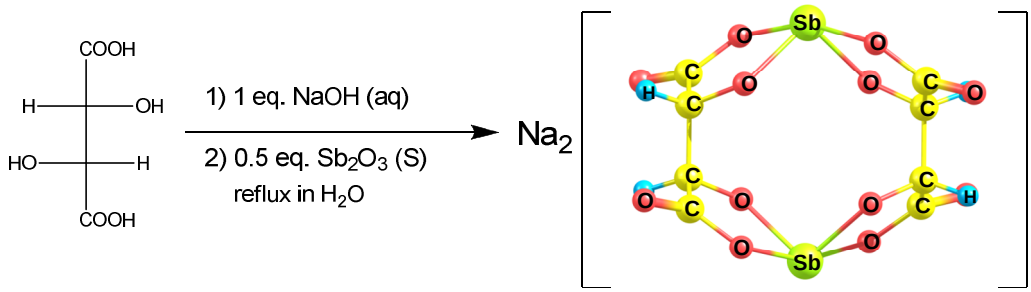

Scheme 4.1 Synthesis of Na_2[*L*-Sb_2-tar_2]. Reprinted from reference 80 with permission from John Wiley & Sons, Inc.

4.2.2.2 Single-Stage ESI-MS Competitive Binding Experiments

A Thermo LCQ Deca XP quadrupole ion trap instrument equipped with a conventional ESI source (Thermo-Fisher Scientific, West Palm Beach, FL) was used in all ESI-MS experiments. Solution-phase targeting mass spectra was obtained by direct infusion of respective solutions into the source by an in-built syringe pump. In between separate solution analyses, the ESI source and external tubing were flushed with LC-MS grade water for an extended period by direct infusion using the syringe pump (capacity, 500 µL) at 100 µL/min.

Single-stage ESI-MS competitive binding experiments were performed using three types of solvent systems (ACN/H_2O (75/25 v/v), H_2O (100%) and H_2O/MeOH (25/75 v/v)), each containing the chiral selector (100 µM), either Na_2[*L*-Sb_2-tar_2] or Na_2[*D*-Sb_2-tar_2], and enantiomeric isotopomeric chiral selectands of each amino acid (AA) type (100 µM each), *D*-AA and *L*-dX-AA (X represents 4, 8, 10 and 8 for the amino acids Ala, Val, Leu and Phe, respectively). All solutions with chiral selectands and selectors were freshly prepared before ESI-MS analysis. These volume ratios of water and organic modifiers were the optimal ratios required to have all amino acids and *D*,*L*-antimony(III)-tartrates to be fully dissolved. It was assumed that utility of 75% of the organic modifiers in these solutions were sufficient to represent their effect to these chiral molecular recognition systems. Formaldehyde incorporation (~ 100 mM) to enhance spectral quality of previously reported experiments was not practiced in these experiments [79, 143], because the study was focused on studying the effects by electrospray friendly organic solvent modifiers on these chiral recognition systems. It was assumed that formaldehyde incorporation with a high concentration (~ 100 mM) would influence the solvent properties and alter the original form of the solvent system.

Ionization and source parameters were optimized based on maximizing the ion abundance of the protonated antimony(III)-tartrate ions, {[*D*,*L*-Sb_2-tar_2][H]}$^-$ observed at 536.8 Th using the automatic optimization function of the Xcalibur software (Thermo-Fisher Scientific). Prepared solutions were directly infused and data were collected in five trials, using a minimum of 70 scans for each replicate. All solutions analyzed with solvent systems ACN/H_2O (75/25 v/v) and MeOH/H_2O (75/25) were pumped at a flow rate of 10 µL/min. However aqueous solutions were pumped at a higher flow rate (20 µL/min) while keeping a 4-5 times higher sheath gas flow rates compared to the other two solvent systems. These higher sheath gas flow rates were used in order to facilitate solvent evaporation and obtain clear mass spectra of aqueous solutions. It was observed that use of lower sheath gas flow rates and lower syringe pump flow rates of aqueous solutions result in mass spectra with substantially less responsive signals.

Analysis of relative responses of ionic complexes formed between the chiral selector ions ({[*D*,*L*-Sb_2-tar_2][H]}$^-$ and [*D*,*L*-Sb_2-tar_2]$^{2-}$) and enantiomeric isotopomeric chiral selectands of each amino acid type were used to calculate enantioselectivity (e.g. complex ion intensity of *D*-AA divided by complex ion intensity of *L*-dX-AA). Enantioselectivity values were separately calculated for each singly-charged and doubly-charged isotopomeric diastereomeric complex-ion pairs. Average enantioselectivity values ($\boldsymbol{\alpha}_{MS,1-}$ and $\boldsymbol{\alpha}_{MS,2-}$) and the standard deviations were then calculated using the selectivity values obtained from the five replicates of each experiment.

In order to monitor and normalize any deuterium isotope effects [44] influencing the chiral molecular recognition capacity of *D*,*L*-antimony(III)-tartrate salts, a second set of control experiments were also carried out substituting *D*-forms of the amino acids by the *L*-forms. Selectivity and average selectivity values for these experiments were also calculated for these sets of experiments. Adjusted enantioselectivity values ($\boldsymbol{\alpha}^*_{MS,1-}$ and $\boldsymbol{\alpha}^*_{MS,2-}$) were then calculated for each chiral ionic species (dianionic and mono-anionic of *D*,*L*-antimony(III)-tartrate salts). Adjusted enantioselectivity values mathematically normalize and correct for any deuterium isotope effects that might influence average enantioselectivity values. Standard deviations were calculated using standard statistical error propagation methods. There are three signals observed in each ionic complex which corresponds to the three combinations of ^{121}Sb and ^{123}Sb isotopes. Only the central peak was used in all calculations. The central ion was selected in all calculations so that complications that arise due to merged signals in experiments involved with Ala could be avoided (see Figure 4.2A).

4.3 Results and Discussion

The main focus of this study was to evaluate whether *D*,*L*-antimony(III)-tartrate salts maintain their previously reported proton-assisted enantioselectivity with other similar neutral-side chain amino acid enantiomeric isotopomers Ala, Val, Leu and Phe in different electrospray solvent systems. Evaluation of the effect of different hydrophobic substituent groups of amino acids on proton-assisted enantioselective capacity of *D*,*L*-antimony(III)-tartrate was a secondary

focus. Figure 4.2 illustrates a series of mass spectra obtained in competitive binding experiments performed in MeOH/H_2O (75/25 v/v) solutions, containing the chiral selector, Na_2[*D*-Sb_2-tar_2] (100 µM), and the chiral selectands, enantiomeric isotopomers of amino acids (100 µM each). In general, it is clear that in all these systems enantiomeric discrimination capacity originates from complexation with the {[*D*-Sb_2-tar_2][H]}$^-$ ion, and that the diasteromeric complex ion forms with the deuterated *L*-amino acid produced higher intensities with respect to that observed for the diastereomeric complexes with *D*-amino acids. Doubly-negatively charged complexes did not show distinguishable binding preferences. The opposite binding preference, but consistent proton-assisted enantioselectivity, was observed with {[*L*-Sb_2-tar_2][H]}$^-$ ion (mass spectra not shown).

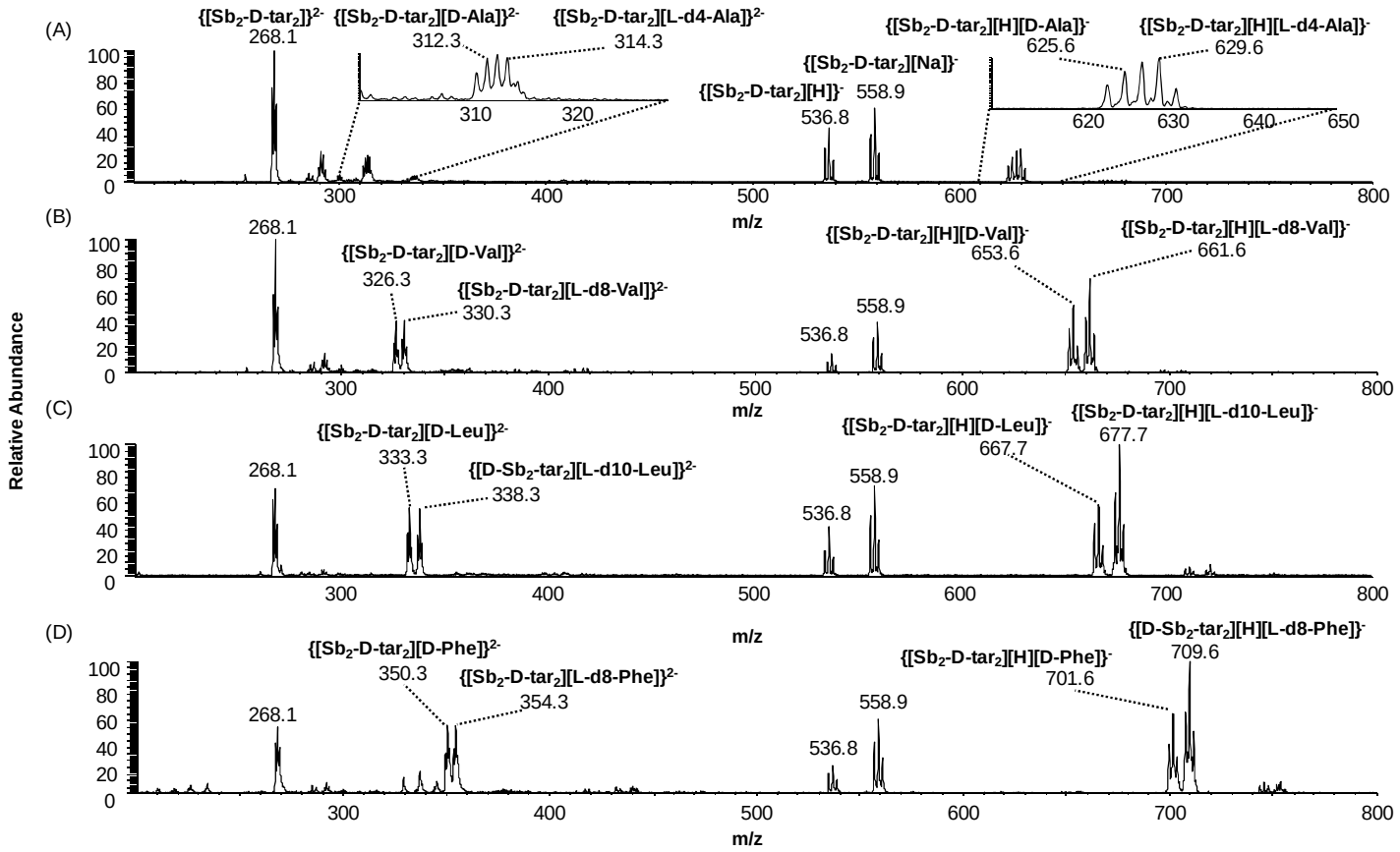

Figure 4.2 Competitive binding ESI mass spectra obtained by direct infusion of a solution containing equimolar (100 μM) Na_2[*D*-Sb_2-tar_2] and enantioisotopomeric amino acids A) *D*-Ala, *L*-d4-Ala B) *D*-Val, *L*-d8-Val C) *D*-Leu, *L*-d10-Leu and D) *D*-Phe, *L*-d8-Phe MeOH/H_2O (75/25 v/v). Reprinted from reference 80 with permission from John Wiley & Sons, Inc.

Enantioselectivity and adjusted enantioselectivity values calculated for amino acid enantiomers of Ala, Val, Leu and Phe from all ESI-MS competitive binding experiments for singly charged {[*D*,*L*-Sb_2-tar_2][H]}$^-$ ions are summarized in Table 4.1. Values obtained for each solvent system are separately included. It is apparent that {[*L*-Sb_2-tar_2][H]}$^-$ ion has binding preference towards the *D*-form of all the amino acids studied and {[*D*-Sb_2-tar_2][H]}$^-$ ion has the opposite chiral preference which is towards the *L*-forms of the respective amino acids. This is consistent with our previous report [79]. Deuterium isotope effects are observed in some cases, but are negligible compared to the average enantioselectivity values obtained. In all cases, values calculated show close cross-chiral or reciprocal binding relationships with respect to the {[*L*-Sb_2-tar_2][H]}$^-$ and {[*D*-Sb_2-tar_2][H]}$^-$ ions and their preference for *D*- or *L*-amino acids, respectively.

In general, comparison of adjusted enantioselectivity values indicate that Leu and Phe amino acid enantiomers show the largest values compared to the other two amino acids regardless of the solvent system. Except for one case, interestingly, Val enantiomers show the lowest adjusted enantioselectivity values. The exception is observed in aqueous solutions with {[*L*-Sb_2-tar_2][H]}$^-$ ion, where comparable adjusted selectivity values are observed for Val and Ala enantiomers. Therefore, a general trend of increasing adjusted selectivity can be organized as Val ≤ Ala < Leu ≈ Phe. The higher adjusted enantioselectivity values observed for Leu and Phe can be attributed to larger steric interactions resulting from their bulkier side chain groups. Enantiomers of Ala show slightly higher or comparable adjusted enantioselectivity values compared to Val enantiomers. This indicates that the size of the hydrophobic side chains of Ala and Val provide less on the chiral molecular recognition capacity of {[*D*, *L*-Sb_2-tar_2][H]}$^-$ ion, while other interactions such as electrostatic and hydrogen bonding are expected to be predominant.

.

Table 4.1 Calculated average enantioselectivity values $\alpha_{MS,1-}$ (n = 5) for singly charged proton associated {[*D*- and *L*-Sb_2-tar_2][H]}$^{1-}$ chiral ionic species and standard deviations from competitive binding experiments in three different solvent systems, ACN/H_2O (75/25 v/v), H_2O (100%) and MeOH/H_2O (75/25 v/v). 'c.p.' denotes configurational preference and 'np' denotes no preference. Reprinted from reference 80 with permission from John Wiley & Sons, Inc.

Antimony(III)-X-tartrate (Chiral Selector/SO)	Amino Acid (Chiral Selectands/SAs)	Avg. Selectivity ($\alpha_{MS,1-}$ ± SD (c.p.)) (n=5)			Adjusted Selectivity ($\alpha^*_{MS,1-}$ ± SD (c.p.))		
		Solvent System			Solvent System		
		ACN/H_2O 75/25 (v/v%)	H_2O 100%	MeOH/H_2O 75/25 (v/v%)	ACN/H_2O 75/25 (v/v%)	H_2O 100%	MeOH/H_2O 75/25 (v/v%)
L	D-**Ala** vs L-d4-**Ala**	1.61 ± 0.03 (**D**)	1.23 ± 0.07 (**D**)	1.39 ± 0.04 (**D**)	**1.63 ± 0.05** (**D**)	**1.28 ± 0.13** (**D**)	**1.48 ± 0.06** (**D**)
	L-**Ala** vs L-d4-**Ala**	0.99 ± 0.02 (np)	0.96 ± 0.08 (np)	0.94 ± 0.03 (np)			
	D-**Val** vs L-d8-**Val**	1.35 ± 0.02 (**D**)	1.23 ± 0.07 (**D**)	1.26 ± 0.04 (**D**)	**1.44 ± 0.05** (**D**)	**1.30 ± 0.08** (**D**)	**1.33 ± 0.06** (**D**)
	L-**Val** vs L-d8-**Val**	0.94 ± 0.03 (np)	0.95 ± 0.02 (np)	0.95 ± 0.03 (np)			
	D-**Leu** vs L-d10-**Leu**	1.63 ± 0.05 (**D**)	1.38 ± 0.04 (**D**)	1.52 ± 0.04 (**D**)	**1.77 ± 0.05** (**D**)	**1.53 ± 0.07** (**D**)	**1.65 ± 0.06** (**D**)
	L-**Leu** vs L-d10-**Leu**	0.92 ± 0.01 (np)	0.90 ± 0.03 (np)	0.92 ± 0.02 (np)			
	D-**Phe** vs L-d8-**Phe**	1.75 ± 0.04 (**D**)	1.68 ± 0.03 (**D**)	1.66 ± 0.02 (**D**)	**1.74 ± 0.08** (**D**)	**1.72 ± 0.06** (**D**)	**1.67 ± 0.04** (**D**)
	L-**Phe** vs L-d8-**Phe**	1.01 ± 0.04 (np)	0.98 ± 0.03 (np)	1.00 ± 0.02 (np)			
D	D-**Ala** vs L-d4-**Ala**	1.73 ± 0.06 (**L**)	1.33 ± 0.04 (**L**)	1.31 ± 0.02 (**L**)	**1.68 ± 0.07** (**L**)	**1.28 ± 0.05** (**L**)	**1.25 ± 0.03** (**L**)
	L-Ala vs L-d4-Ala	1.03 ± 0.02 (np)	1.04 ± 0.02 (np)	1.05 ± 0.02 (np)			
	D-**Val** vs L-d8-**Val**	1.37 ± 0.02 (**L**)	1.22 ± 0.04 (**L**)	1.28 ± 0.02 (**L**)	**1.27 ± 0.03** (**L**)	**1.16 ± 0.05** (**L**)	**1.21 ± 0.03** (**L**)
	L-**Val** vs L-d8-**Val**	1.08 ± 0.02 (np)	1.06 ± 0.04 (np)	1.06 ± 0.02 (np)			
	D-**Leu** vs L-d10-**Leu**	1.89 ± 0.01 (**L**)	1.78 ± 0.07 (**L**)	1.79 ± 0.02 (**L**)	**1.71 ± 0.05** (**L**)	**1.59 ± 0.10** (**L**)	**1.61 ± 0.03** (**L**)
	L-**Leu** vs L-d10-**Leu**	1.10 ± 0.03 (np)	1.11 ± 0.05 (np)	1.11 ± 0.02 (np)			
	D-**Phe** vs L-d8-**Phe**	1.71 ± 0.04 (**L**)	1.63 ± 0.03 (**L**)	1.65 ± 0.05 (**L**)	**1.72 ± 0.05** (**L**)	**1.64 ± 0.05** (**L**)	**1.59 ± 0.05** (**L**)
	L-**Phe** vs L-d8-**Phe**	1.00 ± 0.02 (np)	0.99 ± 0.02 (np)	1.04 ± 0.01 (np)			

Figure 4.3 illustrates a series of mass spectra obtained in competitive binding experiments performed to study binding of enantiomeric isotopomers of Ala (*D*-Ala (100 µM) and *L*-d4-Ala (100 µM)) towards the chiral selectors, Na_2[*L*-Sb_2-tar_2] (100 µM) and Na_2[*D*-Sb_2-tar_2] (100 µM), respectively in the three different solvent systems: (A) MeOH/H_2O (75/25 v/v); (B) ACN/H_2O (75/25 v/v); and (C) H_2O (100%). It is clearly observed that regardless of the solvent system utilized, previously reported proton-assisted enantioselectivity is maintained [79]. Close inspection of adjusted enantioselectivity values in Table 4.1 shows that the three solvent systems have small, but statistically significant, contributions towards the resolving capacity of {[*D*, *L*-Sb_2-tar_2][H]}$^-$ ion on neutral side-chain amino acids. In all cases, the ACN/H_2O (75/25 v/v) solvent system produced the highest adjusted enantioselectivity values. Either comparable or slightly smaller values were observed for the other two solvent systems. Since the ACN/H_2O (75/25 v/v) solvent system produced the highest adjusted enantioselectivity values compared to MeOH/H_2O (75/25 v/v) and H_2O (100%) solvent systems, it can be surmised that ACN, as an organic modifier, in some form facilitates chiral resolving capacity of amino acid enantiomers by {[*D*, *L*-Sb_2-tar_2][H]}$^-$ ions. It is likely that the decreased hydrogen bonding capacity of ACN molecules allows chiral selector ions (in particularly the anions, {[*D*,*L*-Sb_2-tar_2][H]}$^-$) and amino acids to interact to a greater degree through hydrogen bonding, which leads to an increase in adjusted enantioselectivity values. When MeOH and H_2O solvent molecules are present, the degree of hydrogen bonding interactions between chiral selector ions and amino acids can be expected to be reduced, due to competitive hydrogen bonding effects. Additionally, the presence of 25% H_2O in the ACN/H_2O (75/25 v/v) may be contributing to a reduced enantioselectivity, compared to what might be expected in 100% ACN. Unfortunately, the system is not soluble in 100% ACN and could not be studied in that solvent.

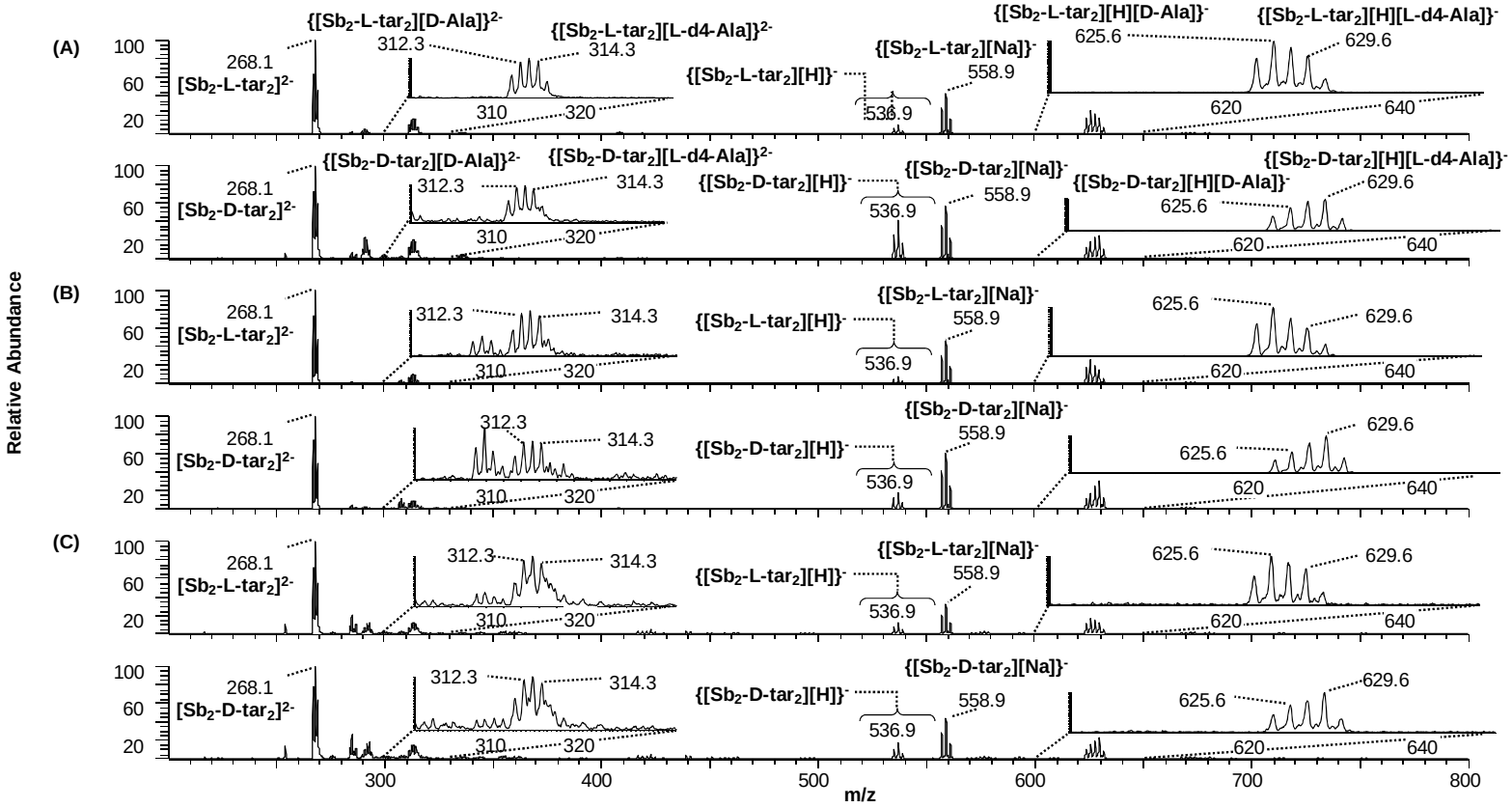

Figure 4.3 Competitive binding ESI mass spectra obtained by direct infusion of a solution containing equimolar (100 μM) enantioisotopomeric amino acids *D*-Ala and *L*-d4-Ala and chiral selectors Na_2[*L*- and *D*-Sb_2-tar_2] in A) MeOH/H_2O (75/25 v/v) B) ACN/H_2O (75/25 v/v) and C) H_2O (100 100%). Reprinted from reference 80 with permission from John Wiley & Sons, Inc.

Table 4.2 summarizes the selectivity values and the adjusted selectivity values calculated for the dianionic {[*D*,*L*-Sb_2-tar_2] }$^{2-}$ diastereomeric complex ion forms. For different solvent systems, enantiosselectivity values and adjusted enantioselectivity values are separately indicated. In general, regardless of the solvent system, {[*D*,*L*-Sb_2-tar_2] }$^{2-}$ ion forms showed no significant selectivity towards the amino acid enantiomers studied. This observation is also consistent with the previous work which signifies that absence of a proton associated to the {[*D*,*L*-Sb_2-tar_2] }$^{2-}$ ionic core, fail to show enantiomeric discrimination character towards neutral side-chain amino acids [79]. It is also apparent that the variation in solvent system does not alter this effect. The non-enantioselective character of {[*D*,*L*-Sb_2-tar_2] }$^{2-}$ is believed to be due to some alterations in its structural/symmetry features. Other theoretical and experimental studies to elucidate the nature of the {[*D*,*L*-Sb_2-tar_2] }$^{2-}$ ion forms are underway and will be reported in due course.

Table 4.2 Calculated average enantioselectivity values $\alpha_{MS,1-}$ (n = 5) for singly charged proton associated {[*D*- and *L*-Sb_2-tar_2][H]}$^{1-}$ chiral ionic species and standard deviations from competitive binding experiments in three different solvent systems, ACN/H_2O (75/25 v/v), H_2O (100%) and MeOH/H_2O (75/25 v/v). 'c.p.' denotes configurational preference and 'np' denotes no preference. Reprinted from reference 80 with permission from John Wiley & Sons, Inc.

Antimony(III)-X-tartrate (Chiral Selector/SO)	Amino Acid (Chiral Selectands/SAs)	Avg. Selectivity ($\alpha_{MS,2-}$ ± SD) (n=5)			Adjusted Selectivity ($\alpha^*_{MS,2-}$ ± SD)		
		Solvent System			Solvent System		
		ACN/H_2O 75/25 (v/v%)	H_2O 100%	MeOH/H_2O 75/25 (v/v%)	ACN/H_2O 75/25 (v/v%)	H_2O 100%	MeOH/H_2O 75/25 (v/v%)
L	D-**Ala** vs L-d4-**Ala**	0.96 ± 0.03	0.94 ± 0.04	0.93 ± 0.04	**1.21 ± 0.12**	**1.06 ± 0.09**	**1.07 ± 0.05**
	L-**Ala** vs L-d4-**Ala**	0.79 ± 0.08	0.89 ± 0.07	0.87 ± 0.02			
	D-**Val** vs L-d8-**Val**	1.24 ± 0.05	1.09 ± 0.04	1.04 ± 0.03	**1.18 ± 0.09**	**1.11 ± 0.06**	**1.08 ± 0.05**
	L-**Val** vs L-d8-**Val**	1.05 ± 0.06	0.99 ± 0.04	0.96 ± 0.03			
	D-**Leu** vs L-d10-**Leu**	0.91 ± 0.05	0.89 ± 0.04	0.87 ± 0.01	**0.92 ± 0.06**	**0.92 ± 0.06**	**0.92 ± 0.03**
	L-**Leu** vs L-d10-**Leu**	0.99 ± 0.04	0.96 ± 0.05	0.95 ± 0.03			
	D-**Phe** vs L-d8-**Phe**	0.98 ± 0.07	0.92 ± 0.03	0.91 ± 0.03	**0.95 ± 0.09**	**0.95 ± 0.04**	**0.91 ± 0.04**
	L-**Phe** vs L-d8-**Phe**	1.03 ± 0.07	0.97 ± 0.02	1.00 ± 0.04			
D	D-**Ala** vs L-d4-**Ala**	1.07 ± 0.06	1.03 ± 0.08	1.12 ± 0.03	**0.94 ± 0.15**	**0.91 ± 0.09**	**1.00 ± 0.09**
	L-**Ala** vs L-d4-**Ala**	1.14 ± 0.16	1.13 ± 0.08	1.12 ± 0.10			
	D-**Val** vs L-d8-**Val**	1.05 ± 0.02	1.00 ± 0.05	1.05 ± 0.03	**1.02 ± 0.04**	**1.00 ± 0.06**	**1.02 ± 0.03**
	L-**Val** vs L-d8-**Val**	1.03 ± 0.03	1.01 ± 0.04	1.03 ± 0.01			
	D-**Leu** vs L-d10-**Leu**	0.88 ± 0.05	0.97 ± 0.03	0.97 ± 0.02	**0.91 ± 0.08**	**0.89 ± 0.04**	**0.91 ± 0.05**
	L-**Leu** vs L-d10-**Leu**	0.96 ± 0.06	1.10 ± 0.03	1.07 ± 0.05			
	D-**Phe** vs L-d8-**Phe**	0.88 ± 0.02	0.95 ± 0.03	1.06 ± 0.04	**090 ± 0.03**	**0.94 ± 0.04**	**0.97 ± 0.04**
	L-**Phe** vs L-d8-**Phe**	0.97 ± 0.02	1.02 ± 0.04	1.09 ± 0.02			

4.4 Conclusions

In summary, we have demonstrated, with a series of single-stage ESI-MS competitive binding experiments, that *D*,*L*-antimony(III)-tartrates and neutral side-chain amino acid binding systems maintain the previously reported proton-assisted enantioselectivity regardless of the common electrospray organic modifiers (ACN and MeOH) added to aqueous solutions. More specifically, it was consistently observed in all three solvent systems that protonated mono-anionic $\{[D, L\text{-}Sb_2\text{-}tar_2][H]\}^-$ species has the capacity to resolve enantiomers of neutral side chain amino acids, whereas the dianionic $\{[D, L\text{-}Sb_2\text{-}tar_2]\}^-$ species was incapable. However, close inspection of the adjusted selectivity values obtained for $\{[D, L\text{-}Sb_2\text{-}tar_2][H]\}^-$ species in three different solvent systems showed small but significant differences. In that respect, the ACN/H_2O (75/25 v/v) solvent system consistently provided the largest adjusted selectivity values compared to the other two systems.

It was also observed that amino acid enantiomers employed in this study showed a general trend of increasing adjusted selectivity in an increasing order of Val ≤ Ala < Leu ≈ Phe. This observation was independent of the solvent system employed. It can be inferred that larger hydrophobic side chains found in Leu and Phe contribute significantly for the chiral discrimination capacity of $\{[D, L\text{-}Sb_2\text{-}tar_2][H]\}^-$ ion species based on steric interactions. However, when the hydrophobic side chains are either moderate or small in size (in the case of Val and Ala), contributions by other interactions such as electrostatic and hydrogen bonding are expected to predominantly control the chiral discrimination capacity of $\{[D, L\text{-}Sb_2\text{-}tar_2][H]\}^-$ ionic species.

CHAPTER 5

GAS PHASE CHIRAL RECOGNITION CAPACITY OF TARTAR EMETIC TOWARDS NEUTRAL SIDE-CHAIN AMINO ACIDS

5.1 Introduction

The ability to glean information on both solvent-mediated solution phase and solvent-free gas phase molecular recognition from a qualitative and quantitative stand-point is a major advantage of ESI-MS. Many reviews on this subject are available, recounting research progress in a general sense [37, 38, 122], as well as those focused more closely on biomacromolecular [159, 161] and stereoselective [10, 12] binding phenomena. General techniques used to directly obtain information relevant to the interactions forged by a system in solution include basic host-guest screening, as well as more rigorous competitive binding and titration experiments. A critical assumption that must be fulfilled for these approaches to provide meaningful information is that equilibrium has been established in solution and is not significantly perturbed during the ESI process. Thus, when an association reaction is kinetically stable on the time-scale of the electrospray process (~ 0.1 – 1 msec) [162], ESI-MS can provide a snap-shot of the distribution of species, and the shift in this distribution as a function of concentration can be probed to obtain quantitative binding information. The results of such experiments should be validated by data from complementary solution phase binding determination methods (e.g. UV/Vis, fluorescence, NMR, capillary electrophoresis, calorimetry [39-41]) when possible.

The isolation of complexes in the gas phase for interrogation by a variety of collisional, photonic, and electronic processes by tandem mass spectrometry provides additional information which can be useful for determination of enantiomeric excess and describing molecular recognition processes. Since isolated ionic complexes are not solvated, such experiments provide details about their relative strength and kinetic stability based solely on

molecular contacts in a low dielectric environment. For example, collision activated dissociation (CAD) [145], where the relative abundance of reactants and products are monitored as a function of activation energy, provides a convenient means for comparing relative gas phase stability. This and other tandem mass spectrometry experiments have both advantages and disadvantages. On one hand, probing the stability of complexes in the absence of solvation can provide new insights into molecular recognition mechanisms, that might not be readily apparent when solvent is present. Such experimental data is particularly amenable for comparison with that from theoretical computations. On the other hand, most molecular recognition processes occur, or are designed to occur, in a solution phase environment. In this case, data from gas phase experiments may be less relevant for studying the system of interest in the context where it will be used.

In general, the coherence between solution phase and gas phase relative affinity data is system dependent. In the case of cinchona alkaloid-carbamates (chiral selectors) and chiral N-blocked amino acids (chiral selectands) enantioselective molecular recognition systems, stripped of solvent, these systems have actually shown a reversal in enantioselective behavior. Chiral selectors, cinchona alkaloid carbamates, have been used primarily for the separation of chiral acids in a variety of liquid phase separation techniques and are available in several commercial HPLC column formats [52]. Early work [55] emphasizes, assignment of cinchona alkaloid carbamates as ion-exchange chiral selectors requiring competing achiral species in solution to tune and modulate their interactions with the enantiomers they are used to separate. In contrast, antimony(III)-*D*- and -*L*-tartrate more or less maintain their enantioselective preference towards a particular enantiomeric configuration in both the solution media and the gas phase, indicating the role of the solvent and/or other solution modifiers to be less pronounced for achieving stereoselective recognition [79]. Antimony(III)- tartrate binuclear complexes have been employed both as mobile phase additives and as immobilized stationary phases for the separation of inorganic and biologically-relevant mixtures of enantiomers [78].

Our group recently reported, antimony(III)- tartrate binuclear complexes have a proton-assisted enantioselective molecular recognition capacity towards the amino acid leucine both in solution media and gas phase [79]. Several extended solution phase-targeted antimony(III) tartrate binding to neutral amino acids, alanine (Ala), valine (Val), and phenylalanine (Phe) (see Figure 4.1 for chiral selectors and selectands employed for this study) were also reported [80]. These studies provided evidence relevant not only to the use of tartar emetic in chiral-separation applications, but also to the interaction of this compound with biologically-relevant compounds. Observation of disparity in enantioselective recognition behavior exhibited by different charge states of antimony(III) tartrate additionally signified the use of ESI-MS for studying such molecular recognition phenomena. However, in order to evaluate the consistency of proton-assisted enantioselective phenomena of antimony(III)-*D*, *L*-tartrates in gas phase with amino acids, alanine (Ala), valine (Val), and phenylalanine (Phe), similar CAD experiments (described in Chapter 3.0) were carried out on the diastereomeric ionic complexes of these amino acids bound dinaionic and protonated-mono anionic antimony(III)-*D*, *L*-tartrates. This chapter shows, antimony(III)-*D*, *L*-tartrates consistently exhibits similar gas-phase proton-assisted enantioselective binding phenomena towards these neutral side-chained amino acids.

5.2 Experimental

All experiments were performed on a Thermo LCQ Deca XP quadrupole ion trap instrument equipped with a conventional ESI source (Thermo-Fisher Scientific, West Palm Beach, FL). Samples were delivered by direct infusion to the source by an in-built syringe pump at 10 µL/min. All bulk solvents (water, methanol (MeOH), acetonitrile (ACN)) used were LC-MS grade and supplied by Mallincrodt-Baker (Phillipsburg, NJ USA).

The sodium salts of antimony(III)-*D*- and -*L*-tartrate as chiral selector hosts were prepared according to a published procedure [85]. Antimony(III) oxide was purchased from Alfa Aesar (Ward Hill, MA USA) and *D*- and *L*-tartrate were from Sigma-Aldrich. Solution-phase host-guest screening experiments were performed by analyzing the relative responses of ionic

complexes formed between the hosts and each of the enantiomerically pure *D*- and *L*-forms of alanine (Ala; Sigma-Aldrich), valine (Val; Fluka), leucine (Leu; Fluka Chemie (Buchs, Switzerland)), and phenylalanine (Phe; Sigma-Aldrich). Each solution was prepared with host and guest present equimolar at 100 μM in 75/25 ACN/water (v/v), including 100 mM formaldehyde (HCHO; Sigma-Aldrich). HCHO was added to the solution to facilitate better signal quality in the negative ionization mode according to a previous report in the literature [143].

For collision activated dissociation (CAD) experiments, the ion abundances of each 1:1 diastereomeric ionic complex of interest were individually optimized. Then, the complex ions were isolated in the ion trap and subjected to collision activated dissociation using a systematic increase in activation voltage (end-cap electrode potential) in regular increments (activation time = 10 msec, q = 0.250). At each voltage, a minimum of 50 scans (where each scan is an average of three microscans) were recorded and averaged to obtain each data point. Each experiment was performed in triplicate.

5.3 Results and Discussion

Figure 5.1A shows a typical mass spectrum of disodium antimony(III)-*L*-tartrate (without selectand present), where the dominant signals correspond to dianionic $[Sb_2\text{-}L\text{-}tar_2]^{2-}$ (m/z = 268.1 Th), sodiated monoanionic $\{[Sb_2\text{-}L\text{-}tar_2][Na]\}^{1-}$ (m/z = 558.9 Th), and protonated monoanionic $\{[Sb_2\text{-}L\text{-}tar_2][H]\}^{1-}$ (m/z = 536.8 Th) ion forms (the m/z of the most abundant signal which corresponds to equivalent contributions from ^{121}Sb (57.2 % natural abundance) and ^{123}Sb (42.8 %) is given). Upon addition of the selectand *D*-leucine, as shown in Figure 5.1B, significant complexation only forms with the dianionic and protonated monoanionic forms. Furthermore, comparing the degree of complexation with different enantiomers of leucine, only the protonated monoanionic form showed appreciable enantioselectivity based on the relative abundance of ionic complexes, whereas the dianionic form provided no significant enantioselectivity [79].

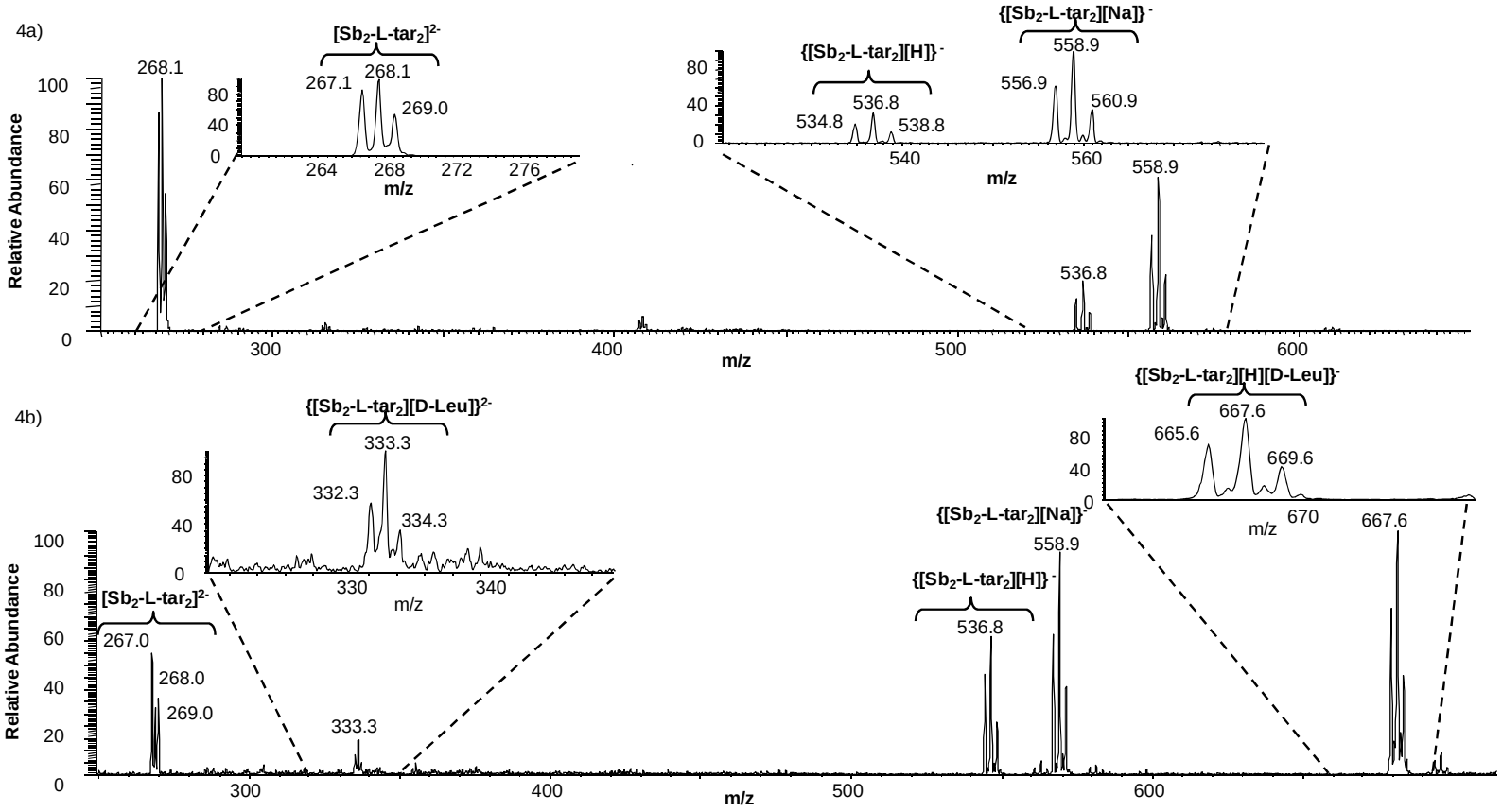

Figure 5.1 Negative ionization mode ESI mass spectra for A) antimony(III)-*L*-tartrate and B) antimony(III)-*L*-tartrate in complex with *D*-Leu. Reprinted from reference 15 with permission from CRC Press, Taylor & Francis Group, LLC.

Gas phase-targeted CAD experiments were performed in a similar manner to that described in Chapter 3. This was performed to check both the proton-assisted enantioselectivity and configurational preference of antimony(III)-tatrate in the gas phase, for a wider range of amino acids. In these gas phase experiments, the stabilities of isolated ionic complexes were monitored as a function of activation voltage [145, 146] (q = 0.250; 30 msec activation time). Figures 5.2, 5.3 and 5.4 represent the CAD plots generated for the diastereomeric ionic complexes of antimony(III)-*D*,*L*-tartrates associating to amino acids, Ala, Val and Phe, respectively. A consistent pattern is observed when these plots are compared to the CAD plots observed for diastereomeric ionic complexes of antimony(III)-*D*,*L*-tartrates associating to Leu (Figure 3.8) . For CAD of the protonated monoanionic complexes, configurational preferences equivalent to the solution phase data were observed, with a cross-chiral relationship in going from antimony(III)-*L*-tartrate to antimony(III)-*D*-tartrate. Also consistent with previous results, dissociation of the dianionic forms revealed no enantioselective discrimination. The applied end-cap voltage values required to dissociate 50% of the precursor ion complexes (V_{50}) were obtained from the CAD plots of protonated monoanionic diastereomeric ionic complexes. ΔV_{50} values were then calculated (with error propagation) and compared in Table 5.1. The differences in V_{50} values which are indicative of $\Delta(\Delta G)$ for the dissociation of the diastreomeric complexes provide a means to calculate enantioselectivity values (α_{CAD}) in gas phase. Calculated enantioselectivity values (α_{CAD}) of the protonated monoanionic complexes indicate, quantitative cross-chiral relationships in going from antimony(III)-*L*-tartrate to antimony(III)-*D*-tartrate for all amino acids.

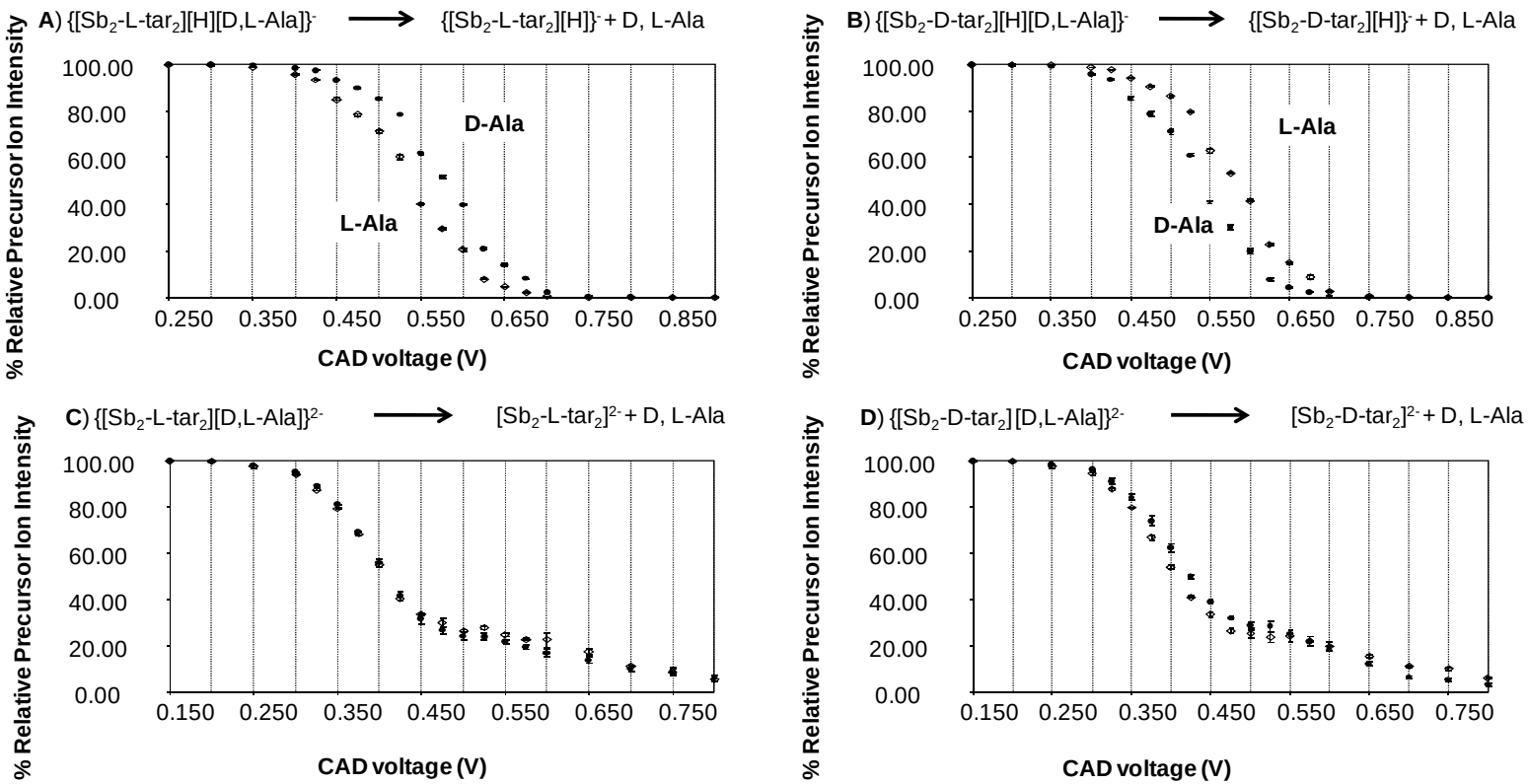

Figures 5.2 Collision activated dissociation of protonated monoanionic (A, B) and dianionic (C, D) diastereomeric complexes between antimony(III)-*D*, *L*-tartrates and alanine.

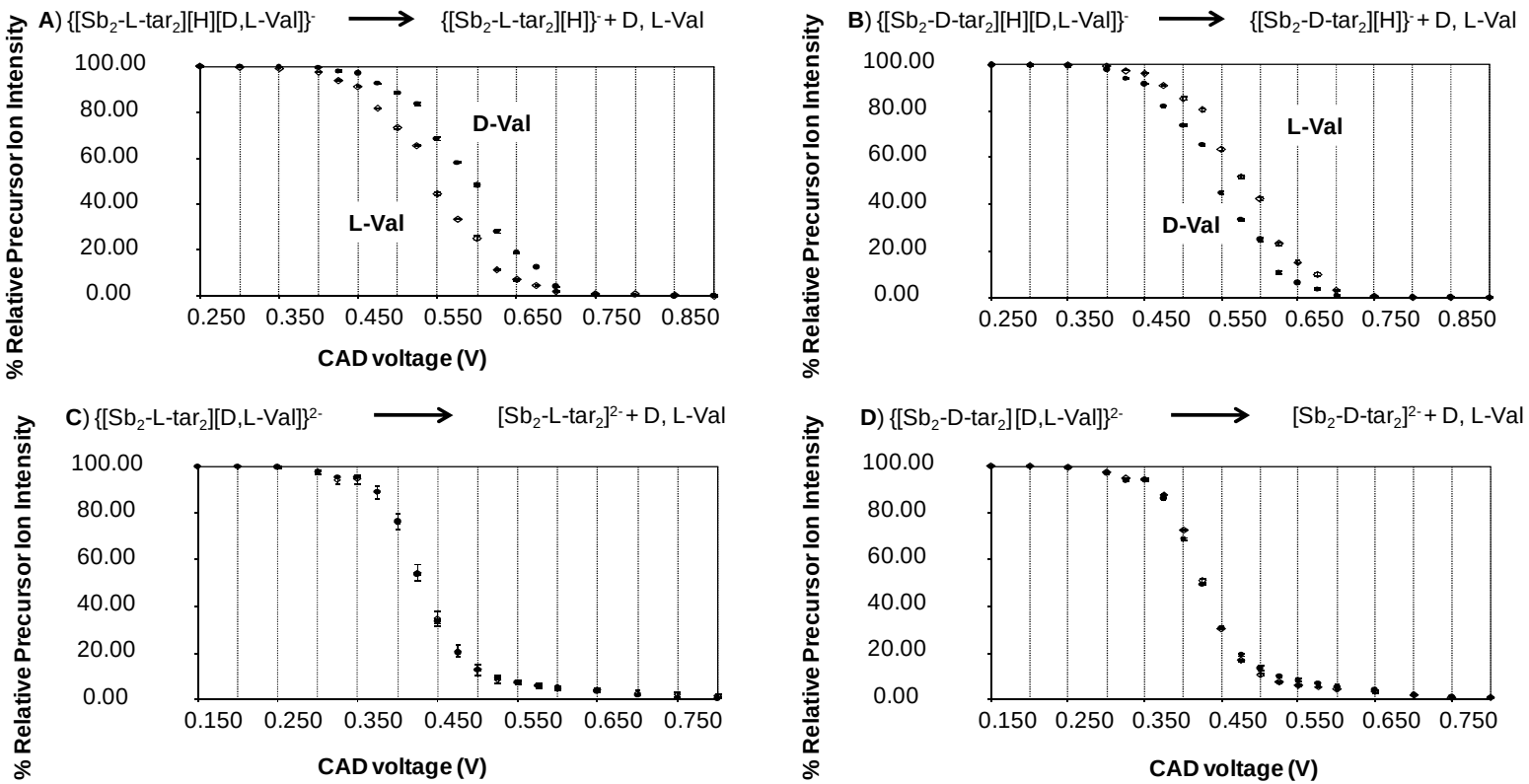

Figures 5.3 Collision activated dissociation of protonated monoanionic (A, B) and dianionic (C, D) diastereomeric complexes between antimony(III)-*D*, *L*-tartrates and valine.

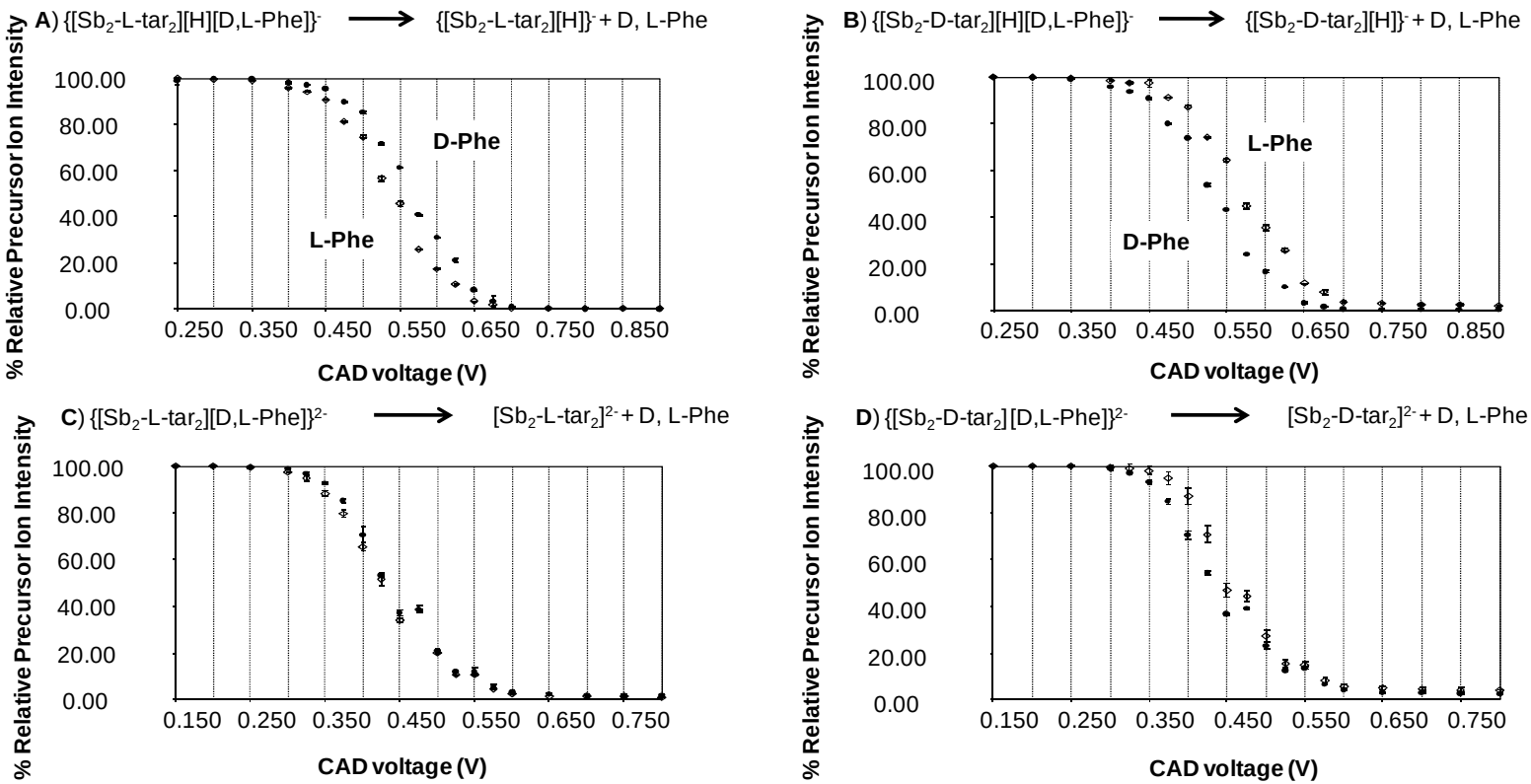

Figures 5.4 Collision activated dissociation of protonated monoanionic (A, B) and dianionic (C, D) diastereomeric complexes between antimony(III)-*D*, *L*-tartrates and phenylalanine.

Table 5.1 V_{50} and enantioselectivity values recorded for dissociation of protonated monoanionic diastereomeric complexes by collision threshold dissociation

Selector (SO)	Selectand (SA)	V_{50} ± SD [n = 3] / V	Selectivity α_{CTD} (ΔV_{50}) ± SD
$[Sb_2\text{-L-tar}_2][H^+]$	D-Ala	0.750 ± 0.005	0.040 ± 0.007 (D)
	L-Ala	0.790 ± 0.005	
	D-Val	0.760 ± 0.005	0.040 ± 0.007 (D)
	L-Val	0.800 ± 0.005	
	D-Leu	0.575 ± 0.005	0.040 ± 0.007 (D)
	L-Leu	0.615 ± 0.005	
	D-Phe	0.735 ± 0.005	0.025 ± 0.007 (D)
	L-Phe	0.760 ± 0.005	
$[Sb_2\text{-D-tar}_2][H^+]$	L-Ala	0.785 ± 0.005	0.040 ± 0.007 (L)
	D-Ala	0.750 ± 0.005	
	L-Val	0.790 ± 0.005	0.040 ± 0.007 (L)
	DVal	0.750 ± 0.005	
	L-Leu	0.610 ± 0.005	0.040 ± 0.007 (L)
	D-Leu	0.570 ± 0.005	
	L-Phe	0.770 ± 0.005	0.035 ± 0.007 (L)
	D-Phe	0.735 ± 0.005	

These gas phase-targeted molecular recognition data indicates that either a fundamental difference exists in the structural and functional arrangement of stereoselective recognition motifs between the dianionic or protonated monoanionic forms, or that some other unforeseen factor is contributing to the decreased stereoselective performance provided by the dianionic form. The fact that some of the CAD plots for the dissociation of the dianionic diastereomeric complexes do not follow a clean sigmoidal shape (e.g. kinetic shifts were observed as seen in Figures 5.2C, 5.2D and Figures 5.4C, 5.4D) may lend support to the latter notion. Further work is required to elucidate this aspect, however these data provide some insight into where those efforts might be channeled.

5.4 Conclusions

In summary, we have demonstrated, with a series of gas phase CAD experiments, that antimony(III)- *D*,*L*-tartrates and neutral side-chain amino acid binding systems maintain the previously reported proton-assisted enantioselectivity in gas phase. More specifically, it was consistently observed in all cases, protonated mono-anionic {[*D*, *L*-Sb_2-tar_2][H]}$^-$ species has the capacity to resolve enantiomers of neutral side chain amino acids, whereas the dianionic {[*D*, *L*-Sb_2-tar_2]}$^-$ species was incapable. From the results of both solution phase [79, 80] and gas phase data [79], it can be speculated that the protonated monoanionic form of antimony(III)-tartrate is mainly responsible for its observed enantioselective discrimination in various applications. Importantly, this information would be difficult to ascertain without the use of mass spectrometric experiments as described in this work and previously reported work [79, 80]. This hypothesis is supported also by the results of Martin et al. [69] where the resolution of Ru(II) tris-diimine complexes was achieved at a pH of 2.5 using antimony(III) tartrate as a chiral selector in the run buffer. These conditions would favor the presence of the protonated monoanionic form (and possibly even a doubly-protonated neutral form). The mass spectrometric experiments also reveal the consistency of configurational preference in the presence and absence of solvent, contrary to the cinchona alkaloid carbamate experiments. Thus, for the protonated monoanionic form of antimony tartrate, the stereochemical arrangement of the associates that give rise to enantioselective binding appear to be less influenced by the presence of solvent. Whether the magnitude of the enantioselectivity can be tuned or optimized based on changing the percent organic, ionic strength, or pH of the solution remains to be further investigated. In addition to this, in future experiments we will also investigate the effects of different activation conditions in CAD experiments to gain more insight into the kinetics of the dissociation process. Through such experiments, it may be possible to learn more about apparent kinetic shifts observed at high activation voltages for the dianionic complexes in the present experiments. Theoretical computations and molecular modeling will

also be pursued to provide a more comprehensive description of possible structural and functional differences between the different ion forms.

CHAPTER 6

SOLVENT MOLECULES UNDERGO HOMOLYTIC CLEAVAGE AND RADICAL RECOMBINATION PROCESSES DURING NEGATIVE-MODE ELECTROSPRAY IONIZATION: ADDUCT FORMATION WITH ANTIMONY(III)-TARTRATE DIANION

6.1 Introduction

The capability to ionize intact molecules from a flowing liquid with no or minimal fragmentation has made the electrospray ionization (ESI) technique a versatile tool for mass spectrometry (MS) [32, 33]. Low sample consumption, high sensitivity, and rapid analysis times have made ESI-MS highly attractive compared to other analytical methods. Compared to the applications performed using positive-ionization mode ESI-MS, negative-ionization mode applications have been more limited [163]. This is due, in part, to instabilities in ionization, which can arise from electron- or corona-discharge at the tip of the ESI spray capillary. However, the utility of negative-ionization mode ESI-MS to detect negatively-charged ions is significantly increasing, especially in areas such as lipidomics and metabalomics [164-167], among others, where acidic analytes are prevalent. In conjunction with these efforts, there is a need to provide means through which high quality negative-ionization mode ESI-mass spectra can be generated.

To produce improved negative-ionization mode ESI mass spectra, researchers have used sharpened spray capillary tips [168], or they have incorporated electron scavenger gases such as O_2 [169] and SF_6 [170]. These modifications reduce the incidence of corona discharge. Incorporation of additives into electrosprayed solutions, such as 2,2,2-trifluoroethanol, formaldehyde, and weak acids, can also provide enhanced negative-ionization mode ESI mass spectra of various analytes [143], as well as noncovalent complexes [79]. Cole and co-workers have contributed substantially to a more refined understanding of negative-ionization mode ESI-

MS [33, 163, 164]. For example, they have shown that chlorinated solvents are also capable of suppressing corona discharge to produce higher quality mass spectra.

For effective modifications of various experimental conditions to further advance the applicability of ESI-MS for monitoring negatively-charged ions, a thorough understanding of the ionization process is required. Though many indirect pieces of evidences have been reported, the direct observation of chloride ions by Cole and co-workers, produced during ESI of chlorinated solvents, provided crucial insight [33, 163, 171]. Chloride ions were proposed to be generated by an electron capture process. If chlorinated solvents are subject to such processes, it could be immediately questioned: To what types of processes are common ESI solvents, such as water (H_2O), acetonitrile (CH_3CN) and methanol (CH_3OH) subjected? For a complete understanding of the ionization mechanism, it would be desirable to have a greater understanding of the fate and participation of high abundance solvent constituents in the ESI process.

The formation of pseudomolecular ions comprised of adducts between various ionic species and unmodified solvent molecules has been widely reported [30, 172]. To our knowledge, direct evidence for the presence of neutral solvent reaction products, generated from solvents such as H_2O, CH_3CN and CH_3OH, during ESI has not been previously reported. Of course, targeted monitoring of active or inactive neutral species with ESI-MS is difficult. This is due to the rapid rate of the ESI process, and, because of their neutrality, no responses would be expected to be recorded by the mass spectrometer. Nevertheless, more insight into the ESI mechanism, specifically the role and fate of solvents, could be gained if an ionic species were capable of associating with neutral solvent reaction intermediates or products, so that they could be observed as adduct ions in the mass spectra.

Antimony(III)-*L*-tartrate or *L*-tartrato(4-)-antimony(III)-bridged complexes, drew our attention in recent years, because of their turbulent history as a remedial indication for diseases like typhoid, bronchitis, pneumonia, and various parasite infections [65]. Though they have also

been shown to be useful as a chiral selector for separation of enantiomers in liquid phase separations and through diastereomeric salt formation [78], little is known about their detailed enantioselective and biomolecular recognition mechanism. In order to obtain more insight into their enantioselective character, we investigated the solution and gas-phase binding of antimony(III)-*D*,*L*-tartrates to several neutral amino-acids using ESI-MS and MS/MS [15, 79, 80]. While these were not the first studies of antimony(III)-tartrate recognition by ESI-MS [136, 137], they did reveal, for the first time, the presence of an enantioselective recognition phenomenon, whereby different charge states of the chiral selector showed different binding selectivities towards neutral amino acid enantiomers.

While further investigation of enantioselective recognition phenomena for antimony(III)-tartrate continues, this manuscript reports a rather serendipitous finding, which arose from those previous studies [15, 79, 80]. Detailed investigation of negative-ionization mode ESI-mass spectra have allowed us to show that the dianionic antimony(III)-tartrate ($[Sb_2\text{-}tar_2]^{2-}$) complex is capable of adducting to neutral solvent reaction products that are generated during the negative-ionization mode electrospray process. By carrying out a systematic variation of solvent composition and ionization parameters, new experimental insight regarding the participation of solvent molecules during negative-ionization mode ESI was revealed.

When disodium antimony(III)-tartrate ($Na_2[Sb_2\text{-}tar_2]$) salt solutions, in H_2O/CH_3CN and H_2O/CH_3OH solvent systems, were analyzed in negative-ionization mode ESI-MS, adducted ions between antimony(III)-tartrate dianion and unusual solvent reaction intermediates were observed in respective mass spectra. However, when the spray voltage was systematically lowered, the relative intensity of the adducted ions diminished. This observation suggests that the solvent reaction products are produced during negative-ionization mode ESI, and that they adduct to the dianionic antimony(III)-tartrate ($[Sb_2\text{-}tar_2]^{2-}$). Changes in relative ion intensities of the adducted ions were also monitored as the composition of the solvent system was systematically varied. The identities of the adducted ions were further confirmed by carrying out

experiments using deuterated solvent systems. Consequently, experimental evidence provided herein prompts a hypothesis that neutral solvent reaction-product species are produced by homolytic cleavage of solvent molecules during ESI. This process is proposed to be initiated by high-energy electrons, available at the highly negatively-charged spray capillary, to produce radical species. The radical species then recombine and adduct to the antimony(III)-tartrate to produce a series of quasi-molecular ions which can be detected by the mass spectrometer.

6.2 Neutral reaction products generated from acetonitrile (CH_3CN) and water (H_2O) solvent systems

Disodium antimony(III)-tartrate was synthesized in-house, as previously described [85], and was analyzed by negative-ionization mode ESI-MS (100 µM, in CH_3CN/H_2O 75/25 (v/v)). All experiments were carried out using a Thermo LCQ Deca XP ion trap instrument (Thermo-Fisher Scientific, Inc., San Jose, CA, USA) equipped with a conventional electrospray ion source. Changes in mass spectral intensities of solvent product adducts were monitored as a function of spray capillary voltage (-3.5 kV to -5.5 kV; in 0.5 kV increments) (Figure 6.1; 75/25 CH_3CN/H_2O (v/v)). Along with the doubly charged dianion, $[^{121,123}Sb_2\text{-}tar_2]^{2-}$ (268.1 Th), two prominent ion signals at 285.0 Th and 307.9 Th (initially unobserved with spray voltage of – 3.5 kV; Figure 6.1A) began to emerge, and increased in intensity, as the negative spray voltage was increased. Two other less prominent peaks were also observed to emerge at 276.1 Th and 292.0 Th. Interestingly, all these newly emerging peaks carried the isotopic pattern of two Sb(III) ions (^{121}Sb, 57.36% and ^{123}Sb, 42.64% natural abundance). The isotopic peak separations of 1 Th were also characteristic of the dianionic species, $[Sb_2\text{-}tar_2]^{2-}$, which suggested, these new species were adducts of $[Sb_2\text{-}tar_2]^{2-}$. The m/z values prompted us to assign the more prominent peaks at 285.0 Th and 307.9 Th as $\{[Sb_2\text{-}tar_2][H\text{-}O\text{-}O\text{-}H]\}^{2-}$ and $\{[Sb_2\text{-}tar_2][NC\text{-}CH_2\text{-}CH_2\text{-}CN]\}^{2-}$, respectively. Less prominent peaks at 276.1 Th and 292.0 Th were assigned as $\{[Sb_2\text{-}tar_2][O]\}^{2-}$ and $\{[Sb_2\text{-}tar_2][HO\text{-}CH_2\text{-}OH]\}^{2-}$, respectively.

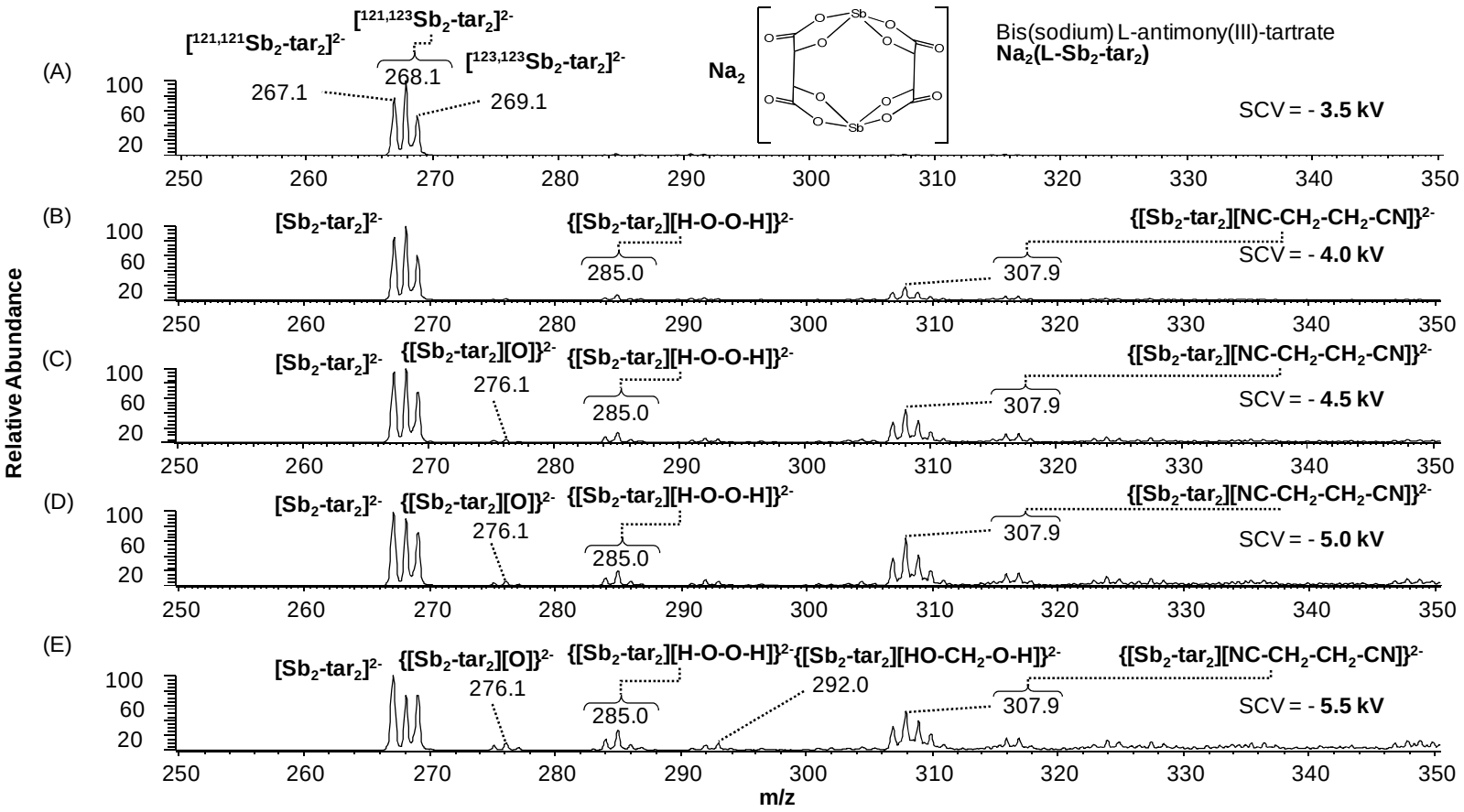

Figure 6.1 Negative-ionization mode ESI mass spectra of $Na_2[Sb_2\text{-}tar_2]$ (100 μM) in CH_3CN/H_2O (75/25 v/v) at different spray capillary voltages (SCV): A) -3.5 kV, B) -4.0 kV, C) -4.5 kV, D) -4.0 kV and E) -5.5 kV. Reprinted from reference 81 with permission from American Chemical Society.

The assignment of prominent peaks presumed that neutral species [H-O-O-H] and [NC-CH_2-CH_2-CN] were generated from solvent molecules during negative-ionization mode ESI. To support this assignment, additional experiments were carried out to generate and compare mass spectra for $Na_2[Sb_2\text{-}tar_2]$ (100 µM) in a series of deuterated and nondeuterated solvent systems: A) CH_3CN/H_2O 75/25 (v/v); B) CD_3CN/H_2O 75/25 (v/v); C) CH_3CN/D_2O 25/75 (v/v); and D) CD_3CN/D_2O 25/75 (v/v) (see Figure 6.2; spray capillary set at -5.0 kV). It was clearly observed that a change in solvent system from CH_3CN/H_2O 75/25 (v/v) to CD_3CN/H_2O 75/25 (v/v), or from CH_3CN/D_2O 25/75 (v/v) to CD_3CN/D_2O 25/75 (v/v), shifted the peak position for the signal at 307.9 Th to 309.9 Th. The signal at 309.9 Th can be assigned to the ionic species, $\{[Sb_2\text{-}tar_2][NC\text{-}CD_2\text{-}CD_2\text{-}CN]\}^{2-}$. This confirms that the neutral species [NC-CH_2-CH_2-CN] is generated by CH_3CN, and is associated to the dianion $[Sb_2\text{-}tar_2]^{2-}$, during negative-ionization mode ESI. Similarly, when the solvent system was composed of D_2O (75%), three $[Sb_2\text{-}tar_2]^{2-}$ dianion-bound neutral species, [D-O-O-D], [H-O-O-D], and [H-O-O-H], replaced the signal observed solely at 285.0 Th in the absence of deuterated solvent (compare Figure 6.1C, 6.1D with 6.1A, 6.1B). The signal at 286.0 Th, assigned to the ionic species $\{[Sb_2\text{-}tar_2][D\text{-}O\text{-}O\text{-}D]\}^{2-}$, confirms that [D-O-O-D] is produced during negative-ionization mode ESI of D_2O. It is prudent to note here that D_2O is extremely hygroscopic and is prone to contamination with H_2O, either during preparation of solutions or during ESI-MS analysis. This fact is believed to be responsible for the additional ionic responses at 285.5 Th and 285.0 Th, which were assigned as the ions, $\{[Sb_2\text{-}tar_2][D\text{-}O\text{-}O\text{-}H]\}^{2-}$ and $\{[Sb_2\text{-}tar_2][H\text{-}O\text{-}O\text{-}H]\}^{2-}$, respectively, when 75% D_2O was incorporated into the experiment.

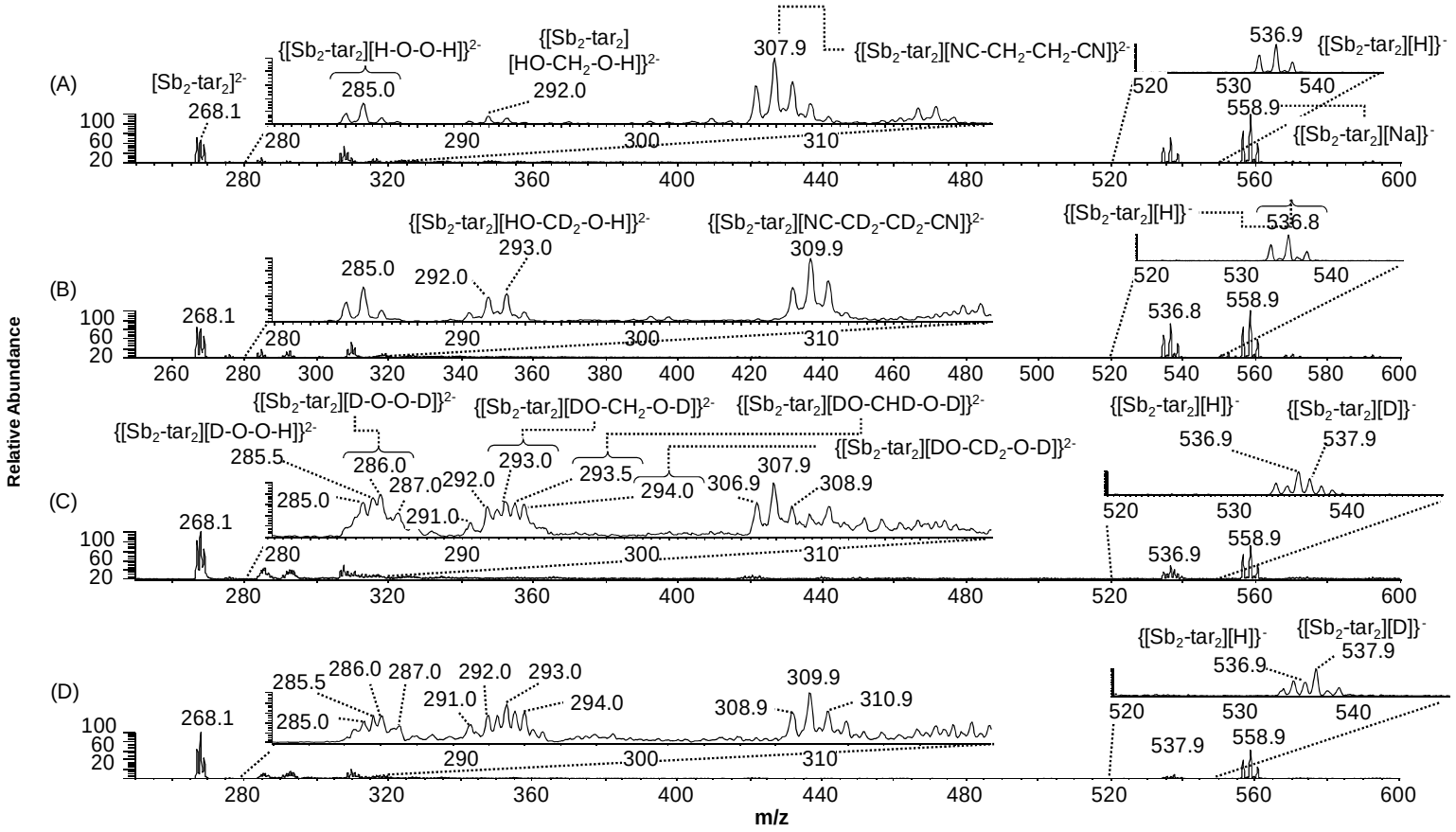

Figure 6.2 Negative mode ESI mass spectra obtained by direct infusion (20 µL/min) of $Na_2[Sb_2\text{-}tar_2]$ (100 µM) in A) CH_3CN/H_2O 75/25 (v/v), B) CD_3CN/H_2O 75/25 (v/v), C) CH_3CN/D_2O 25/75 (v/v) and D) CD_3CN/D_2O 25/75 (v/v), with spray capillary voltage at -5.0 kV. Reprinted from reference [81] with permission from American Chemical Society.

Observation of peaks at 292.0 Th, 293.0 Th, 293.5 Th and 294.0 Th, which are assigned as $\{[Sb_2\text{-}tar_2][HO\text{-}CH_2\text{-}OH]\}^{2-}$, $\{[Sb_2\text{-}tar_2][HO\text{-}CD_2\text{-}OH]\}^{2-}$ or $\{[Sb_2\text{-}tar_2][DO\text{-}CH_2\text{-}OD]\}^{2-}$, $\{[Sb_2\text{-}tar_2][DO\text{-}CHD\text{-}OD]\}^{2-}$ or $\{[Sb_2\text{-}tar_2][HO\text{-}CD_2\text{-}OD]\}^{2-}$ and $\{[Sb_2\text{-}tar_2][\ DO\text{-}CD_2\text{-}OD]\}^{2-}$, respectively, indicates the chaotic environment in the ESI source. Consistent observation of the signal at 276.1 Th, which was dianionic (according to the isotope pattern and peak separation) and separated by 8 m/z units from the molecular ion at 268 Th ($[Sb_2\text{-}tar_2]^{2-}$), suggests that active oxygen-radical species (Figure 6.1 and Figure 6.2) are also generated and associated to $[Sb_2\text{-}tar_2]^{2-}$ during the experiment.

To further confirm that dianionic $[Sb_2\text{-}tar_2]^{2-}$ binds to hydrogen peroxide, an equimolar (100 µM) solution of $Na_2[Sb_2\text{-}tar_2]$ and hydrogen peroxide (H_2O_2) in CH_3CN/H_2O 75/25 (v/v) was analyzed. The spray voltages were held at reduced values (– 3.0 kV and – 3.5 kV; compare Figure 6.3A with 6.3B and 6.3C) to limit response from ESI-generated adducts (see Figure 6.1A). Observation of the expected signal at 285.0 Th further confirmed that neutral H_2O_2 binds to $[Sb_2\text{-}tar_2]^{2-}$. A similar set of experiments was performed to confirm generation and adduction of a succinonitrile ($NCCH_2CH_2CN$) solvent product. An equimolar (100 µM) solution of $Na_2[Sb_2\text{-}tar_2]$ and succinonitrile ($(CH_2CN)_2$) in CH_3CN/H_2O 75/25 (v/v) was analyzed. The spray voltages were again held at reduced values (– 3.0 kV and – 3.5 kV; compare Figure 6.4A with 6.4B and 6.4C) to limit response from ESI-generated adducts. The adduction of succinonitrile by the antimony-tartrate dianion was consistent with that observed for hydrogen peroxide. At this point, no speculation is made about the specificity of such interactions, although further work is underway to investigate this aspect experimentally and computationally.

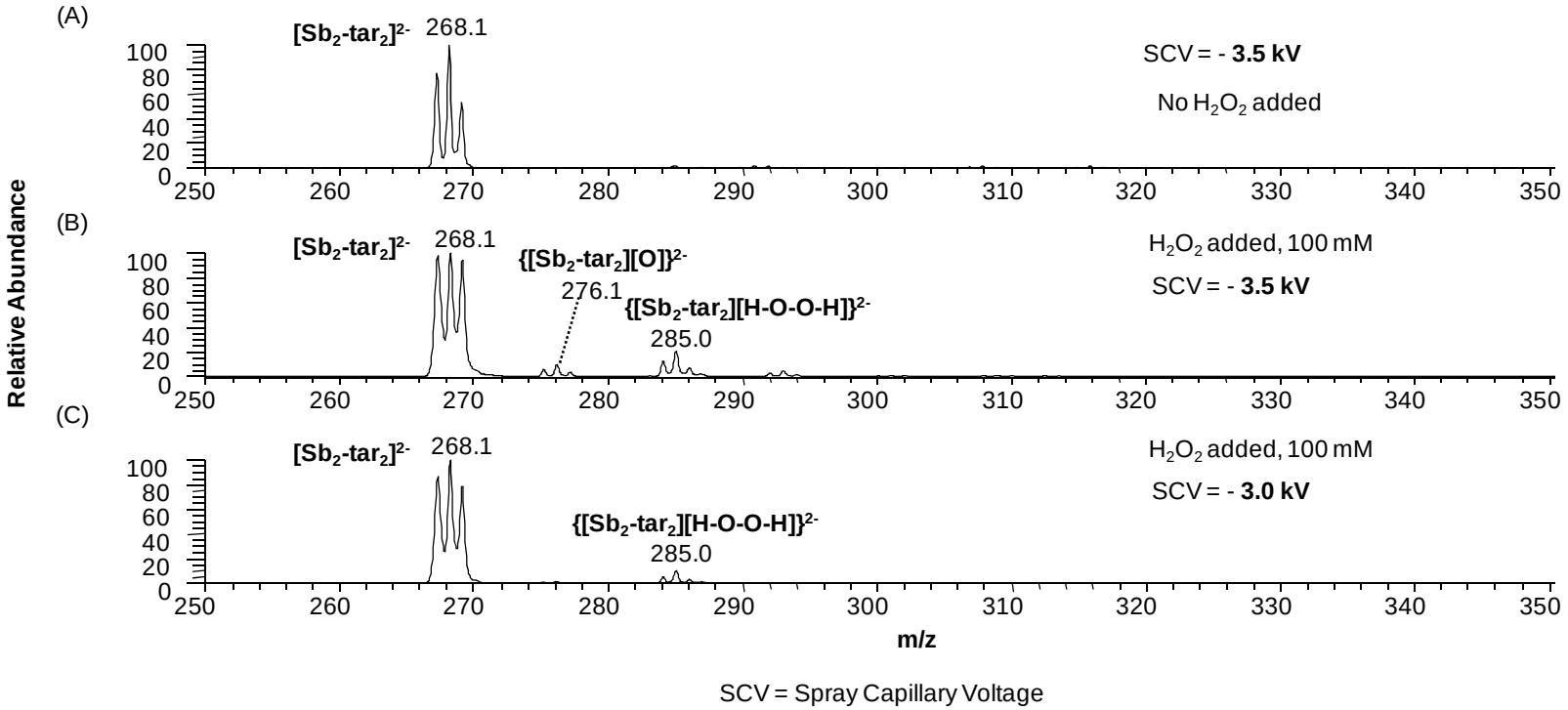

Figure 6.3 Negative mode ESI mass spectra obtained by direct infusion (5 µL/min) of $Na_2[Sb_2\text{-}tar_2]$ (100 µM) in CH_3CN/H_2O 75/25 (v/v): A) no H_2O_2 added at – 3.5 kV SCV; B) H_2O_2 added (100 µM) at – 3.5 kV SCV; and C) H_2O_2 added (100 µM) at – 3.0 kV SCV. Reprinted from reference 81 with permission from American Chemical Society.

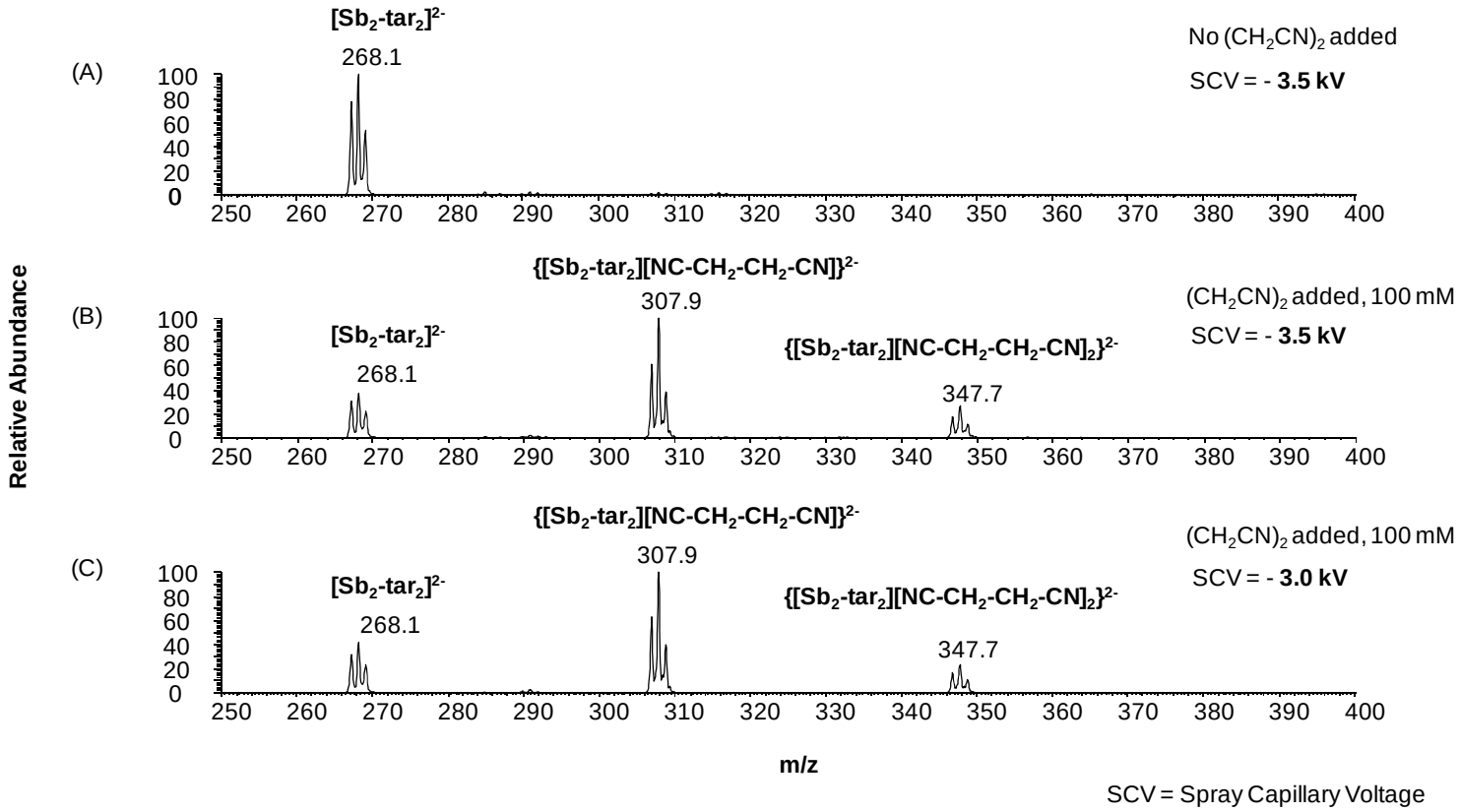

Figure 6.4 Negative mode ESI mass spectra obtained by direct infusion (5 µL/min) of $Na_2[Sb_2\text{-}tar_2]$ (100 µM) in CH_3CN/H_2O 75/25 (v/v): A) no $(CH_2CN)_2$ added at – 3.5 kV SCV; B) $(CH_2CN)_2$ added (100 µM) at – 3.5 kV SCV; and C) $(CH_2CN)_2$ added (100 µM) at – 3.0 kV SCV. Reprinted from reference 81 with permission from American Chemical Society.

To monitor how solvent composition affects the production of these neutral solvent products, negative-ionization mode ESI-MS analysis of $Na_2[Sb_2\text{-}tar_2]$ (100 µM) in three CH_3CN/H_2O solvent compositions was performed: A) 25/75 (v/v); B) 50/50 (v/v); and C) 75/25 (v/v) (Figure 6.5; spray capillary -4.0 kV). Figures 6.5A, 6.5B and 6.5C clearly illustrate that the response for 285.0 Th (H_2O_2 adduct) increases as the volume percent of H_2O increases, and that the response for 307.9 Th (NC-CH_2-CH_2-CN adduct) increases as the volume percent of CH_3CN increases. The effect of spray voltage for each of these solvent systems was also monitored. The average normalized adduct-ion abundances (calculated from five trials and normalized to the abundance of the molecular ion at 268.1 Th) for signals at 285.0 Th and 307.9 Th were plotted as a function of spray voltage. Figures 6.5D, 6.5E and 6.5F clearly show the increase of adduct-ion responses as the spray voltage is increased. This indicates that a greater number of neutral solvent intermediates, which are associated to $[Sb_2\text{-}tar_2]^{2-}$, are produced when negative ESI potentials are increased.

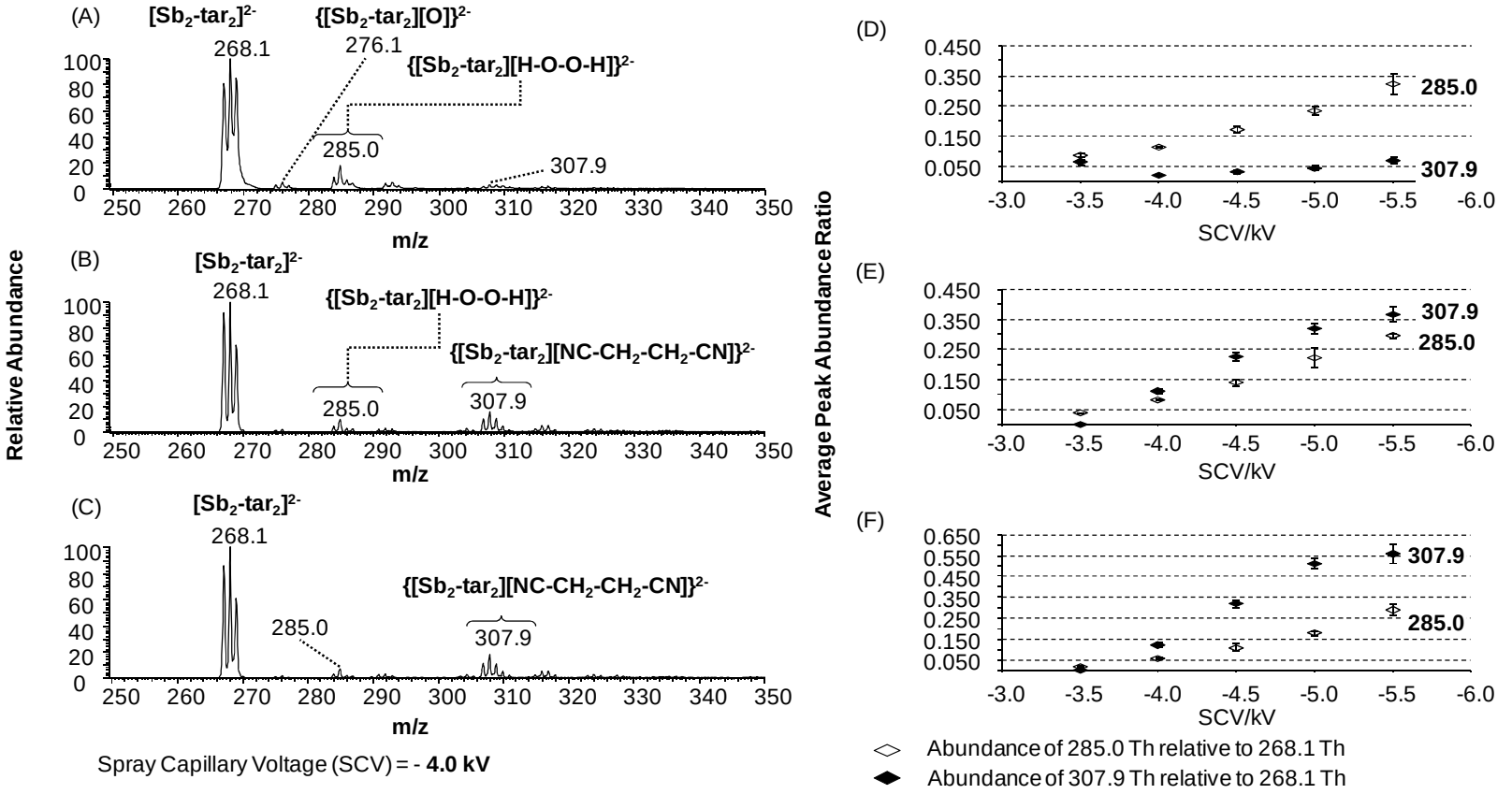

Figure 6.5 Negative-ionization mode ESI mass spectra of $Na_2[Sb_2\text{-}tar_2]$ (100 μM) in A) CH_3CN/H_2O 25/75 (v/v), B) CH_3CN/H_2O 50/50 (v/v) and C) CH_3CN/H_2O 75/25 at a spray capillary voltage (SCV) of -4.0 kV, and plots of normalized adduct ion response vs. SCV for peaks at 268.1 Th and 307.9 Th in solutions of D) CH_3CN/H_2O 25/25 (v/v), E) CH_3CN/H_2O 50/50 (v/v), and F) CH_3CN/H_2O 75/25. Reprinted from reference 81 with permission from American Chemical Society.

6.3 Neutral reaction products generated from methanol (CH_3OH) and water (H_2O) solvent systems

A similar picture was revealed in the presence of another ESI-friendly solvent, methanol. When negative-ionization mode ESI-mass spectra of $Na_2[Sb_2\text{-}tar_2]$ (100 µM) in CH_3OH/H_2O 75/25 (v/v) were generated as a function of spray capillary voltage (see Figure 6.6), two new adduct ion signals at 285.0 Th and 291.9 Th were observed. A low intensity signal at 276.1 Th was also consistently observed to emerge at high voltages. Prominent ions were assigned as adduct ions of $[Sb_2\text{-}tar_2]^{2-}$ with [H-O-O-H] and [H-O-CH_2-O-H]. The signal at 276.1 Th was assigned as $\{[Sb_2\text{-}tar_2][O]^{2-}\}$, as before. In order to confirm these assignments, negative mode ESI-MS analysis of $Na_2[Sb_2\text{-}tar_2]$ (100 □M) in CD_3OH/H_2O 75/25 (v/v) was performed (see Figure 6.7; spray capillary -5.5 kV). A signal at 292.9 Th was observed and assigned as the adduct ion $\{[Sb_2\text{-}tar_2][HO\text{-}CD_2\text{-}OH]\}^{2-}$, which confirmed the previous assignment for the signal at 291.9 Th. The solvent composition effects on the responses at 285.0 Th and 291.9 Th were also monitored for CH_3OH/H_2O solvent systems. Figures 6.8A, 6.8B and 6.8C illustrate the response intensity variation of peaks at 285.0 Th and 291.9 Th as the CH_3OH/H_2O solvent composition is varied (at a constant spray capillary voltage). Additionally, an observed increase of adduct-ion responses (285.0 Th and 291.9 Th) with an increase in spray voltage was consistent with what was observed for CH_3CN solvent systems.

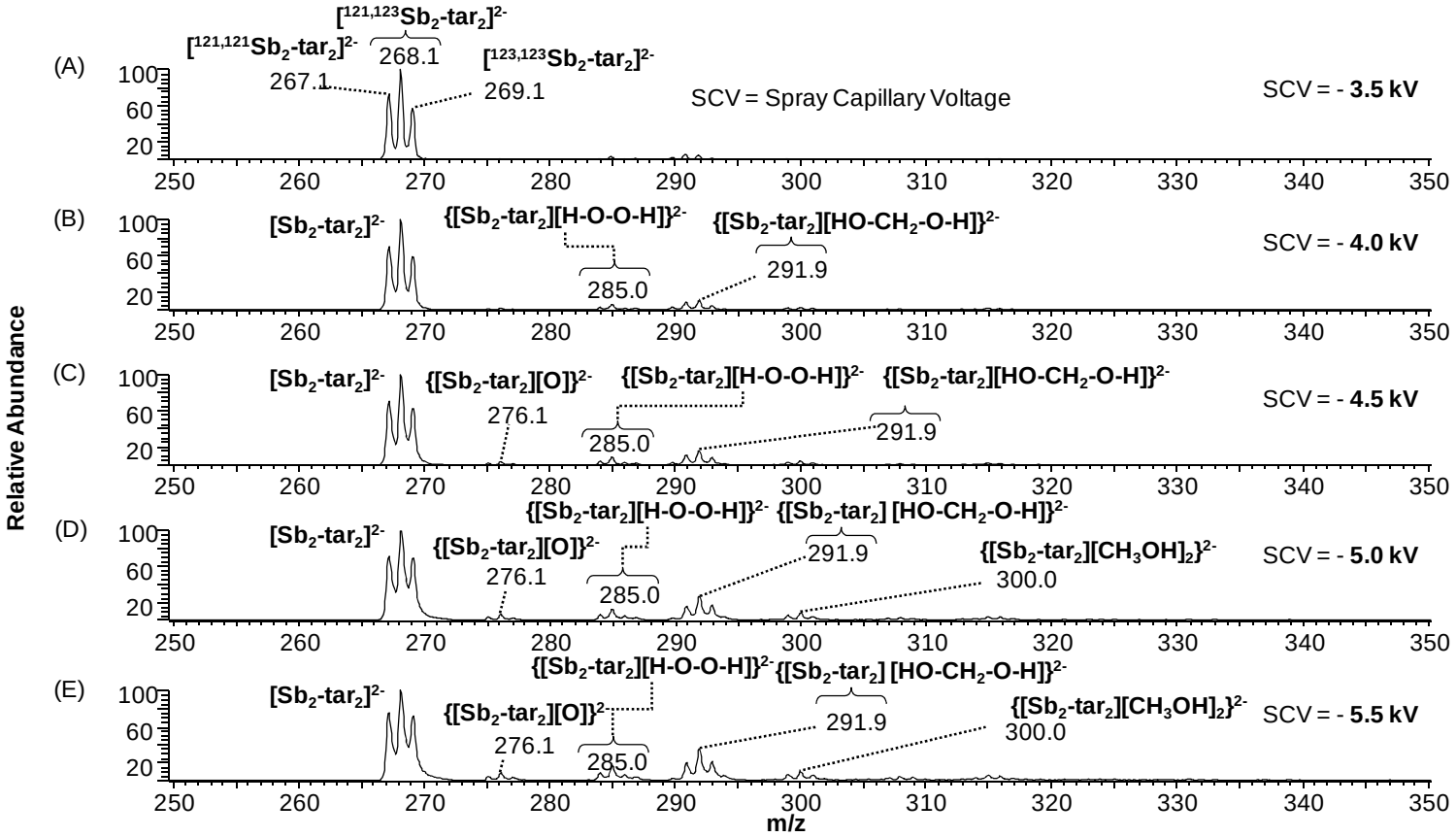

Figure 6.6 Negative mode ESI mass spectra obtained by direct infusion (10 µL/min) of $Na_2[Sb_2\text{-}tar_2]$ (100 µM) in CH_3OH/H_2O (75/25 v/v) at different spray capillary voltages (SCVs): A) -3.5 kV; B) -4.0 kV; C) -4.5 kV; D) -4.0 kV; and E) -5.5 kV. Reprinted from reference 81 with permission from American Chemical Society.

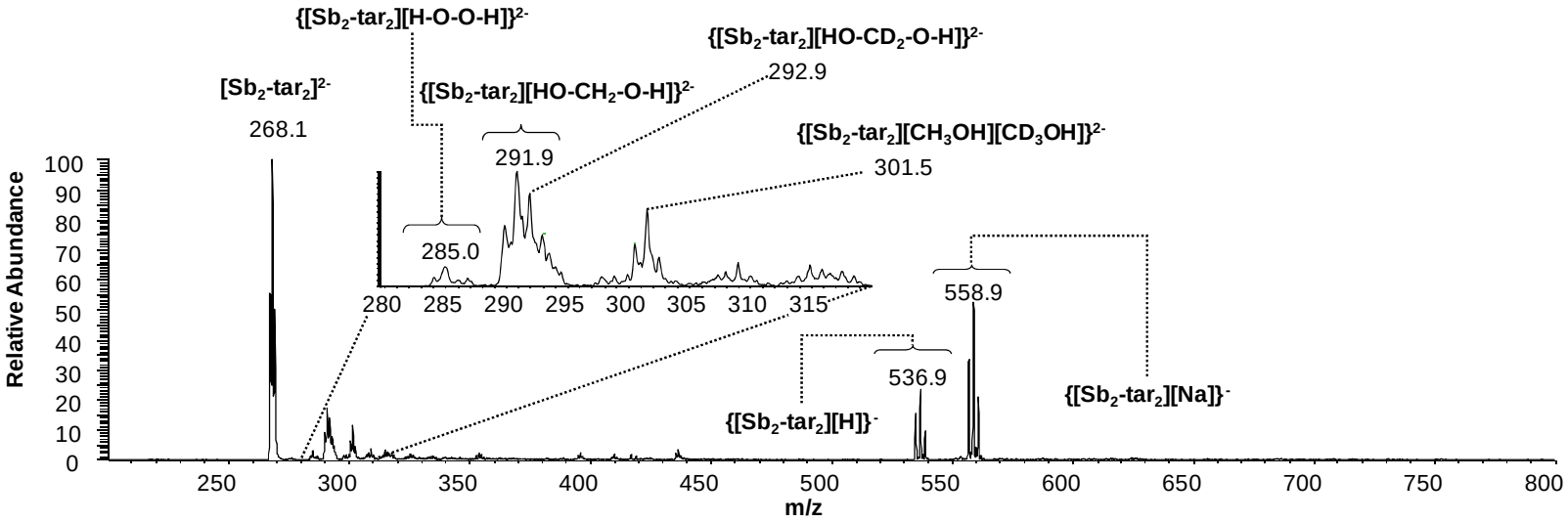

Figure 6.7 Negative mode ESI mass spectra obtained by direct infusion (70 µL/min) of $Na_2[Sb_2\text{-}tar_2]$ (100 µM) in CD_3CN/H_2O 75/25 (v/v), keeping the spray capillary voltage at -5.5 kV. Reprinted from reference 81 with permission from American Chemical Society.

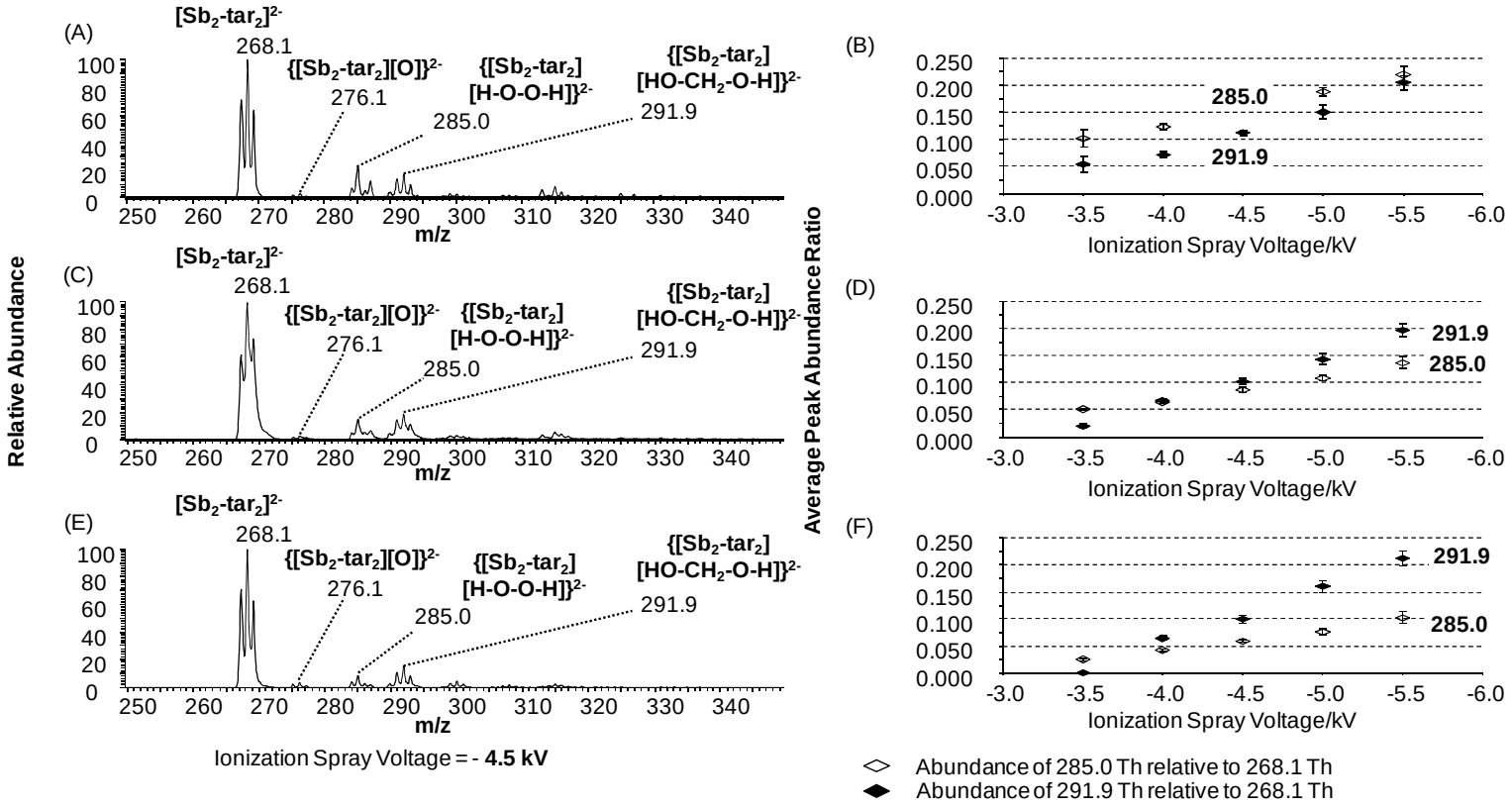

Figure 6.8 Negative-ionizaton mode ESI mass spectra of $Na_2[Sb_2\text{-}tar_2]$ (100 μM) in A) CH_3OH/H_2O 25/75 (v/v), B) CH_3OH/H_2O 50/50 (v/v) and C) CH_3OH/H_2O 75/25 at a spray capillary voltage (SCV) of -4.5 kV, and plots of normalized adduct ion response vs. SCV for peaks at 285.0 Th and 291.9 Th in solutions of D) CH_3CN/H_2O 25/25 (v/v), E) CH_3CN/H_2O 50/50 (v/v) and F) CH_3CN/H_2O 75/25. Reprinted from reference 81 with permission from American Chemical Society.

6.4 Proposed reaction scheme for methanol (CH_3OH) or acetonitrile (CH_3CN) and water (H_2O) solvent systems

Based on these findings, we propose that neutral solvent products, generated during the ESI process in the negative-ionization mode, are produced by homolytic cleavage of C-H bonds from CH_3CN and CH_3OH molecules, and O-H bonds from H_2O molecules, to produce a series of radicals (Figure 6.9). The formation of such species is reasonable, based on previous work [173-175]. The generation of OH radical species as well as reactive oxygen species during positive-mode electrospray (and in conjunction with corona discharge events) have been postulated [176-179]. The formation of free radicals in negative-ionization mode ESI is plausible given the high flux of electrons at the spray capillary tip. Once free radicals are formed, self-recombination or cross-recombination is a logical next step to produce the observed neutral solvent product molecules. In CH_3CN/H_2O solvent systems, homolytic cleavage, followed by self-recombination to produce [H-O-O-H] and [NC-CH_2-CH_2-CN] products, was consistently observed. Generation of [H-O-O-H] and [H-O-CH_2-O-H] products from CH_3OH/H_2O solvent systems indicates that homolytic cleavage is followed by self-recombination and cross-recombination of radicals to produce a wider array of products. Homolytic cleavage is assumed to take place by the impact of electrons (which are available at the tip of the capillary) with bonding electrons in solvent molecules to cleave their respective covalent bonds. The high electronegativity of O-atoms and the capacity of cyanide groups (-CN) to delocalize radical electrons provide driving forces to generate the predicted free radical species. Thus, recombination of radical species in a random fashion, and subsequent adduction of these products with the dianion to generate the observed adduct ions, is a reasonable proposition.

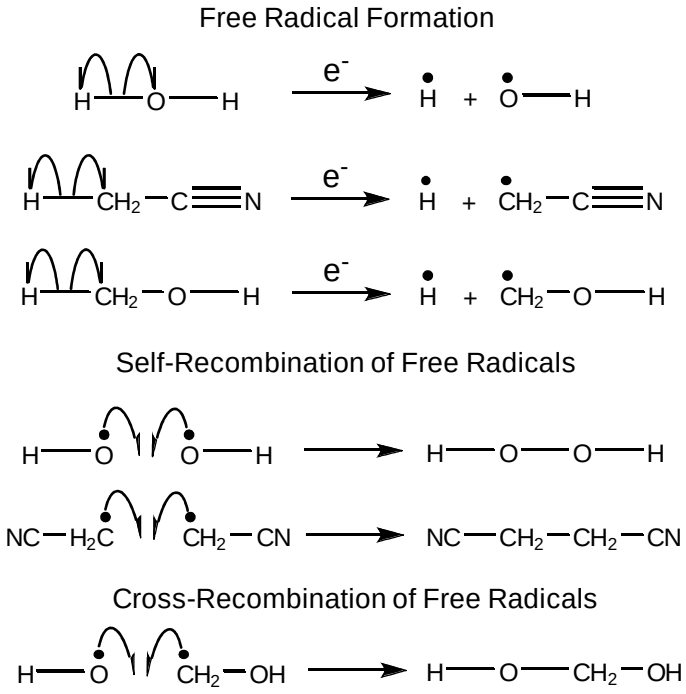

Figure 6.9 Proposed formation mechanism for solvent reaction intermediates produced using negative-ionization mode ESI. Reprinted from reference 81 with permission from American Chemical Society.

6.5 Summary

In summary, we have demonstrated that dianionic antimony(III)-tartrate ($[Sb_2\text{-}tar_2]^{2-}$) is capable of adducting to solvent reaction products, which are proposed to be generated during negative-ionization mode ESI. It should be noted that close inspection of mass spectra from previous ESI-MS studies (from our group and from Arakawa et al.) on antimony(III)-tartrate noncovalent complex formation do show the existence of these adduct ions [15, 80, 136, 137, 168]; however, the signals were never assigned as such. The experiments detailed in the present work provide new insight into the fate of solvent molecules during the ESI process, although further experimental and theoretical work is needed to fully understand the role of radical-recombination processes in the overall ionization process. We proposed, during negative-ionization mode electrospray, ESI-friendly H_2O, CH_3CN and CH_3OH solvent molecules undergo homolytic cleavage of O-H and C-H bonds to produce free radicals, followed by radical self-recombination or cross-recombination to produce neutral solvent intermediates. We are

currently investigating computational methods to more fully elucidate the molecular-level nature of adduct ion formation between the solvent products and antimony(III)-tartrate. Additional MS experiments are also warranted to gain a better appreciation for this phenomenon, and to gain further insight on the fundamental mechanism of negative-ionization mode ESI.

CHAPTER 7

NEW STRUCTURAL INSIGHT FOR ANTIMONY(III)-TARTRATE

7.1 Introduction

"Tartar emetic", bis-potassium salt of dianionic antimony(III)-*L*-tartrate, is a colorless crystalline substance which can be prepared inexpensively from tartaric acid and antimony oxide [85]. The long history of tartar emetic traces back to medieval times [65, 85]. The term "emetic" signifies its original use, a medicine that was taken to induce vomiting [65]. As a drug, it was also used in the 17th and 18th centuries to treat widespread inflammatory conditions, like bronchitis and pneumonia. Recent medicinal applications have been mainly in the treatment of schistosomiasis, as a valuable anthelmintic agent for the control of schistosomal blood flukes [64, 65, 85]. According to the Carter center, schistosomiasis is the second most socioeconomically devastating parasitic disease after malaria; approximately 200 million people in 74 countries are currently affected [180]. Bactericidal activity of tartar emetic at higher concentrations (compared to penicillin) has also been reported [65]. Further, the asymmetric nature of this economical and easily synthesizable anionic metal complex has prompted its use as a chiral resolving agent [78]. Despite initial few reports on its potential capacity as a drug and a resolving agent [64-66, 78, 85], further developments of its applications have not materialized. This is likely due, in part, to the lack of understanding of its structure and molecular recognition chemistry.

Our recent attempts to understand its chiral biomolecular recognition capacity using electrospray ionization-mass spectrometry (ESI-MS) uncovered an unprecedented proton-assisted enantioselective character of tartar emetic for binding of neutral side-chained amino acids (Ala, Val, Leu and Phe) [15, 79, 80]. More specifically, it was observed that, in order for

tartar emetic to show enantioselective association/dissociation phenomena, a proton association to the antimony(III)-*L*-tartrate dianionic core was crucial. When a proton was not attached, the antimony(III)-*L*-tartrate dianion failed to show enantioselective molecular recognition properties. The use of ESI-MS was crucial for visualizing this disparity in enantioselective biomolecular recognition capacity between the proton-bound and unbound antimony(III)-*D*,*L*-tartrate complexes.

Additionally, a serendipitous finding from our chiral biomolecular recognition studies was the observation of antimony(III)-tartrate's capability to adduct with unusual solvent reaction products that were proposed to be generated during negative ionization mode electrospray [81]. Studies on adduct ion formation between dianionic antimony(III)-*L*-tartrate and species like hydrogen peroxide and succinonitrile have provided new insight into the processes that are relevant to the fundamental understanding of the electrospray process. Nevertheless, the structure of dianionic antimony(III)-*L*-tartrate is of critical importance in trying to understand the binding chemistry of antimony(III)-*L*-tartrate with biomolecules, such as amino acids, and other small molecules, like hydrogen peroxide and succinonitrile.

The accepted structure for the antimony(III)-*L*-tartrate dianion has a binuclear tartrato(4-) bridged geometry as depicted in Figure 7.1 [66, 181]**.** This structure was determined using solid-state X-ray crystallography. The Sb(III) ion in this complex assumes a four coordinate, pseudo-trigonal-bipyramidal coordination geometry. The fifth coordination position of Sb(III) has been presumed to contain a lone pair of electrons [66]. This structure is similar to that of the binuclear vanadyl tartrate complex, which is often used as a model to explain most of the tartrato(4-) metal complexes [66]. Enantioselective molecular recognition properties of tartar emetic in solution and in the gas phase have often been explained based on this particular geometry [78]. However, explicating our observations [15, 79-81], particularly the proton-assisted enantioselective character of tartar emetic was not trivial using this particular structure alone. Also, in several instances, it was mentioned that the anti-parasitic and anti-bacterial

activity of tartar emetic is still not fully understood [64, 65]. Thus, it is not unrealistic to speculate that the solution and gas phase structure(s) of this compound are different from that which has been reported by X-ray crystallography. Further studies are required to investigate this hypothesis.

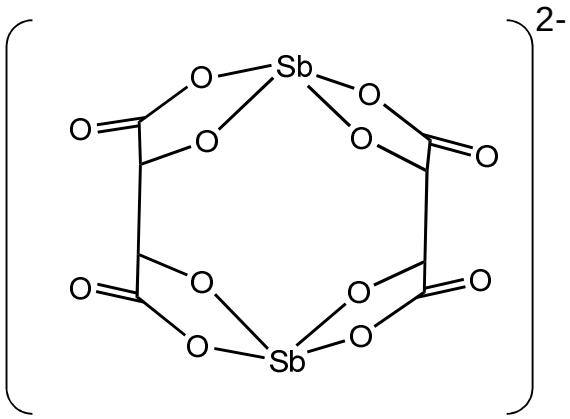

Figure 7.1 Ab initio (MP2) and DFT (in parenthesis) level predicted isomeric equilibrium of dianionic antimony(III)-*L*-tartrate.

Here we report, by carrying out theoretical calculations and NMR (nuclear magnetic resonance) experiments, antimony(III)-*L*-tartrate dianion can assume a previously unreported structural isomer. The isomer is shown to be stable in the gas phase and present in the solution phase. Results provided herein, in fact, provide a new insight for the structural character of the dianionic antimony(III) binuclear tartrato(4-) complex. This report also urges that tartar emetic's solution phase and gas phase biomolecular recognition chemistry and enantiomeric resolving chemistry should be reevaluated using both these structures.

7.2 Gas phase-targeted theoretical calculations on dianionic structure of antimony(III)-*L*-tartrate

Theoretical calculations for dianionic antimony(III)-*L*-tartrate were carried out using both density functional theory (DFT) and ab initio (MP2) approaches (details of these calculations, including Cartesian coordinates of all models are available in Appendix A). Initially, the crystallographic antimony(III)-*L*-tartrate dianion, as reported in the literature, was extracted from recent structural determinations [181]. Subsequent ab initio (MP2) and DFT calculations of this

structure (in vacuum at 0 K) resulted in the discovery of a closely spaced low-energy isomeric form (Figure 7.2), which is only 2.2 (2.4) kcal mol^{-1} higher in energy (the DFT result is given in parenthesis).

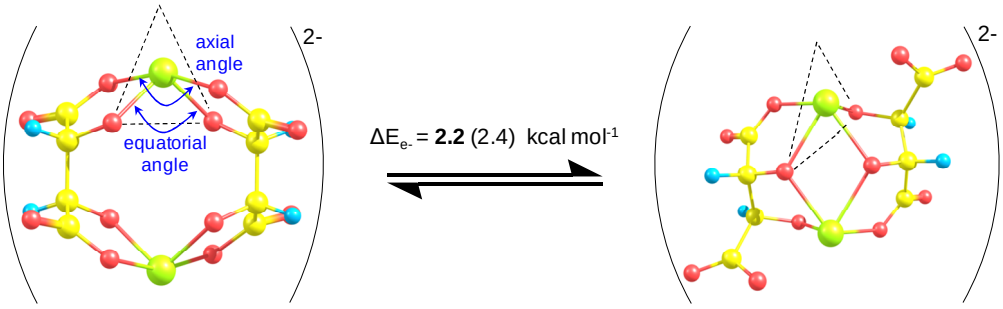

(A) $[Sb_2(L\text{-tar})_2]^{2-}$ (B) $[Sb_2(L\text{-tar})_2]^{2-}{}_{[Sb\text{-}O\text{-}Sb]}$

Figure 7.2 Ab initio (MP2) and DFT (in parenthesis) level predicted isomeric equilibrium of dianionic antimony(III)-*L*-tartrate.

The new isomer revealed by computation is denoted as $[Sb_2\text{-}L\text{-}tar_2]^{2-}{}_{[Sb\text{-}O\text{-}Sb]}$ (Figure 7.2B), because there are two oxygen atoms (one on each tartrato(4-) ligand) bridging the antimony(III) ions. Some analogous structures have been reported for titanium and indium tartrates in crystallographic studies [61, 90]. A report by Sharpless and Lippard et al. [61] indicated that the presumed structure of titanium tartrate, which resembled vanadyl tartrate and was similar to the structure depicted in Figure 7.2A, was an unsatisfactory model for explaining the catalytic activity observed in their experiments [182]. A new, more reasonable, metal-oxygen-bridged structure was revealed by X-ray crystallography of the titanium tartrate ester complex. Nevertheless, to our knowledge the metal-oxygen-bridged isomeric structure Figure 7.2B has not been previously described for antimony(III)-tartrate.

Table 7.1 Comparison of bond angles and bond lengths of reported and computationally determined structures

Structure-Type	Bond angle [a]		Bond length [a]		Sb-Sb distance	Ref.
	Axial	Equatorial	Axial	Equatorial		
Perfect trigonal bipyramid	180°	120°				66
$K_2[Sb_2\text{-L-tar}_2].3H_2O$ (tartar-emetic)			2.163(28) [b]	1.987(13) [b]		181
$K_2[Sb_2\text{-D-tar}_2].3H_2O$					5.05	66
[c] Sb_1	148	99	2.11	1.97		
			2.11	1.99		
[c] Sb_2	152	95	2.18	1.98		
			2.19	2.01		
$[Sb_2\text{-L-tar}_2]^{2-}$	161.8	102.9	2.177	2.005	4.998	MP2
			2.177	2.005		
	161.2	102.1	2.172	1.998	5.030	DFT
			2.172	1.998		
$[Sb_2\text{-L-tar}_2]^{2-}{}_{\{Sb\text{-}O\text{-}Sb\}}$	124.4	108.3	2.175	2.035	3.664	MP2
			2.181	2.249		
	124.2	108.4	2.162	2.023	3.657	DFT
			2.179	2.256		

[a] Bond angles are in degrees and lengths in Angstroms. [b] Average values as in reported literature. [c] Original literature reported nomenclature was used for these crystallographically non-equivalent Sb-atoms.

Table 7.1 compares the Sb(III) coordination sphere bond angles and bond lengths for the reported and computed antimony(III)-tartarate structures with respect to the perfect trigonal bipyramidal geometry. Values clearly show that both axial and equatorial bond lengths are kept at around 2.1 Å (± 0.1 Å). However, there is a noted difference observed in axial and equatorial bond angles for the newly identified structure, $[Sb_2\text{-L-tar}_2]^{2-}{}_{[Sb\text{-}O\text{-}Sb]}$. A large decrease for the axial bond angles (~ 40 ^{o}) and a small, but significant, increase (~ 7 ^{o}) for the equatorial bond angles was calculated. Also, the newly identified structure exhibits a Sb(III)-Sb(III) distance of ~ 3.600 Å, which is markedly smaller compared to the Sb(III)-Sb(III) distance of the reported structures (~ 5.000 Å). These similarities and differences indicate that the isomerization of the two structures takes place with minute changes in coordination bond lengths (O-Sb), while the Sb(III)-Sb(III) distance and coordination angles change to a more significant degree.

7.3 Solution phase-targeted NMR studies on structure of antimony(III)-*L*-tartrate dianionic

In order to see whether a similar phenomenon is present in solution, ^{1}H and ^{13}C-NMR experiments were carried out. Since $Na_2[Sb_2\text{-}L\text{-tar}_2]$ and $K_2[Sb_2\text{-}L\text{-tar}_2]$ are only sparingly soluble in dimethylsulfoxide (DMSO), $[P(Bu)_4]_2[Sb_2\text{-}L\text{-tar}_2]$ was prepared (Scheme 7.1, using methods described in literature [85]) and used instead.

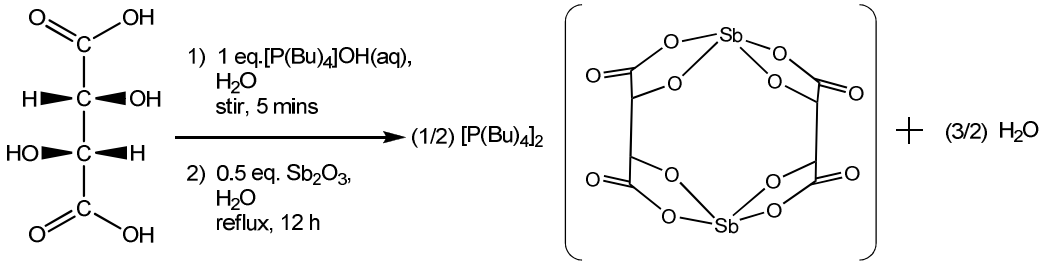

Scheme 7.1 Synthesis of bis(tetrabutylphosphonium) antimony(III)-*L*-tartrato(4-) complex, $[P(Bu)_4]_2[Sb_2\text{-}L\text{-tar}_2]$.

DMSO was selected as the solvent for these analyses to eliminate any proton abstraction processes possible by the antimony(III)-tartrate dianion [15, 79-81]. During the synthesis, $[P(Bu)_4][OH](aq)$ was used instead of NaOH(aq) or KOH(aq) which enabled the change in the counter cation from Na^+ or K^+ to tetrabutylphosphonium. This change in the cation

made the complex highly soluble in DMSO and provided the ability to carry out the desired NMR experiments. Characterization of the $[P(Bu)_4]_2[Sb_2$-*L*-$tar_2]$ salt was performed using ESI-MS (Figure 7.3). These experiments were carried out using a Thermo LCQ Deca XP ion trap instrument (Thermo-Fisher Scientific, Inc., San Jose, CA, USA) equipped with a conventional electrospray ion source. NMR experiments were performed on a JEOL 500 MHz instrument in d_6-DMSO at room temperature.

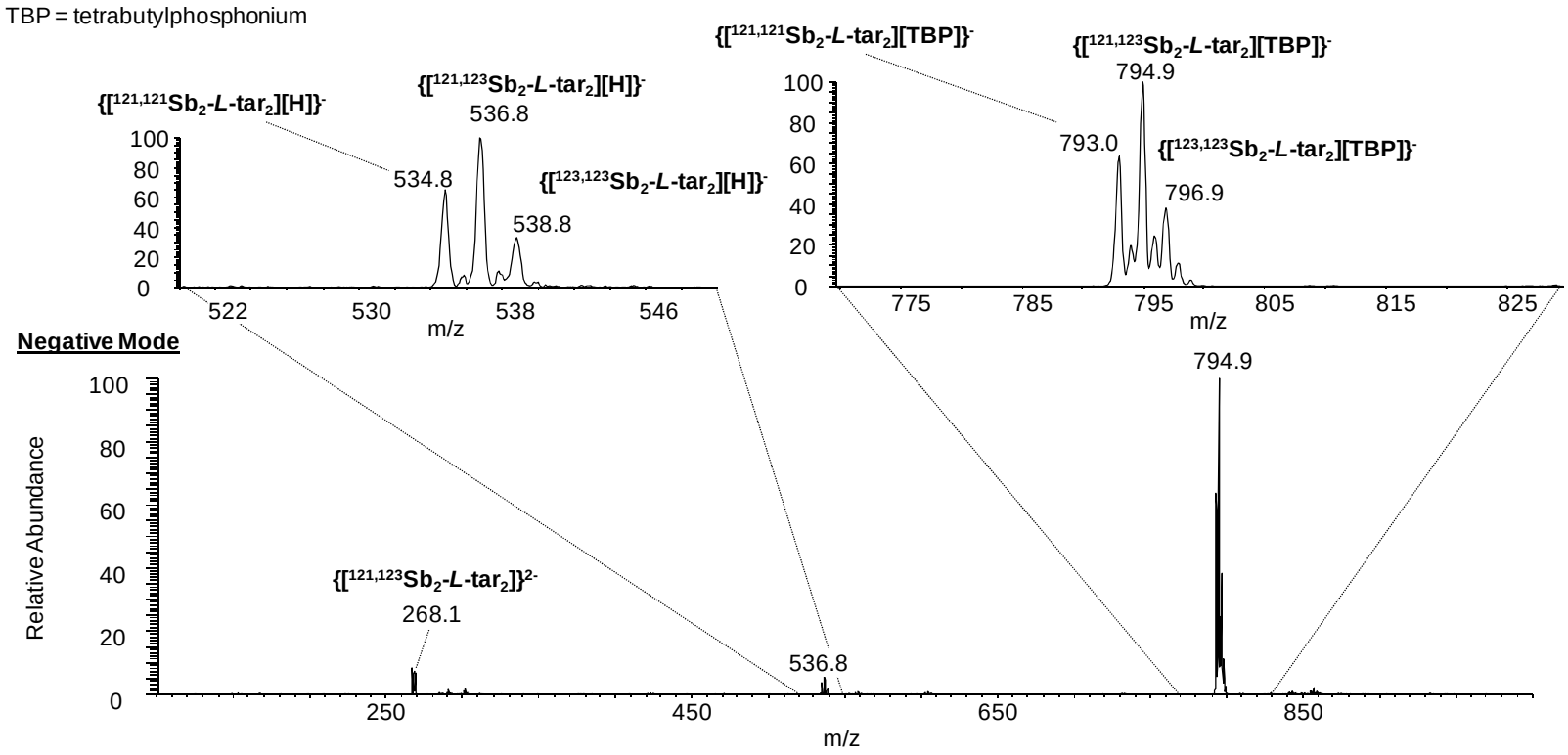

Figure 7.3 Negative mode ESI-mass spectrum of $[TBP]_2[Sb_2\text{-}L\text{-}tar_2]$ complex in MeOH at 5 mL/min flow rate.

If the two isomeric forms co-existed in solution, the $[Sb_2\text{-}L\text{-}tar_2]^{2-}_{[Sb\text{-}O\text{-}Sb]}$ structure was expected to show two distinct ^{1}H-NMR signals, corresponding to the protons **H**-C-$O_{bridging}$ and **H**-C-$COO^-_{non\text{-}coordinating}$, compared to the crystallographically-determined structure. The crystallographically-determined structure (i.e. $[Sb_2\text{-}L\text{-}tar_2]^{2-}$) was expected to show a separate signal which corresponded to the **H**-C-$COO^-_{coordinating}$ protons. Figure 7.4 illustrates the ^{1}H-NMR spectrum obtained for $[P(Bu)_4]_2[Sb_2\text{-}L\text{-}tar_2]$ in d6-DMSO at room temperature. ^{1}H-NMR signals labeled with **a**, **b**, **c** and **d** represents the protons on the butyl-group of the tetrabutylphosphonium cation. Observation of the peaks labeled with **2p** and **2q** (observed at δ (ppm) = 4.5 and 3.3, respectively) along with the peak labeled with **1** (observed at δ (ppm) = 4.2) illustrate the co-existence of the isomeric structures predicted for the gas phase. However, though this qualitative picture provides information to infer the co-existence of the isomeric structures, the integral values obtained for 1, 2p and 2q peaks in ^{1}H-NMR (Figure 7.4) indicate an inexplicable observation. The three peaks represent seven hydrogens instead of four and the peak integrals of 2p (3H) and 2q (3.5H) do not match each other. But collectively, peaks 1 and 2q represent four hydrogens. It was also observed that the intensities of these peaks to change over time. More specifically, when the peak intensity of 1 increased with time, the peak intensity of 2p completely diminished, and that of 2q was reduced. Due to these reasons, it is not fully clear whether both 2p and 2q represent the $[Sb_2\text{-}L\text{-}tar_2]^{2-}_{[Sb\text{-}o\text{-}Sb]}$ structure, or if only 2q represents the $[Sb_2\text{-}L\text{-}tar_2]^{2-}_{[Sb\text{-}o\text{-}Sb]}$ structure and 2p is an artifact originating from another sources, such as an interaction of $[TBP]_2[Sb_2\text{-}L\text{-}tar_2]$ with solvent molecules. Therefore more experiments are needed to fully detail these observations and are currently underway in our labs. Nevertheless, ^{13}C-NMR experiments were carried out to validate the co-existence of the gas-phase isomeric structure predicted by computation, with that in solution. The $[Sb_2\text{-}L\text{-}tar_2]^{2-}_{[Sb\text{-}o\text{-}Sb]}$ structure was expected to show two distinct ^{13}C-NMR signals corresponding to **C**H-$O_{bridging}$ and **C**H-$COO^-_{non\text{-}coordinating}$ for the carbons of the tartrato(4-) ligands. Also, both isomeric forms were expected to show two more common ^{13}C-NMR signals corresponding to **C**H-

$O_{coordinating}$ and **C**H-$COO^-_{coordinating}$ for the carbons of the tartrato(4-) ligands. Figure 7.5 illustrates the ^{13}C-NMR spectrum obtained for $[P(Bu)_4]_2[Sb_2$-*L*-$tar_2]$ in d6-DMSO at room temperature. ^{13}C-NMR signals labeled with **a**, **b**, **c** and **d** in Figure 7.5 represent the carbons of the butyl-group of tetrabutylphosphonium cation. Observation of the peaks labeled with **2p** and **2q** (observed at δ (ppm) = 76.6 and 179.3, respectively), along with the peaks labeled with **1p** and **1q** (observed at δ (ppm) = 77.9 and 179.5, respectively), clearly illustrate the co-existence of the predicted isomeric structures.

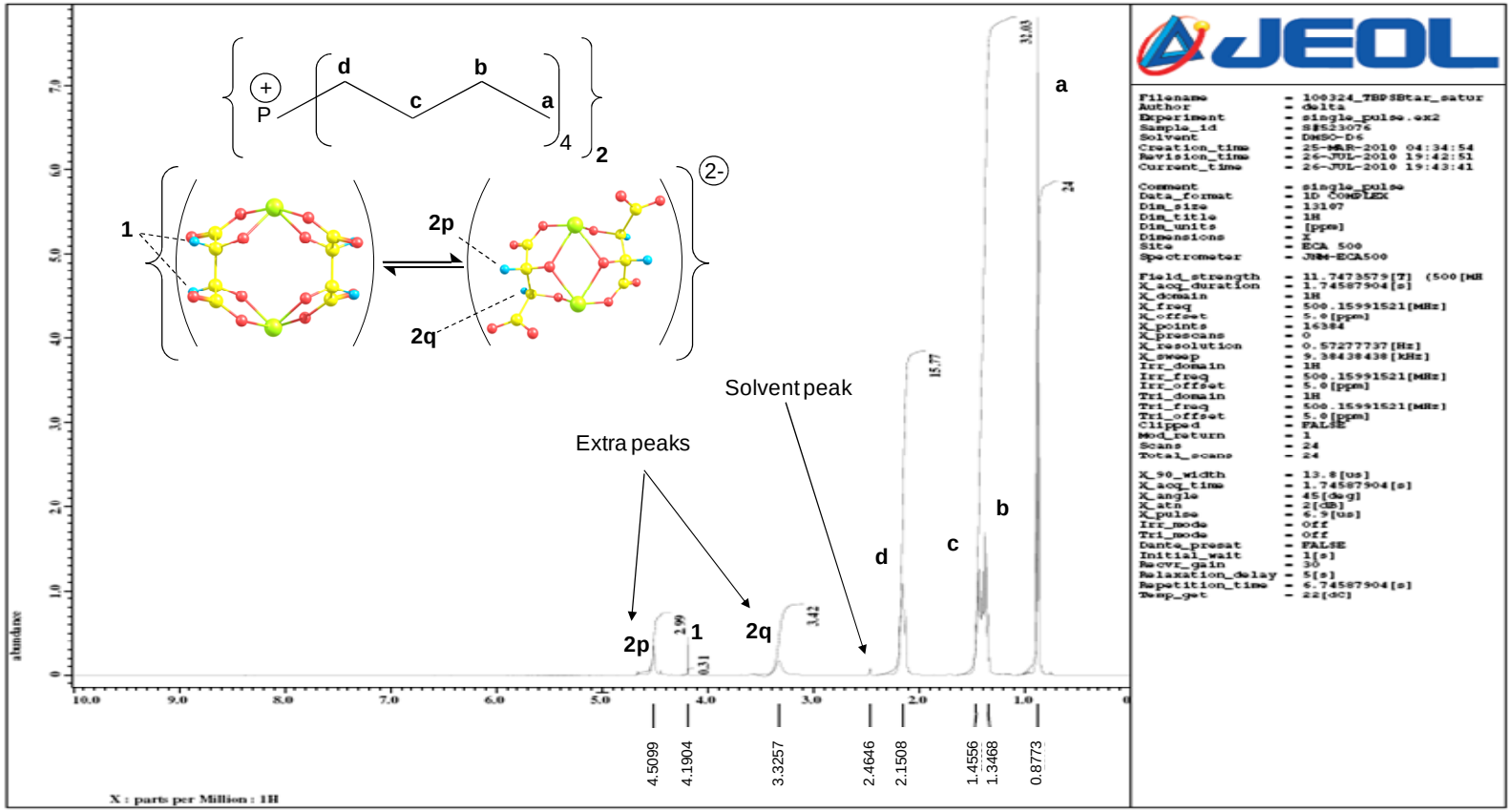

Figure 7.4 ^{1}H-NMR spectrum of $[P(Bu)_4]_2[Sb_2$-*L*-$tar_2]$ in d6-DMSO at room temperature.

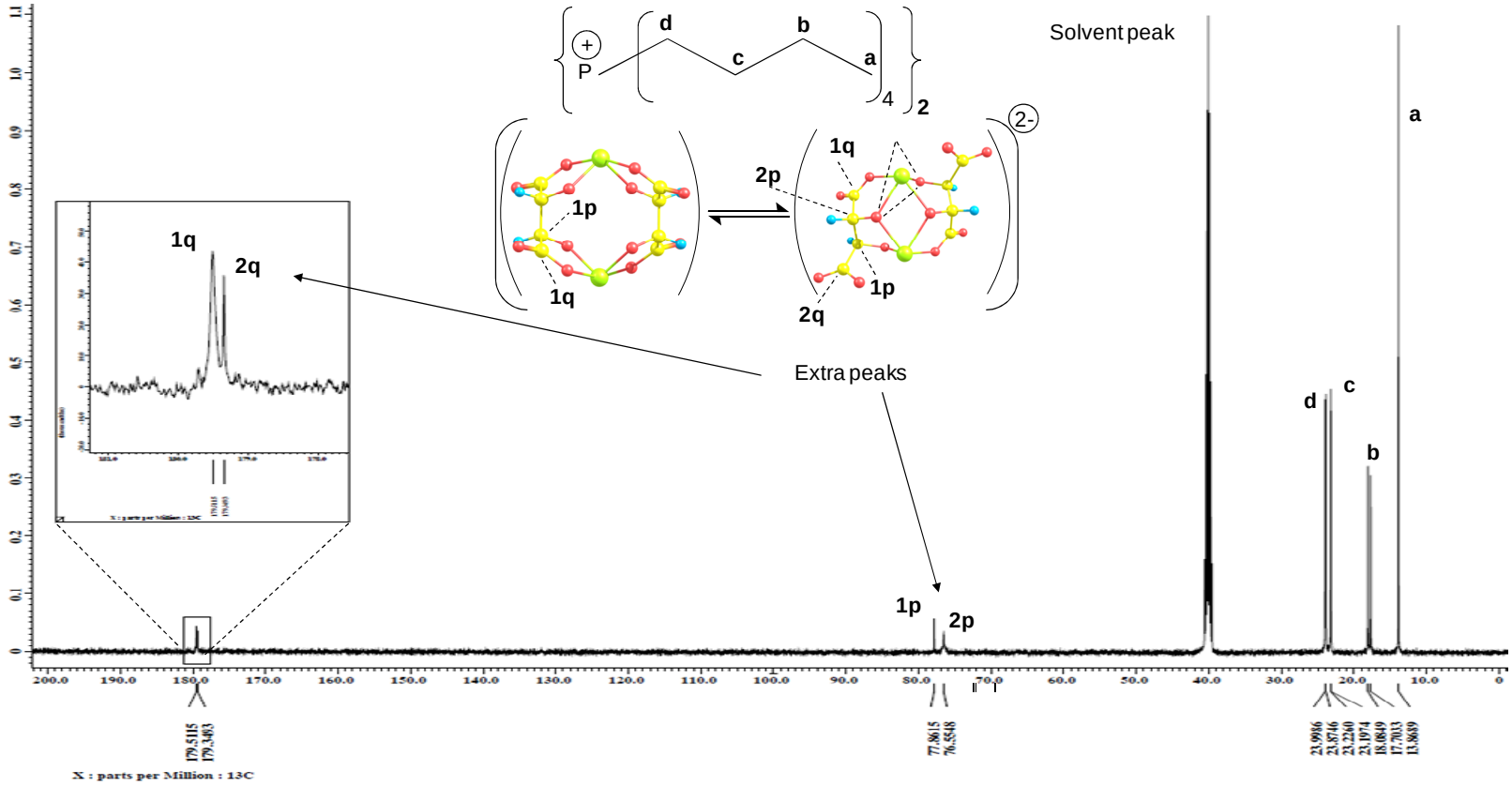

Figure 7.5 ^{13}C-NMR spectrum of $[P(Bu)_4]_2[Sb_2$-*L*-$tar_2]$ in d6-DMSO at room temperature.

7.4 Summary

In summary, theoretical calculations (using both DFT and ab initio (MP2) levels) and both ^{1}H and ^{13}C-NMR experiments have revealed a new structural isomer for the antimony(III)-*L*-tartrate dianion, which is predicted to co-exist in solution and in the gas phase. Structural evaluation of the co-existing structures indicate a significant change in Sb(III)-Sb(III) distance (~ 3.6 Å) for the newly identified structure, $[Sb_2\text{-}L\text{-}tar_2]^{2-}{}_{[Sb\text{-}o\text{-}Sb]}$, which is ~ 1.4 Å less than that for the previously reported crystallographically-determined structure, which carries a Sb(III)-Sb(III) distance of ~ 5.0 Å. In addition, the newly identified structure shows a large decrease in its axial bond angle (~ 40^{o}) and a small but significant increase in its equatorial bond angles (~ 7^{o}) compared to the crystallographically-determined structure. The coordinating bond distances (O-Sb) remained around 2.1 Å (± 0.1 Å) in both isomers. Both ^{1}H and ^{13}C-NMR spectra obtained for $[P(Bu)_4]_2[Sb_2\text{-}L\text{-}tar_2]$ in d6-DMSO at room temperature confirmed that the new isomer co-exists with the crystallographically-determined structure in solution. In these experiments, the use of a $[P(Bu)_4]^{+}$ counter-cation, instead of Na^{+} or K^{+} cations, provided a significant solubility increase in aprotic DMSO and eliminated the problems associated in obtaining clear NMR spectra. Overall, these studies provided new insight into a dynamic structural character for antimony(III)-*L*-tartrate, which is a drug, a chiral selector, and a compound which has provided new information about the mechanism of electrospray ionization. This communication urges researchers to revisit and consider both structures when explicating the molecular recognition properties of antimony(III)-*L*-tartrate.

CHAPTER 8

CONCLUSIONS AND FUTURE WORK

While the emphasis on using enantiomerically-pure compounds continuingly increases, separation techniques, such as HPLC, GC and CE still remain the current methods of choice determine the enantiomeric purity of non-racemic mixtures. However, compared to NMR and IR techniques used to study molecular level enantioselective recognition phenomena, MS methods still hold a unique place in analytical techniques that are used to study such phenomena. Among many ionization techniques coupled to MS, ESI has been the most popular choice to evaluate the capacity of chiral compounds to discriminate enantiomers. Its capability to produce gas phase ions from preformed solution phase noncovalent interactions in respective full scan mass spectra has made it more attractive compared to other ionization techniques. ESI-MS based gas-phase targeting tandem MS techniques allow for an additional level of information on noncovalently bound complexes in the absence of solvent. Acquiring such information is not possible with any other single experimental technique.

Although it is tricky to always match solution-phase based measurements to respective ESI-MS based enantiomeric discrimination results, studies have shown that ESI-MS is capable of providing information about solution phase association phenomena. In order to extend our efforts to signify that ESI-MS is an invaluable analytical tool to study chiral intermolecular interactions, a chiral reference with not very well understood chiral molecular recognition properties was identified. This identified chiral reference, namely antimony(III)-*D*/*L*-tartrate falls under the general category of organo-metallic metal-tartrate complexes.

This dissertation initially (in chapter 2) summarized the current knowledge of molecular recognition properties of tartrates and metal-tartrates pertaining to the gas phase and solution media, in conjunction with their application to enantiomeric separation sciences and MS

discrimination studies. Our initial ESI-MS based chiral molecular recognition studies on antimony(III)-*L*-tartrate ("tartar emetic") association to leucine enantiomers were then discussed in chapter 3. It was revealed, in both solution phase targeting full scan MS studies and gas-phase targeting CTD-MS studies, that antimony(III)-*D*/*L*-tartrate complexes require an association of a proton to become enantioselective. Interestingly, the dianionic selector itself was unable to show enantiomeric discrimination properties. These studies clearly showed the promise of ESI-MS for examination of such a disparity in enantioselective binding phenomena between the dianionic and the protonated monoanionic representatives of antimony(III)-*D*/*L*-tartrates.

The effect of solvent systems on antimony(III)-*D*/*L*-tartrates and amino acid binding systems were evaluated and discussed in chapter 4. Similar solution phase targeting ESI-MS studies were also extended to several other neutral amino acids (Ala, Val and Phe). These studies have revealed the proton-assisted enantioselective character of antimony(III)-*D*/*L*-tartrate and amino acid binding systems is consistent with all four amino acids evaluated and the effect of solvent systems on this chiral recognition property of antimony(III)- *D*,*L*-tartrates is small, but not negligible. Amino acid enantiomers have also shown a general trend of increasing selectivity order of Val ≤ Ala < Leu ≈ Phe towards the binding of protonated $\{[Sb_2\text{-}\ D,\ L\text{-}tar_2][H]\}^-$ ionic species. This observed order has been independent of the solvent systems employed. In chapter 5, extended gas-phase targeting collision threshold dissociation (CTD) ESI-MS experiments carried out on diastereomeric ions generated by the association of dianionic as well as protonated monoanionic antimony(III)-*D*,*L*-tartrates with alanine (Ala), valine (Val) and phenylalanine (Phe) amino acid enantiomers were discussed. Similar to full-scan MS analyses, also in gas phase, a consistent pattern of proton-assisted enantioselectivity was observed for all diastereomeric ions analyzed.

In chapter 6, some unexpected observations that eventually have resulted in providing new insights into the fundamental understanding of the electrospray process was discussed. It

was revealed during the negative-ionization mode ESI-MS analysis of antimony(III)-tartrate in frequently used solvent systems (ACN/H_2O and MeOH/H_2O), that antimony(III)-tartrate dianions are capable of associating to solvent reaction products generated by free radical formation and recombination during negative-ionization mode electrospray. Products such as H_2O_2, $NCCH_2CH_2CN$, and $CH_2(OH)_2$ adducted to antimony(III)-tartrate dianion were confirmed by experiments carried out with deuterated and non-deuterated solvent mixtures. Relative intensity changes of these adducted-ions with the change in volume composition of each solvent system further indicated the effect of solvent composition on the relative formation of these species. Based on these pieces of evidence, this chapter has proposed that homolytic cleavage of C-H bonds for CH_3CN and CH_3OH molecules, and O-H bonds for H_2O molecules, produces a series of free radicals during negative-ionization mode ESI, and subsequent self-recombination or cross-recombination of these free radicals then occurs to form the neutral solvent products, which are observed in mass spectra as dianionic [Sb_2-tar_2]-adducted ionic species.

In order to explain ESI-MS observations using crystallographically-determined structure of dianionic antimony(III)-*L*-tartrate, particularly the proton-assisted enantioselective character of tartar emetic, has not been trivial. Therefore theoretical calculations and NMR (nuclear magnetic resonance) studies were carried out on the structure of dianionic antimony(III)-*L*-tartrate. The results were discussed in chapter 7. It was revealed a new structural isomer for the antimony(III)-*L*-tartrate dianion, which is predicted to co-exist in solution and in the gas phase. Overall, these studies have provided a new insight into a dynamic structural character for antimony(III)-*L*-tartrate. Currently, extended theoretical calculations are being carried out to fully detail the proton-assisted enantioselective phenomena that were observed in ESI-MS based association and dissociation studies.

Density functional theory (DFT) and post Hartree-Fock MP2 calculations were performed to calculate electronic energies for all four free antimony tartrate anions, as well as their respective binding energies with *D*- and *L*-Leu. The preliminary computational results for

the dianionic forms are shown in Figure 8.1, while those for the protonated monoanionic forms are summarized in Figure 8.2. A structural determination for the proton-bound monoanion of antimony tartrate has never been reported. According to the computational data, the protonated {[Sb_2-*L*-tar_2]$^{2-}$[H^+]} monoion exists predominantly in the [Sb-O-Sb] isomer form (Figure 8.2). Additionally, and consistent with the experimental results, this ion form was computed to show a slight preference for binding to *D*-Leu. In contrast, the higher energy crystallographic form was predicted to have a stronger binding affinity to *L*-Leu. For the [Sb_2-*L*-tar_2]$^{2-}$ dianion, the crystallographic and the [Sb-O-Sb] isomer forms were close in energy, with the former computed to be slightly more stable than the latter, in contrast with the results for the monoanion (Figure 8.1). Consistent with the monoanion results, the [Sb-O-Sb] form was predicted to have a higher binding affinity to *D*-Leu, whereas the crystallographic form preferred *L*-Leu. Overall, these results are also consistent with the experimental observations showing a lack of enantioselective binding by the dianion form. The minimal variation in stability between the isomeric structures would support the notion that both are present at equilibrium, and consequently, their individual enantioselective preferences would cancel. Some information may also be gleaned about the nature of the noncovalent interactions formed between antimony(III)-tartrate and the leucine enantiomers. While still speculative, the predicted involvement of antimony in the protonated complex (Figure 8.2) may also be key for the observed enantioselectivity. It is well know that at least three interaction points, which can be either attractive or repulsive, are necessary to achieve stereoselective discrimination. However, even with these high level gas-phase calculations, it is difficult to infer the arrangement of binding partners, which would occur in solution.

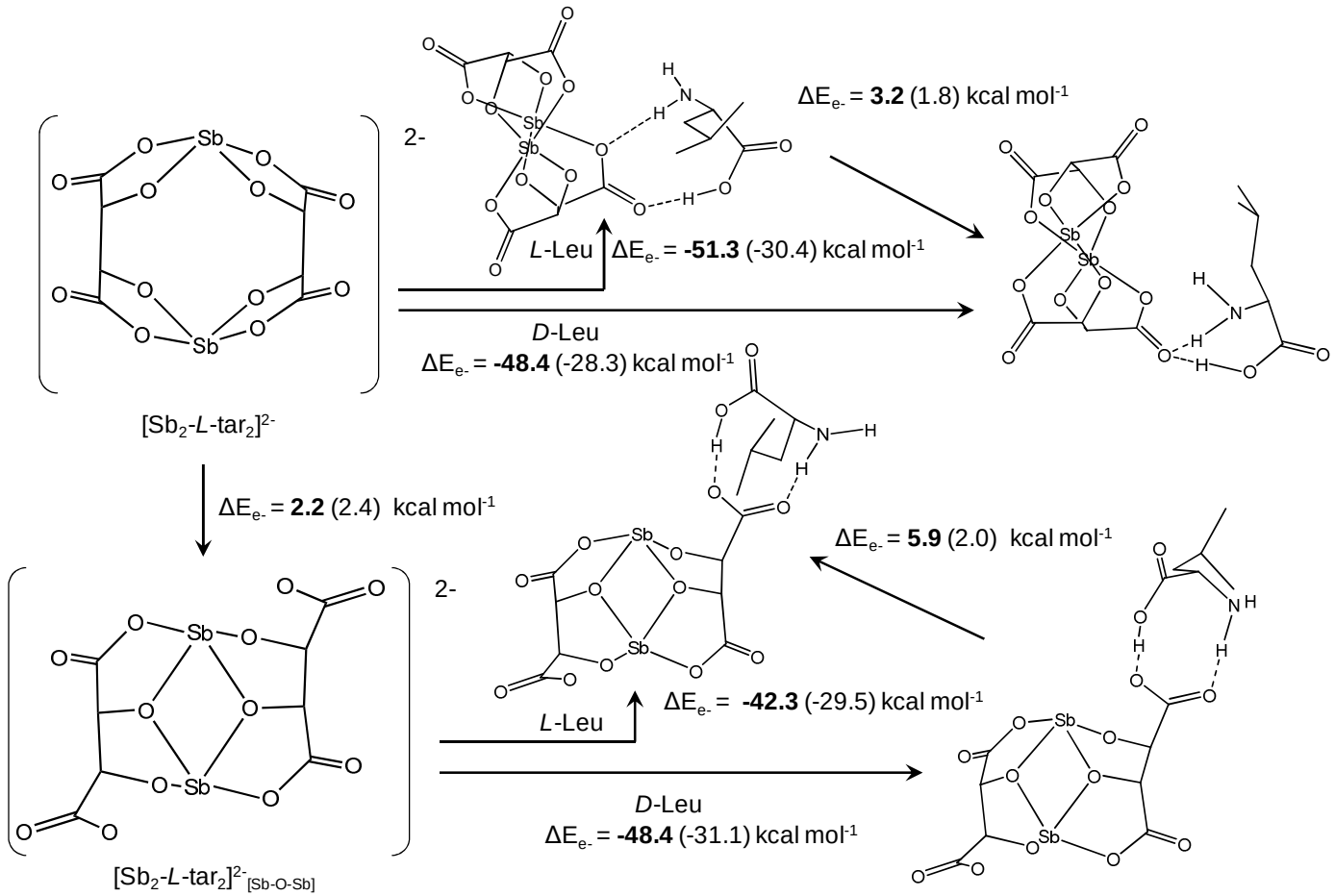

Figure 8.1 Relative gas phase binding energies to *D*- and *L*-Leu and inter-conversion energy for calculated isomers of dianionic [Sb_2-*L*-tar_2]$^{2-}$ obtained by the MP2 method. Values in brackets were obtained from DFT at B3LYP level for comparison.

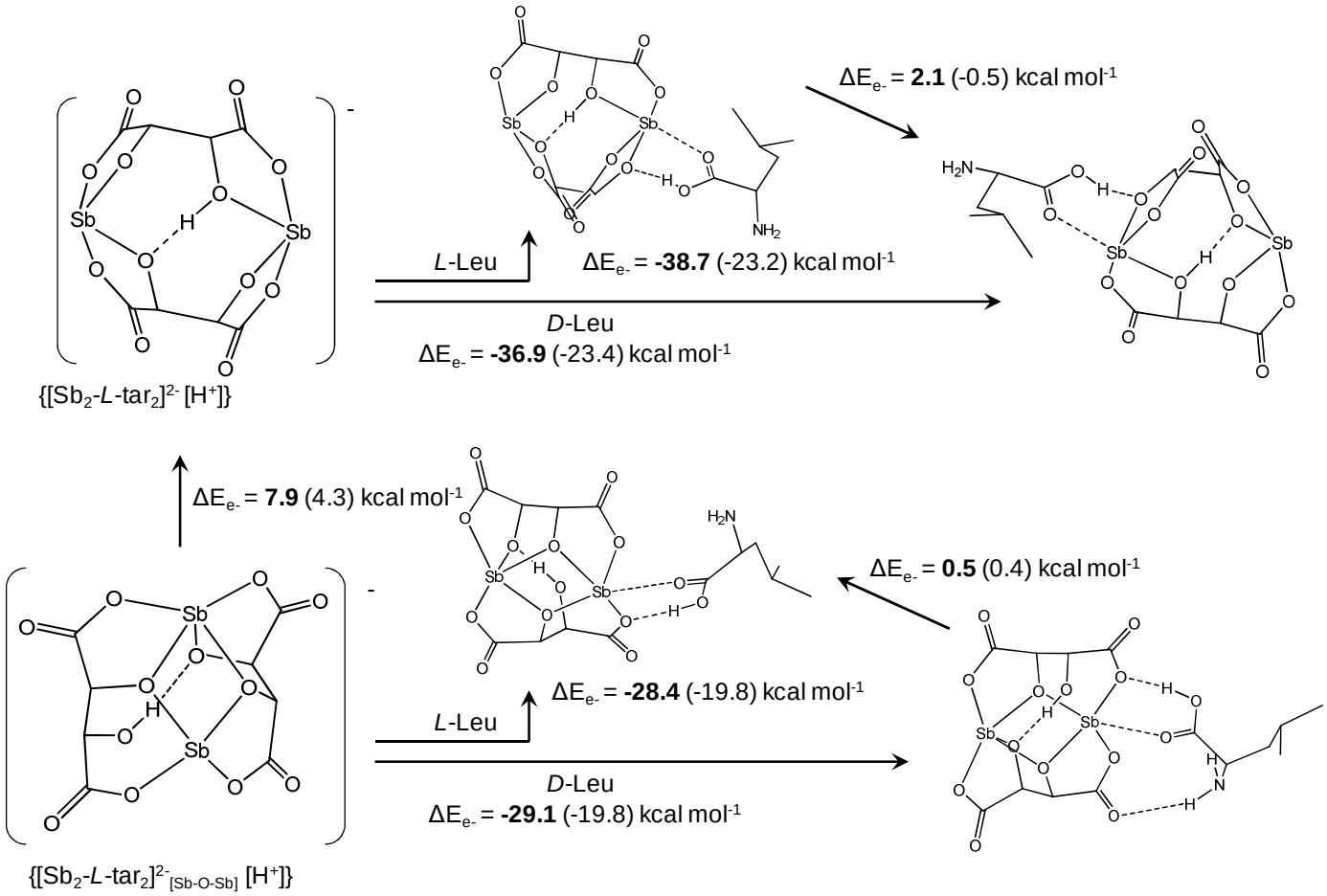

Figure 8.2 Relative gas phase binding energies to *D, L*-Leu and interconversion energy for calculated isomers for monoanionic {[Sb_2-*L*-tar_2]$^{2-}$[H]$^+$} obtained by the MP2 method. Values in brackets were obtained from DFT at B3LYP level for comparison.

While the work which was discussed in this dissertation has significantly supported to our ongoing efforts to show that ESI-MS is an important analytical tool to study molecular recognition phenomena, several extended studies are currently being carried out to further elucidate this assertion. One area of focus is given towards similar ESI-MS chiral molecular recognition studies associated to metal-tartrates carrying different metal- or metal-oxo- ion centers. In fact, preliminary studies carried out using arsenyl(III)-*D*/*L*-tartrates have shown similar proton-assisted enantioselectivity phenomena to that observed with antimony(III)-*D*/*L*-tartrates (Chapter 3). However, significantly higher enantioselectivity values for protonated $\{[As_2\text{-}\ D,\ L\text{-}tar_2][H]\}^-$ ionic species were returned both in solution-phase-targeted single-stage mass spectra and gas-phase-targeted CTD studies. These studies suggest that arsenyl(III)-*D*/*L*-tartrates might be a better alternative for enantiomeric separations that were carried out using antimony(III)-*D*/*L*-tartrates. These studies also revealed that dianionic $[As_2\text{-}L\text{-}tar_2]^{2-}$ ionic species also carry similar adducting capabilities to solvent reaction products generated during negative mode electrospray ionization. Extended studies to fully evaluate its adducting capacity towards these solvent reaction products are currently underway.

Since, it was the protonated antimony(III)-*D*/*L*-tartrates that have shown the enantioselective binding to neutral amino acids, a simple method to synthesize $[H]_2[Sb_2\text{-}D/L\text{-}tar_2]$ was evaluated. During the synthesis, ESI-MS was used to identify the starting materials and the product generated during the synthesis. $[H]_2[Sb_2\text{-}D/L\text{-}tar_2]$ was separated from starting materials by precipitation in ethanol and purity of products were effectively monitored using ESI-MS. Future studies on synthesized $[H]_2[Sb_2\text{-}D/L\text{-}tar_2]$ include, its applicability for enhanced enantiomeric separations as well as for antimicrobial/antifilarial therapeutics. Identification of similar solvent reaction products generated during positive mode electrospray ionization was not possible using $[Na]_2[Sb_2\text{-}L\text{-}tar_2]$. However, during the synthesis and ESI-MS analysis of $[H]_2[Sb_2\text{-}D/L\text{-}tar_2]$, it was realized that cation, $\{[H]_3[Sb_2\text{-}D/L\text{-}tar_2]^+$, is capable of adducting to similar solvent reaction products as well as free radicals that are believed to be generated

during positive mode electrospray. Extended studies of these phenomena are currently underway to further prove that similar solvent reaction products are also generated during positive mode electrospray.

APPENDIX A

OPTIMIZED GEOMETRIES FROM COMPUTATION

D-Leu

Atomic Number	B3LYP= -83.8026709 Hartree			Atomic Number	MP2= -82.7197709 Hartree		
	Coordinates (Angstroms)				Coordinates (Angstroms)		
	X	Y	Z		X	Y	Z
7	-1.7647	1.73567	0.019179	7	-1.93096	1.607542	0.013106
6	-0.64863	0.803877	0.27942	6	-0.70148	0.805144	0.30355
6	-1.26032	-0.58147	0.346261	6	-1.13321	-0.64598	0.367044
8	-1.26141	-1.34023	1.317113	8	-1.01833	-1.42537	1.335388
6	0.510443	0.924119	-0.74729	6	0.446801	1.046927	-0.71591
6	1.830833	0.158795	-0.46195	6	1.789099	0.310375	-0.43747
6	2.441443	0.527331	0.906565	6	2.235767	0.482763	1.037649
6	1.706778	-1.3716	-0.61897	6	1.740533	-1.19164	-0.82259
8	-1.86794	-0.93195	-0.85226	8	-1.70692	-1.04873	-0.85788
1	-1.59438	2.69263	0.302145	1	-1.76005	2.60121	0.128518
1	-2.17158	1.661426	-0.90647	1	-2.28712	1.414672	-0.91902
1	-0.28269	1.013129	1.285282	1	-0.37254	1.075318	1.306914
1	0.740636	1.997116	-0.80061	1	0.63133	2.131169	-0.70352
1	0.124795	0.633767	-1.73288	1	0.079912	0.786709	-1.71738
1	2.53124	0.505567	-1.23607	1	2.538603	0.792746	-1.08008
1	3.443622	0.094777	1.009776	1	3.255141	0.103044	1.17816
1	1.833954	0.14187	1.734784	1	1.570596	-0.07844	1.708521
1	2.531819	1.614591	1.025686	1	2.215345	1.540329	1.334116
1	2.698207	-1.83902	-0.5817	1	2.745375	-1.62849	-0.76366
1	1.245465	-1.63706	-1.57774	1	1.359089	-1.31915	-1.84319
1	1.108504	-1.81479	0.185085	1	1.09588	-1.75371	-0.13604
1	-2.30522	-1.80256	-0.78459	1	-2.01788	-1.97094	-0.7988

L-Leu

Atomic Number	B3LYP= -83.8026709 Hartree			Atomic Number	MP2= -82.7197709 Hartree		
	Coordinates (Angstroms)				Coordinates (Angstroms)		
	X	Y	Z		X	Y	Z
7	-0.62152	1.664317	-0.69126	7	-0.33944	-1.02665	1.318405
6	-0.46803	0.237229	-0.3687	6	-0.49205	0.15279	0.417948
6	-1.83918	-0.35846	-0.13253	6	-1.94551	0.246404	-0.00459
8	-2.23912	-1.45125	-0.53781	8	-2.67238	1.260879	0.02153
6	0.445521	-0.10071	0.856571	6	0.394555	0.166229	-0.86216
6	1.960803	-0.23365	0.547117	6	1.92943	0.274509	-0.61207
6	2.267674	-1.49316	-0.28925	6	2.267458	1.322814	0.478082
6	2.577737	1.021017	-0.10506	6	2.599861	-1.08825	-0.29244
8	-2.62781	0.450083	0.676014	8	-2.40068	-0.98889	-0.51526
1	0.228867	2.129693	-0.97801	1	0.572691	-1.0458	1.758089
1	-1.14861	2.192569	-0.00522	1	-0.514	-1.89971	0.828434
1	-0.08354	-0.26994	-1.25535	1	-0.28322	1.040445	1.01459
1	0.11593	-1.05127	1.297596	1	0.080614	1.031803	-1.46498
1	0.280047	0.675976	1.613455	1	0.176516	-0.73643	-1.4481
1	2.446928	-0.36447	1.525116	1	2.360851	0.628376	-1.55869
1	3.349117	-1.61402	-0.42384	1	3.349446	1.497712	0.51925
1	1.818228	-1.4348	-1.28887	1	1.948805	0.970116	1.469644
1	1.882367	-2.39674	0.19737	1	1.765561	2.278935	0.279089
1	3.668344	0.922887	-0.16305	1	3.692442	-0.98267	-0.30592
1	2.350674	1.928757	0.466422	1	2.311242	-1.84529	-1.03281
1	2.214803	1.158983	-1.13256	1	2.3118	-1.45446	0.700424
1	-3.50428	0.047899	0.831272	1	-3.33463	-0.91939	-0.78664

[Sb-*L*-tar]$^{2-}$

Atomic Number	B3LYP= -83.8026709 Hartree			Atomic Number	MP2= -82.7197709 Hartree		
	Coordinates (Angstroms)				Coordinates (Angstroms)		
	X	Y	Z		X	Y	Z
51	-2.51504	0.000349	-0.00017	51	2.493902	0.000296	0.000022
8	-1.25935	-1.31736	0.824665	8	1.244683	-1.32325	-0.84199
8	-2.17962	-1.40069	-1.62614	8	2.150464	-1.37303	1.654446
8	-1.2586	1.317636	-0.82454	8	1.244339	1.323509	0.842045
8	-2.17954	1.401043	1.626024	8	2.150086	1.373518	-1.6544
6	-1.39142	2.445122	1.37365	6	1.364642	2.441667	-1.39504
6	-0.76743	2.424037	-0.03695	6	0.765305	2.446082	0.030608
8	-1.20569	3.411351	2.148725	8	1.161821	3.411508	-2.18852
1	-1.05687	3.349929	-0.5445	1	1.07375	3.360213	0.540851
6	0.768239	2.423914	0.037328	6	-0.76594	2.445914	-0.03059
1	1.05783	3.349666	0.54504	1	-1.07458	3.359973	-0.54084
6	1.392116	2.445153	-1.37332	6	-1.36536	2.441386	1.39503
8	1.206411	3.411493	-2.14827	8	-1.16254	3.411128	2.188627
8	1.259307	1.317304	0.824651	8	-1.2447	1.323242	-0.84204
51	2.515031	-0.00038	-0.00018	51	-2.49393	-0.0003	-4.6E-05
8	2.179712	1.400771	-1.62609	8	-2.1505	1.373009	1.654396
8	2.17941	-1.40092	1.626091	8	-2.15003	-1.3735	-1.65447
8	1.258671	-1.31774	-0.82456	8	-1.24441	-1.32351	0.842022
6	1.391321	-2.44503	1.373744	6	-1.36474	-2.44174	-1.39502
8	1.205763	-3.41133	2.148773	8	-1.16149	-3.41135	-2.18867
6	0.767431	-2.42407	-0.0369	6	-0.76536	-2.44609	0.030615
1	1.056896	-3.35	-0.54437	1	-1.0738	-3.36021	0.540884
6	-0.76824	-2.42394	0.037298	6	0.765889	-2.4459	-0.03054
1	-1.05786	-3.3497	0.544961	1	1.07456	-3.35998	-0.54075
6	-1.39208	-2.44511	-1.37337	6	1.365181	-2.44131	1.395134
8	-1.2064	-3.41145	-2.14833	8	1.162751	-3.41129	2.188542

[Sb-*L*-tar]$^{2-}$ [Sb-O-Sb]

Atomic Number	B3LYP= -83.8026709 Hartree			Atomic Number	MP2= -82.7197709 Hartree		
	Coordinates (Angstroms)				Coordinates (Angstroms)		
	X	Y	Z		X	Y	Z
51	1.168545	-1.40627	-0.56336	51	1.16341	-1.41507	-0.57159
8	0.98953	0.761545	-0.6992	8	0.982344	0.754146	-0.70476
8	-0.98951	-0.76153	-0.69916	8	-0.98233	-0.75413	-0.70475
8	0.034002	-2.63713	0.805471	8	0.035419	-2.65978	0.809654
8	1.938825	-0.69826	1.168476	8	1.937145	-0.7289	1.181218
8	3.459839	-0.95618	-0.97122	8	3.455945	-0.951	-1.0094
6	3.926391	-0.07657	-0.10103	6	3.933642	-0.07208	-0.11508
8	5.096599	0.389848	-0.05742	8	5.117224	0.411108	-0.07526
6	2.822013	0.411851	0.856917	6	2.832482	0.402871	0.854904
1	3.234893	0.827325	1.771925	1	3.235735	0.810454	1.775402
6	1.974482	1.486103	0.098063	6	1.98362	1.48145	0.109718
1	2.625364	2.053055	-0.5736	1	2.623545	2.043207	-0.57222
6	1.272252	2.50926	1.006834	6	1.279934	2.492685	1.038859
8	1.94631	3.204885	1.799823	8	1.965537	3.157117	1.875639
8	-0.03399	2.637099	0.805503	8	-0.03542	2.65978	0.809652
51	-1.16856	1.406277	-0.56334	51	-1.16342	1.415067	-0.57157
8	-3.45981	0.956144	-0.97125	8	-3.45594	0.950941	-1.00942
8	-1.93886	0.698262	1.168496	8	-1.93715	0.728883	1.18123
6	-3.92638	0.076537	-0.10106	6	-3.93366	0.072101	-0.11504
8	-5.09659	-0.38988	-0.05747	8	-5.1172	-0.4112	-0.07531
6	-2.82202	-0.41186	0.856925	6	-2.83248	-0.40289	0.854907
1	-3.23492	-0.82734	1.771926	1	-3.23572	-0.81049	1.775401
6	-1.97447	-1.4861	0.098092	6	-1.98363	-1.48145	0.109679
1	-2.62533	-2.05306	-0.57358	1	-2.62355	-2.04316	-0.5723
6	-1.27223	-2.50926	1.006863	6	-1.27997	-2.49279	1.038737
8	-1.94627	-3.20484	1.799896	8	-1.96551	-3.15688	1.875842

{[Sb-*L*-tar][H]}$^{-}$

Atomic Number	B3LYP= -83.8026709 Hartree			Atomic Number	MP2= -82.7197709 Hartree		
	Coordinates (Angstroms)				Coordinates (Angstroms)		
	X	Y	Z		X	Y	Z
51	2.640361	0.548126	-0.00998	51	2.641647	0.533613	-0.00833
8	0.660317	1.061546	0.642053	8	0.669353	1.085223	0.667514
8	1.862076	1.850596	-1.48932	8	1.86611	1.801779	-1.52524
8	1.852096	-1.04893	-0.88272	8	1.846179	-1.06554	-0.88789
8	2.561443	-0.81491	1.619463	8	2.516271	-0.78603	1.658798
6	2.013442	-2.02228	1.389882	6	1.949348	-2.0103	1.432408
6	1.434942	-2.15149	-0.03314	6	1.417159	-2.16995	-0.01032
8	1.956877	-2.95171	2.208323	8	1.849686	-2.93188	2.281406
6	-0.09307	-2.24635	0.041688	6	-0.10895	-2.26179	0.028825
6	-0.73436	-2.54988	-1.32593	6	-0.71816	-2.517	-1.36839
8	-0.27581	-3.4316	-2.0689	8	-0.23071	-3.37946	-2.14472
8	-0.6919	-1.04167	0.63121	8	-0.69806	-1.04741	0.647536
51	-2.60713	-0.57683	-0.00597	51	-2.59991	-0.56872	-0.00311
8	-1.85696	-1.8535	-1.53934	8	-1.85741	-1.80799	-1.5836
8	-2.59005	0.850243	1.607778	8	-2.54897	0.834836	1.64639
8	-1.86952	1.05169	-0.8999	8	-1.87439	1.069614	-0.90973
6	-2.06642	2.053559	1.359691	6	-2.01548	2.05358	1.394118
8	-2.01709	3.009858	2.152717	8	-1.92625	3.012627	2.20975
6	-1.47573	2.162402	-0.06481	6	-1.46792	2.184364	-0.05057
6	0.048829	2.27133	0.029767	6	0.056271	2.289025	0.008974
6	0.733461	2.550587	-1.31753	6	0.712849	2.506459	-1.36889
8	0.302864	3.426986	-2.07905	8	0.254625	3.351505	-2.17637
1	1.790198	-3.07656	-0.48869	1	1.794243	-3.09017	-0.45155
1	-0.31397	-3.08072	0.716946	1	-0.35831	-3.09327	0.693406
1	-1.82425	3.085161	-0.5313	1	-1.8325	3.102755	-0.5073
1	0.274344	3.091049	0.717242	1	0.311236	3.111296	0.678183
1	0.057315	0.169082	0.702832	1	0.074747	0.215055	0.70276

{[Sb-*L*-tar][H]}$^{-}_{[Sb\text{-}O\text{-}Sb]}$

Atomic Number	B3LYP= -83.8026709 Hartree			Atomic Number	MP2= -82.7197709 Hartree		
	Coordinates (Angstroms)				Coordinates (Angstroms)		
	X	Y	Z		X	Y	Z
51	1.294938	-1.17869	-1.119	51	1.332619	-1.13501	-1.14349
8	0.798504	0.810472	-0.71347	8	0.762089	0.835986	-0.7279
8	-0.89341	-1.11086	-0.89595	8	-0.87179	-1.12046	-0.89683
8	0.890401	-2.51871	0.352446	8	1.005079	-2.48337	0.34242
8	1.282374	0.347027	2.062144	8	1.24786	0.205343	1.978925
8	3.00029	-0.72419	-0.12125	8	3.06503	-0.61555	-0.20788
6	3.351955	0.179773	0.837866	6	3.365529	0.265671	0.821415
8	4.508119	0.259397	1.260533	8	4.530231	0.385408	1.263794
6	2.227825	1.119758	1.286663	6	2.180695	1.113077	1.294968
6	1.587288	1.787995	0.048366	6	1.52806	1.815656	0.079546
6	0.685943	2.983628	0.435502	6	0.588931	2.97339	0.513201
8	1.206122	3.986759	0.950424	8	1.08777	3.957703	1.124371
8	-0.60776	2.849198	0.141241	8	-0.70532	2.85104	0.144849
51	-1.44773	1.11859	-0.75063	51	-1.49194	1.083073	-0.76782
8	-3.44818	0.483249	-0.16343	8	-3.48112	0.368203	-0.20854
8	-1.23189	0.36736	1.138753	8	-1.2638	0.386881	1.150817
6	-3.47039	-0.46048	0.79185	6	-3.47097	-0.5719	0.781704
8	-4.4841	-1.03479	1.222948	8	-4.47639	-1.20101	1.209622
6	-2.04559	-0.82698	1.240245	6	-2.0342	-0.8609	1.25417
6	-1.44492	-1.87023	0.229725	6	-1.37761	-1.88937	0.272291
6	-0.34858	-2.73149	0.859655	6	-0.22804	-2.67181	0.926296
8	-0.59121	-3.5668	1.734852	8	-0.42325	-3.45661	1.881478
1	0.325903	0.450312	1.795934	1	0.294752	0.400877	1.765381
1	2.663878	1.905915	1.904753	1	2.532229	1.883567	1.979234
1	2.372735	2.179512	-0.60303	1	2.298755	2.239309	-0.56509
1	-2.03769	-1.21108	2.256415	1	-2.00443	-1.22325	2.276239
1	-2.22776	-2.53635	-0.13642	1	-2.12124	-2.60286	-0.08129

{[Sb-*L*-tar][H][D-Leu]}$^{-}$

Atomic Number	B3LYP= -83.8026709 Hartree			Atomic Number	MP2= -82.7197709 Hartree		
	Coordinates (Angstroms)				Coordinates (Angstroms)		
	X	Y	Z		X	Y	Z
8	-2.39744	0.929032	-2.07426	8	-2.43862	1.148273	-2.05831
6	-1.34566	0.227363	-1.96055	6	-1.3744	0.434626	-2.00201
8	-1.3257	-1.00572	-1.52375	8	-1.35147	-0.85043	-1.67265
6	0.011569	0.806672	-2.37222	6	-0.01905	1.068554	-2.33598
1	-0.04518	1.112006	-3.42234	1	-0.04702	1.473254	-3.34922
51	0.652737	-2.02354	-1.58915	51	0.648432	-1.81588	-1.80276
8	0.723504	-1.80541	0.396779	8	0.639657	-1.7375	0.202953
8	1.055405	-0.18005	-2.24612	8	1.066232	0.086804	-2.28417
8	2.70932	-2.41458	-1.19192	8	2.703974	-2.23992	-1.39702
6	3.107783	-2.38891	0.086715	6	3.055072	-2.34713	-0.08827
8	4.240684	-2.72552	0.485816	8	4.189135	-2.72028	0.326704
6	1.994563	-1.97734	1.069679	6	1.901715	-2.04071	0.893353
1	1.875513	-2.78091	1.803284	1	1.714421	-2.91824	1.516197
6	0.315991	2.068649	-1.54623	6	0.24116	2.22535	-1.36255
1	-0.42975	2.820146	-1.82366	1	-0.5196	2.987524	-1.53749
8	0.17095	1.799766	-0.13409	8	0.057526	1.75406	0.017584
51	1.738054	2.102484	1.081007	51	1.60325	1.990964	1.290831
8	0.752146	0.896132	2.589237	8	0.578755	0.63906	2.644305
6	1.264272	-0.3115	2.825578	6	1.125237	-0.58823	2.789415
8	0.929761	-1.06247	3.768484	8	0.771734	-1.44426	3.656304
6	1.708344	2.636107	-1.88889	6	1.639094	2.834102	-1.61215
8	1.969553	3.051728	-3.03853	8	1.921866	3.374245	-2.72254
6	2.386059	-0.71137	1.848214	6	2.284114	-0.87708	1.814518
1	3.276207	-0.96068	2.434792	1	3.165202	-1.17822	2.383501
8	2.727126	0.368216	0.95308	8	2.652775	0.297559	1.02263
8	2.527736	2.696503	-0.84049	8	2.453617	2.783374	-0.53484
1	-3.94347	0.580285	-1.81905	1	-3.99965	0.694058	-1.69464
8	-4.94471	0.439817	-1.75033	8	-4.98366	0.548598	-1.57152
6	-5.50702	0.388897	-0.51351	6	-5.39822	0.380194	-0.25748
8	-6.73188	0.197872	-0.39795	8	-6.62035	0.200363	-0.0135
6	-4.58338	0.511214	0.700188	6	-4.31655	0.341588	0.820426
1	-5.2547	0.644983	1.552265	1	-4.84383	0.354685	1.77573
7	-3.77087	1.746432	0.581698	7	-3.48992	1.598899	0.759978
1	-3.26606	1.9531	1.436198	1	-2.80189	1.586635	1.508482
1	-3.10888	1.717603	-0.19255	1	-2.95918	1.632141	-0.11184
1	-4.40716	-1.64919	0.515862	1	-4.109	-1.76012	0.223574
6	-3.78722	-0.81776	0.884691	6	-3.49753	-0.98409	0.709352
1	-2.89783	-0.79486	0.244483	1	-2.63635	-0.82155	0.04874
6	-3.38715	-1.15942	2.3422	6	-3.02391	-1.53353	2.082248
1	-4.32149	-1.34338	2.900738	1	-3.91644	-1.90948	2.612901
6	-2.61661	-0.03974	3.072494	6	-2.35922	-0.44891	2.964737
1	-2.28549	-0.38639	4.059465	1	-1.97025	-0.89321	3.889265
1	-1.71431	0.260209	2.528775	1	-1.50034	0.009548	2.458115

1	-3.24674	0.846829	3.229213	1	-3.07892	0.339765	3.231307
6	-2.55842	-2.46356	2.348219	6	-2.03603	-2.70845	1.844914
1	-1.60843	-2.31695	1.818503	1	-1.15348	-2.34941	1.290896
1	-3.10537	-3.27991	1.855667	1	-2.51798	-3.50061	1.251131
1	-2.32148	-2.77248	3.374501	1	-1.69042	-3.12559	2.801056

{[Sb-*L*-tar][H][L-Leu]}$^{-}$

Atomic Number	B3LYP= -83.8026709 Hartree			Atomic Number	MP2= -82.7197709 Hartree		
	Coordinates (Angstroms)				Coordinates (Angstroms)		
	X	Y	Z		X	Y	Z
6	-0.31647	-0.96632	2.292157	6	-0.53808	-0.67012	2.481246
6	-0.17889	0.561771	2.411552	6	-0.4616	0.859234	2.407212
1	0.649312	0.757323	3.100163	1	0.263921	1.202632	3.148151
6	0.924393	-1.55191	1.611224	6	0.801153	-1.28174	2.039767
1	-0.37749	-1.36831	3.30923	1	-0.74376	-0.95489	3.515516
6	-0.76479	1.521179	-2.50527	6	-0.05848	1.166397	-2.53931
1	-2.13735	-0.76087	-3.22073	1	-1.23574	-1.24052	-3.23737
8	0.161195	1.142971	1.134542	8	0.056092	1.253355	1.095574
8	2.076226	-1.37815	2.103979	8	1.903367	-0.95591	2.593991
6	-2.12387	0.990581	-2.00478	6	-1.50802	0.679164	-2.33046
6	-3.55021	-1.07434	-1.63134	6	-2.99632	-1.32245	-1.9736
8	-1.82214	0.914481	4.173336	8	-2.38912	1.331884	3.844888
1	-2.90704	1.41371	-2.64259	1	-2.11583	1.000386	-3.17893
6	-2.20265	-0.53656	-2.15187	6	-1.5546	-0.85081	-2.26924
8	-1.5182	-1.33536	1.587285	8	-1.6514	-1.16034	1.662624
8	0.693046	-2.24683	0.519731	8	0.713029	-2.18483	1.056223
8	-0.40786	1.366037	-3.69388	8	0.626276	0.788575	-3.53762
8	-0.07954	2.193252	-1.5807	8	0.372811	2.039659	-1.60226
8	-2.38956	1.394102	-0.64415	8	-2.11997	1.246452	-1.12357
8	-1.08483	-1.18113	-1.49711	8	-0.58917	-1.34194	-1.27658
8	-3.424	-1.94783	-0.62201	8	-3.11437	-2.03279	-0.82149
8	-4.63166	-0.76011	-2.16731	8	-3.93991	-1.09731	-2.78478
8	-2.03294	2.079124	2.206261	8	-2.33231	2.235453	1.699803
51	-1.0535	2.519685	0.328152	51	-1.03456	2.521263	-0.01664
51	-1.4464	-2.49284	-0.03781	51	-1.29365	-2.49964	0.211116
6	-1.45288	1.190557	3.011271	6	-1.84144	1.484716	2.712718
7	3.048426	-2.07285	-1.36613	7	2.561445	-2.0388	-1.20971
6	3.996295	-0.96898	-1.07269	6	3.521284	-0.90583	-0.94402
6	4.987187	-1.42544	0.004208	6	4.616715	-1.39845	0.001996
8	6.209797	-1.50775	-0.22071	8	5.81276	-1.57213	-0.3459
6	3.297446	0.367272	-0.71585	6	2.805946	0.342411	-0.38383
6	4.229158	1.562425	-0.40626	6	3.728507	1.55729	-0.11659
6	5.125454	1.938118	-1.60503	6	4.286076	2.116699	-1.45161
6	3.376019	2.769021	0.039893	6	2.912865	2.65222	0.620012
8	4.513952	-1.73576	1.239416	8	4.264589	-1.66138	1.327976
1	4.610248	-0.83619	-1.96567	1	4.018383	-0.67324	-1.88685
1	2.632626	0.211986	0.139645	1	2.283287	0.082386	0.540297

1	2.637831	0.629956	-1.5544	1	2.02158	0.643809	-1.08544
1	2.646701	-1.97498	-2.29411	1	1.871123	-1.71023	-1.88789
1	2.289295	-2.16011	-0.6867	1	2.021594	-2.20501	-0.35604
1	4.885611	1.279766	0.430892	1	4.564508	1.236061	0.525033
1	5.734833	2.822995	-1.37277	1	4.900795	3.01311	-1.2778
1	4.507824	2.174897	-2.48287	1	3.435637	2.384634	-2.09738
1	5.80902	1.123713	-1.87099	1	4.899206	1.371929	-1.97564
1	2.703306	3.080629	-0.76994	1	2.145305	3.031154	-0.06919
1	4.010485	3.622989	0.318273	1	3.558697	3.485227	0.939343
1	2.745608	2.500059	0.895354	1	2.386122	2.220807	1.480314
1	3.530211	-1.61725	1.450192	1	3.34808	-1.40152	1.616464

{[Sb-*L*-tar][Sb-O-Sb][D-Leu]}$^-$

Atomic Number	B3LYP= -83.8026709 Hartree			Atomic Number	MP2= -82.7197709 Hartree		
	Coordinates (Angstroms)				Coordinates (Angstroms)		
	X	Y	Z		X	Y	Z
51	0.145604	1.354109	-0.14131	51	0.092869	1.512896	-0.39958
8	0.358432	-0.74843	0.324672	8	0.064461	-0.54701	0.312288
8	2.005012	0.559621	-1.0351	8	1.897296	0.45647	-1.09299
8	1.620049	2.83202	0.16621	8	1.66219	2.944486	-0.25588
8	0.137227	1.275153	1.87427	8	0.137068	1.685346	1.625387
8	-2.26646	0.86047	0.751069	8	-2.29609	1.337595	0.487502
6	-2.11464	0.354077	1.960862	6	-2.22545	1.058881	1.797778
8	-3.0574	-0.0095	2.718041	8	-3.22863	0.976937	2.586876
6	-0.64608	0.15387	2.349064	6	-0.79801	0.720086	2.230081
6	-0.12921	-1.14289	1.640293	6	-0.49054	-0.71174	1.672461
6	0.969283	-1.90329	2.407864	6	0.460038	-1.55932	2.544975
8	0.783802	-2.23253	3.598107	8	0.209598	-1.70914	3.777264
8	2.025816	-2.24038	1.675198	8	1.453122	-2.17169	1.869126
51	2.371318	-1.5264	-0.33075	51	1.98966	-1.58392	-0.14519
8	6.020973	0.045307	-2.02513	8	5.988455	-0.51097	-1.47457
8	3.694239	-0.34918	0.64199	8	3.277955	-0.40563	0.896458
6	4.972946	-0.31768	-1.43461	6	4.826322	-0.71759	-0.99436
8	4.242715	-1.3898	-1.70704	8	4.020541	-1.76241	-1.26663
6	4.329567	0.530139	-0.32088	6	4.125	0.306791	-0.08093
6	3.200743	1.398485	-0.97041	6	3.188005	1.182002	-0.97784
6	2.894929	2.692419	-0.20416	6	2.959531	2.603544	-0.42975
8	3.781592	3.549369	-0.02471	8	3.940419	3.380047	-0.24691
7	-5.74997	-0.27469	1.492292	7	-5.62258	-0.23632	1.271564
6	-5.75948	-0.20305	0.019777	6	-5.3076	-0.57047	-0.1497
6	-5.53933	1.221007	-0.52862	6	-5.3519	0.650194	-1.08976
8	-6.45849	1.81764	-1.13126	8	-6.2613	0.769986	-1.9625
6	-4.74399	-1.21664	-0.54587	6	-3.94837	-1.30518	-0.18765
6	-4.63794	-1.26865	-2.08708	6	-3.38443	-1.55091	-1.60864
6	-3.51146	-2.23808	-2.49958	6	-2.03535	-2.30297	-1.49039
6	-5.97077	-1.65659	-2.76004	6	-4.39039	-2.33875	-2.4852
8	-4.35111	1.828922	-0.32876	8	-4.41276	1.641823	-0.93404

1	-4.82722	-0.17115	1.931907	1	-4.85065	0.260701	1.729634
1	-3.5758	1.352522	0.166275	1	-3.64563	1.466783	-0.27985
1	-6.43824	0.331216	1.928064	1	-6.48111	0.301568	1.35235
1	-0.53536	0.059751	3.426649	1	-0.67328	0.738417	3.308229
1	-0.95876	-1.84402	1.507818	1	-1.42428	-1.27247	1.570558
1	5.059965	1.162457	0.176205	1	4.83025	0.9342	0.453116
1	3.491406	1.681929	-1.98503	1	3.612254	1.273993	-1.97771
1	-6.76491	-0.46851	-0.31723	1	-6.09317	-1.2339	-0.5192
1	-5.03018	-2.20416	-0.1577	1	-4.07805	-2.2657	0.331512
1	-3.75386	-0.98918	-0.13478	1	-3.20758	-0.72662	0.375243
1	-4.36053	-0.26577	-2.44262	1	-3.19996	-0.57216	-2.07489
1	-3.38462	-2.25866	-3.59003	1	-1.57716	-2.45248	-2.47887
1	-3.73824	-3.26087	-2.16591	1	-2.20137	-3.28786	-1.02554
1	-2.55516	-1.94445	-2.05107	1	-1.33287	-1.73836	-0.86072
1	-5.84853	-1.73093	-3.84902	1	-3.95388	-2.56153	-3.46905
1	-6.75229	-0.91531	-2.56175	1	-5.31615	-1.76916	-2.63678
1	-6.31947	-2.63331	-2.39295	1	-4.63811	-3.29328	-1.99326

{[Sb-*L*-tar][Sb-O-Sb][L-Leu]}$^{-}$

Atomic Number	B3LYP= -83.8026709 Hartree			Atomic Number	MP2= -82.7197709 Hartree		
	Coordinates (Angstroms)				Coordinates (Angstroms)		
	X	Y	Z		X	Y	Z
51	0.133353	-0.96877	0.28604	51	-0.25877	0.335261	-0.97081
8	0.870718	1.0529	0.510255	8	0.98004	-1.45452	-0.67419
8	2.294833	-0.99706	0.711829	8	1.82208	0.926238	-1.04537
8	0.949601	-2.46776	-0.95742	8	-0.24088	2.277013	-0.09619
8	-0.27729	-0.0692	-1.47448	8	-0.50416	-0.15608	0.97509
8	-2.16742	0.28492	0.389857	8	-2.17857	-1.38763	-0.72553
6	-2.13002	1.202628	-0.5573	6	-2.04125	-1.95528	0.48308
8	-3.07958	1.983062	-0.84889	8	-2.92203	-2.6806	1.059908
6	-0.77565	1.275255	-1.26934	6	-0.69394	-1.61206	1.123984
6	0.23183	2.042496	-0.34644	6	0.455385	-2.36487	0.366126
6	1.299804	2.859286	-1.09845	6	1.600816	-2.85336	1.28128
8	0.952688	3.696949	-1.95725	8	1.341004	-3.64226	2.236834
8	2.546663	2.659419	-0.6827	8	2.838628	-2.45516	0.916604
51	3.107153	1.09002	0.686138	51	3.120303	-0.87118	-0.5173
8	6.397412	-1.68685	0.313675	8	5.387306	2.744309	0.299696
8	3.702576	0.210304	-1.03212	8	2.940135	0.250746	1.167128
6	5.397841	-0.92555	0.301305	6	4.632012	1.727217	0.16801
8	5.132559	0.044922	1.164492	8	4.873081	0.64646	-0.60217
6	4.258146	-1.09295	-0.72169	6	3.235497	1.652806	0.818698
6	3.123713	-1.93441	-0.04418	6	2.192641	2.126104	-0.24995
6	2.257722	-2.72431	-1.03483	6	0.933253	2.802722	0.330736
8	2.767951	-3.57923	-1.78414	8	1.041435	3.824035	1.066162
7	-5.70287	1.411332	0.389193	7	-5.30319	-0.81471	0.810625
6	-5.86626	0.04878	0.923875	6	-5.20816	0.323805	-0.15125
6	-5.13591	-0.18083	2.264806	6	-5.29773	-0.11809	-1.6247

8	-5.77987	-0.45108	3.301505	8	-6.24494	0.248123	-2.37813
6	-5.44706	-1.03011	-0.10209	6	-3.92641	1.167052	0.072948
6	-6.2956	-1.13842	-1.40043	6	-3.76456	1.824299	1.475731
6	-7.80836	-1.23058	-1.11043	6	-5.10138	2.427588	1.975576
6	-5.99929	-0.02804	-2.43028	6	-3.16716	0.8449	2.521505
8	-3.79202	-0.05953	2.310898	8	-4.32254	-0.96621	-2.10862
1	-3.2375	0.128803	1.457813	1	-3.54702	-1.17793	-1.48138
1	-4.7896	1.611494	-0.03741	1	-4.4743	-1.41488	0.820229
1	-0.86538	1.782884	-2.22644	1	-0.67546	-1.8511	2.182015
1	-0.3135	2.749433	0.285827	1	0.04868	-3.23952	-0.1423
1	4.602664	-1.5777	-1.63085	1	3.163166	2.262312	1.712634
1	3.564335	-2.65661	0.647503	1	2.660329	2.839971	-0.92822
1	-5.96353	2.133838	1.053959	1	-6.12005	-1.38974	0.616588
1	-6.92038	-0.09217	1.176317	1	-6.08327	0.956501	0.012332
1	-5.50041	-1.99858	0.416024	1	-3.93133	1.958255	-0.69176
1	-4.39524	-0.88097	-0.3727	1	-3.05201	0.540204	-0.12798
1	-5.99269	-2.09359	-1.85817	1	-3.03481	2.634972	1.337653
1	-8.36377	-1.46372	-2.02903	1	-4.93839	3.009451	2.893574
1	-8.18962	-0.27763	-0.72337	1	-5.81015	1.617248	2.198014
1	-8.03003	-2.01205	-0.37114	1	-5.55061	3.087926	1.218145
1	-6.52467	-0.23333	-3.37457	1	-2.99719	1.373653	3.47208
1	-4.9263	0.036773	-2.64307	1	-2.1997	0.468916	2.157954
1	-6.316	0.946208	-2.0474	1	-3.85247	0.005684	2.68916

{[Sb-*L*-tar][H][D-Leu]}$^{-}$

Atomic Number	B3LYP= -83.8026709 Hartree			Atomic Number	MP2= -82.7197709 Hartree		
	Coordinates (Angstroms)				Coordinates (Angstroms)		
	X	Y	Z		X	Y	Z
51	0.923763	0.931552	-1.65886	51	-1.07098	2.043145	0.798777
8	-1.09367	0.049272	-1.55933	8	0.853088	1.104895	1.316721
8	1.181297	-1.1307	-1.18346	8	-1.52437	0.083937	1.555856
8	0.631296	1.184443	0.353861	8	-0.80503	1.215479	-1.02769
8	-0.08445	2.829268	-1.48794	8	0.256644	3.439614	-0.16873
6	-0.51764	3.253833	-0.29724	6	0.74318	3.128927	-1.40028
6	-0.23024	2.253752	0.834808	6	0.211959	1.781445	-1.93041
8	-1.09077	4.331912	-0.06977	8	1.524853	3.836516	-2.08732
6	-1.52795	1.712492	1.438377	6	1.332717	0.765918	-2.12224
6	-1.26339	0.846497	2.68626	6	0.768185	-0.58697	-2.61777
8	-0.42371	1.187936	3.537454	8	-0.15942	-0.63567	-3.47176
8	-2.32506	0.971318	0.46101	8	2.091008	0.57666	-0.86345
51	-3.50327	-0.54841	1.2102	51	2.971909	-1.27791	-0.64968
8	-2.07452	-0.20985	2.767437	8	1.411122	-1.65407	-2.0866
8	-4.29831	-0.68916	-0.78292	8	3.940951	-0.36205	1.04361
8	-2.27753	-1.88426	0.366978	8	1.672189	-1.72086	0.817964
6	-3.65008	-1.47007	-1.65305	6	3.265071	-0.3764	2.219045
8	-4.00211	-1.71373	-2.8201	8	3.669231	0.099346	3.31482
6	-2.3488	-2.06159	-1.06518	6	1.874551	-1.05087	2.106618

6	-1.14594	-1.41764	-1.76332	6	0.781862	-0.00197	2.323994
6	0.203388	-2.02884	-1.35778	6	-0.62771	-0.61283	2.296203
8	0.351018	-3.25885	-1.30471	8	-0.90231	-1.63596	2.97645
7	5.901867	1.461895	-0.07616	7	-5.62281	-0.38533	0.739213
6	5.068076	0.518331	0.685338	6	-4.61118	-0.83177	-0.25121
6	3.585567	0.683669	0.386226	6	-3.62108	0.252757	-0.63576
8	2.762918	0.529689	1.412157	8	-2.90977	-0.03643	-1.76022
6	5.550949	-0.93057	0.412536	6	-3.82221	-2.039	0.352773
6	4.875812	-2.04156	1.266697	6	-2.905	-2.8082	-0.65306
6	3.764446	-2.77752	0.491379	6	-1.40523	-2.49423	-0.41916
6	5.934928	-3.04483	1.772387	6	-3.14393	-4.33517	-0.52628
8	3.174901	0.971962	-0.78535	8	-3.42167	1.304682	0.056211
1	-1.65389	0.440113	-0.76485	1	1.395791	0.898159	0.454214
1	0.299488	2.769749	1.639358	1	-0.27945	1.933668	-2.89184
1	-2.10989	2.589422	1.745392	1	2.034069	1.173117	-2.85603
1	-2.30484	-3.12974	-1.28264	1	1.760087	-1.79896	2.889342
1	-1.28375	-1.55909	-2.83918	1	0.96216	0.487672	3.281815
1	5.77076	2.432284	0.193992	1	-6.0874	0.469943	0.445529
1	5.790712	1.360412	-1.0815	1	-5.17416	-0.21128	1.63652
1	5.196534	0.730739	1.749547	1	-5.11814	-1.16535	-1.16048
1	1.763293	0.7255	1.137622	1	-2.02897	0.456673	-1.73183
1	6.6294	-0.90168	0.602676	1	-4.59573	-2.70886	0.747548
1	5.420313	-1.14788	-0.65688	1	-3.22459	-1.6759	1.20105
1	4.418806	-1.56675	2.145797	1	-3.17171	-2.49357	-1.66899
1	2.996459	-2.10642	0.094591	1	-1.21824	-1.41644	-0.3783
1	3.258613	-3.5077	1.133903	1	-0.7773	-2.91326	-1.21457
1	4.194158	-3.32309	-0.36093	1	-1.08645	-2.90557	0.549072
1	5.469267	-3.82882	2.381868	1	-2.51357	-4.88507	-1.23811
1	6.700994	-2.54763	2.381518	1	-4.19721	-4.58687	-0.71605
1	6.440117	-3.53294	0.927258	1	-2.88627	-4.66636	0.490938

{[Sb-*L*-tar][H][L-Leu]}$^{-}$

Atomic Number	B3LYP= -83.8026709 Hartree			Atomic Number	MP2= -82.7197709 Hartree		
	Coordinates (Angstroms)				Coordinates (Angstroms)		
	X	Y	Z		X	Y	Z
51	0.852693	0.634324	-1.89165	51	0.973519	0.86219	-1.80253
8	-1.14602	-0.24338	-1.54739	8	-0.96388	-0.16389	-1.59421
8	1.16742	-1.29828	-1.0511	8	1.403861	-1.04951	-0.93742
8	0.614206	1.243948	0.055058	8	0.627145	1.461485	0.10572
8	-0.18164	2.522808	-2.02594	8	-0.27828	2.598022	-2.05864
6	-0.59278	3.145773	-0.91811	6	-0.78075	3.212334	-0.95404
6	-0.24655	2.374658	0.366232	6	-0.34511	2.533379	0.360358
8	-1.18707	4.235389	-0.86932	8	-1.51414	4.235011	-0.94662
6	-1.50874	1.938043	1.112718	6	-1.54551	1.967739	1.11244
6	-1.17635	1.327203	2.488966	6	-1.10846	1.316981	2.445711
8	-0.31404	1.837958	3.22568	8	-0.21739	1.843111	3.167541

8	-2.32113	1.011188	0.325825	8	-2.27588	0.98863	0.272866
51	-3.43197	-0.36219	1.390051	51	-3.27716	-0.48299	1.317385
8	-1.95435	0.288885	2.798639	8	-1.82662	0.209577	2.74981
8	-4.30182	-0.87811	-0.50641	8	-4.0914	-0.98157	-0.6183
8	-2.20911	-1.80992	0.75116	8	-1.94877	-1.84967	0.681097
6	-3.66922	-1.79154	-1.24974	6	-3.37324	-1.83998	-1.38397
8	-4.06045	-2.24704	-2.33814	8	-3.69927	-2.2713	-2.52349
6	-2.33269	-2.24625	-0.62098	6	-2.03595	-2.26065	-0.72354
6	-1.17275	-1.72299	-1.4755	6	-0.87752	-1.65906	-1.52129
6	0.204483	-2.22828	-1.02053	6	0.501333	-2.06058	-0.97245
8	0.382157	-3.42536	-0.75011	8	0.761617	-3.25812	-0.68385
1	0.303869	3.036708	1.039465	1	0.147579	3.260183	1.006782
1	-2.09936	2.847723	1.27193	1	-2.23417	2.794938	1.305566
1	-2.27368	-3.33541	-0.6422	1	-1.9245	-3.34299	-0.75757
1	-1.34862	-2.06356	-2.5	1	-0.97468	-1.98288	-2.55836
7	5.483305	1.326808	1.59549	7	5.603976	1.161578	1.872401
6	5.064791	0.716659	0.326429	6	4.935358	0.265396	0.882288
6	3.567318	0.802263	0.067911	6	3.572358	0.778285	0.447408
8	2.778957	0.817362	1.127952	8	2.698379	0.936349	1.470676
6	5.585802	-0.7453	0.216806	6	4.762232	-1.14256	1.506751
6	5.033544	-1.75443	1.264188	6	3.847333	-2.08399	0.684063
6	3.865069	-2.58832	0.700875	6	4.403202	-2.33104	-0.73972
6	6.165938	-2.67716	1.763937	6	3.647758	-3.42309	1.4317
8	3.115104	0.871336	-1.12435	8	3.280012	1.022156	-0.77417
1	5.001475	0.942551	2.402671	1	5.013141	1.27788	2.692778
1	5.406342	2.339155	1.601383	1	5.823891	2.073569	1.480688
1	5.53052	1.279928	-0.48695	1	5.560318	0.223385	-0.00963
1	6.673087	-0.65898	0.320978	1	4.322391	-1.01052	2.505316
1	5.377018	-1.11505	-0.79484	1	5.763015	-1.58059	1.627694
1	4.660137	-1.19455	2.132651	1	2.866672	-1.61189	0.565093
1	3.046095	-1.97863	0.307864	1	4.48242	-1.39164	-1.3024
1	3.443887	-3.24222	1.473723	1	3.719349	-2.99116	-1.28761
1	4.216859	-3.22686	-0.12177	1	5.3971	-2.80435	-0.68871
1	5.787318	-3.3969	2.499947	1	2.938613	-4.05247	0.880342
1	6.973858	-2.09938	2.230034	1	3.245306	-3.24634	2.438488
1	6.594935	-3.24797	0.928457	1	4.607294	-3.95574	1.526236
1	-1.68112	0.276518	-0.81386	1	-1.52884	0.291175	-0.84869
1	1.762323	0.954157	0.85178	1	1.771763	1.177657	1.117141

{[Sb-*L*-tar][H][Sb-O-Sb][D-Leu]}$^{-}$

Atomic Number	B3LYP= -83.8026709 Hartree			Atomic Number	MP2= -82.7197709 Hartree		
	Coordinates (Angstroms)				Coordinates (Angstroms)		
	X	Y	Z		X	Y	Z
51	0.335277	0.194219	-1.01686	51	0.292513	0.310266	-1.14955
8	-1.47282	1.222949	-0.69253	8	-1.53286	1.220478	-0.71743

8	-1.25748	-1.35745	-0.87549	8	-1.19721	-1.33935	-0.93705
8	0.820367	-0.93969	0.604602	8	0.931905	-0.7494	0.475588
8	-1.13887	1.392264	2.159276	8	-0.97925	1.328152	2.126569
8	1.122406	1.732671	0.175228	8	1.095354	1.891982	-0.05196
6	0.575516	2.662934	1.023669	6	0.566958	2.757619	0.904009
8	1.286521	3.550142	1.505968	8	1.281463	3.669111	1.382417
6	-0.92098	2.54343	1.31282	6	-0.89547	2.535585	1.293134
6	-1.71674	2.491057	-0.00406	6	-1.78596	2.469944	0.037199
6	-3.23436	2.670672	0.240562	6	-3.29262	2.559421	0.404659
8	-3.64876	3.758484	0.673357	8	-3.71941	3.616497	0.942782
8	-3.99359	1.62348	-0.07866	8	-4.04504	1.488685	0.067609
51	-3.23603	-0.18973	-0.88311	51	-3.24336	-0.28248	-0.81652
8	-4.22786	-2.05197	-0.33831	8	-4.09419	-2.20519	-0.24985
8	-2.68449	-0.53155	1.058295	8	-2.56761	-0.58232	1.100216
6	-3.6384	-2.71518	0.66909	6	-3.40268	-2.84471	0.739863
8	-3.96564	-3.83608	1.093137	8	-3.63776	-4.00571	1.169173
6	-2.4151	-1.94691	1.197332	6	-2.20472	-2.0007	1.212084
6	-1.17886	-2.26037	0.274596	6	-0.99765	-2.23347	0.236698
6	0.140283	-2.0346	1.003496	6	0.328809	-1.89457	0.914695
8	0.563665	-2.79908	1.88064	8	0.840001	-2.61829	1.80631
7	4.190741	-1.78302	1.69709	7	3.893497	-1.56556	1.884924
6	4.682413	-1.17935	0.441796	6	4.477662	-1.13983	0.580216
6	3.683444	-0.15003	-0.06501	6	3.635999	-0.07264	-0.10007
8	3.580505	0.954043	0.700726	8	3.543086	1.086709	0.632677
6	6.081104	-0.58015	0.667764	6	5.915953	-0.6255	0.803526
6	6.736028	0.070318	-0.57187	6	6.580745	-0.04624	-0.4709
6	8.058224	0.753428	-0.16685	6	8.000638	0.466875	-0.12916
6	6.974137	-0.94302	-1.71042	6	6.637868	-1.09984	-1.60569
8	2.94853	-0.33268	-1.0706	8	3.043864	-0.22231	-1.21105
1	-1.7417	0.693232	1.778104	1	-1.5994	0.64298	1.755845
1	-1.22185	3.44316	1.851727	1	-1.22509	3.389892	1.882966
1	-1.40237	3.310554	-0.65652	1	-1.5561	3.307102	-0.62373
1	-2.21142	-2.19862	2.234497	1	-1.93041	-2.2257	2.237741
1	-1.21238	-3.29519	-0.06878	1	-0.97169	-3.26587	-0.10851
1	4.133232	-1.10832	2.456114	1	3.833643	-0.76447	2.511073
1	3.299713	-2.26768	1.605006	1	2.9527	-1.9506	1.782185
1	4.718939	-1.96789	-0.31139	1	4.478965	-2.00652	-0.08123
1	2.725105	1.461114	0.518736	1	2.749952	1.620822	0.341517
1	6.718224	-1.39035	1.04564	1	6.512248	-1.46535	1.186147
1	6.004526	0.171703	1.463361	1	5.886771	0.152685	1.578098
1	6.059198	0.852495	-0.94551	1	5.977106	0.80548	-0.81389
1	7.892366	1.501011	0.617948	1	7.956688	1.228674	0.659592
1	8.521731	1.25695	-1.02436	1	8.485105	0.90374	-1.0127
1	8.77461	0.01389	0.217043	1	8.622257	-0.36647	0.230685
1	7.478439	-0.46297	-2.55826	1	7.165856	-0.69569	-2.47974
1	6.036032	-1.36895	-2.08258	1	5.631979	-1.39827	-1.92384
1	7.610362	-1.76963	-1.36436	1	7.176061	-1.99469	-1.25706

{[Sb-*L*-tar][H][Sb-O-Sb][L-Leu]}$^{-}$

Atomic Number	B3LYP= -83.8026709 Hartree			Atomic Number	MP2= -82.7197709 Hartree		
	Coordinates (Angstroms)				Coordinates (Angstroms)		
	X	Y	Z		X	Y	Z
51	0.463682	0.230464	-0.79143	51	0.376058	0.484785	-1.09355
8	-1.44647	1.116109	-0.79519	8	-1.61954	1.038461	-0.84754
8	-1.00125	-1.43962	-0.66921	8	-0.76671	-1.40672	-0.75167
8	0.847123	-0.69417	0.981977	8	1.106291	-0.24327	0.670488
8	-1.51631	1.591831	2.046461	8	-1.26063	1.544955	1.976479
8	0.961586	1.94942	0.312691	8	0.771323	2.313159	-0.17168
6	0.236642	2.89186	0.999517	6	0.022756	3.141275	0.662133
8	0.807158	3.876612	1.479187	8	0.504839	4.228993	1.056125
6	-1.27186	2.666961	1.111555	6	-1.3822	2.6565	1.022861
6	-1.8792	2.415371	-0.28018	6	-2.16435	2.279976	-0.25071
6	-3.42533	2.476921	-0.24629	6	-3.67812	2.094951	0.044376
8	-3.97863	3.558363	0.012088	8	-4.33936	3.090378	0.445908
8	-4.05022	1.338189	-0.54289	8	-4.18043	0.865657	-0.20614
51	-3.05119	-0.46697	-1.04567	51	-2.98574	-0.78602	-0.84465
8	-3.95101	-2.35331	-0.42692	8	-3.47091	-2.77269	-0.09617
8	-2.73478	-0.56389	0.973024	8	-2.3944	-0.73694	1.122583
6	-3.445	-2.85641	0.710339	6	-2.73288	-3.14834	0.990481
8	-3.73006	-3.95808	1.209057	8	-2.75771	-4.28194	1.540049
6	-2.37026	-1.9264	1.298432	6	-1.76314	-2.03024	1.414331
6	-1.00077	-2.20705	0.577751	6	-0.47139	-2.10859	0.527367
6	0.186924	-1.78276	1.435354	6	0.708576	-1.42962	1.219422
8	0.526883	-2.39687	2.453678	8	1.287203	-1.92755	2.218294
7	4.457966	-1.08303	2.151	7	3.95312	-0.12468	2.345357
6	4.961119	-0.2841	1.007787	6	4.599295	0.181945	1.030765
6	3.784641	0.456303	0.387598	6	3.650901	0.970506	0.13108
8	3.46653	1.599906	1.02209	8	3.315747	2.195561	0.660363
6	5.682341	-1.18999	0.004338	6	5.03209	-1.12603	0.352959
6	6.366459	-0.46104	-1.17555	6	5.939182	-0.91565	-0.88562
6	7.522226	0.449083	-0.71053	6	7.346286	-0.42518	-0.46041
6	6.871025	-1.49216	-2.2055	6	6.048336	-2.23554	-1.68595
8	3.098174	0.007673	-0.56736	8	3.149089	0.546858	-0.95206
1	3.752808	-1.768	1.885997	1	3.145441	-0.74057	2.227046
1	-2.00817	0.807423	1.671808	1	-1.72495	0.719209	1.669767
1	2.542747	1.933528	0.769452	1	2.451076	2.512989	0.274842
1	-1.70722	3.586035	1.507013	1	-1.91426	3.47611	1.504047
1	-1.54756	3.194998	-0.97188	1	-2.06678	3.073344	-0.99339
1	-2.28572	-2.0546	2.374079	1	-1.51802	-2.08531	2.470112
1	-0.90089	-3.26988	0.35265	1	-0.21365	-3.14399	0.309259
1	4.103585	-0.50904	2.911156	1	3.628883	0.730979	2.790197
1	5.640269	0.463897	1.420452	1	5.465637	0.815679	1.235989
1	6.426703	-1.76679	0.567717	1	5.562452	-1.7327	1.098456
1	4.952683	-1.90447	-0.39729	1	4.127513	-1.67563	0.058055
1	5.611113	0.16346	-1.67191	1	5.465879	-0.16052	-1.52427

1	7.179768	1.234255	-0.02711	1	7.288303	0.498143	0.12923
1	7.997064	0.942514	-1.56769	1	7.975186	-0.23269	-1.33971
1	8.291984	-0.13883	-0.19133	1	7.833979	-1.19365	0.158267
1	7.341234	-0.9968	-3.06424	1	6.68005	-2.10906	-2.57572
1	6.046623	-2.11122	-2.57887	1	5.053258	-2.57089	-2.00469
1	7.616324	-2.16062	-1.75245	1	6.491443	-3.02093	-1.05533

APPENDIX B

COMPUTATIONAL DETAILS

Calculations were performed at all levels and on every one of the systems with the Gaussian03 program suite [183]. The electronic configuration of the molecular systems was described by the Stuttgart Relativistic Core ECP Basis Sets. In the case of carbon, nitrogen and oxygen atoms, we chose the quasi-relativistic two core electrons basis set, ECP2MWB [184], while for antimony atoms we opted for the 46 core electrons fully relativistic basis set, ECP46MDF [185]. The hydrogen valence description is from the Binkley et. al. 3-21G basis set augmented by polarizing functions, SBKJC (s,2p) [186-188]. Basis sets were chosen considering the limits in MP2 calculations. Geometry optimizations were performed at the GGA level with the popular functional B3LYP. B3LYP utilizes Becke's three parameter hybrid exchange functional together with the correlation functional [189, 190]. Results at DFT level were refined with Hartree-Fock optimizations including Møller-Plesset correlation energy corrections truncated at second-order, MP2 [191-197].

APPENDIX C

FULL CITATIONS OF CHAPTERS 2-7

Chapter 2: Aruna B. Wijeratne; Kevin A. Schug. Molecular recognition properties of tartrates and metal-tartrates in solution and gas phase. Journal of Separation Science, 2009, 32(10), 1537-1547.

Chapter 3: Aruna B. Wijeratne; Sandra E. Spencer; Jose Gracia; Daniel W. Armstrong; Kevin A Schug. Antimony(III)-D, L-tartrates exhibit proton-assisted enantioselective binding in solution and in the gas Phase. Journal of the American Society for Mass Spectrometry, 2009, 20(11), 2100-2105.

Chapter 4: Aruna B. Wijeratne; Samuel H. Yang; Jose Gracia; Daniel W. Armstrong; Kevin A. Schug. ESI-MS investigation of solvent effects on the chiral recognition capacity of tartar emetic towards neutral side-chain amino acids. Chirality, (in press, available online). 2010.

Chapter 5: Kevin A. Schug; Aruna B. Wijeratne; Billal. H. Bazzi; Daniel W. Armstrong, Solution phase vs. gas phase chiral recognition by ESI-MS: A case study of two chiral selector classes. In Chiral Recognition in the Gas Phase; Zehnacker, A., Ed.; Taylor & Francis/CRC Press: Boca Raton, FL, 2010, ISBN: 9781420082272.

Chapter 6: Aruna B. Wijeratne; Samuel H. Yang; Daniel W. Armstrong; Kevin A. Schug. Solvent Molecules Undergo Homolytic Cleavage and Radical Recombination Processes during Negative-Mode Electrospray Ionization: Adduct Formation with Antimony(III)-Tartrate Dianion. Analytical Chemistry, 2010, 82(12), 5141-5146.

Chapter 7: Aruna B. Wijeratne; Jose Gracia; Samuel H. Yang; Peter Kroll; Daniel W. Armstrong; Kevin A. Schug. New Structural Insight for Antimony(III)-Tartrate. (Submitted), 2010.

REFERENCES

1. Agranat, I.; Caner, H.; Caldwell, J. Putting chirality to work: The strategy of chiral switches. *Nature Reviews*. **2002**, 1, 753-768.

2. Zehnacker, A., Ed. *Chiral recognition in the gas phase*, Taylor & Francis/CRC Press: Boca Raton, FL, 2010.

3. Mislow, K., Molecular chirality. *Top. Stereochem*. **1999**, *22*, 1–82.

4. Bonner, W. A. Parity violation and the evolution of biomolecular homochirality. *Chirality*. **2000**, *12*, 114–126.

5. Agranat, I.; Sarel, S. Introduction. Reflections on chiral discrimination. *Enantiomer*, **1996**, *1*, 249–250.

6. Caldwell, J. Through the looking glass in chiral drug development. *Modern Drug Discov*. **1999**, *2*, 51–60.

7. Eichelbaum, M.; Testa, B.; Somogyi, A., Eds. Stereochemical aspects of drug action, Springer, Heidelberg, 2002.

8. Eichelbaum, M.; Gross, A. S. Stereochemical aspects of drug action and disposition. *Adv. Drug Res.* **1996**, 28, 1–64.

9. Shah, R. R.; Midgley, J. M.; Branch, S. K. Stereochemical origin of some clinically significant drug safety concerns: Lessons for future drug development. *Adv. Drug React. Toxicol. Rev*. **1998**, 17, 145–190.

10. Schug, K.A.; Lindner, W. Chiral molecular recognition for the detection and analysis of enantiomers by mass spectrometric methods. *J. Sep. Sci.* **2005**, *28*, 1932–1955.

11. Finn, M.G. Emerging methods for the rapid determination of enantiomeric excess. *Chirality* **2002**, *14*, 534-540.

12. Schug, K. A. Solution phase enantioselective recognition and discrimination by electrospray ionization—mass spectrometry: State-of-the-art, methods, and an eye towards increased throughput measurements. *Comb. Chem. High Throughput Screen*. **2007**, *5*, 301-316.

13. Compiled by McNaught, A. D.; Wilkinson, A. *IUPAC. Compendium of Chemical Terminology, 2nd ed. (the "Gold Book")*, Blackwell Scientific Publications, Oxford, 1997.

14. Morrsion, J. D., Ed. Asymmetric Synthesis, Academic Press, New York, 1983.

15. Schug, K.A; Wijeratne, A.B; Bazzi, B.H.; Armstrong, A.B. Solution phase vs. gas phase chiral recognition by ESI-MS: A case study of two chiral selector classes. In *Chiral Recognition in the Gas Phase*; Zehnacker, A., Ed.; Taylor & Francis/CRC Press: Boca Raton, FL, 2010; p 181.

16. Fales, H.M.; Wright, G.J. Detection of chirality with the chemical ionization mass spectrometer. “meso” ions in the gas phase. *J. Am. Chem. Soc*. **1977**, *99*, 2339-2340.

17. Sawada, M.; Shizuma, M.; Takai, Y.; Yamada, H.; Kaneda, T.; Hanafusa, T. Enantioselectivity in FAB mass spectrometry. *J. Am. Chem. Soc*. **1992**, *114*, 4405-4406.

18. Sawada, M. Chiral recognition detected by fast atom bombardment mass spectrometry. *Mass Spectrom. Rev*. **1997**, *16*, 73-90.

19. So, M.P.; Wan, T.S.M. Differentiation of enantiomers using matrix-assisted laser desorption/ionization mass spectrometry. *Rapid Commun. Mass Spectrom*. **2000**, *14*, 692-695.

20. Speranza, M. Enantioselectivity in gas-phase ion-molecule reactions. *Int. J. Mass Spectrom*. **2004**, *232*, 277-317.

21. Grigorean, G.S.; Gronert, S.; Lebrilla, C.B. Enantioselective gas-phase ion-molecule reactions in a quadrupole ion trap. *Int. J. Mass Spectrom*. **2002**, *219*, 79-87.

22. Dearden, D.V.; Liang, Y.; Nicoll, J.B.; Kellersberger, K. Study of gas-phase molecular recognition using fourier transform ion cyclotron resonance mass spectrometry. *J. Mass Spectrom*. **2001**, *36*, 989-997.

23. Tao, W.A.; Cooks, R.G. Chiral analysis by MS. *Anal. Chem*. **2003**, *75*, 25A-31A.

24. Gronert, S.; Fagin, A.E.; Okamoto, K. Stereoselectivity in the collision-activated reactions of gas phase salt complexes. *J. Am. Soc. Mass Spectrom*. **2004**, *15*, 1509-1516.

25. Czerwenka, C.; Lindner, W. Enantiomer discrimination of peptides by tandem mass spectrometry: Influence of the peptide sequence on chiral recognition. *Rapid Commun. Mass Spectrom.* **2004**, *18*, 2713-2718.

26. Schug, K.A.; Joshi, M.D.; Frycak, P.; Maier, N.M.; Lindner, W. Investigation of monovalent and bivalent enantioselective molecular recognition by electrospray ionization – mass spectrometry and tandem mass spectrometry. *J. Am. Soc. Mass Spectrom*. **2008**, *19*, 1629-1642.

27. Filippi, A.; Giardini, A.; Piccirillo, S.; Speranza, M. Gas-phase enantioselectivity. *Int. J. Mass Spectrom*. **2000**, *198*, 137-163.

28. Speranza, M.; Rondino, F.; Satta, M.; Paladini, A.; Giardini, A.; Catone, D.; Piccirillo, S. Molecular and supramolecular chirality: R2PI spectroscopy as a tool for the gas-phase recognition of chiral systems of biological interest. *Chirality* **2009**, *21*, 119-144.

29. Speranza, M.; Satta, M.; Piccirillo, S.; Rondino, F.; Paladini, A.; Giardini, A.; Filippi, A.; Catone, D. Chiral recognition by mass-resolved laser spectroscopy. *Mass Spectrom. Rev*. **2005**, *24*, 588-610.

30. Yamashita, M.; Fenn, J. B. Electrospray ion source. Another variation on the free-jet theme. *J. Phys. Chem.* **1984**, *88*, 4451–4459.

31. Cole, R. B. Some tenets pertaining to electrospray ionization mass spectrometry. *J. Mass Spectrom.* **2000**, *35*, 763–772.

32. Fenn, J. B.; Mann, M.; Meng, C. K.; Wong, S. F.; Whitehouse, C. M. Electrospray ionization for mass spectrometry of large biomolecules. *Science* **1989**, *246*, 64-71.

33. Cole, R. B. *Electrospray ionization mass spectrometry*; John Wiley and Sons: New York, 1997.

34. Taylor, G. I. Disintegration of water drops in an electric field. *Proc. R. Soc. London A* **1964**, *280*, 383-397.

35. Rayleigh, L. On the equilibrium of liquid conducting masses charged with electricity. *Philos. Mag.* **1882**, *14*, 184.

36. Ganem, B.; Li, Y.T.; Henion, J. Detection of noncovalent receptor-ligand complexes by mass spectrometry. *J. Am. Chem. Soc.* **1991**, *113*, 6294-6296.

37. Daniel, J. M.; Friess, S. D.; Rajagopalan, S.; Wendt, S.; Zenobi, R. Quantitative determination of noncovalent binding interactions using soft ionization mass spectrometry. *Int. J. Mass Spectrom.* **2002**, *216*, 1-27.

38. Schalley, C.A. Molecular recognition and supramolecular chemistry in the gas phase. *Mass Spectrom. Rev.* **2001**, *20*, 253-309.

39. Jelesarov, I.; Bosshard, H.R. Isothermal titration calorimetry and differential scanning calorimetry as complementary tools to investigate the energetics of biomolecular recognition. *J. Molec. Recog.* **1999**, *12*, 3-18.

40. Fielding, L. Determination of association constants (Ka) from solution NMR data. *Tetrahedron* **2000**, *56*, 6151-6170.

41. Hirose, K. A Practical guide for the determination of binding constants. *J. Incl. Phenom. Macrocyc. Chem*. **2001**, *39*, 193-209.

42. Czerwenka, C.; Maier, N.M.; Lindner, W. Enantiomer discrimination by mass spectrometry: Noncovalent interactions of an N-derivatized dipeptide with various cinchona alkaloid derivatives and comparison with enantioselective liquid-phase separations. *Anal. Bioanal. Chem*. **2004**, *379*, 1039-1044.

43. Schug, K.A.; Frycak, P.; Maier, N.M.; Lindner, W. Measurement of solution-phase chiral molecular recognition in the gas phase using electrospray ionization – mass spectrometry. *Anal. Chem*. **2005**, *77*, 3660-3670.

44. Schug, K.A.; Maier, N.M.; Lindner, W. Deuterium isotope effects observed during competitive binding chiral recognition electrospray ionization – mass spectrometry of cinchona alkaloid-based systems. *J. Mass Spectrom*. **2006**, *41*, 157-161.

45. Schug, K.A.; Maier, N.M.; Lindner, W. Chiral recognition mass spectrometry: Remarkable effects observed from the relative ion bbundances of ternary diastereomeric complexes using electrospray ionization. *Chem. Commun*. **2006**, 414-416.

46. Frycak, P.; Schug, K.A. On-line dynamic titration: Determination of dissociation constants for noncovalent complexes using gaussian concentration profiles by electrospray ionization mass spectrometry. *Anal. Chem*. **2007**, *79*, 5407-5413.

47. Frycak, P.; Schug, K.A. High throughput multiplexed method for evaluation of enantioselective performance of chiral Selectors by HPLC-ESI-MS and dynamic titration: Cinchona alkaloid carbamates discriminating N-blocked amino acids. *Chirality* **2009,** *21*, 929-936.

48. Laemmerhofer, M.; Lindner, W. Quinine and quinidine derivatives as chiral selectors I. Brush type chiral stationary phases for high-performance liquid chromatography based on cinchona carbamates and their application as chiral anion exchangers. *J. Chromatogr. A* **1996**, *741*, 33-48.

49. Mandl, A.; Nicoletti, L.; Laemmerhofer, M.; Lindner, W. Quinine versus carbamoylated quinine-based chiral anion exchangers. A comparison regarding enantioselectivity for N-protected amino acids and other chiral acids. *J. Chromatogr. A* **1999**, *858*, 1-11.

50. Maier, N.M.; Nicoletti, L.; Laemmerhofer, M.; Lindner, W. Enantioselective ion exchangers based on cinchona alkaloid-derived carbamates: influence of C8/C9 stereochemistry on chiral recognition. *Chirality* **1999**, *11*, 522-528.

51. Schefzick, S.; Laemmerhofer, M.; Lindner, W.; Lipkowitz, K.; Jalaie, M. Comparative molecular field analysis of quinine derivatives used as chiral selectors in liquid chromatography: 3D QSAR for the purposes of molecular design of chiral stationary phases. *Chirality* **2000**, *12*, 742-750.

52. Gasparrini, F.; Misiti, D.; Villani, C. High-performance liquid chromatography chiral stationary phases based on low-molecular-mass selectors. *J. Chromatogr. A* **2001**, *906*, 35-50.

53. Lah, J.; Maier, N.M.; Lindner, W.; Vesnaver, G. Thermodynamics of binding of (R)- and (S)-dinitrobenzoyl leucine to cinchona alkaloids and their tert-butylcarbamate derivatives in methanol: Evaluation of enantioselectivity by spectroscopic (CD, UV) and microcalorimetric (ITC) titrations. *J. Phys. Chem. B* **2001**, *105*, 1670-1678.

54. Czerwenka, C.; Laemmerhofer, M.; Maier, N.M.; Rissanen, K.; Lindner, W. Direct high performance liquid chromatographic separation of peptide enantiomers: Study on chiral recognition by systematic evaluation of the influence of structural features of the chiral selectors on enantioselectivity. *Anal. Chem*. **2002**, *74*, 5658-5666.

55. Maier, N.M.; Schefzick, S.; Lombardo, G.M.; Feliz, M.; Rissanen, K.; Lindner, W.; Lipkowitz, K.B. Elucidation of the chiral recognition mechanism of cinchona alkaloid carbamate-type receptors for 3,5-dinitrobenzoyl amino acids. *J. Am. Chem. Soc*. **2002**, *124*, 8611-8629.

56. Laemmerhofer, M.; Tobler, E.; Zarbl, E.; Lindner, W.; Svec, F.; Fréchet, J.M. Macroporous monolithic chiral stationary phases for capillary electrochromatography: New chiral monomer derived from cinchona alkaloid with enhanced enantioselectivity. *Electrophoresis* **2003**, *24*, 2986-2999.

57. Czerwenka, C.; Zhang, M.M.; Kaehlig, H.P.; Maier, N.M.; Lipkowitz, K.B.; Lindner, W. Chiral recognition of peptide enantiomers by cinchona alkaloid derived chiral selectors: Mechanistic investigations by liquid chromatography, NMR spectroscopy, and molecular modeling. *J. Org. Chem*. **2003**, *68*, 8315-8327.

58. Bicker, W.; Laemmerhofer, M.; Lindner, W. Direct high-performance liquid chromatographic method for enantioselective and diastereoselective determination of selected pyrethroic acids. *J. Chromatogr A* **2004**, *1035*, 37-46.

59. Laemmerhofer, M.; Lindner, W. Chiral separations by capillary electrophoresis using cinchona alkaloid derivatives as chiral counter-ions. *Methods Mol. Biol*. **2004**, *243*, 323-342.

60. Wirz, R.; Buergi, T.; Lindner, W.; Baiker, A. Absolute configuration modulation attenuated total reflection IR spectroscopy: An in situ method for probing chiral recognition in liquid chromatography. *Anal. Chem*. **2004**, *76*, 5319-5330.

61. Williams, I.D.; Pedersen, S.F.; Sharpless, K.B.; Lippard, S.J. Crystal structures of two titanium tartrate asymmetric epoxidation catalysts. *J. Am. Chem. Soc*. **1984**, *106*, 6340-6341.

62. Plimmer, H.G.; Bateman, H.R. Further results on the experimental treatment of trypanosomiasis: Being a progress report to a committee of the royal society. *Proc. R. Soc. London B* **1908**, *80*, 477-487.

63. Tracy, J. W.; Webster, L. T.; In: Hardman, J. G.; Limbird, L. E.; Molinoff, P. B.; Ruddon, R. W.; Gilman, A. G.; (Eds.) Goodman & Gilman's the Pharmacological

Basis of Therapeutics, 9th ed., McGraw-Hill Book Co., New York, NY. **1996**. pp. 987-1008.

64. Mansour, T. E. Chemotherapy of parasitic worms: New biochemical strategies. *Science* **1979**, *205*, 462-469.

65. Duffin, J.; René, P. "Anti-moine; anti-biotique": the public fortunes of the secret properties of antimony potassium tartrate (tartar emetic). *J. Hist. Med. Allied Sci.* **1991**, *46*, 440-456.

66. Tapscott, E. R.; Belford, R. L.; Paul, I. C. Stereochemistry of tartrato(4-)-bridged binuclear complexes. *Coord. Chem. Rev*. **1969**, *4*, 323-359.

67. Sun, P.; Krishnan, A.; Yadav, A.; Singh, S.; MacDonnell, F. M.; Armstrong, D. W. Enantiomeric separations of ruthenium(II) polypyridyl complexes using high-performance liquid chromatography (HPLC) with cyclodextrin chiral stationary phases (CSPs). *Inorg. Chem*. **2007**, *46*, 10312-10320.

68. Nakazawa, H.; Yoneda, H. Chromatographic study of optical resolution. II. Separation of optically active cobalt(III) complexes using potassium antimony *D*-tartrate as eluent. *J. Chromatogr.* **1978**, *160*, 89-99.

69. Martin, S. E.; Connatser, R. M.; Kane-Maguire, N. A. P.; Wheeler, J. F. Capillary electrophoresis with laser-induced fluorescence detection for chiral analysis and DNA binding studies of ruthenium(II) tris-diimine complexes. *Anal. Chim. Acta*. **2001**, *445*, 21-27.

70. Yoneda, H.; Nakatani, K.; Yamazaki, S. Chromatographic study of optical resolution. XI. Optimum conditions for optical resolution of uncharged complexes. *J. Chromatogr*. **1985**, *319*, 35-41.

71. Miyoshi, K.; Izumoto, S.; Nakai, K.; Yoneda, H. Mechanism of chiral recognition of octahedral metal complexes effected by bis(μ-d-tartrato)diantimonate(III) anion in

solution. 2. Cage complexes of the type [Co(N)6]3+. *Inorg. Chem*. **1986**, *25*, 4654-4657.

72. Izumoto, S.; Miyoshi, K.; Yoneda, H. Chromatographic study of optical resolution. XIV. Optical resolution of amine complex cations of the type [Co(N)6]3+ by reversed-phase ion-pair chromatography using bis(μ-*D*-tartrato)diantimonate(III) and an arsenic analog as an ion-pairing reagent. *Bull. Chem. Soc. Japan* **1987**, *60*, 3199-3205.

73. Oi, N.; Kitahara, H.; Aoki, F. Direct separation of carboxylic acid and amine enantiomers by high-performance liquid chromatography on reversed-phase silica gels coated with chiral copper(II) complexes. *J. Chromatogr. A* **1995**, *707*, 380-383.

74. Mizuta, T.; Sasaki, K.; Yamane, H.; Miyoshi, K.; Yoneda, H. Chromatographic resolution of a diastereomeric mixture of tris(trans-1,2-diaminocyclohexane)cobalt(III) by bis(μ-tartrato)diantimonate(III) anion and association modes found in their diastereomeric salts. *Bull. Chem. Soc. Japan* **1998**, *71*, 1055-1064.

75. Shelton, C.M.; Seaver, K.E.; Wheeler, J.F.; Kane-Maguire, N.A.P. Application of capillary electrophoresis for the assessment of enantiomeric purity of α-diimine transition metal complexes. *Inorg. Chem*. **1997**, *36*, 1532-1533.

76. Harris, J.E.; Desai, N.; Seaver, K.E.; Watson, R.T.; Kane-Maguire, N.A.; Wheeler, J.F. Chiral separations of transition metal complexes using capillary zone electrophoresis. *J. Chromatogr. A* **2001**, *919*, 427-436.

77. Kodama, S.; Yamamoto, A.; Matsunaga, A.; Soga, T.; Hayakawa, K. Direct chiral resolution of malic acid in apple juice by ligand-exchange capillary electrophoresis using copper(II)-*L*-tartaric acid as a chiral selector. *Electrophoresis* **2001**, *22*, 3286-3290.

78. Wijeratne, A. B; Schug, K.S. Molecular recognition properties of tartrates and metal-tartrates in solution and gas phase. *Journal of Separation Science*, **2009**, 32(10), 1537-1547.

79. Wijeratne, A. B; Spencer, S.E.; Gracia, J.; Armstrong, D.W.; Schug, K.S. Antimony(III)-*D*, *L*-tartrates exhibit proton-assisted enantioselective binding in solution and in the gas Phase. *Journal of the American Society for Mass Spectrometry*, **2009**, 20(11), 2100-2105.

80. Wijeratne, A. B; Yang, S.Y.; Gracia, J.; Armstrong, D.W.; Schug, K.S. ESI-MS investigation of solvent effects on the chiral recognition capacity of tartar emetic towards neutral side-chain amino acids. *Chirality*, (*in press, available online)*. **2010.**

81. Wijeratne, A. B; Yang, S.Y.; Armstrong, D.W.; Schug, K.S. Solvent molecules undergo homolytic cleavage and radical recombination processes during negative-mode electrospray ionization: Adduct formation with antimony(III)-tartrate dianion. *Analytical Chemistry*, **2010**, 82(12), 5141-5146.

82. Wijeratne, A. B; Yang, S.Y.; Gracia, J.; Kroll, P.; Armstrong, D.W.; Schug, K.S. New structural insight for antimony(III)-tartrate. (*Submitted*), **2010**.

83. Pasteur, L., *Comptes rendus hebdomadaires de l'Académie des Sciences, Paris.* **1848**, *26*, 535–538.

84. Kostyanovsky, R. G.; Berova, N. Contributions dedicated to the 160th anniversary of Louis Pasteur's discovery. *Chirality*. **2008**, *20*, 1071.

85. Marcovich, D.; Tapscott, R.E. Carbon-13 NMR studies on arsenic(III) and antimony(III) dihydroxydicarboxylate complexes. *J. Am. Chem. Soc.* **1980**, *102*, 5712-5717.

86. Coronado, E.; Galan-Mascaros, J. R.; Gomez-Garcia, C. J.; Murcia Martinez, A. Chiral molecular magnets: synthesis, structure, and magnetic behavior of the series

[M(*L*-tart)] (M = Mn(II), Fe(II), Co(II), Ni(II); *L*-tart = (2R,3R)-(+)-tartrate). *Chem. Eur. J.* **2006**, *12*, 3484-3492.

87. Horikawa, K.; Masuyama, S. Aliphatic hydroxycarboxylic acids as antioxidants. V. Complexes of copper(II) with erythro- and threo-2-methyltartaric, and meso- and threo-2,3-dimethyltartaric acids. *Bull. Chem. Soc. Jap.* **1971**, *44*, 2697-2702.

88. Tatsumi, S.; Izumi, Y., Imaida, M.; Fukuda, Y.; Akabori, S. Studies of C-substituted tartaric acid. I. The preparation of optically active 2-methyltartaric and 2,3-di-O-methyltartaric acid. *Bull. Chem. Soc. Jap.* **1966**, *39*, 602-604.

89. Belford, R. L.; Chasteen, N. D.; So, H.; Tapscott, R. E. Triplet state of vanadyl tartrate binuclear complexes and electron paramagnetic resonance spectra of the vanadyl .alpha.-hydroxycarboxylates. *J. Am. Chem. Soc.* **1969**, *91*, 4675-4680.

90. Au-Yeung, A. S.; Sung, H. H.; Cha, J. A.; John, A. K.; Siu, A. W.; Chui, S. S.; Williams, I. D. Hydrothermal synthesis of indium tartrates: Structures of the chiral polymer [In(*L*-TAR)3-H2O].bul.0.5H2O containing the tartrate trianion, and a microporous hybrid solid [In(OH)(*D*/*L*-TAR)2-].bul.2H2O. *Inorg. Chem. Commun.* **2006**, *9*, 507-511.

91. Gilbert, J. C.; Martin S. F. Experimental Organic Chemistry; 3rd ed.; Brooks/Cole-Thomson Learning: Pacific Grove, CA, USA, 2002.

92. Galsboel, F.; Hammershoei, A.; Larsen, E. The bis[di(2-aminoethyl)sulfide]rhodium(III) ion. Preparation of the u-fac isomer, its resolution, and the determination of the absolute configuration of the (+)*D*-enantiomer. *Acta Chem. Scand. Series A*, **1978**, *32*, 643-646.

93. Garbett, K., Gillard, R. D. Optically active coordination compounds. V. The method of less soluble diastereoisomers and relative configurations. *J. Chem. Soc. A. Inorg., Phys., Theo.* **1966**, 802-805.

94. Anderson, B. F.; Bell, J. D.; Buckingham, D. A.; Cresswell, P. J.; Gainsford, G. J.; Marzilli, L. G.; Robertson, G. B.; Sargeson, A. M. Structures, chemistry, and relative energies of the [Co(trien)(glyO)]2+ ions. 3. .alpha.-(RR,SS)-[Co(trien)(glyO)]2+ and .alpha.-(RR,SS)-[Co(trien)(glyOEt)Cl]2+ ions. *Inorg. Chem.*, **1977**, *16*, 3233-3244.

95. Yasui, T.; Ama, T; Kauffman, G. B.; Radanovic, D. J.; Djuran, M. I. Resolution of the dodecaamminehexa-μ-hydroxotetracobalt(III) ion. *Inorg. Synth.* **1992**, *29*, 169-174.

96. Takabe, K.; Sugiura, M.; Asumi, Y.; Mase, N.; Yoda, H.; Shimizu, H. Practical optical resolution of *DL*-muscone using tartaric acid derivatives as a chiral auxiliary. *Tetrahedron Lett.* **2005**, *46*, 3457-3460.

97. Berrod, G.; Bourdon, J.; Dreux, J.; Longeray, R.; Moreau, M.; Schifter, P. Study of the behavior of chiral alcohols by gas chromatography on chiral phases. *Chromatographia*, **1979**, *12*, 150-152.

98. Prelog, V.; Mutak, S.; Kovacevic, K. Separation of enantiomers by partition between liquid phases. Part 3. Selectivity of lipophilic tartaric acid esters for chiral ammonium salts of different constitution and configuration. *Helv. Chim. Acta*, **1983**, *66*, 2279-2284.

99. Zhou, D.; Liu, J.; Tang, K. Chiral extraction of racemic α-cyclohexyl-mandelic acid with tartaric acid esters as chiral selector. *Fenxi Ceshi Xuebao*, **2006**, *25*, 49-52.

100. Keurentjes, J. Separation of racemic drugs with membranes. Chemisch Magazine (Rijswijk, Netherlands), **1994**, *9*, 352-357.

101. Cai, Y.; Yan, Z. H.; Zi, M.; Yuan, L. M. Preparative enantioseparation of *D*L-α-methylbenzylamine by high-speed countercurrent chromatography using *L*-(+)-tartaric acid as chiral selector. *J. of Liq. Chromato. Related Technol.* **2007**, *30*, 1489-1495.

102. Gyllenhaal, O.; Karlsson, A. Enantiomeric separations of amino alcohols by packed-column SFC on Hypercarb with *L*-(+)- tartaric acid as chiral selector. *J. Biochem. Biophys. Methods*, **2002**, *54*, 169-185.

103. Zhou, L.; Trubig, J.; Dovletoglou, A.; Locke, D. C. Enantiomeric separation of the novel growth hormone secretagogue MK-0677 by capillary zone electrophoresis. *J. Chromatogr. A*, **1997**, *773*, 311-320.

104. Hoedl, H.; Krainer, A.; Holzmueller, K.; Koidl, J.; Schmid, M. G.; Guebitz, G. Chiral separation of sympathomimetics and β-blockers by ligand-exchange CE using Cu(II) complexes of *L*- tartaric acid and *L*-threonine as chiral selectors. *Electrophoresis*, **2007**, *28*, 2675-2682.

105. Kicinski, H. G.; Kettrup, A. Synthesis and characterization of *L*(+)-diacetyltartaric acid silica gel for high-performance liquid chromatography. *Fresenius' Zeitschrift fuer Analytische Chemie*, **1983**, *316*, 39-42.

106. Kicinski, H. G.; Kettrup, A. Determination of enantiomeric catecholamines by ligand-exchange chromatography using chemically modified *L*-(+)- tartaric acid silica gel. *Fresenius' Zeitschrift fuer Analytische Chemie*, **1985**, *320*, 51-54.

107. Lindner, W.; Hirschboeck, I. Tartaric acid derivatives as chiral sources for enantioseparation in liquid chromatography. *J. Pharm. Biomed. Anal.* **1984**, *2*, 183-189.

108. Gennaro, M. C.; Abrigo, C.; Marengo, E. The use of chiral interaction reagents in the separation of D(-)- and *L*(+)-ascorbic acid by ion interaction reversed-phase HPLC. *Chromatographia*, **1990**, *30*, 311-317.

109. Heldin, E.; Lindner, K. J.; Pettersson, C.; Lindner, W.; Rao, R. Tartaric acid derivatives as chiral selectors in liquid chromatography. *Chromatographia*, **1991**, *32*, 407-416.

110. Oi, N.; Kitahara, H.; Aoki, F. Enantiomer separation by chiral ligand exchange HPLC with a (R,R)-tartaric acid mono amide derivative as stationary phase. *Kuromatogurafi*, **1992**, *13*, 307-308.

111. Oi, N.; Kitahara, H.; Aoki, F. Enantiomer separation by high-performance liquid chromatography with (R,R)-tartaric acid mono-amide derivatives as bifunctional chiral selectors. *J. Chromatogr. A*, **1994**, *666*, 457-462.

112. Monser, L. I.; Greenway, G. M.; Ewing, D. F. Novel 2-chrysenyl- and 1-pyrenyl-tartaramide derivatives as liquid chromatographic chiral phases for enantiomeric separation on porous graphitic carbon. *Tetrahedron: Asymmetry*, **1996**, *7*, 1189-1198.

113. Andersson, S.; Balmer, K.; Persson, B. A. Chromatographic resolution of organic acids using the Kromasil-CHI-TBB chiral stationary phase. *Chirality*, **1999**, *11*, 420-425.

114. Chang, P.; Su, K. Tartaric acid derivatives as chiral selectors in separation of enantiomers in HPLC. *Huaxue Shijie*, **2001**, *42*, 492-497.

115. Oxelbark, J.; Sellen, I. Effects from hydrogen bonding and rigidity on selectivity in tartaric acid-based chiral selectors for enantioselective liquid chromatography. *Chirality*, **2003**, *15*, 787-793.

116. Weng, W.; Yao, B. X.; You, X. Li.; Zeng, Q. L. Enantioseparation of BINOL using L-tartaric acid derivative as chiral stationary phase. *Yingyong Huaxue*, **2004**, *21*, 853-855.

117. Oxelbark, J.; Gidlund, P. Investigation of a tartaric acid -based linear polyamide and dimer as chiral selectors in liquid chromatography. *Chirality*, **2005**, *17*, 79-84.

118. Weng, W.; Yao, B. X.; Liu, F.; Zhu, J.; Li, S. Q. Influence of mobile phase composition on thermodynamic parameters of enantioseparation by chiral stationary phase derived from tartaric acid. *Yingyong Huaxue*, **2005**, *22*, 800-803.

119. Bao, Z.; Su, B.; Ren, Q. Kinetic and equilibrium study of the enantioseparation of paroxetine intermediate on amylose and tartaric acid -based chiral stationary phases. *J. Sep. Sci.* **2008**, *31*, 16-22.

120. Maier, N.M.; Franco, P.; Lindner, W. Separation of enantiomers: needs, challenges, perspectives. *J. Chromatogr. A*, **2001**, *906*, 3-33.

121. Gübitz, G.; Schmid, M.G. Chiral separation principles in chromatographic and electromigration techniques. *Mol. Biotechnol.* **2006**, *32*, 159-180.

122. Brodbelt, J.S. Probing molecular recognition by mass spectrometry. *Int. J. Mass Spectrom.* **2000**, *200*, 57-69.

123. Filippi, A.; Giardini, A.; Latini, A.; Piccirillo, S.; Scuderi, D.; Speranza, M. Chiral discrimination of monofunctional alcohols and amines in the gas phase. Int. J. Mass Spectrom. **2001**, *210/211*, 483-488.

124. Baldwin, M. A.; Howell, S. A.; Welham, K. J.; Winkler, F. J. Identification of chiral isomers by fast atom bombardment/ mass spectrometry: dialkyl tartrates. *Biomed. Environ. Mass Spectrom.* **1988**, Volume Date 1987, *16*, 357-360.

125. Hofmeister, G.; Leary, J. A. Chiral recognition of lithium-coordinated diols using tandem mass spectrometry. *Org. Mass Spectrom.* **1991**, *26*, 811-812.

126. Dang, T. T.; Pedersen, S. F.; Leary, J. A. Chiral recognition in the gas phase: Mass spectrometric studies of diastereomeric cobalt complexes. *J. Am. Soc. Mass Spectrom*. **1994**, *5*, 452-459.

127. Frycak, P.; Schug, K. A. Dynamic Titration: Determination of Dissociation Constants for Noncovalent Complexes in Multiplexed Format Using HPLC-ESI-MS. *Anal. Chem.* **2008**, *80*, 1385-1393.

128. Winkler, F. J.; Stahl, D.; Maquin, F., Chirality effects in the chemical ionization mass spectra of dialkyl tartrates. *Tetrahedron Lett.* **1986**, *27*, 335-338.

129. Winkler, F. J.; Medina, R.; Winkler, J.; Krause, H. Mass spectral and semi-empirical studies on chiral discrimination in gaseous aggregation products of protonated dialkyl tartrates. *J. Chromatogr. A*, **1994**, *666*, 549-556.

130. Winkler, F. J.; Medina, R.; Winkler, J.; Kranuse, H. Chirality-directed self-assembly of supramolecular propellers of dialkyl tartrate trimers with hydronium, ammonium and primary aminium ions in CI mass spectra. *J. Mass Spectrom.* **1997**, *32*, 1072-1079.

131. Denisov, E.V.; Shustryakov, V.; Nikolaev, E.N.; Winkler, F.J.; Medina, R. FT ICR investigations of chiral supramolecular propellers of dialkyl tartrate trimers with methylammonium ions. *Int. J. Mass Spectrom. Ion Proces.* **1997**, *167/168*, 259-268.

132. Nikolaev, E. N.; Denisov, E. V.; Nikolaeva, M. I.; Futrell, J. H.; Rakov, V. S.; Winkler, F. J. Elucidation of influence of chirality on formation and decomposition of ion molecular complexes in the dialkyltartrate class using mass spectrometry. *Adv. Mass Spectrom.* **1998**, *14*, Chapter 12/279-Chapter 12/313.

133. Sussmuth, R.; Jung, G.; Winkler, F. J.; Medina, R. Comparative coordination studies of chiral supramolecular propellers of dialkyltartrate trimers with alkali ions using electrospray ionization mass spectrometry. *Eur. Mass Spectrom.* **1999**, *5*, 289-294.

134. Lu, H. J.; Guo, Y. L. Evaluation of chiral recognition characteristics of metal and proton complexes of di-o-benzoyl-tartaric acid dibutyl ester and *L*-tryptophan in the gas phase. *J. Am. Soc. Mass Spectrom.* **2003**, *14*, 571-580.

135. Nikolaev, E. N.; Popov, I. A.; Kharybin, O. N.; Kononikhin, A. S.; Nikolaeva, M. I.; Borisov, Y. V. In situ recognition of molecular chirality by mass spectrometry. Hydration effects on differential stability of homo- and heterochiral dimethyl tartrate clusters. *Int. J. Mass Spectrom.* **2007**, *265*, 347-358.

136. Arakawa, R.; Kobayashi, M.; Ama, T. Chiral recognition in association between antimony potassium tartrate and bis(*L*-alaninate)ethylenediamine cobalt(III)

complexes using electrospray ionization mass spectrometry. *J. Am. Soc. Mass Spectrom.* **2000**, *11*, 804-808.

137. Arakawa, R.; Kobayashi, M.; Fukuo, T.; Shiraiwa, T. Studies on the association of 2-thiazolidinecarboxylic acid and antimony potassium tartrate: chiral recognition and prediction of absolute configuration by electrospray ionization mass spectrometry. *Rapid Commun. Mass Spectrom.* **2001**, *15*, 685-689.

138. Kobayashi, M.; Ama, T.; Arakawa, R. Chiral recognition in association between antimony potassium tartrate and metal complexes by electrospray ionization mass spectrometry. *Adv. Mass Spectrom.* **2001**, *15*,797-798.

139. Gingras, A. -C.; Gstaiger, M.; Raught, B.; Aebersold, R. Analysis of protein complexes using mass spectrometry**.** *Nature Rev*. **2007**, *8*, 645-654.

140. Tian, Z.; Kass, S. R. Does electrospray ionization produce gas-phase or liquid-phase structures? *Journal of the American Chemical Society*, **2008**, 130, 10842-10843.

141. Tian, Z.; Wang, X.; Wang, L.; Kass, S. R. Are Carboxyl Groups the Most Acidic Sites in Amino Acids? Gas-Phase Acidities, Photoelectron Spectra, and Computations on Tyrosine, p-Hydroxybenzoic Acid, and Their Conjugate Bases. *Journal of the American Chemical Society*, **2009**, 131, 1174-1181.

142. Tian, Z.; Kass, Steven R. Gas-phase versus liquid-phase structures by electrospray ionization mass spectrometry. *Angewandte Chemie*, **2009**, 48, 1321-1323.

143. Wu, Z.; Gao, W.; Phelps, M. A.; Wu, D.; Miller, D. D.; Dalton, J. T. Favorable effects of weak acids on negative-ion electrospray ionization mass spectrometry. *Anal. Chem*. **2004**, 76, 839-847.

144. Kita, K; Shiomi, K; Omura, S. Advances in Drug Discovery and Biochemical Studies. *Trends Parasitaol.* **2007**, *23*, 223-229.

145. Wan, K. X.; Gross, M. L.; Shibue, T. Gas-phase stability of double-stranded oligodeoxynucleotides and their noncovalent complexes with DNA-binding drugs as revealed by collisional activation in an ion trap. *J. Am. Soc. Mass Spectrom*. **2000**, *11*, 450-457.

146. Colorado, A.; Brodbelt, J.S. An Empirical Approach to Estimation of Critical Energies by Using a Quadrupole Ion Trap. *J. Am. Soc. Mass Spectrom*. **1996**, *7*, 1116-1125.

147. Wijeratne, A. B.; Gracia, J.; Armstrong, D. W.; Schug, K. A. Charge-state-dependent enantioselective discrimination of leucine enantiomers by antimony(III)-*D*/*L*-tartrate elucidated by ESI-MS, computational modeling and ^{1}H-NMR. *Proceedings of the 57th ASMS Conference on Mass Spectrometry and Allied Topics*, Philadelphia, PA, May 31-June 4, 2009.

148. Wang, X.; Lee, J.-T.; Armstrong, D.W. Separation of Enantiomers by Capillary Electrophoresis using Pentosan Polysulfate. *Electrophoresis* **1999**, *20*, 162-170.

149. Trapp, O.; Trapp, G.; Kong, J.; Hahn, U.; Vogtle, F.; Schurig, V. Probing the Stereointegrity of Troger's Base – a Dynamic Electrokinetic Chromatographic Study. *Chem. Eur. J.* **2002**, *8*, 3629-3634.

150. Bustos, E.; Garcia, J.E.; Bandala, Y.; Godinez, L.A.; Juaristi, E. Enantioselective Recognition of Alanine in Solution with Modified Gold Electrodes Using Chiral PAMAM Dendrimers G4.0. *Talanta* **2009**, *78*, 1352-1358.

151. Camara, E.; Green, M.K.; Penn, S.G.; Lebrilla, C.B. Chiral Recognition is Observed in the Deprotonation Reaction of Cytochrome c by (2R)- and (2S)-2-Butylamine. *J. Am. Chem. Soc*. **1996**, *118*, 8751-8752.

152. Chevalier, A.G. The 'Antimony War': A dispute between Montpellier and Paris. *Ciba Symposia* **1940**, *2*, 418-423.

153. Haller, J.S. The use and abuse of tartar emetic in the 19th-century material medica. *Bull. Hist. Med.* **1975**, *49*, 235-257.

154. Burger, A. *Medicinal Chemistry*; Interscience Publishers: New York, 1960. p 1042-1045.

155. Schulert, A.R.; Abdel Rassoul, A.A.; Mansour, M.; Girgis, N.; McConnell E.; Farid, Z. Biological Disposition of Antibilharzial Antimony Drugs. II. Antimony Fate and Uptake by Schistosoma haematobium Eggs in Man. *Exp. Parasit.* **1966**, *18*, 397-402.

156. Croft, S.L. Recent Developments in the Chemotherapy of Leshmaniasis. *Trends Pharmacol. Sci.* **1988**, *9*, 376-381.

157. Bartter, F.C.; Cowie, D.B.; Most, H.; Ness, A.T.; Forbush, S. The Fate of Radioactive Tartar Emetic Administered to Human Subjects. *Am. J. Trop. Med. Hyg.* **1949**, *27*, 403-411.

158. Mansour, M.M.; Abdel-Rassoul, A.A.; Schulert, A.R. Anti-bilharzial Antimony Drugs. *Nature* **1967**, *214*, 819-820.

159. Heck, A.J.R.; Jorgensen, T.J.D. Vancomycin in vacuo. *Int. J. Mass Spectrom.* **2004**, *236*, 11-23.

160. Lam, H.; Oh, D.; Cava, F.; Takacs, C.N.; Clardy, J.; De Pedro, M.A.; Waldor, M.K. *D*-Amino Acids Govern Stationary Phase Cell Wall Remodeling in Bacteria. *Science* **2009**, *325*, 1552-1555.

161. Nesatyy, V. J. Mass Spectrometry Evaluation of the Solution and Gas-Phase Properties of Noncovalent Protein Complexes. *Int. J. Mass Spectrom*. **2002**, *221*, 147–161.

162. Wortmann, A.; Kistler-Momotova, A.; Zenobi, R.; Heine, M.C.; Wilhelm, O.; Pratsinis, S.E. Shrinking Droplets in Electrospray Ionization and Their Influence on Chemical Equilibria. *J. Am. Soc. Mass Spectrom*. **2007**, *18*, 385-393.

163. Cole, R. B.; Harrata, A. K. Charge-state distributuion and electric-discharge suppression in negative-ion electrospray mass spectrometry using/chlorinated solvents. *Rapid Comm. Mass Spectrom*. **1992**, *6*, 536-539.

164. Murphy, R. C.; Fiedler, J.; Hevko, J. Analysis of nonvolatile lipids by mass spectrometry. *Chem. Rev*. **2001**, *101*, 479-526.

165. Pulfer, M.; Murphy, R. C. Electrospray mass spectrometry of phospholipids. *Mass Spectrom. Rev*. **2003**, *22*, 332-364.

166. Oursel, D.; Loutelier-Bourhis, C.; Orange, N.; Chevalier, S.; Norris, V.; Lange, C. M. Lipid composition of membranes of Escherichia coli by liquid chromatography/tandem mass spectrometry using negative electrospray ionization. *Rapid Comm. Mass Spectrom*. **2007**, *21*, 1721-1728.

167. Edwards, J. L.; Chisolm, C. N.; Shackman, J. G.; Kennedy, R. T. Negative mode sheathless capillary electrophoresis electrospray ionization-mass spectrometry for metabolite analysis of prokaryotes. *J. Chrom. A*. **2006**, *1106*, 80-88.

168. Chowdhury, S. K.; Chait, B. T. Method for the electrospray ionization of highly conductive aqueous solutions. *Anal. Chem.* **1991**, *63*, 1660-1664.\

169. Yamashita, M.; Fenn, J. B. Yamashita, M.; Fenn, J. B. Negative ion production with the electrospray ion source. *J. Phys. Chem*. **1984**, *88*, 4671-4675. *J. Phys. Chem*. **1984**, *88*, 4671-4675.

170. Ikonomou, M. G.; Blades, A. T.; Kebarle, P. Electrospray mass spectrometry of methanol and water solutions suppression of electric discharge with SF_6 gas. *J. Am. Soc. Mass Spectrom.* **1991**, *2*, 497-505.

171. Cole, R. B.; Harrata, A. K. Solvent effect on analyte charge state, signal intensity, and stability in negative ion electrospray mass spectrometry; implications for the mechanism of negative ion formation *J. Am. Soc. Mass Spectrom*, **1993**, *4*, 546-56.

172. Blades, A. T.; Jayaweera, P.; Ikonomou, M. G.; Karbale, P. Studies of alkaline earth and transition metal M++ gas phase ion chemistry. *J. Chem. Phys.* **1990**, *92*, 5900-5906.

173. Joshi, A. A.; Locke, B. R.; Arce, P.; Finney, W. C. Formation of hydroxyl radicals, hydrogen peroxide and aqueous electrons by pulsed streamer corona discharge in aqueous solution. *J. Hazardous Materials*, **1995**, 41, 3-30.

174. Tomizawa, S.; Tezuka, M. Oxidative Degradation of Aqueous Cresols Induced by Gaseous Plasma with Contact Glow Discharge Electrolysis. *Plasma Chemistry and Plasma Processing*, **2006**, 26, 43-52.

175. Kirkpatrick, M. J.; Locke, B. R. Hydrogen, Oxygen, and Hydrogen Peroxide Formation in Aqueous Phase Pulsed Corona Electrical Discharge. *Industrial & Engineering Chemistry Research*, **2005**, *44*, 4243-4248.

176. Boys, B. L.; Kuprowski, M. C.; Noel, J. J.; Konermann, L. Protein Oxidative Modifications During Electrospray Ionization: Solution Phase Electrochemistry or Corona Discharge-Induced Radical Attack? *Anal. Chem.* **2009**, 81, 4027-4034.

177. Wang, W.; Wang, S.; Liu, F.; Zheng, W.; Wang, D. I. C. Optical study of OH radical in a wire-plate pulsed corona discharge. *Spectrochim. Acta, Part A: Molecular and Biomolecular Spectroscopy* **2006**, 63, 477-482.

178. Morand, K.; Talbo, G.; Mann, M. Oxidation of peptides during electrospray ionization. *Rapid. Commun. Mass Spectrum.* **1993**, 7, 738-743.

179. Maleknia, S. D.; Chance, M. R.; Downard, K. M. Electrospray-assisted modification of proteins: a radical probe of protein structure. *Rapid. Commun. Mass Spectrum.* **1999**, 13, 2352-2358.

180. http://www.cartercenter.org/health/schistosomiasis/index.html (date visited 09/16/2009)

181. Palenik, R. C.; Abboud, K. A.; Palenik, G. J. Bond valence sums and structural studies of antimony complexes containing Sb bonded only to O ligands. *Inorganica Chimica Acta*, **2005**, *358*, 1034-1040.

182. Lu, L.D.; Johnson, R.A.; Finn, M.G.; Sharpless, K.B. Two new asymmetric epoxidation catalysts. Unusual stoichiometry and inverse enantiofacial selection. *J. Org. Chem.* **1984**, *49* 728-731.

183. Gaussian 03, Revision C.02, Frisch, M. J.; Trucks, G. W.; Schlegel, H. B.; Scuseria, G. E.; Robb, M. A.; Cheeseman, J. R.; Montgomery, Jr., J. A.; Vreven, T.; Kudin, K. N.; Burant, J. C.; Millam, J. M.; Iyengar, S. S.; Tomasi, J.; Barone, V.; Mennucci, B.; Cossi, M.; Scalmani, G.; Rega, N.; Petersson, G. A.; Nakatsuji, H.; Hada, M.; Ehara, M.; Toyota, K.; Fukuda, R.; Hasegawa, J.; Ishida, M.; Nakajima, T.; Honda, Y.; Kitao, O.; Nakai, H.; Klene, M.; Li, X.; Knox, J. E.; Hratchian, H. P.; Cross, J. B.; Bakken, V.; Adamo, C.; Jaramillo, J.; Gomperts, R.; Stratmann, R. E.; Yazyev, O.; Austin, A. J.; Cammi, R.; Pomelli, C.; Ochterski, J. W.; Ayala, P. Y.; Morokuma, K.; Voth, G. A.; Salvador, P.; Dannenberg, J. J.; Zakrzewski, V. G.; Dapprich, S.; Daniels, A. D.; Strain, M. C.; Farkas, O.; Malick, D. K.; Rabuck, A. D.; Raghavachari, K.; Foresman, J. B.; Ortiz, J. V.; Cui, Q.; Baboul, A. G.; Clifford, S.; Cioslowski, J.; Stefanov, B. B.; Liu, G.; Liashenko, A.; Piskorz, P.; Komaromi, I.; Martin, R. L.; Fox, D. J.; Keith, T.; Al-Laham, M. A.; Peng, C. Y.; Nanayakkara, A.; Challacombe, M.; Gill, P. M. W.; Johnson, B.; Chen, W.; Wong, M. W.; Gonzalez, C.; Pople, J. A. Gaussian, Inc., Wallingford CT 2004.

184. Bergner, A.; Dolg, M.; Kuechle, W.; Stoll, H.; Preuss, H. Ab initio energy-adjusted pseudopotentials for elements of groups 13-17. *Moecular Physics*, **1993**, *80*, 1431-1441.

185. Stoll, H.; Metz, B.; Dolg, M. Relativistic energy-consistent pseudopotentials-recent developments. *J. Comp. Chem.*, **2002**, *23*, 767-777.

186. Labello, N. P.; Ferreira, A. M.; Kurtz, H. A. An augmented effective core potential basis set for the calculation of molecular polarizabilities. *J. Comp. Chem.*, **2005**, *26*, 1464-1471.

187. Labello, N. P.; Ferreira, A.M.; Kurtz, H.A. Correlated, relativistic, and basis set limit molecular polarizability calculations to evaluate an augmented effective core potential basis set. *Int. J. Quan. Chem.* **2006**, *106*, 3140-3148.

188. Binkley, J. S.; Pople, J. A.; Hehre, W. J. Self-consistent molecular orbital methods. 21. Small split-valence basis sets for first-row elements. *J. Am. Chem. Soc.*, **1980**, *102*. 939-947.

189. Becke, A. D. Density-functional thermochemistry. III. The role of exact exchange. *J. Chem. Phys.* 1993, 98, 5648-5652.

190. Stephens, P. J.; Devlin, F. J.; Chabalowski, C. F.; Frisch, M. J. Ab Initio Calculation of Vibrational Absorption and Circular Dichroism Spectra Using Density Functional Force Fields. *J. Phys. Chem.* **1994**, 98, 11623-11627.

191. Moller, C.; Plesset, M. S. Note on the approximation treatment for many-electron systems. *Physical Review*, **1934**, 46, 618-622.

192. Head-Gordon, M.; Pople, J. A.; Frisch, M. J. MP2 energy evaluation by direct methods. *Chem. Phys. Lett.* **1988**, 153, 503-506.

193. Frisch, M. J.; Head-Gordon, M.; Pople, J. A. A direct MP2 gradient method. *Chem. Phys. Lett.* **1990**, *166*, 275-280.

194. Frisch, M. J.; Head-Gordon, M.; Pople, J. A. Semidirect algorithms for the MP2 energy and gradient. *Chem. Phys. Lett.* **1990**, *166*, 281-289.

195. Almloef, J.; Korsell, K.; Faegri Jr. K. Principles for a direct SCF approach to LCAO-MO ab initio calculations. *J. Comp. Chem.*, **1982**, *3*, 385-399.

196. Head-Gordon, M.; Head-Gordon, T. Analytic MP2 frequencies without fifth-order storage. Theory and application to bifurcated hydrogen bonds in the water hexamer. *Chem. Phys. Lett.* **1994**, *220*, 122-128.

197. Saebo, S.; Almlof, J. Avoiding the integral storage bottleneck in LCAO calculations of electron correlation. *Chem. Phys. Lett*. **1989**, *154*, 83-89.

BIOGRAPHICAL INFORMATION

Aruna (W.M.) B. Wijeratne, the elder son of Mrs. S. Wijeratne and late Mr. W. M. A. B. Wijeratne, has obtained his K-12 education at Dharmaraja College, Knady, Sri Lanka. During his initial days of education, his interests were in Mathematics, English & Music. At Dharmaraja College he was known for his extracurricular activities in music, drama and drumming and has been a regular performer in ceremonies and festivals. His performances have won him and his school several national awards in national-level competitions. He was also in U-13 & U-15 cricket teams, representing the college. After successful completion of G.C.E.-O/L examination, he has focused in studying Pure Mathematics, Applied Mathematics, Physics and Chemistry to take G.C.E.-A/L examination in Physical Sciences. During this time he has also represented the college “Chemistry-Quiz” team. While studying sciences, he has continued learning traditional Kandyan Dancing and Drumming under the supervision of Mr. P. B. Gamagedara. He is a traditionally coronated “Kandyan Wes Dancer” and also has taken part in international cultural dancing tours to Austria and Hungary representing Sri Lanka. After successful completion of G.C.E.-A/L examination, he was selected to enter the University of Peradeniya, Sri Lanka to study physical sciences and started reading in Chemistry, Computer Science and Geology towards a bachelor’s degree. He has received a B.Sc.-Special degree in Chemistry with honors with a subsidiary in Computer Science. During his final year of undergraduate studies, he has conducted research in digitizing a DTA (differential thermal analysis) instrument and conducted a seminar on solar cells. He moved to the University of Texas at Arlington to obtain his doctoral degree in Analytical Chemistry. He conducts multi-disciplinary work and his research interests are in molecular recognition mass spectrometry, new ionization techniques for mass spectrometric studies, fundamentals of electrospray ionization and synthesis/characterization of metal-complexes and ionic liquids for various analytical techniques.